Early woody plant diversity and biology: An integrative evolutionary and palaeoenvironmental study

A thesis submitted for the degree of Doctor of Philosophy

January 2026

Thibault Ulrich Frédéric Durieux

Department of Botany

School of Natural Sciences

Trinity College Dublin, the University of Dublin

Declaration

I declare that this thesis has not been submitted as an exercise for a degree at this or any other university and it is entirely my own work.

I agree to deposit this thesis in the University's open access institutional repository or allow the Library to do so on my behalf, subject to Irish Copyright Legislation and Trinity College Library conditions of use and acknowledgement.

I consent to the examiner retaining a copy of the thesis beyond the examining period, should they so wish (EU GDPR May 2018).

Thibault Durieux

Summary

The Devonian-Carboniferous (about 420 to 300 million years ago [Mya]) period witnessed the diversification of all the major groups that will form today's floras, i.e. lycophytes, ferns *s.l*, and seed plants, and the appearance of numerous structures, such as leaves, roots, seeds, and wood. In extant flora, the wood is only produced by seed plants from a bifacial cambium; however, during the Devonian and the Carboniferous, numerous lycophytes and ferns *s.l* were also able to produce it, and such, from another type of cambium (a unifacial cambium). The Devonian-Carboniferous fossil record then represents an exceptional window on the evolution of wood. However, our knowledge of anatomically preserved specimens from these periods is limited due to the rarity of the localities including such fossil types. This limits our understanding of the diversity of woody plants and the impact of a major biological crisis happening at the end of the Devonian on them.

In this work, I have contributed toward a better understanding of anatomically preserved Devonian-Carboniferous plants by studying and/or collecting specimens from Ireland and France. Studied Irish specimens have been collected during three fieldtrips of two weeks in Irish Late Devonian localities (County Kerry and County Wexford), leading to the creation of a collection comprising around 200 new specimens from historical and new localities.
The early Carboniferous specimens have been collected before this work in the French localities of the Montagne Noire (southern France). This material has been prepared using classic methods in palaeobotany for anatomically preserved fossils (thin sections, wafers, and acetate peels), allowing observation of cellular and sub-cellular details. Using this material, this thesis aims to contribute towards a better understanding of the Devonian-Carboniferous woody plant taxonomical (aim 1) and anatomical diversity (aim 2), which contributes to the debate on the impact on plants of the Devonian-Carboniferous crisis (aim 3). In addition, new specimen descriptions and reviews of historical slides also focused on observations of potential fungal-plant interaction, especially in woody tissue, contributing to the debate on the origin of wood degradation (aim 4).

The first part of my work has focused on the description of a new species from the Late Devonian of Ireland, *Callixylon seamrogia*, that has been found in the Hook Peninsula (Co. Wexford, Ireland). This study increases our understanding of the taxonomical and anatomical diversity of the genus by describing the first Irish *Callixylon* species, which also possesses a unique root anatomy (aims 1 and 2). The second part of my work led to the architectural reconstruction of an early Carboniferous cladoxylopsid, *Cladoxylon taeniatum*. This study, using 53 specimens of *Cladoxylon* from the Montagne Noire (early Carboniferous, France), leads to a reassessment of the taxonomical diversity of the genus from this assemblage and hypotheses about its growth (including the reconstruction of an atypical growth of its wood), organotaxis, and habit (aims 1 and 2). The third

part focused on the re-study of a species that also comes from the Montagne Noire, *Stauroxylon beckii*. Its re-description and the addition of a new specimen to the species lead to a better understanding of the species' anatomical diversity and organotaxis (aim 2). In addition, the phylogenetic study conducted during this study led to the inclusion of *S. beckii* into the aneurophytalean progymnosperms, indicating that this group crossed the Devonian-Carboniferous boundary (aim 3). The fourth part focused on a single slide of *Sphenophyllum* coming from the early Permian of Autun (France). Studying this slide led to the description of the first fungal remains found inside a fossil sphenophyte stem and provides the first description of fossil fungus preserved as trace fossils. This contributes to the debate on the origin of wood degradation by providing a prime example of how highly biased our understanding of fossil fungi is (aim 4).

This work has contributed to a better understanding of the taxonomical and morphological diversity of Devonian-Carboniferous woody plants. It also shows that a group previously only known in the Devonian crossed the Devonian-Carboniferous boundary and provides a prime example of how bias affects our understanding of fossil fungi and their interactions.

Acknowledgements

There are way too many people that I want to thank, but I'm truly afraid to forget someone, so I will try to reduce a maximum the name-dropping.

First, for all their support throughout my life and since the beginning of my project to becoming a "scientist", I would like to thank the family members who have always been there for me. I also want to thank all my friends, from the ones that I have known since I was a kid to the ones that I have met during these last years. My life in France and Ireland would never have been that great without all of you, thank you so much for that! Merci pour tout!

I also want to thank my supervisors, Carla J. Harper, Anne-Laure Decombeix, and Peter Moonlight. Carla, thank you so much to have been able to enroll me in a PhD, and for being so supportive of me all these years, whether for personal issues or my work. Anne-Laure, thanks for all. You have been an amazing supervisor in responding to all my queries in about a day, whether to respond to my questions, give advice, sign a paper, or even help me when I'm dumb enough to miss a flight or break my leg. Peter, thank you for agreeing to take the follow-up of Carla's supervision of me, answering all my paperwork questions, and fixing my English writing. Without you all allowing me to work in a field I love with amazing supervision, I would never have been able to complete a PhD, so thanks a million!

I would like to thank all the people I have met in Trinity (I know it's overlapping with the previous parts, but it's easier to write it like that). I have found my Dublin family inside these walls, and my life during these last years will be sad without the amazing tea/coffe/lunch breaks discussions, crazy Christmas parties, Sunday's climbs, Sate's 2 pm 2 am cooking parties, Richa's diverse competitions events, and all the parties we have done Friday or/and Saturday nights.

I also want to thank people whom I have met during my numerous stays in the AMAP lab. This place is an amazing working environment full of great people. I especially want to thank Brigittte for all her advice and discussion, Gilles for his ability to always find me a desk during my stays and lead the canteen gathering, Merlin for his help with the material preparation, and Gaelle for agreeing to come with us in the field to take hundreds of pictures.

I also want to thank the people whom I have met during my journey into the field of Palaeobotany. They have helped me during fieldwork, visiting collections, writing papers, and give me feedback and advice on my work. Thank you, Mihai Tomescu, Michael Krings, Cyrille Prestianni, and Chris Mays, for that. I also want to thank members of Agora Paleobotanica with wich we have formed a great group of friends during conferences, it was so much fun sharing these moments with you.

And lastly, I want to thank my reviewers, Jennifer McElwain and Sandy Hetherington, for agreeing to review my PhD thesis.

Merci à tout le monde!

List of main contributors to each chapter

Chapter	Name of contributor	Contributions
1: Introduction	Thibault Durieux	Conceptualization; writing.
	Anne-Laure Decombeix	Review; editing.
	Peter Moonlight	Review; editing.
2: Increasing the diversity of Devonian–Carboniferous woody plants: A new *Callixylon* species Published as: Durieux, T., Decombeix, A.-L., Harper, C.J., Ramel, M., Mays, C., Prestianni, C., 2025. *Callixylon seamrogia* sp. nov., a new species from the uppermost Famennian (Upper Devonian) of Ireland. Review of Palaeobotany and Palynology 334, 105256. https://doi.org/10.1016/j.revpalbo.2024.105256	Thibault Durieux	Conceptualization; data acquisition; investigation; visualization; writing – original draft; writing – review, and editing
	Anne-Laure Decombeix	Conceptualization; data acquisition; funding acquisition; writing – review, and editing.
	Carla J. Harper	Data acquisition; funding acquisition; writing – review, and editing.
	Merlin Ramel	Data acquisition; visualization; writing – review, and editing.
	Chris Mays	Data acquisition; writing – review, and editing.
	Cyrille Prestianni	Data acquisition, review.
3: Same component, different structure, the asymmetrical wood growth of *Cladoxylon*. Under minor revision in	Thibault Durieux	Conceptualization; data acquisition; funding acquisition; investigation; visualization; writing – original draft; writing – review and editing

International Journal of Plant Sciences in August 2025 as: Durieux, T., Decombeix, A.-L., Harper, C.J. Reconstructing the architecture of *Cladoxylon taeniatum*, an early Carboniferous nonarborescent cladoxylopsid.	Anne-Laure Decombeix Carla J. Harper	Conceptualization; data acquisition; funding acquisition; writing; review, and editing. Funding acquisition; review.
4: Woody plants and palaeoenvironments: a new group crossing the Devonian–Carboniferous boundary Durieux, T., Decombeix, A.-L., and Harper, C.J. 2024. Re-investigation of *Stauroxylon beckii*, a possible aneurophytalean progymnosperm from the Mississippian of France. International Journal of Plant Sciences, 729412. https://doi.org/10.1086/729412	Thibault Durieux Anne-Laure Decombeix Carla J. Harper Jean Galtier	Conceptualization; data acquisition; investigation; visualization; writing – original draft; writing – review and editing Conceptualization; data acquisition; funding acquisition; writing – review, and editing. Conceptualization; data acquisition; funding acquisition; writing – review, and editing. Data acquisition; writing – review, and editing.
5: Co-evolution of woody plants and wood-degrading microorganisms: another exquisite example of common human bias Published as: Durieux, T., Harper, C.J., Decombeix, A.-L., Krings, M. (2025). A rare permineralized *Sphenophyllum* (Sphenophyta,	Thibault Durieux Carla J. Harper	Conceptualization; data acquisition; investigation; visualization; writing – original draft; writing – review and editing Conceptualization; preliminary investigation; funding acquisition.

Sphenophyllales) stem containing abundant fungal remains from the Permian of Autun, central France. Review of Palaeobotany and Palynology, 105416. https://doi.org/10.1016/j.revpalbo.2025.105416	Anne-Laure Decombeix Michael Krings	Data acquisition, review, and editing. Conceptualization; data acquisition; investigation; visualization; writing – original draft; writing – review and editing
6: Conclusion	Thibault Durieux Anne-Laure Decombeix Peter Moonlight	Conceptualization; writing. Review, editing. Review, editing.

Table of Contents

List of Tables

List of Figure

List of Appendices

Chapter 1

Introduction

1. Introduction

1.1 The importance of Devonian flora in plant evolution

Vascular plants belong to the monophyletic group of the tracheophytes (Kenrick and Crane, 1997), which are defined by the presence of tracheary elements (i.e. specialized conducting tissues, [Decombeix et al., 2019a]). This group is thought to have originated in the late Ordovician based on the latest phylogenetic study using molecular data calibrated with fossils (Harris et al., 2022). The earliest evidence of this group from the fossil record are late Ordovician trilete spores, however, they are not conclusive evidence of the presence of vascular plants during this period because some extant bryophytes are also known to produce them (Gerrienne et al., 2016).

The first tracheophyte macrofossil dates from the mid-Silurian, and the earliest unambiguous anatomical evidence of tracheids dates from the late Silurian (Gerrienne et al., 2016, and references therein). These early plants were morphologically and anatomically "simple", i.e., radial symmetry, no axial branching, terminal sporangia, and absence of stem-leaf-root organotaxis, until their major diversification during the Devonian (Bateman et al.,1998; Sanders et al., 2009; Meyer-Berthaud et al., 2010; Crepet and Niklas, 2018). It is during this period that plants evolve structures that will change ecosystems worldwide, i.e. leaves (Hao and Beck, 1993; Hao and Xue, 2013), rooting systems (Morris et al., 2015), seeds (Gerrienne et al., 2004), and secondary growth (Gerrienne et al., 2011; Hoffman and Tomescu, 2013).

Nearly all extant plants from the major clades that originated during the Devonian (Figure 1.1), such as seed plants, lycophytes, ferns, and sphenophytes, are known to possess leaves (Tomescu, 2009) while only extant seed plants possess wood. However, the absence of wood or tissues in extant plant groups other than the seed plants does not necessarily imply their absence in their fossil ancestors. Indeed,wood was present across all major clades during the Devonian (Decombeix et al., 2019a), marking it out as one of the key periods to work on to increase our knowledge about wood diversity and the early stages of its evolution.

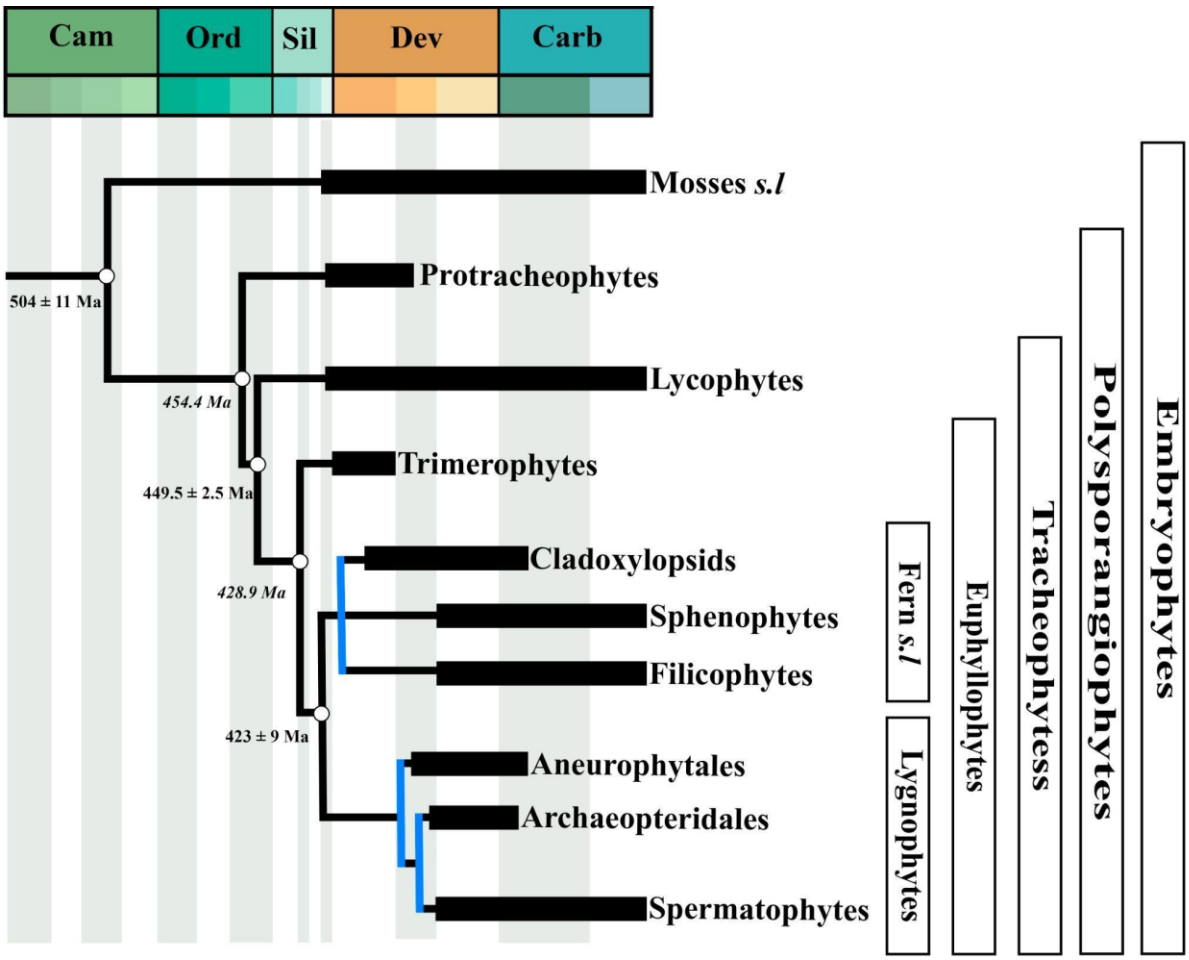

Figure 1.1 Simplified phylogenetic tree of embryophytes

The phylogenetic relationship and groups included in this tree are inspired by Figure 1 of Decombeix et al. (2019a). Dates in black at nodes represented by white circles are inferred from 1) Gerrienne et al. (2016) when they are in italics, and 2) Harris et al. (2022) when a confidence interval is given. All these dates are coming from molecular phylogenies. The blue nodes are inferred from morphological phylogenies. The node that includes ferns *s.l.* is inferred from the node of *Psilophyton* with the most basal cladoxylopsids in Durieux et al. (2021) Figure 9. The node at the base of lygnophytes and the one including the archaeopteridales with the spermatophytes are inferred from Toledo et al. (2021) Fig. 5.

1.2 The Devonian-Carboniferous wood diversity, an overview

Wood is a tissue produced by a secondary meristem called the vascular cambium. This cambium is initially located between the primary xylem and the primary phloem and produces its secondary xylem toward the center and its secondary phloem toward the outside (Esau, 1977). When the meristem can produce these two types of tissue, the cambium is called a bifacial cambium found in all extant woody plants (except in the special case of the *Isoetes* [Tomescu and Groover, 2019; Decombeix et al., 2019a]). However, some fossil plants are known to produce only secondary xylem, this type of cambium is then called a unifacial cambium (Phillips and Leisman, 1966; Cichan, 1985b; Cichan and Taylor, 1990; Donoghue, 2005). In this thesis, the term “wood” will be

equivalent to secondary xylem, a tissue that can be composed of multiple types of cells (vessel, tracheids, fibers, parenchyma [review in Esteban et al., 2024]) or can be "simpler' with the presence of only 2 types of cells, the tracheids, for the water transport, and the parenchyma cells forming ray, for transporting and storing nutrients. In all cases, to be identified as secondary xylem (see characters in Table 1.1 for a review), the tissue needs to show: 1) radially aligned tracheids; and 2) a radial system formed by parenchyma cells (i.e. rays) or/and tracheids in rare cases (Hoffman and Tomescu, 2013; Pfeiler and Tomescu, 2023; and see Rothwell and Karrfalt [2008] for a special case of absence of secondary xylem despite the above criteria).

The oldest evidence of wood in the fossil records dates from the Early Devonian of France (late Pragian/earliest Emsian; Gerrienne et al., 2011), and from 4 species and few unnamed woody plants that have been described from slightly younger localities in Canada (Gerrienne et al., 2011; Hoffman and Tomescu, 2013; Gensel, 2018; Pfeiler and Tomescu, 2021, 2023; Toledo et al., 2021). All these early woody plants possess a unifacial cambium, which is also the case for later diverging clades such as ferns (rhacophytalean and basal filicopsids), sphenopsids, cladoxylopsids (basal to ferns and sphenophytes), and lycophytes that will evolve during the Devonian (Gerrienne et al., 2011; Hoffman and Tomescu, 2013; Decombeix et al., 2019a; Tomescu and Groover, 2019). The Middle Devonian was also the period when the lignophytes, a group that includes the seed plants and the progymnosperms, evolved a bifacial cambium recognized as the synapomorphy of the clade (Rothwell and Serbet, 1994; Toledo et al., 2018, 2021). In addition, outside the lignophytes clade, other Carboniferous plants belonging to the sphenophytes and lycophytes have been hypothesized to possess a bifacial cambium based on the identification of secondary phloem (Eggert and Gaunt, 1973; Wilson and Eggert, 1974; D'Antonio and Boyce, 2021). Then, even if today, the wood production is restricted to seed plants (i.e. angiosperms and gymnosperms), during the Devonian, it was also produced by ferns, sphenophytes, lycophytes, and seed plant-related groups such as progymnosperms and stenokoleales (Table1.1 and references therein). In addition, this taxonomic diversity of secondary growth is also linked with some variation in the anatomy of the secondary xylem that can be determinate, indeterminate, with differences in ray types, pitting location and type, and frequency of cambial division (see Cichan [1984] and Cichan and Taylor [1990] for a review).

Group	Radially aligned tracheids	Secondary xylem rays	Radially aligned phloem cells	Secondary phloem rays	Anticlinal division	Difference in diameter between aligned tracheids and phloem cells	Type of secondary growth/ cambium type	References
Lycophytes	Yes	Yes	Yes (debated)	Yes (debated)	Rare (if present)	Yes	Determinate /Debated	D'Antonio and Boyce (2021)
Trimerophytes	Yes	Yes (but see [1])	No	No	Yes	Not applicable	Determinate/ Unifacial	[1]Pfeiler and Tomescu (2023)
Cladoxylopsids	Yes	Yes	No	No	Yes (rare)	Not applicable	Determinate/ Unifacial	Chapter III
Sphenophytes	Yes	Yes	Yes (can vary based on their position)	Yes	No[1]	Yes[2] and no[3]	Determinate/ Debated	[1]Cichan and Taylor (1982) [2]Wilson and Eggert (1974) [3]Eggert and Gaunt (1973)

Filicophytes (i.e. Rhacophytales and Zygopteridales)	Yes	Yes	No	No	No[1]	Not applicable	Determinate/ Unifacial	Andrews and Phillips (1968) Dennis (1974) Cichan and Taylor (1990) Phillips and Galtier (2005) [1]Tomescu and Groover (2019)
Aneurophytales	Yes	Yes	Yes	Yes	Yes	No	Indeterminate?/ Bifacial	Beck (1957) Scheckler and Banks (1971a)
Archaeopteridales	Yes	Yes	Yes	Yes	Yes	No	Indeterminate/ Bifacial	Decombeix and Meyer-Berthaud (2013)
Spermatophytes	Yes	Yes	Yes	Yes	Yes	No (but yes in Medullosa[1])	Indeterminate/ Bifacial	[1]Smoot (1984) Decombeix et al. (2014)

Table 1.1 Anatomical characters of cambial growth.

Note that information from Cichan and Taylor (1990) and Decombeix et al. (2019a) has also been included for multiple groups.

Even if the wood is not needed to attain a tree habit (e.g. in cladoxylopsids and actual palm trees and tree ferns) and is thought to have primarily evolved to increase the water conduction and not for mechanical support (Rowe and Speck, 2003; Gerrienne et al., 2011), it is during the Devonian and the Carboniferous that all major clades include species reaching the tree habit (Cichan and Taylor, 1990) with wood in variable amounts (Meyer-Berthaud and Decombeix, 2009; Meyer-Berthaud et al., 2010). The most famous representative of Devonian tree-sized species is *Archaeopteris* (Beck, 1962a). Even if not the oldest tree, it is the first to possess a large amount of wood and a deep rooting system (Meyer-Berthaud et al., 2010; Stein et al., 2020). This innovation, along with the spread of seed plants, is thought to have significantly altered global nutrient and weathering fluxes, leading some researchers to propose it as a potential trigger for the mass extinction events of the Devonian (Algeo et al., 1995, 1998; Algeo and Scheckler, 2010; Carmichael et al., 2016; Algeo and Shen, 2023; Qie et al., 2023).

1.3 Overview of the study localities

This thesis includes studies based on specimens from existing collections, as well as samples collected during our field trips. Specimens from collections reported in chapters 3, 4, and 5 of this work have been found in two geological formations (i.e. the Lydienne formation and Millery formation) in France. Information on the different geological settings and localities is available in the materials and methods sections of these studies (i.e. part 3.3, 4.3.1, and 5.3).
As part of the work for this thesis, three fieldtrips (two of one week, one of two) have been conducted in the south east of Ireland (Figure 1.2A, red star), and led to the collection of more than 250 anatomically preserved specimens from seven different localities. All these localities (summarised in Appendix A.1) are located around the Hook Peninsula (Co. Wexford) and represent localities already reported by previous authors (Figure 1.2B, black arrows) as well as new ones (Figure 1.2B, white arrows).

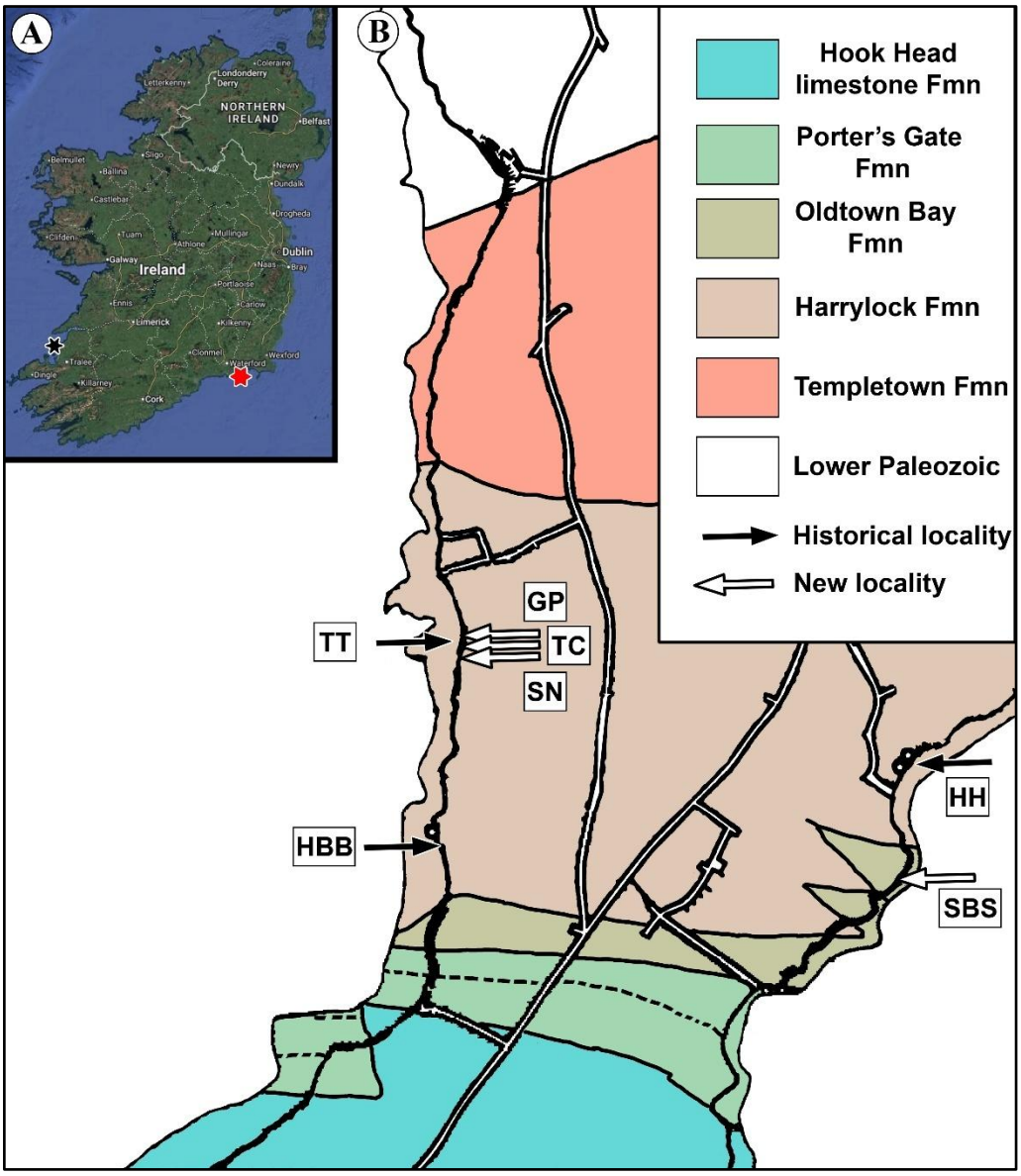

Figure 1.2 Map of the Irish localities sampled during the fieldtrips.

(A) Map of Ireland showing the location of the Kerry Head localities (black star) and the Hook Head localities (red star). (B) Geological map of part of the Hook Peninsula modified from Matten (1995) with location of the sampled localities (arrows). The color code of the geological formations is from the Geological Survey of Ireland map available online.

Three localities corresponding to outcrops of the Harrylock formation had already been reported as preserving plant remains in previous work (Figure 1.2B, black arrows; Appendix A.1).
First, the locality that has been the most sampled during our work (about 180 specimens collected) is located on the east coast of the Hook Peninsula, at Sandeel beach (Figure 1.2B, HH). This locality, corresponding to outcrops dated from the latest Famennian (LL miospore biozone), was first reported by Matten in 1982 and later studied for its fossil and or geological setting by Sleeman

et al. (1983, 76/2271), Matten (1989, locality 7; 1995, locality 4), MacCarthy and Higgs (2013), Decombeix et al. (2023), and Veenma et al (2023, "upper Sandeel Bay plant bed"). This locality provided the 5 specimens described in Chapter 2 of this work (Durieux et al., 2025).
Second, is a locality located on the west coast of the Hook Peninsula, slightly south of Oldtown Bay (Figure 1.2B, HBB). There, more than 50 anatomically preserved specimens have been collected. This locality also contains outcrops dating from the latest Famennian (LE miospore zone) and has been reported as "Higgs'locality H" by Sleeman et al (1983) and as "locality 1" by Matten (1995).
The third locality is also located on the west coast of the Hook Peninsula, on the beach of Harrylock Bay (Figure 1.2B, TT), and yielded 12 anatomically preserved specimens. According to Figure 4 of Sleeman et al. (1983), the outcrop likely corresponds to the LL miospore biozone and has already been reported by Matten (1989, "locality 2"; 1995, "locality 3") and Veenma et al. (2023, "Fossil log jam").
The four new localities (Figure 1.2B, white arrows) that have not been previously reported as containing anatomically preserved plants have been discovered during the different fieldtrips. Three of them are located in a perimeter of about 50 m around locality 3 of Matten (1995), which corresponds to an outcrop of the Harrylock formation that might be part of the LL miospore biozone. In these three localities, respectively, 7 (Figure 1.2B, GP), 9 (Figure 1.2B, TC), and 8 (Figure 1.2B, SN) anatomically preserved specimens have been collected. The remaining new locality is located on the east coast of the Hook Peninsula, about 300 m south of the Sandeel beach locality (Figure 1.2B, SBS). Based on Sleeman et al. (1983)'s map, it might correspond to their sample 76/2188 or 76/2273, which corresponds to the Oldtown Bay formation that might be part of the VI miospore biozone. Six anatomically preserved specimens have been sampled from this last locality. This locality, then, might have the potential to be the first well-dated European locality with anatomically preserved plants from the beginning of the Carboniferous known to date.

Stratigraphic and sedimentological details of the above localities are not provided in this work. This is because it represents ongoing work in collaboration with geologists and palynologists (i.e. Dr Chris Mays and Dr Cyrille Prestianni) that will provide updated/new dating, palynological biozones, and sedimentological interpretations. In addition, fieldwork has also been conducted in Kerry Head (Co. Kerry) on the beach near the village of Ballyheigue (Figure 1.2A, black star), leading to the imaging of tens of anatomically and morphologically preserved specimens directly in the field. The latter flora, also dating from the latest Famennian and first described by Matten et al (1980), will also allow further comparison with the co-occurring and paleogeographically nearby flora of Hook Head. However, studies on this flora will not be presented here because this is part of

an ongoing broader project aiming to reassess the Late Devonian-early Carboniferous Flora of Ireland, which my thesis belongs to.

1.4 The Devonian-Carboniferous Crisis

The Late Devonian is characterized by multiple extinction events, with the two major ones occurring at the boundary between the Frasnian and Famennian stages and at the Devonian-Carboniferous boundary (Sepkoski, 1986; Caplan and Bustin, 1999; Kaiser et al., 2016; Algeo and Shen, 2023). These events are respectively called the Kellwasser and the Hangenberg events. The first is considered one of the famous "Big Five" mass extinction events in the Phanerozoic (Raup and Sepkoski, 1982; Sepkoski, 1986), which is not the case for the Hangenberg event. However, its impact on aquatic organisms seems equivalent to the Kellwasser event (Kaiser et al., 2016). Nevertheless, as with numerous major past crises, its effects on terrestrial organisms are still debated (Lucas, 2021; Sahoo et al., 2023).

The Hangenberg event is characterized by the presence of black shale layers in Europe, Russia, North America, and China (Caplan and Bustin, 1999) and has been identified in at least 37 countries on all continents (except Antarctica) using different proxies (Kaiser et al., 2016; see Carmichael et al. [2016] for the use of different proxies). These carbon-rich sediments are hypothesized to result from multiple global marine anoxia events associated with significant sea level changes (Caplan and Bustin, 1999; Carmichael et al., 2016). Multiple causes of this extinction event have been hypothesized, including: a bolide impact (McLaren and Goodfellow, 1990), massive UV-B radiation caused by global warming or a supernova (Fields et al., 2020; Marshall et al., 2020), a large volcanic event (Pisarzowska et al., 2020; Rakociński et al,. 2020), rifting-hydrothermal pollution (Shun-Liang, 2001), or linked to the plant evolution (Algeo et al., 1995).

According to the latest review (Kaiser et al., 2016; Algeo and Shen, 2023) the non-identification of a "significant" and simultaneous crater (Caplan and Bustin, 1999) or large igneous province with the Hangenberg event, as well as the fact that this event is hypothesised to be a large carbon burial event (Caplan and Bustin, 1999) weaken the volcanism and the impact hypotheses. In addition, the results of a recent isotopic study also weaken the volcanism hypothesis (Qie et al., 2023).

The UV-B radiation hypothesis is based primarily on the identification in east Greenland of a large portion of malformed spores close to the D-C boundary, followed by an absence of plants in the study's Tournaisian section (early Carboniferous [Marshall et al., 2020]). However, an increase in temperature seems unlikely to significantly increase UV-B exposure (Fields et al., 2020), and a supernova will leave radioisotopic signals that are yet to be discovered to add more weight to this

hypothesis (Fields et al., 2020). In addition, whether a supernova can be a cause of mass extinction events is still debated, a recent study based on models concluded that "*nearby SN* [supernovae] *are unlikely to have caused mass extinctions on Earth*" (Christoudias et al., 2024: p. 5), thanks to the Earth's atmosphere and its geomagnetic field.

The hypothesis of the land plant-driven mass extinction suggests that during the Frasnian and the Famennian plants grew larger with deeper root systems, ultimately leading to thicker soil. In addition, seed plants will spread during the Famennian leading plants to colonize areas that were previously plantless (Algeo et al., 1995, 1998; Algeo and Scheckler, 2010). This increase in biotic weathering and soil formation is expected to result in water eutrophication, leading to major anoxia events and Earth cooling induced by CO2 burial (Algeo et al., 1995, 1998). This hypothesis is supported by isotopic studies (Carmichael et al., 2016; Qie et al., 2023), however, it does not preclude the other hypothesis from being true. Note that this hypothesis is also used to explain the Kellwasser extinction event (Whiteside and Grice, 2016; Smart et al., 2023).

All of these hypotheses are still debated, and it is possible that the Hangenberg extinction event had multiple causes. The latter would then explain that the extinction happened in different groups from different ecological niches at different periods spread over 50 to 100 ka intervals around 359 Ma (Myrow et al., 2014; Carmichael et al., 2016; Kaiser et al., 2016).
Then, even if it is not the only one, plant evolution (i.e. apparition of deep rooting systems and the spread of seed plants) is one of the processes that is thought to be one of the strong triggers of the Hangenberg mass extinction event. Nevertheless, the impact of this event on plant diversity is still debated with evidence coming from spores seeming to show an extinction event (Caplan and Bustin [1999] and reference therein; Marshall et al., 2020) whereas the taxonomical diversity of plant macrofossils seeming to show a transition from one type of flora towards another (Cleal and Cascales-Miñana, 2014; Capel et al., 2021).

1.5 Wood-degrading fungi and bias in the fossil record

The knowledge about the taxonomical diversity and phylogenetic relationships of the Devonian-Carboniferous fossil plants increases thanks to the numerous anatomically and/or morphologically preserved specimens that are described and published each year. However, reports of interactions between plants and other organisms, such as fungi, are rarer (Figure 1.2) during these periods especially if we exclude the Rhynie chert. The latter deposit, dating from the Early Devonian (about 410 Ma) and known since the early 1900s (Mackie, 1914; Kidston and Lang, 1917), is the

foundation of much of our knowledge about the early fungal lineage and their interactions (Taylor et al., 2004; Krings et al., 2017c). However, direct fossil evidence of one of today's major interactions, i.e. the ability of the fungi to degrade the tracheids and most especially its thickening major component, the lignin, has not been found in this deposit despite the presence of plants possessing this cell type (i.e. tracheophytes).

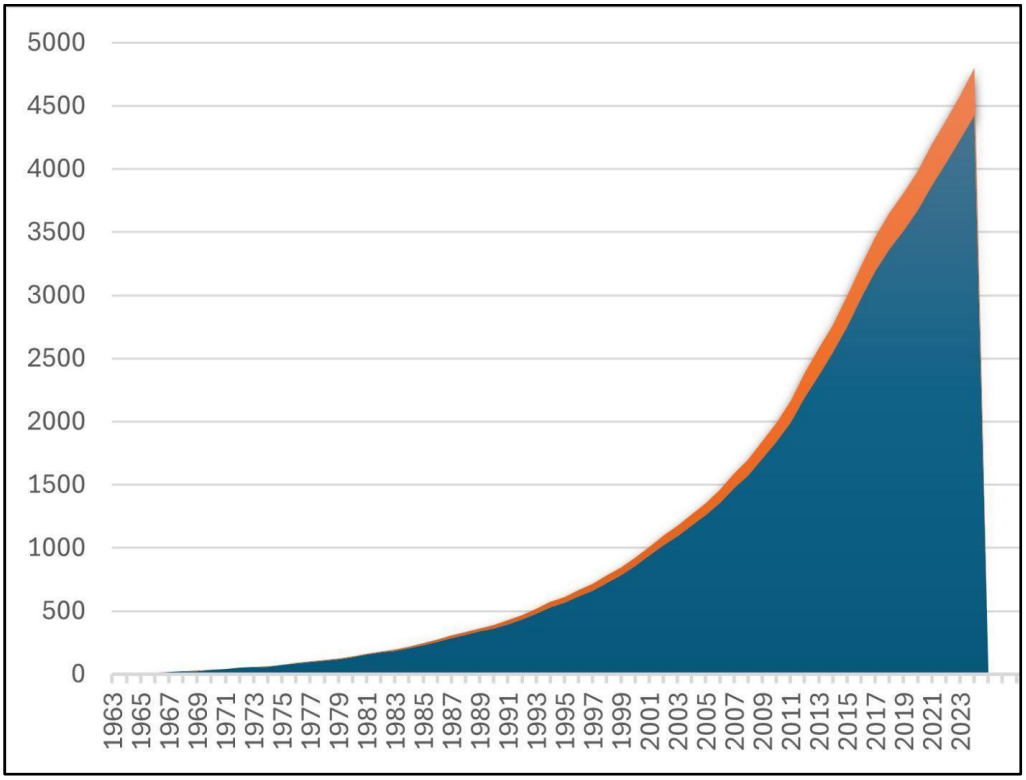

Figure 1.3 Cumulative graph of the number of publications including words "fossil" and "plant" (in blue; n = 4456) and "fossil" and "fungi" (in orange; n = 372) from 1963 to 2024.

Data from Scopus and details of the search in Appendix A.1; A.2, 1963 correspond to the first publication including "fungi" and "fossil" in the database.

In plants, lignin is mostly present in primary and secondary xylem tracheids (about 20-30 % of lignin [Kirk and Farrell, 1987]), fibers, and sclereids (Jarvis, 2012; Crang et al., 2018). Plants and especially wood are the major biomass components of today's ecosystem (Bar-On et al., 2018) and, their decomposition being mostly done by fungi (Kirk and Farrell, 1987), this type of interaction is common in today's ecosystems. However, despite the diversity of plants known to possess wood during the Devonian (see part I.2), the only potential fossil evidence of wood degradation by fungi during this period dates from the Late Devonian (Stubblefield et al., 1985), and the first occurrence

of the group that is known to be the major one with this role in today's ecosystems (i.e. the Basidiomycota) dates from the early Carboniferous (Visean [Krings et al., 2011a]).

After a review of the literature on this subject, I see mainly two hypotheses to explain this apparent lack of fossil evidence: 1) fungi cannot degrade the lignin during this period (Floudas et al., 2012), or 2) the process indeed occurs in this period, but due to numerous biases, fossil evidence has yet to be discovered.

Some bacteria species can degrade the wood (review in Grgas et al. [2023]), however, fungi are the main organisms able to significantly degrade plant lignin in extant ecosystems (Kirk and Farrell, 1987; Sigoillot et al., 2012; Janusz et al., 2017). Within the fungi, the Basidiomycota and more precisely the agaricomycetes (mainly white rot fungi but also brown rot) are "*The only organism capable of substantial lignin decay*" (Floudas et al., 2012: p. 1715). A study based on extant fungal species belonging to this group concluded that the origin of the lignin enzymatic decomposition dates from the end of the Carboniferous (Floudas et al., 2012). This study has led to the above first hypothesis that the lack of fossil evidence is due to the absence of lignin degradation by fungi, in addition to explaining the unique high organic carbon burial during the Carboniferous (Floudas et al., 2012). Nevertheless, some authors (Nelsen et al., 2016) disagree strongly because (1) other enzymes than those studied by Floudas et al. (2012) can be used to degrade the lignin (Nelsen et al., 2016); (2) other fungal groups (e.g. ascomycetes, zygomycetes) able to degrade lignin are present during the Carboniferous (Taylor and Taylor, 1997; Holman et al., 2024 and reference therein); and (3) they have not have taken into account (or even mentioned) fossil evidence such as the potential evidence of decaying wood during the Late Devonian (Stubblefield et al., 1985) or the earliest fossil clamp connection indicating the presence of the basidiomycetes during the early Carboniferous (Krings et al., 2011a). In addition, the high carbon burial in the Carboniferous can be due to "*a unique combination of climate and tectonics during the Pangea formation*" (Nelsen et al., 2016: p. 2442) and not to the lack of fungi able to degrade the lignin. Note that there is no peak of organic carbon burial during the Middle to Late Devonian when *Archaeopteris* trees spread all over the world, which are more "woody" than species that dominated the coal deposit during the Carboniferous (i.e. lycophytes, calamites). Conversely, the Paleogene burial peak happens even when all enzymes able to decay lignin were present (Nelsen et al., 2016). Furthermore, if the fungi were able to degrade lignin only at the end of the Carboniferous, then it induces a gap of more than 100 Ma between lignin's appearance and the evolution of a mechanism able to degrade what is today one of the most abundant carbon resources on the planet.

The second hypothesis is based on the numerous biases leading to the scarcity of reports of fungi in the fossil record (Taylor and Krings, 2005; Taylor et al., 2015; Halbwachs et al,. 2021). There are

multiple explanations for that, but they are mainly of two types: the taphonomical bias and the human bias.

Belonging to the first type is the fact that fungi are indeed rarer than plants in the fossil record due to their specific preservation requirements (Taylor and Taylor, 1997; Taylor et al., 2015; review in Halbwachs et al. [2021] and Harper and Krings [2021]). In addition, the likelihood that fossil plants preserved information about fungal interactions (Harper and Krings, 2021) is even lower because the burial of the specimens has to happen at a precise time of the life of the fungi and the host, e.g. for observing a fossil of wood that is degraded by fungi, the specimens need to have been buried not before the fungus arrives and not after everything is degraded (Halbwachs et al., 2021).

The human bias is due to (1) the development of the acetate peel technique for the study of anatomically preserved fossil plants (Joy et al., 1956), which leads to the loss of the plant cellular contents during the preparation, i.e. where the fungal remains are potentially preserved (Taylor et al., 2011), and (2) the lack of expertise on fossil fungi (Taylor and Taylor, 1997; Taylor et al., 2015). Note that after the 90s, there has been an increase in interest/awareness about fossil fungi and their role in past ecosystems (Harper et al., 2016b; Halbwachs et al., 2021). Harper and Krings (2021: p. 81) summarize also well a kind of paradox that can be explained by the quality of the preservation and the lack of expertise "*Evidence of decay attributable to fungi is frequently encountered in fossil wood; however, studies focusing on fossil fungal wood degradation are rare (see Harper et al. 2016 for a review; Wan et al. 2017), and documented example of (partially) decayed fossil wood containing well-preserved fungal remains are even rarer.*".

Another piece of evidence that supports the ability of fungi to degrade lignin as far back as the early Devonian is provided by a recent biomarker study (Holman et al., 2024). In it, Holman and collaborators (2024) show evidence of perylene in silicified plant fragment from the Rhynie Chert. The presence of perylene, being one of the known biomarkers of the lignin-degrading fungi, suggests that the fungi were likely degrading the lignin. Note that, while the Basidiomycota are the ones responsible for most of the lignin degradation today (see above), this biomarker is restricted to Ascomycota (Holman et al., 2024). In any case, this finding seems to support that this lignin degrading fungi where present even before the current oldest woody plants (Late Pragian/earliest Emsian; Gerrienne et al., 2011; Hoffman and Tomescu, 2013), making the second hypothesis for explaining the lack of fossil evidence of wood-degrading fungi even more likely.

1.6 Thesis aims and structure

This thesis aims to increase our knowledge of the taxonomic (aim 1) and anatomical diversity of Devonian-Carboniferous woody plants (aim 2) in providing new specimens descriptions that will further the debates about the impact of the Devonian-Carboniferous crisis on plants (aim 3), and the absence of unequivocal evidence of wood-degrading interactions in these periods (aim 4). Following these different aims, this work encompasses four chapters that correspond to four studies that are currently published (chapters 2, 4, and 5), and submitted (chapter 3), and a sixth chapter consisting of a general conclusion. Each of those constitutes a chapter of this thesis, organized as follows:

Chapter 2 aims to increase the diversity of the Devonian–Carboniferous woody plants. During this thesis, three fieldtrips were conducted in two Irish fossil localities, resulting in the collection of over 200 new anatomically preserved specimens. These localities date from the Late Devonian (latest Famennian) and are located in Kerry Head (Co. Kerry) and Hook Head (Co. Wexford) (Decombeix et al., 2022). In the latter, specimens belonging to the genus *Callixylon* have been discovered, and their unique characters led to the description of a new species, *Callixylon seamrogia* (Figure 1.3 A, B; Durieux et al., 2025b). This species shows a specific combination of wood characters that expands the known diversity of this genus, and by extension, the diversity of the Late Devonian woody plants.

Chapter 3 focuses on describing the architecture (*sensu* Barthélémy and Caraglio [2007]) of an atypical woody plant called *Cladoxylon taeniatum* (Figure 1.3 C, D). This study has been conducted on 28 specimens assigned to *C. taeniatum* from early Carboniferous (Tournaisian) localities of southern France (Montagne Noire, Hérault). From them, the primary and secondary growth of this species, as well as its lateral organ emission process, have been described. The wood growth of *C. taeniatum* is reconstructed as asymmetrical around its numerous primary xylem bundles. The cell type and the tissue organization of this wood are not different from most of the woody plants from this period, but its growth pattern is atypical. This species then represents an example of how from the same wood components different growth patterns can evolve, increasing the known diversity of secondary growth in the early Carboniferous.

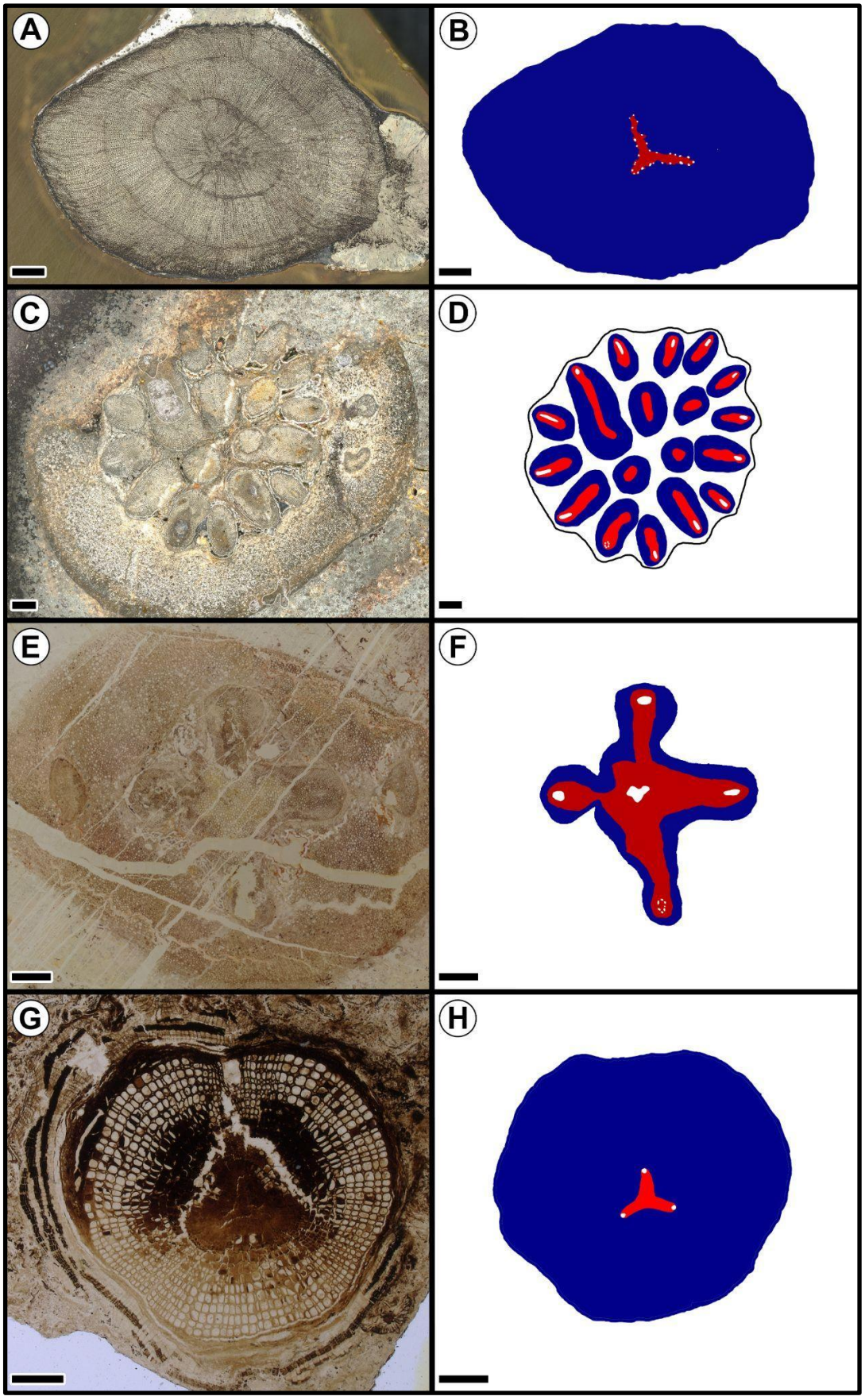
A
B
C
D
E
F
G
H

Figure 1.4 Overview of the anatomical diversity of the study plants.

(A) *Callixylon seamrogia* paratype in cross-section (Late Devonian, Ireland) with its associated explicative drawing (B); Scale bar = 1 mm; Slide n°HH10 DS 6. (C) *Cladoxylon taeniatum* in cross-section (early Carboniferous, France) with its associated explicative drawing (D); Scale bar = 1 mm; Waffer n° MN268 3 AS 1. (E) *Stauroxylon beckii* holotype in cross-section (early Carboniferous, France) with its associated explicative drawing (F); Scale bar = 1 mm; Slide n°MN410-AI 01. (G) *Sphenophyllum plurifolium* (early Permian, France) in cross-section with its associated explicative drawing (H); Scale bar = 1 mm.
Color coding of the drawings, in: White: protoxylem; Red: Metaxylem; Blue: Secondary xylem.

Chapter 4 is based on the study of *Stauroxylon beckii* (Figure 1.3 E, F; Durieux et al., 2024), a species initially described in 1970 (Galtier, 1970) that, despite showing an unusual combination of characters, has never been included in recent phylogenetic studies. This plant has also been found in the Montagne Noire (Tournaisian), in the same site as part of the *Cladoxylon* specimens. The holotype and an additional specimen have been (re)described and included in phylogenetic analyses encompassing lignophytes and closely related groups (i.e. radiotopsids [Toledo et al., 2018, 2021; Durieux et al., 2024]). The result of the analyses, in addition to strengthening previous finding of radiotopsids phylogenies, places *S. beckii* in the aneurophytales, making it the first representative of this group found after the Devonian. This study thus provides a new example of a group known to have survived the Hangenberg event and crossing the Devonian-Carboniferous boundary.

Chapter 5 provides a prime example of human-linked bias in the study of fossil fungi and their interactions with plants. In this study, a slide containing a cross-section of *Sphenophyllum* stem (Figure 1.3 G, H; Durieux et al., 2025a) dating from the early Permian of Autun (central France) has been studied. This plant specimen shows fungal remains inside almost all of these cells, providing the first evidence of fungi inside a *Sphenophyllum* stem and an unusual type of fossil remains for fungi. However, this finding is unexpected because 1) this slide came from the historical collection of Auguste Roche, who was, among others, the co-worker of Bernard Renault, one of the fathers of palaeomycology (Galtier, 2016), 2) *Sphenophyllum* is a genus possessing an extensive fossil record of anatomically preserved specimens (Renault, 1876, 1878; Williamson and Scott, 1894; Baxter, 1948; Schabilion and Baxter, 1971; Good, 1973; Terreaux De Felice et al., 2019), and 3) the slide has been found in a collection that is already known to contain fungal remains (Krings et al., 2009b; Taylor et al., 2012; Strullu-Derrien et al., 2021). This study then represents a prime example of that, even with the perfect condition, i.e. specimens containing

abundant fungal remains, in a collection already studied by palaeomycologists, and in a genus that has never been reported to include fungi, fungal remains can be overlooked.

Chapter 6 concludes this work by reviewing the main results and their application to broader questions. These results include new knowledge on the targeted topics, i.e., increasing our knowledge about the taxonomical and anatomical diversity of the Devonian-Carboniferous plants, the impact of the Hangenberg event on woody plants, and plant-microorganism interaction. In addition, this chapter also reviewed other results leading to new insight into the architecture and the character evolution of the Devonian-Carboniferous plants, which were not included in the primary aims of this work. However, such findings are primordial for a better understanding of fossil plant and their evolution. The last part encompasses the future steps that my research can undertake to continue working on these questions.

Chapter 2

Increasing the diversity of Devonian–Carboniferous woody plants: A new *Callixylon* species.

Published as: Durieux, T., Decombeix, A.-L., Harper, C.J., Ramel, M., Mays, C., Prestianni, C., 2025. *Callixylon seamrogia* sp. nov., a new species from the uppermost Famennian (Upper Devonian) of Ireland. Review of Palaeobotany and Palynology 334, 105256. https://doi.org/10.1016/j.revpalbo.2024.105256

Figure, table, section numbers, and citation style have been modified to fit the manuscript's purpose.

2. *Callixylon seamrogia* sp. nov., a new species from the uppermost Famennian (Upper Devonian) of Ireland.

2.1 Abstract

The fossil record of the Devonian tree *Archaeopteris*/*Callixylon* is extensive worldwide, however, the underground parts of these plants remain scarcely known. To date, there are only three studies that provide detailed anatomical descriptions of their roots. This study describes new anatomically preserved roots and stems of *Callixylon* from uppermost Famennian (Upper Devonian) deposits of Sandeel Bay, County Wexford, Ireland. The wood is characterized by tracheids with the pitting pattern typical of *Callixylon* (i.e., radial pits forming groups separated by non-pitted areas), and the presence of numerous ray tracheids that are smaller than the parenchyma ray cells in tangential section and unevenly arranged inside the rays. The roots are characterized by a three-lobed actinostele with multiple exarch protoxylem strands, an unusual organization reported for the first time in *Callixylon* roots. The stems are eustelic, with an heterocellular pith composed of thin and some thick-walled cells. Based on their unique combination of characters, the specimens are assigned to a new species, *Callixylon seamrogia*, the first species of *Callixylon* reported from Ireland. Based on comparisons with previous architectural studies of *Callixylon,* the stems are hypothesized to correspond to main axes of the new species, one of them bearing an apically emitted non-persistent branch. These new specimens from Ireland provide new information on the rooting system of *Archaeopteris/Callixylon* and improve our understanding of the anatomical and systematic diversity within the genus.

2.2 Introduction

During the Late Devonian, forests were dominated by the first trees with extensive wood production belonging to the genus *Archaeopteris/Callixylon* (Beck, 1960a, 1964, 1981; Beck and Wight, 1988; Meyer-Berthaud et al., 1999, 2010). After being assigned to two different groups of plants for decades, fern-like foliage bearing sporangia of *Archaeopteris* (Dawson, 1871) and woody stems of *Callixylon* (Zalessky, 1911) were found in anatomical connection by Beck in 1960 (Beck, 1960a). This led to the erection of the progymnosperms (Beck, 1960c) an extinct group characterized by a bifacial vascular cambium like the seed plants but with reproduction by spores. Specimens of *Archaeopteris* and *Callixylon* have been found worldwide (Anderson et al., 1995;

Cornet et al., 2012; Meyer-Berthaud et al., 2021; Liu et al., 2024) and numerous species have been erected. However, despite the discovery of palaeosols with remains of *Archaeopteris* roots in multiple localities (Driese et al., 1997; Mintz et al., 2010; Guo et al., 2019; Stein et al., 2020), there are only a few detailed descriptions of the anatomy and the systematic affinities of these roots. Indeed, since the establishment of *Callixylon petryi*, the first morphospecies of *Callixylon* roots in 1953 (Beck, 1953), only three studies have described anatomically preserved roots, with few details regarding their affinities (Andrews et al., 1965; Snigirevskaya, 1984; Meyer-Berthaud et al., 2013).

Andrews and collaborators (1965) reported roots from the Upper Devonian of Ellesmere Island, Canada, found in association with vegetative and fertile specimens of *Archaeopteris*. Since *Archaeopteris fissilis* and *A. obtusa* were the only fossil plants reported in this locality, it was considered "...*highly probable that they are the roots of these plants…*" (Andrews et al., 1965: p. 555). In addition, these roots seem to share numerous features with *Callixylon petryi*. Snigirevskaya (1984) reported a Late Devonian trunk base of *Callixylon trifilievii* with roots attached and an isolated root fragment from the Donetz Basin, Ukraine. Since the latter possessed the same anatomy as the trunk base, all specimens were assigned to *C. trifilievii* (Snigirevskaya, 1984; Meyer-Berthaud et al., 2013).

More recently, Meyer-Berthaud and collaborators (2013) reported anatomically preserved specimens of *Callixylon* roots from an Upper Devonian deposit of Morocco. These specimens were assigned to the *erianum* and *trifilievii* 'groups' proposed by Orlova and Jurina (2011) based on their wood anatomy (Meyer-Berthaud et al., 2013).

Another fossil reported from Upper Devonian deposits of New York, USA, that may conceivably provide information on the anatomy of the roots of *Archaeopteris*/*Callixylon* is *Eddya sullivensis* (Beck, 1967), which is considered a putative young *Archaeopteris*/*Callixylon*. *E. sullivensis* is a nearly complete anatomically preserved plant in which the root system is attached to the stem.

Anatomically preserved *Callixylon* roots have never been described in detail from western European localities despite numerous Middle to Upper Devonian sites known to contain archaeopteridales remains, including in Belgium (Marcelle, 1951; Berry, 2008; Cornet et al., 2012), Scotland (Chaloner, 1972), Germany (Kräusel and Weyland, 1929), and Ireland (Forbes, 1853; Johnson, 1911; Wang, 2011). In Ireland, numerous localities have been reported to contain Archaeopteridales remains (Johnson, 1911; Matten, 1995; Klavins, 1999). However, only three anatomically preserved specimens have been reported, all from the Hook Peninsula, County Wexford, Ireland, and none of them have been formally described (Matten, 1995; Klavins, 1999). One of these Upper Devonian Hook Peninsula localities, Sandeel Bay, has been recently

reinvestigated by our research team, leading to the discovery of several new anatomically preserved *Callixylon* specimens. In this paper, we describe five specimens corresponding to roots (n = 3) and stems (n = 2) and discuss their affinities. This is the first detailed description of anatomically preserved *Callixylon* roots in western Europe, as well as the first formal description of specimens belonging to this genus in Ireland. The five specimens are assigned to *Callixylon seamrogia* sp. nov., increasing the diversity of Late Devonian *Callixylon*.

2.3 Materials and Methods

2.3.1 Locality

The specimens were collected during the 2021 and 2022 field seasons at Sandeel Bay, a beach located on the east coast of the Hook Peninsula, County Wexford, Ireland (52° 09' 40.7"N, 06° 52' 57.4"W). They are from an outcrop of the Harrylock Formation (Sleeman et al., 1983), which represents the uppermost unit of the informal 'Old Red Sandstone' expressed at the Hook Peninsula. This outcrop has been dated to the latest Famennian based on its miospore assemblage (LL Miospore Biozone, Sleeman et al., 1983; Decombeix et al., 2023; Veenma et al., 2023). This outcrop is equivalent to locality 76/2271 of Sleeman et al. (1983), locality 7 of Matten (1989) and locality 4 of Matten (1995). The bed containing the specimens of this study is a grey, stratified mudrock lens, which has been interpreted as a lacustrine deposit (MacCarthy and Higgs, 2013) and has been figured in Decombeix et al. (2023: sup Fig. 1 b) and Veenma et al. (2023: Fig. 9). In this layer, plant macrofossils are preserved as pyritized permineralizations, impressions, and compressions in a grey-green mudstone matrix that also contains spores and cuticle fragments (Decombeix et al., 2023).

The first report of fossil plants from Sandeel Bay was given by Matten in 1982. Since then, macrofossils of lycophytes (*Wexfordia hookense* [Matten 1989 emend. Klavins 2004], cf. *Cyclostigma* [Klavins, 1999]), gymnosperms (three seed morphotaxa [Klavins, 1999]) and progymnosperms *(Archaeopteris hibernica* and *Callixylon* [Klavins, 1999; Decombeix et al., 2023]) have been reported.

2.3.2 Material preparation and observation

The five specimens of this study were prepared as wafers at UMR AMAP (Botany and Modelling of Plant Architecture and Vegetation, Montpellier, France) using the protocol detailed in Decombeix et al. (2023). In total, 40 wafers were prepared from three specimens identified as roots (specimens HH10, HH24, and HH40), and 13 from two specimens identified as stems or branches (specimen numbers HH37 and HH45). We identified no organic connections between stem and branch specimens.

Images of all the specimens were taken with a Keyence VHX 7000 digital microscope using reflected light. The software ImageJ (https://imagej.nih.gov/ij/) was used to outline specific areas of specimens and for all measurements. The function "analyze particles" was used to measure certain cells to determine differences in cell sizes. Adobe Photoshop (ver. 25.11; San Jose, CA) was used for drawings, plate construction, and minimal homogeneous image adjustment (brightness, contrast, and color). Fossil specimens and slides are currently stored at UMR AMAP Montpellier under specimen numbers HH10, HH24, HH37, HH40, and HH45, and will be ultimately transferred and deposited to the Trinity Geological Museum, Trinity College Dublin, Dublin, Ireland.

2.4 Results

Systematic descriptions

Class: Progymnospermopsida Beck, 1960

Order: ARCHAEOPTERIDALES Zimmermann, 1930

Genus: *Callixylon* Zalessky, 1911

Species: *Callixylon seamrogia* Durieux, Decombeix, Harper, Ramel, Prestianni sp. nov. (Figure 2.1 to 2.5).

Etymology: Seamrogia is the Latinisation of ”seamróg”, the Irish word for shamrock. Irish (Gaeilge) is an official language of the Republic of Ireland; the ‘shamrock’ may refer to the plants, *Trifolium dubium* or *T. repens*, which are characterized by trifoliate, oval to heart shaped leaflets, commonly known as a three-leaf clover (e.g., Burdon, 1983), and is one of the symbols of the Republic of Ireland with significant cultural importance. The shape of the root stele of this species is reminiscent of the three leaves of a shamrock with its three lobed actinostelic roots.

Type locality: Sandeel Beach, County Wexford, Ireland.

Holotype: Specimens HH40.

Paratypes: Specimens HH10 and HH24.

Stratigraphy and age: Harrylock Formation, LL Miospore Biozone, latest Famennian.

Repository: Trinity Geological Museum, Trinity College Dublin, Dublin, Ireland.

Specific diagnosis: Eustelic stems and associated 3-lobed actinostelic roots, both with secondary xylem. Eustelic axes with mesarch vascular bundles in contact with the secondary xylem and a heterocellular pith with thin and thick-walled cells.

Actinostelic axes with 3-lobed primary xylem more than 2 mm wide with numerous exarch protoxylem strands located at the tips and along the lobes. Secondary xylem in both types of axes with uniseriate rays up to 30 cells in height. Two types of cells in rays, parenchyma and ray tracheids. Ray tracheids numerous, unevenly arranged inside rays, and shorter than parenchyma cells in tangential section.

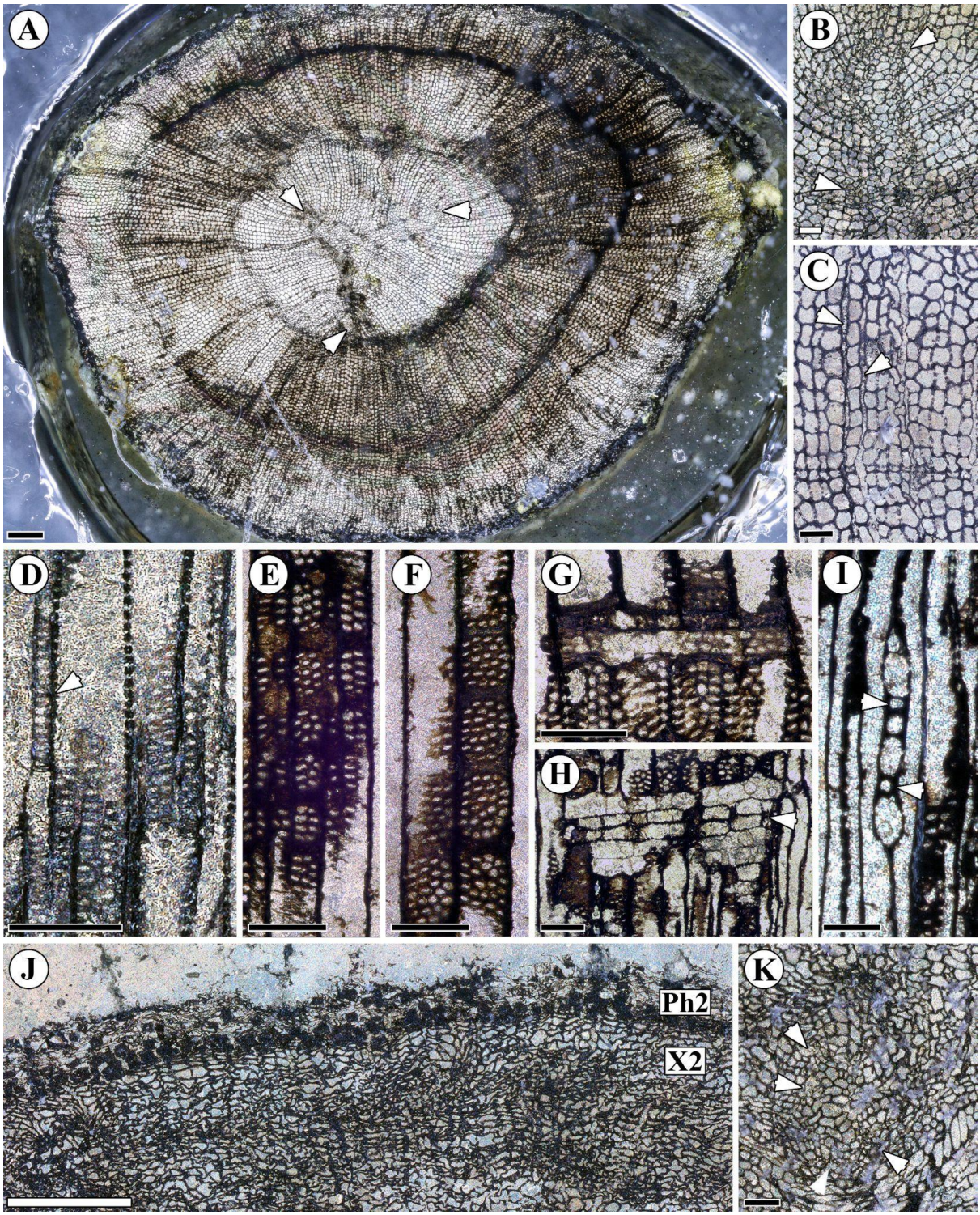

Figure 2.1 Root anatomy of *Callixylon seamrogia* sp. nov.

(A) General view of specimen HH40 (holotype) in transverse section with arrows pointing to the tips of the three lobes of the actinostele; scale bar = 500 µm; slide HH40 B A. (B) Tip of one of the lobes; arrows pointing to two of its protoxylem strands; scale bar = 100 µm; slide HH10 DS06. (C) Detail of the wood in transverse section showing tracheids and rays composed of parenchyma and ray tracheids (arrows); note the

row of tracheids with a reduced tangential diameter; scale bar = 100 µm; slide HH40 A S2. (D) Primary xylem in radial view showing a protoxylem tracheid with helical thickening (arrow) and metaxylem tracheids with multiseriate pits; scale bar = 100 µm; slide HH24 B Lg2. (E) and (F) Detail of the secondary xylem in radial view showing pits in groups separated by unpitted areas; scale bars = 100 µm; slide HH40 Lg2. (G) Cross-field pitting; scale bar = 100 µm; slide HH40 Lg 2. (H) Rays in radial view showing parenchyma cells and ray tracheids (arrow); scale bar = 100 µm; slide HH40 Lg2. (I) Uniseriate ray in tangential view showing parenchyma cells and ray tracheids (arrows); scale bar = 50 µm; slide HH10 C G2. (J) Transverse section of the most peripheral part of specimen HH40; two types of tissue are preserved, secondary xylem (X2) and secondary phloem (Ph2); scale bar = 500 µm; slide HH40 B S. (K) Vascular trace in transversal view with arrows pointing potential protoxylem strands; scale bar = 100 µm; slide HH24 B S3.

2.4.1 *Callixylon seamrogia* sp. nov. roots (Figure 2.1, 2.2)

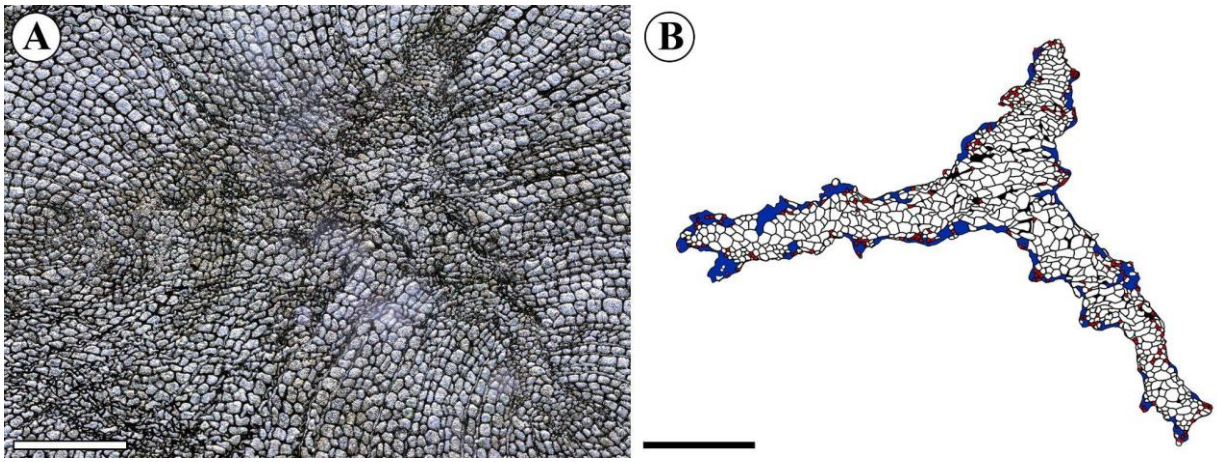

Figure 2.2 Stele of *Callixylon seamrogia* sp. nov. roots in transversal view.

(A) Three-lobed actinostele of HH10 (paratype) surrounded by secondary xylem; scale bar = 500 µm; slide HH10 DS06. (B) Drawing of the stele in (A) with, blue are the unpreserved zones; red are the smallest cells corresponding to the first quartile of the primary xylem cells area; scale bar = 500 µm.

The following description combines all three specimens (HH24, HH10, and HH40). Details of their respective measurements are reported in Table 2.1.

Specimen number	Stele type	Diameter (in mm)	Protoxylem tracheid diameter (in µm)	Metaxylem tracheid diameter (in µm)	Radial diameter tracheid X2 (in µm)	Tangential diameter tracheid X2 (in µm)
HH10	**Actinostele**	**12 x 7.1**	**10–19.7 (mean = 14.4; n = 11)**	**12.4–75.2 (mean = 36.6; n = 50)**	**36.8–77.5 (mean = 54.9; n = 50)**	**26.2–70.3 (mean = 45; n = 50)**
HH24	**Actinostele**	**8.8 x 6.2**	**10.1–28.1 (mean = 15.2; n = 10)**	**12.1–91.5 (mean = 49; n = 50)**	**34.7–89.6 (mean = 54; n = 50)**	**19.1–76.5 (mean = 46.6; n = 50)**
HH40	**Actinostele**	**9.8 x 8.1**	**13–30.7 (mean = 19.5; n = 30)**	**22.2–88.7 (mean = 51.1; n = 50)**	**34.5–83.4 (mean = 55.7; n = 50)**	**21.8–94.4 (mean =53.1; n = 50)**
HH37	**Eustele**	**16.5 x 3.4**	**7.2–30.2 (mean = 16.9; n = 50)**	**17.3–74.8 (mean = 41.3; n = 50)**	**11.2–64.8 (mean = 24.3; n = 50)**	**13.3–55.9 (mean = 25.8; n = 50)**
HH45	**Eustele**	**13.9 x 2.4**	**7.6–35.2 (mean = 20; n = 50)**	**26.3–79.4 (mean = 42.3; n = 50)**	**11.8–43.8 (mean = 25.6; n = 50)**	**13.5–48.7 (mean = 25.1; n = 50)**

Specimen number	Length non-pitted area (in µm)	Pits apperture (in µm)	Ray height (in cells)	Ray cell height (in µm)	Ray cell wideness (in µm)	Parenchyma ray cells height (in µm)	Ray tracheids height (in µm)
HH10	**17.8–30.7**	**4–11 (mean = 6.5; n = 50)**	**1–15**	**13.9–46.3 (mean = 28.7; n = 50)**	**8.4–34.8 (mean = 19.9; n = 50)**	**not observed**	**not observed**
HH24	**10–28.8**	**4.5–14.5 (mean = 9.5; n = 50)**	**1–20**	**14.7–54.6 (mean = 30; n = 50)**	**12.6–30.6 (mean = 20; n = 50)**	**19.8–40.1 (mean = 29.1; n =19)**	**19.1–32.4 (mean = 23.6; n = 6)**
HH40	**8.8–30.1**	**4–14.5 (mean = 9; n = 50)**	**1–30**	**13.5–62.8 (mean = 32.8; n = 50)**	**7.3–41.1 (mean = 19.3; n = 50)**	**17–49.6 (mean = 35.6; n = 20)**	**20.9–43.4 (mean = 28; n = 20)**
HH37	**None entirelly preserved**	**4–10 (mean = 6.5; n = 50)**	**1–17**	**33.7–69.9 (mean = 49.4; n = 50)**	**18.6–48.8 (mean = 32; n = 50)**	**20.2–42 (mean = 29; n = 20)**	**10–30.7 (mean = 17.9; n = 20)**
HH45	**7.5–22.3**	**4.5–12.5 (mean = 8; n = 50)**	**1–43**	**15–82.9 (mean = 36.2; n = 50)**	**11.9–47.5 (mean = 27.1; n = 50)**	**14.8–55.1 (mean = 32.4; n = 20)**	**8–42.3 (mean = 19.9; n = 50)**

Table 2.1 Detail anatomical structures measurements of *Callixylon seamrogia* specimens (X2 = secondary xylem; n = number of structures measured).

The specimens are decorticated axes that are respectively 12 x 7.1 (HH10), 8.8 x 6.2 (HH24), and 9.8 x 8.1 mm (HH40) in diameter, and about 18, 10, and 11 cm long. In transversal view, the specimens possess a three-lobed actinostele with one lobe shorter than the two others (Figure 2.1, A, arrows; Figure 2.2). Protoxylem strands are exarch, located at the lobe tips and likely occur at other locations along the sides of the lobes (Figure 2.1, B, arrows; Figure 2.2). This unusual protoxylem location is inferred from the location of smaller tracheids and the presence of irregular zones in the outline of the stele formed by either a group of small tracheids or by an unpreserved central zone surrounded by small tracheids (Figure 2.1, B, arrows; Figure 2.2). If the latter, the unpreserved parts might correspond to parenchyma cells that are less likely to be preserved. The protoxylem tracheids are 10–31 µm wide (n = 50) and the metaxylem is composed of polygonal tracheids 12–92 µm wide (n = 150).

In radial view, the tracheids of the metaxylem bear alternate to opposite, oval to circular bordered pits (Figure 2.1, D), and protoxylem tracheids are recognized based on their helical thickenings (Figure 2.1, D, arrow).

In transversal view, the secondary xylem is up to 5.4 mm wide and forms three growth rings (Figure 2.1, A; note that in HH24, the third ring is only visible in half of the specimen). Ring boundaries (Figure 2.1, A) are mostly recognizable by a layer of deformed tracheids, but well-preserved parts show that they can consist of a single layer of tracheids with highly reduced radial diameter (Figure 2.1, C). The secondary xylem is composed of rays and rectangular to polygonal tracheids 35–90 µm wide radially (n = 150) and 19–94 µm wide tangentially (n = 150). Rays are composed of two types of cells, parenchyma cells (Figure 2.1, C) and ray tracheids (Figure 2.1, C, arrow).

In radial view, the secondary xylem tracheids bear alternate to opposite bordered pits arranged into groups separated by non-pitted areas that are 9–31 µm in height (Figure 2.1, E–F). These groups are composed of 12–22 bordered pits arranged in 3–4 rows for HH10, 9–22 pits in 2–5 rows for HH24, and 8–26 pits in 2–4 rows for HH40 (Figure 2.1, E–F). Pits are circular to oval with an aperture of 4–15 µm in diameter (Figure 2.1, E–F; n = 150). Groups of 4–5 (HH24) and 7–10 (HH40) cross-field pits have been observed in 2 of the 3 specimens (Figure 2.1, G). Rays cells observed in radial view show parenchymatous cells 17–50 µm high (n = 39) (Figure 2.1, H) and up to 233 µm long (n = 32), and tracheids 19–43 µm high (n = 26) and up to 153 µm long (n = 26) (Figure 2.1, H, arrow). These two types of cells seem to be randomly arranged inside the rays. Even

if their height ranges overlap, the parenchyma cells are on average higher than the ray tracheids (Table 1), a tendency that seems to be confirmed by qualitative observations in radial and tangential views (Figure 2.1, I).

In tangential view, rays are uniseriate and from 1 to 30 cells in height (Figure 2.1, I). The distinction between the 2 types of ray cells (i.e., parenchyma or tracheids) is not always clear, so the following measurement includes the two cell types. The ray cells are 13.5–63 µm (n = 150) high and 7–49 µm (n = 150) wide, with ray tracheids having smaller cells with thicker walls.

In some transverse views of HH10 and HH40, layers of tissue external to the secondary xylem are preserved in some parts of the specimens (Figure 2.1, J). These layers seem to be composed of 2 types of cells (Figure 2.1, J), one filled with black contents (22–47 µm wide radially, 26–54 µm wide tangentially, n = 27) and the other appears to have thinner walls than tracheids (9–44 µm wide radially, 17–69 µm wide tangentially, n = 51). These layers are interpreted as a secondary phloem based on the radial alignment of the cells and their direct contact with the secondary xylem.

A vascular trace to a lateral organ can be observed in the wood on sections of HH24. It is emitted at a very acute angle from the main axis with a course almost parallel to it on the available sections (Figure 2.1, K). The primary xylem of this trace is radially elongated, facing the shortest arms of the actinostele, and it seems to possess its own secondary xylem (Figure 2.1, K). At least one exarch protoxylem strand can be identified (Figure 2.1, K), however, based on the same recognition criteria applied to the main axis, there might be more than one protoxylem strand in this trace (up to 4; Figure 2.1, K, arrows). Another putative trace can be seen in HH40.

2.4.2 Stems of *C. seamrogia* sp. nov. (Figure 2.3–2.6)

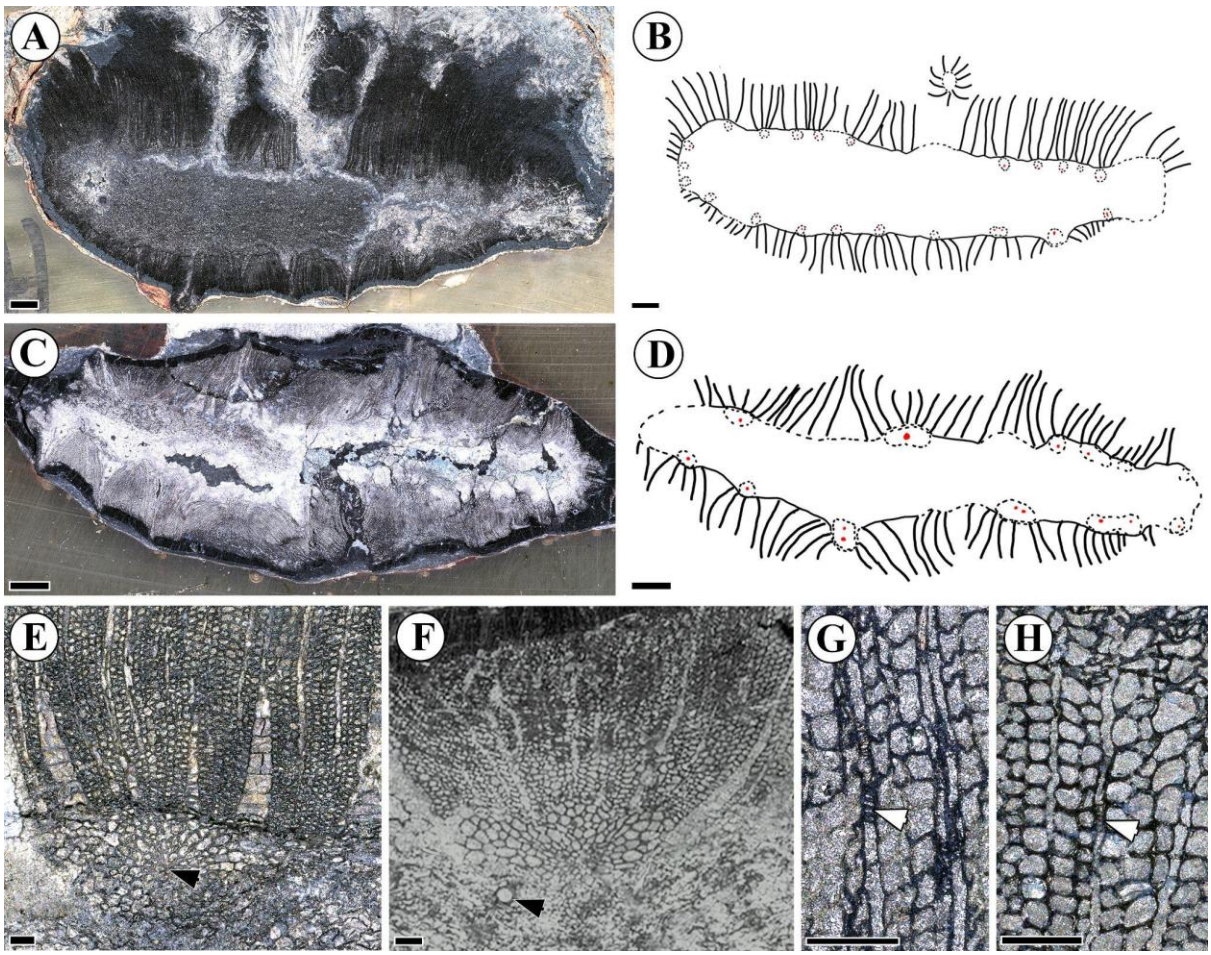

Figure 2.3 Stem anatomy of *Callixylon seamrogia* sp. nov. in transverse section.

(A) General view of specimen HH37; scale bar = 1 mm; slide HH37 S2 sup. (B) Drawing of specimen HH37 (same slide as (A)) illustrating its stele, secondary xylem, primary vascular bundles (small circles in dotted line), and the protoxylem strands (red dots), scale bar = 1 mm. (C) General view of specimen HH45; scale bar = 1 mm; slide HH45 A-4. (D) Drawing of specimen HH45 (same slide as (C)) illustrating the stele, the secondary xylem, primary vascular bundles (small circles in dotted line), and the protoxylem strands (red dots), scale bar = 1 mm. (E) Details of specimen HH37 showing a primary vascular bundle and secondary xylem; arrow pointing to the protoxylem; scale bar = 100 µm; slide H37 I3. (F) Detail of specimen HH45 showing a primary vascular bundle and secondary xylem; arrow pointing to a thick-walled pith cell; scale bar = 100 µm; slide H45 A-4. (G) and (H) Rays of specimens HH37 and HH45 (respectively) showing ray tracheids (arrows); scale bars = 100 µm; slide H37 S2 (G) and slide HH45 A-2 (H).

The two specimens, HH37 and HH45, have a eustele (Figure 2.3, A–D) composed respectively of 22 and 14 mesarch primary vascular bundles (Figure 2.3, E–F) surrounding a poorly preserved parenchymatous central zone. These primary tissues are surrounded by secondary xylem composed of tracheids and rays consisting of parenchyma cells and ray tracheids (Figure 2.3, G–H). Both

specimens are decorticated and their primary tissues and secondary xylem are incompletely preserved.

Specimen HH37 is 5 cm long, 1 cm in width, and possesses a compressed stele at its center that is 16.5 mm in its larger dimension and 3.4 mm in its smaller one.

In transversal view, this specimen has up to 22 preserved primary vascular bundles 0.19–0.43 mm (n = 19) in radial diameter, (Figure 2.3, A–B) made of protoxylem tracheids 7–30 µm wide (n = 50) (Figure 2.3, E, arrow) and polygonal metaxylem tracheids 17–75 µm in diameter (n = 50) (Figure 2.3, E). The primary xylem has a mesarch maturation, and protoxylem strands seem to be composed of tracheids only. In radial view, the protoxylem tracheids bear annular to scalariform pits (Figure 2.4, A, arrow), and the metaxylem tracheids bear scalariform to bordered pits (Figure 2.4, A).

The vascular bundles surround a poorly preserved zone recognized as the pith, containing thin-walled cells 22–101 µm wide (n = 50) with the occasional presence of thicker-walled cells 49–114 µm (n = 20) wide (Figure 2.3, A). Some pith cells can be observed in longitudinal view, specifically the well-preserved ones close to vascular bundles. In this view, pith cells are parenchymatous, arranged in vertical files, and look subrectangular (Figure 2.4, B). They are 23–71 µm (n = 50) high and 23–127 µm (n = 50) wide (Figure 2.4, B). The other type of cells observed in the pith (with thick walls) are mostly circular with a diameter of 19–104 µm (n = 20) in tangential view (Figure 2.4, C).

Toward the periphery of the stele, the bundles are in contact with the secondary xylem (Figure 2.3, E). In transversal view, this tissue forms a layer up to 5.2 mm wide, lacks growth rings (Figure 2.3, A), and is composed of rays (parenchyma or ray tracheids (Figure 2.3, G) and square to polygonal tracheids (Figure 2.3, A, E, G). These tracheids are 11–65 µm (n = 50) in radial diameter, and 13–56 µm (n = 20) in tangential diameter.

In radial view, pits are poorly preserved but the secondary xylem tracheids seem to bear 1–3 rows of opposite bordered pits arranged in groups of 8 to 10 separated by unpitted zones (Figure 2.4, D). These pits possess circular apertures 4–10 µm (n = 50) wide. Cross-field pitting is well preserved and consists of 4 to 6 circular to oval pits (Figure 2.4, E). Rays are 1–17 cells high and are composed of two types of cells in an uneven arrangement (Figure 2.4, G). Parenchyma ray cells are 20–42 µm (mean = 29 µm; n = 20) high and 35–126 µm (mean = 86.1µm, n = 20) wide. Ray tracheids are smaller than the parenchyma cells, with a height of 10–31 µm (mean = 17.9 µm, n = 20), and might be shorter (16–91.5 µm [mean = 44.8 µm, n = 20]) (Figure 2.4, G, arrows). In tangential view, in the oldest wood, some tracheids bear circular pits and the few of the observed rays are uniseriate with cells that are 13–28 µm wide (mean = 20.2 µm, n = 30) (Figure 2.4, F).

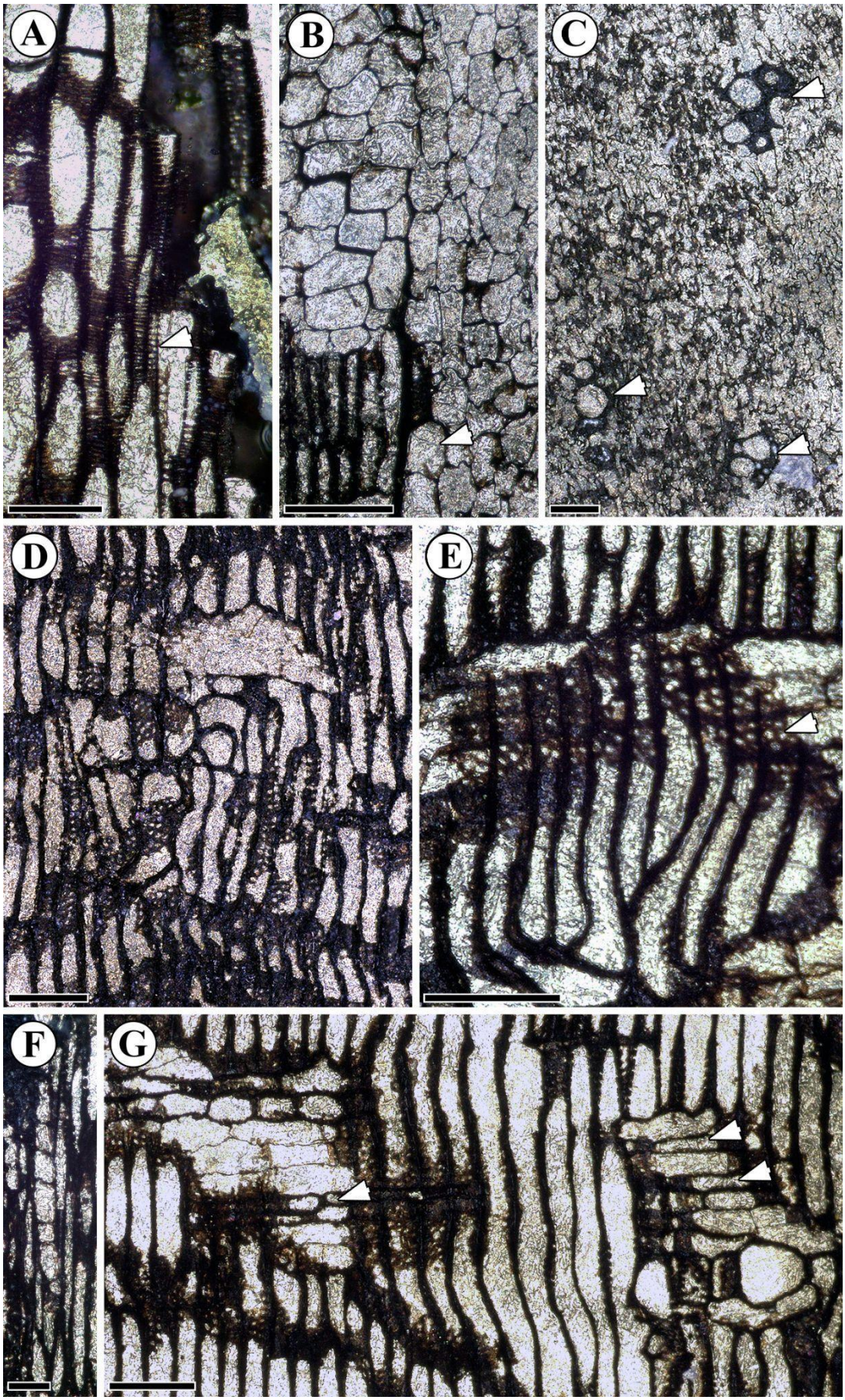
A
B
C
D
E
F
G

Figure 2.4 *Callixylon seamrogia* sp. nov., stem anatomy of specimen HH37 in longitudinal section.

(A) Primary xylem pitting pattern with protoxylem tracheid bearing annular (arrow) to scalariform pits, and metaxylem tracheids bearing scalariform to bordered pits (top right); scale bar = 100 µm; slide HH37 Lg2. (B) Pith parenchyma cells (arrow) close to the secondary xylem, scale bar = 100 µm; slide HH37 Lg1. (C) Pith in tangential view composed of thin-walled cells and three clusters of well-preserved thick-walled cells (arrows); scale bar = 100 µm; slide HH37 Lg1. (D) Detail of the secondary xylem in radial view with poorly preserved pits; scale bar = 100 µm; slide HH37 Lg1. (E) Cross-field pits (arrow); scale bar = 100 µm; slide HH37 Lg2. (F) Uniseriate ray in tangential view, scale bar = 50 µm; slide HH37 Lg2. (G) Rays in radial view showing parenchyma cells and ray tracheids (arrows); scale bar = 100 µm; slide HH37 Lg1.

Specimen HH45 is about 22 cm long, 14 x 6.5 mm in diameter, and its center is a compressed stele that is 14.2 mm in its larger dimension and 2.4 mm in its smaller one (Figure 2.3, C–D). Note that the specimen is not entirely preserved, in the same way as specimen HH37 (i.e., missing the outer layers and part of the stele).

In the transversal view, up to 14 primary vascular bundles (0.23–0.45 mm [n = 10] in diameter when measured radially) are preserved, with some being partially fused (Figure 2.3, F, D). The primary xylem has a mesarch maturation (Figure 2.3, F) and protoxylem strands contain polygonal protoxylem tracheids that are 7.5–35 µm (n = 50) in diameter, with a centrally unpreserved/thin-walled small zone in some strands that can be interpreted as parenchyma.

The metaxylem is composed of polygonal to rectangular tracheids 26–79 µm wide (mean = 42.3 µm, n = 50) (Figure 2.3, F). In radial view, protoxylem tracheids bear an annular to scalariform pitting pattern (Figure 2.5, A), and the metaxylem tracheids bear scalariform to bordered pits (Figure 2.5, B). The presence of protoxylem parenchyma is confirmed by the observation of two protoxylem tracheids surrounding a column of parenchymatous cells that are 72–98 µm high and 18–24 µm wide (n = 6) (Figure 2.5, A, arrow).

In transversal view, the primary vascular bundles are in contact with the secondary xylem and surround a central zone identified as a pith (Figure 2.3, F). This pith is poorly preserved but appears to be composed of two types of cells, one with thick walls and the other with thinner walls. The thinner-walled cells have been measured in longitudinal view, however, the thick-walled ones have only been observed on transversal view. When measured in this view, the thick-walled cells were measured as 25–73 µm (n = 7) wide (Figure 2.3, F, arrow). In radial view, well-preserved pith parenchyma cells are preserved in most peripheral parts and are composed of thin-walled cells 24–141 µm (mean = 60.7 µm; n = 50) high and 19–54 µm (mean = 38.8 µm; n = 50) wide (Figure 2.5, C). These cells are square to rectangular and arranged in vertical columns.

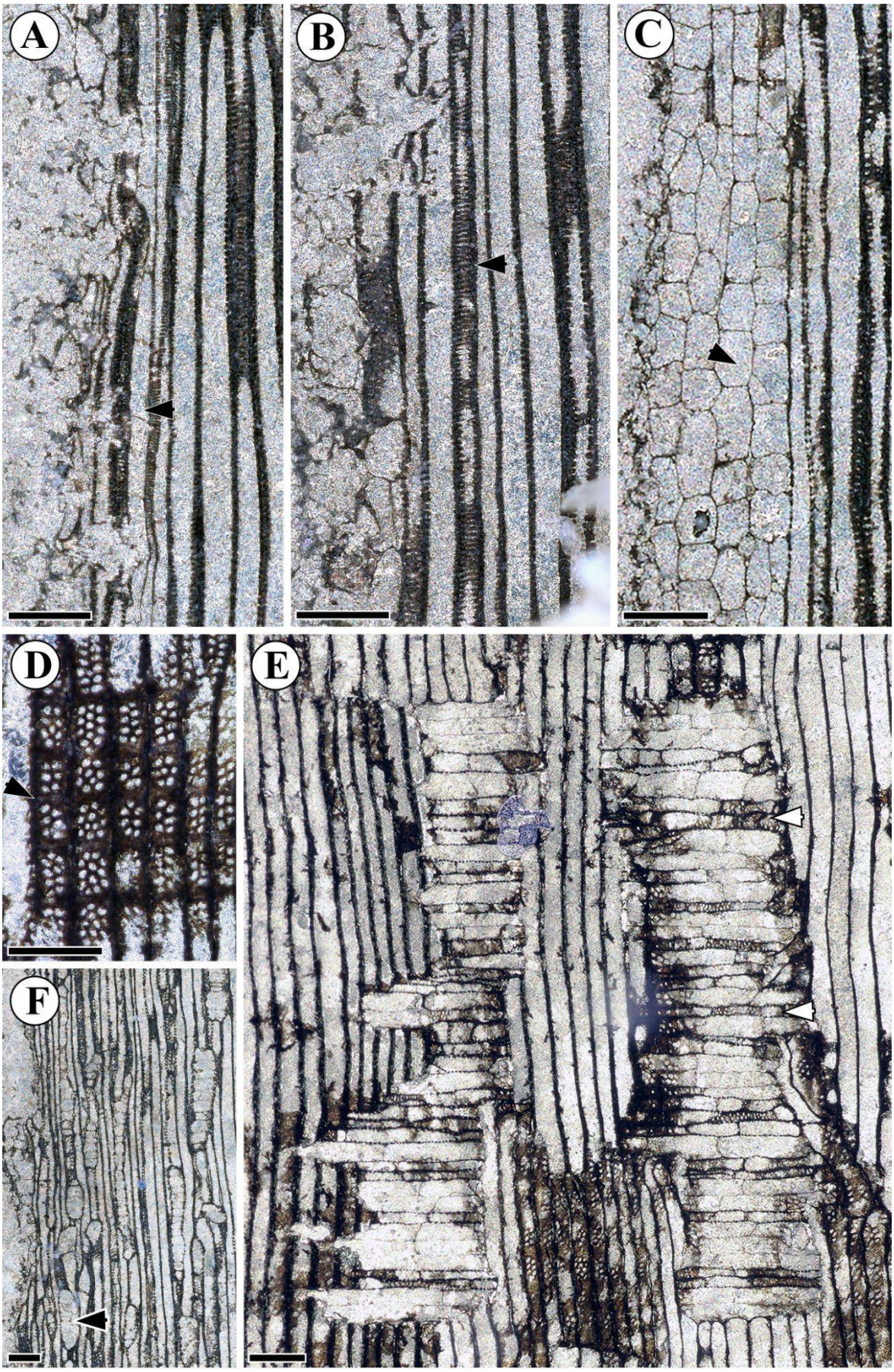
A
B
C
D
E
F

Figure 2.5 *Callixylon seamrogia* sp. nov., stem anatomy of specimen HH45 in longitudinal section.

(A) Primary xylem strand showing a column of protoxylem parenchyma (arrow) surrounded by protoxylem tracheids bearing spiral to scalariform pitting and metaxylem tracheids bearing scalariform to circular pits; scale bar = 100 µm; slide HH45 F Lg2. (B) Metaxylem tracheids with scalariform to bordered pits (arrow); scale bar = 100 µm; slide HH45 F Lg2. (C) Pith parenchyma cells (arrow); scale bar = 100 µm; slide HH45 F Lg2. (D) Detail of the secondary xylem tracheids in radial view with circular bordered pits in groups separated by unpitted areas (arrow); scale bar = 100 µm; slide HH45 F Lg1. (E) Ray in radial view showing parenchyma cells and ray tracheids (two are indicated by arrow); scale bar = 100 µm; slide HH45 F Lg1. (F) Rays in tangential view with one biseriate ray (arrow); scale bar = 100 µm; slide HH45 F Lg1.

In transversal view, a layer of secondary xylem up to 1.9 cm thick and lacking growth rings surrounds the primary vascular tissues (Figure 2.3, C). The secondary xylem is composed of rays with parenchyma cells and ray tracheids (Figure 2.3, H, arrow) and polygonal to square tracheids 12–44 µm radially (mean = 25.6 µm, n = 50) and 13.5–49 µm tangentially (mean = 25.1 µm, n = 50) (Figure 2.3, F, H).

In radial view, the secondary xylem tracheids bear alternate to opposite bordered pits that are approximately circular with apertures 4.5–12.5 µm wide (mean = 8 µm, n = 50) (Figure 2.5, D). These pits are arranged in 2 to 3 rows, forming groups of 8 to 14 pits separated by unpitted zones that are 7.5 to 22 µm long (Figure 2.5, D). The rays are 1–43 cells high (Figure 2.5, E) and composed of parenchyma cells and ray tracheids (Figure 2.5, E, arrows) in an uneven arrangement. The parenchyma cells are 15–55 µm in height (mean = 32.4 µm; n = 50) and 26–251 µm in length (mean = 123.6 µm; n = 50). This is higher than the ray tracheids, which are 8–42 µm in height (mean = 19.9 µm, n = 50) but about the same length as the parenchyma cells (25.5–249 µm, [mean = 119.8 µm, n = 50]).

In tangential view, the rays are mostly uniseriate with few occurrences of rays showing a local biseriation (Figure 2.5, F, arrow). Ray tracheids can be recognized based on their thicker walls and smaller diameters. In the oldest wood, some tracheids bear circular pits and lack unpitted zones (Figure 2.5, F).

In specimen HH37, a vascular trace to a lateral organ has been observed, located away from the primary vascular bundles. The following description of the emission pattern is based on observations of this single trace at different levels (Figure 2.6, A–C).

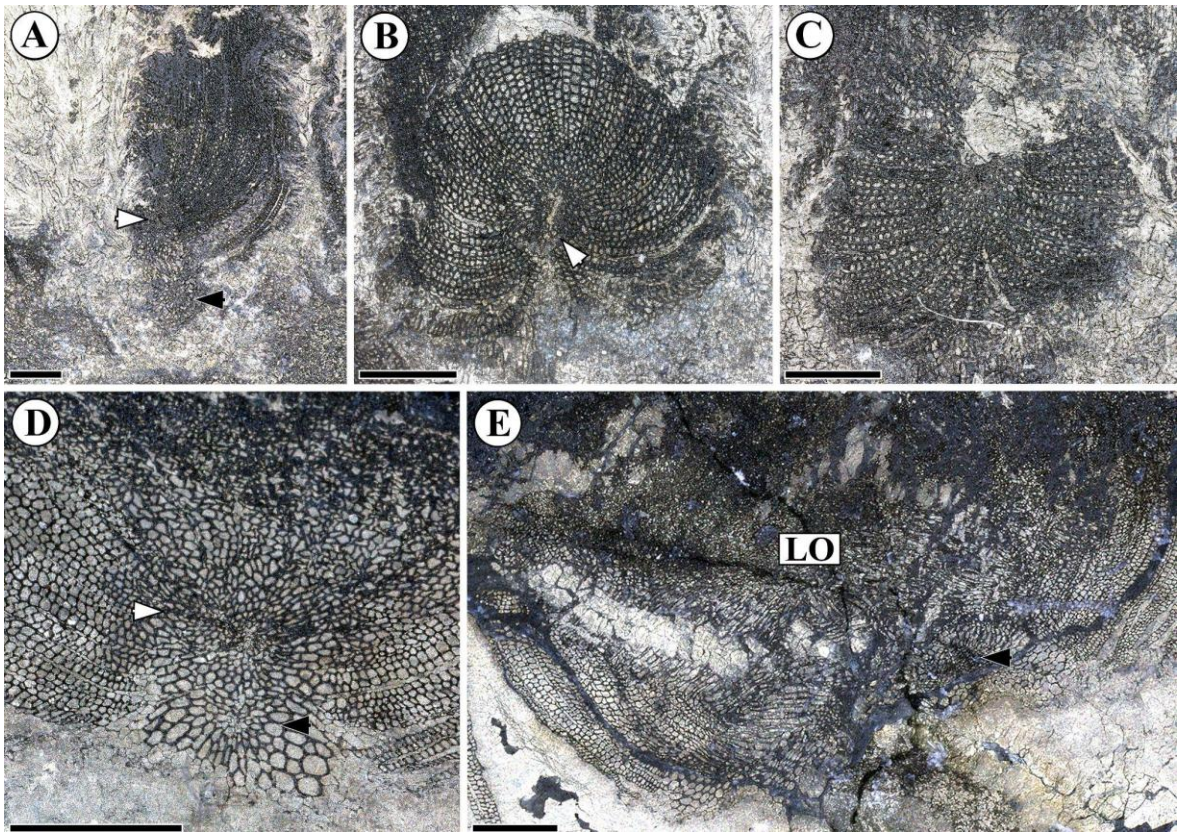

Figure 2.6 *Callixylon seamrogia* sp. nov., lateral organ emission in stems in transverse section.

(A) Earliest observed stage of emission in HH37; white arrow pointing to the vascular trace and black arrow pointing to the vascular bundle of the parental axis; note the radial alignment of the two bundles; scale bar = 500 µm; slide HH37 I2. (B) Vascular trace showing primary xylem in the center (arrow) surrounded by secondary xylem; scale bar = 500 µm; slide HH37 S1. (C) The vascular trace as in (B), but section from a more distal portion; scale bar = 500 µm; slide HH37 S2. (D) Radial division of a primary xylem strand (black arrow) corresponding to an early stage of lateral organ emission (white arrow) in specimen HH45; scale bar = 500 µm; slide HH45 A-4. (E) Stem vascular bundle disturbed (black arrow) by a putative lateral organ emission (LO); scale bar = 500 µm; slide HH45 A-2.

Early stages of emission are poorly preserved. Observation shows that it originates from the radial division of a single stele primary xylem bundle (Figure 2.6, A, bottom arrow), however, the early stage shape of the trace and its protoxylem can not be fully observed.

The preservation is better in the latter stages of the process showing that when the trace becomes free, it is circular and has the same diameter as the stele primary xylem bundle with a single central protoxylem strand (i.e., 450 µm) (Figure 2.6, A, upper arrow). At this stage, the trace has secondary xylem toward its peripheral part that will surround it and seems to reduce in thickness during its radial emission. During this process, the primary xylem of the trace remains mostly circular, with a

slight radial elongation giving it an oval shape (Figure 2.6, B–C). The trace protoxylem strand remains circular and centrally located during all the observed trace emission. The stele primary xylem bundle is devoid of secondary xylem, creating a gap of likely unpreserved parenchymatous tissues between the trace and the parental bundle (Figure 2.3, A–B).

On the observed sections of specimen HH45, there is no trace crossing the wood. However, one seems to be in an early emission stage, with the attached trace appearing as large as the stele primary xylem bundle and slightly larger tangentially than radially (Figure 2.6, D). A central zone in this trace might correspond to a large and tangentially elongated protoxylem strand. In this specimen, divisions and/or fusions of primary vascular bundles around the stele seem to happen based on the close proximity of several pairs of bundles. However, one of them exhibits a different process (Figure 2.6, E). This bundle seems disturbed by an emission based on its split in two with some longitudinal orientation of the cells visible in one of the sections (compare the upper central strand in Figure 2.3, B and Figure 2.6, E).

2.5 Discussion

2.5.1 Comparison with previously described *Callixylon* species

All the specimens described in this study have radial pits on secondary xylem tracheids arranged in groups separated by unpitted zones, a diagnostic feature of the genus *Callixylon* (Zalessky, 1911; Orlova and Jurina, 2011). According to the latest review of the genus (see Table 1 of Tanrattana al., 2018), 20 species of *Callixylon* can be found in the literature, with only nine considered valid by Orlova and Jurina (2011): *C. newberryi* (Dawson, 1871), *C. trifilievii* (Zalessky, 1911; Lemoigne et al., 1983), *C. erianum* (Arnold, 1930), *C. zalesskyi* (Arnold, 1930), *C. whiteanum* (Arnold, 1934), *C. brownii* (Read, 1936), *C. petryi* (Beck, 1953), and *C. arnoldii* (Beck, 1962a). Since this review, a tenth species has been described, *C. wendtii* (Tanrattana et al., 2018).

In their review, Orlova and Jurina (2011) proposed four *Callixylon* groups based solely on secondary xylem characters: the *trifilievii* group, the *erianum* group, the *newberryi* group, and the *arnoldii* group. The new specimens can be assigned to the *erianum* group, which is distinguished by the presence of narrow rays (Orlova and Jurina, 2011; Cornet et al., 2012; Tanrattana et al., 2018) and radial tracheids in the rays (Orlova and Jurina, 2011: p. 584). In addition, the new specimens share almost all of their wood characters, with the only notable differences being the maximum observed ray height between two specimens (17 cells for specimen HH37 and 43 cells

for HH45) and the tracheid diameter (11–60 μm for root specimens and 19–94 μm for stem specimens). However, there seems to be little taxonomic value in the ray maximum heights due to the observed increase of the number of ray cells from the first produced wood toward the periphery in *Callixylon* (Lemoigne et al., 1983; Orlova and Jurina, 2011) and the roots and stems of extant plants also exhibit distinct secondary xylem tracheid diameters (McElrone et al., 2004; Machado et al., 2007).

The numerous similarities in wood anatomy between the five specimens, the fact that they have been found in the same horizon, and the typical combination of the ray tracheids characters, i.e., 1) found in a high quantity, 2) shorter than parenchyma cells in tangential section, and 3) unevenly distributed inside the rays, lead us to include all of them inside a single new species, *C. seamrogia*.

Orlova and Jurina (2011) placed in the following taxa in the erianum group: *Callixylon erianum*, *C. zalesskyi*, *C. petryi*, *C. beckii* (Chitaley and Cai, 2001), and *C. bristolense* (Arnold, 1930), the latter two of which they considered to be synonyms of *C. zalesskyi* and *C. erianum*, respectively. Here, we provide comparisons between the presently described specimens and the above species, in addition to: *C. wendtii* (Tanrattana et al., 2018), *C. velinense* (Marcelle, 1951), *C. schmidtii* (Kräusel and Weyland, 1937), and two specimens described by Meyer-Berthaud and collaborators (2013).

Callixylon zalesskyi, *C. petryi*, *C. beckii*, and specimen MD 600 3/2 of Meyer-Berthaud et al. (2013) have been reported to possess only a few ray tracheids (Orlova and Jurina, 2011; Decombeix and Meyer-Berthaud, 2013). *Callixylon erianum* possess evenly arranged ray tracheids (Arnold, 1930; Meyer-Berthaud et al., 1997), and *C. zalesskyi*, *C. petryi*, and *C. velinense* possess ray tracheids that have the same height in tangential section as their ray tracheids (Arnold, 1930; Marcelle, 1951; Beck, 1953; Decombeix and Meyer-Berthaud, 2013). The combination of ray tracheid characters make *C. seamrogia* different from all the above *Callixylon* species/specimens.

The amount of ray tracheids has been reported as “few” in *C. beckii* by Orlova and Jurina (2011), whereas this species has been reported to have abundant ray tracheids by Tanrattana et al. (2018). Based on the images in the original description by Chitaley and Cai (2001, Plate I Fig. 2, 5, 6–8; Plate II Fig. 4, 5; Plate III Fig. 2), we consider *C. beckii* as a species that is most likely to possess abundant ray tracheids.

Callixylon bristolense possesses secondary xylem tracheids that bear a “vertical pit orifice” as a defining character (Arnold, 1930: p. 21), this is not found in the new species.

Callixylon beckii (Chitaley and Cai, 2001) and *C. wendtii* (Tanrattana et al., 2018) possess ray seriation that are respectively, uni- to partially biseriate with some occurrence of triseriation, and mostly uniseriate with some biseriate and fewer partly triseriate. The ray seriation has been established as an important character for species differentiation in *Callixylon* (Beck, 1953), *C. seamrogia* been close to exclusively uniseriate, *C. beckii* and *C. wendtii* are then different from the new species.

Specimen MD 151 of Meyer-Berthaud et al. (2013) and *C. schmidtii* (Kräusel and Weyland, 1937) have small rays, respectively 1–10 and 1–12 cells high. *Callixylon seamrogia* possess higher rays, however, these two species/specimens can not be differentiated from the Irish species by only this wood character because: 1) HH10 has only slightly higher rays (up to 15 cells), and 2) there is considerable debate about the taxonomic value of this character (Beck, 1953; Lemoigne et al., 1983; Orlova and Jurina, 2011). Nevertheless, MD 151 can be differentiated from *C. seamrogia* based on the number of pits per group (four to five for MD 151 and a minimum of eight for *C. seamrogia*); this is quite distinct given the similar tracheid diameter. According to Lemoigne et al. (1983), *C. schmidtii* possesses biseriate rays. This character and the apparent inconsistency regarding the presence or absence of ray tracheids between Lemoigne et al (1983) and Kraüsel and Weyland (1937) differentiate this species from the new specimens.

In summary, *C. seamrogia* can be differentiated from all the specimens/species previously assigned to *Callixylon* based on wood anatomy.

In addition, the new species can also be distinguished based on features of its primary tissues, except in the cases of *Callixylon schmidtii* and *C. bristolense* that are only based on wood fragments (Kräusel and Weyland, 1937; Arnold, 1940). For the eustelic specimens, most of the species can be differentiated from the stem of *C. seamrogia* sp. nov. based on their pith compositions. *Callixylon beckii* and *C. erianum* possess a homocellular pith, *C. wendtii* possesses sclerotic nests, and *C. zalesskyi* has groups of tracheids in the pith (Tanrattana et al., 2018). Information on the pith of *C. velinence* is lacking (Marcelle, 1951; Tanrattana et al., 2018).

Actinostelic specimens of *Callixylon seamrogia* have an actinostele that is three-lobed with multiple protoxylem strands, whereas all the other species/specimens have an actinostele that is four-lobed with no more than two protoxylem strands at the rib tips (Meyer-Berthaud et al., 2013). Thus, *C. seamrogia* possesses a unique combination of primary and secondary tissue characters in its stems and roots and can be distinguished from all previously described specimens of *Callixylon*.

2.5.2 Position of the new specimens within the whole plant

Archaeopteris/Callixylon has been reconstructed as a tree with multiple orders of branching that are relatively well known and a deep rooting system that is less understood (Beck, 1962b; Meyer-Berthaud and Decombeix, 2009).

For the aerial axes, two authors (Scheckler, 1978; Trivett, 1993) have proposed architectural models of *Archaeopteris/Callixylon* that, among other characters, allow the use of the anatomy of the axes and the trace emission patterns to recognize the axis order and the type of lateral organs that it bears.

Scheckler's (1978) model hypothesized three axis categories: 1) a main axis, 2) penultimate branches, and 3) ultimate branches, plus fertile or vegetative leaves. All axis orders can bear leaves, but the main axis can only bear penultimate branches, and the latter can only bear ultimate branches. The two specimens identified as aerial organs of *Callixylon* in the present study possess a eustele with circular cauline strands and a significant amount of secondary xylem. Using these characters, both can be identified as main axes according to Scheckler's (1978) model. The trace emitted by specimen HH37 is about the same size as the stele primary xylem bundle and it does not seem to have been tangentially elongated. Such characters do not correspond to a leaf trace but more to a branch emission (Scheckler, 1978). Thus, according to Schekler's model, the two new eustelic specimens represent main axes of *Callixylon seamrogia*, with one of them bearing a penultimate branch trace.

In her "Beck's model" Trivett (1993) used the previously described axis categories and added the different growth Types (I to V) that the axes can show. These growth types are mainly defined by the stele diameter, the diameter of the trace that the axis can emit, and the growth types of the lateral organs. In this model, axes showing only Type I growth correspond to ultimate branches that exclusively emit leaves and possess steles with diameters less than 0.5 mm wide.
Axes with Type II growth possess the three phases of growth defined by Eggert (1961): during the early and late phases of growth (i.e., beginning of the epidogenesis, end of the apoxogenesis, respectively), axes are similar to Type I growth in being only able to emit leaves (with larger trace primordia then axes Type I), whereas between these phases of growth, axes with growth Type II emits branches with Type I growth intermixed with leaves. Axes showing growth Type II correspond to penultimate branches with stele diameters between 0.5 and 3 mm.
Type III growth axes are similar to Type II growth, except that they can reach a larger primary xylem diameter (up to 5.75 mm) during which it produces only branches in "*more than two orthostichies*" (Trivett, 1993; p. 306). Axes with Type III growth are also penultimate branches that

experience this type of growth when their steles are 3 to 5.75 mm wide.
The axes showing a Type IV growth correspond to the main axes with an extensive epidogenesis phase of growth, reaching a stele diameter up to 32 mm wide. During their growth, these axes experience Types I, II, and III growth and, once reaching a 6 mm wide stele, start their Type IV growth: emitting laterals with Type II or Type III growth.
Axes with Type V growth are also main axes following the same type of growth as Type IV axes. However, this type of growth implies an epidogenesis leading to a larger stele than the Type IV axes and during which it can emit axes with Type IV growth.
According to "Beck's model" (Trivett, 1993), the type and the diameter of steles shown by the new eustelic specimens reported in the present study correspond to axes experiencing Type IV growth. The diameter of the trace emitted by specimen HH37 is typical of a Type II axis. Based on the two models proposed by Scheckler (1978) and Trivett (1993), the two new eustelic specimens can thus be identified as main axes showing a Type IV growth. One of them bears a penultimate branch trace, corresponding to an axis with a Type II growth.

A later study of *Archaeopteris/Callixylon* architecture described different types of trace emissions that are not included in the previous models (Meyer-Berthaud et al., 2000) and distinguished three different types of vascular trace emissions in a young trunk of *Callixylon erianum*. The main characters to differentiate them are their origin (emitted from the stele or not), their primary anatomy (shape and diameter), the presence/absence of secondary growth, and their emission angle. Meyer-Berthaud et al., (2000) recognized: 1) Type-A branches, which correspond to apically produced short-lived branches; 2) Type-B branches, which seem to be not apical in origin but produce long-lived branches forming the "*...major architectural units of the tree*" (Meyer-Berthaud et al., 2000: p. 467); and 3) Type-H emissions, which have been identified as adventitious traces that can potentially form root primordia.The trace found in the new specimen HH37 shares most of its characters with the Type-A traces of Meyer-Berthaud et al. (2000), i.e., it is emitted from the stele with a radial emission proximally and the presence of secondary xylem. We thus consider that the trace observed in specimen HH37 corresponds to that of an apically emitted short-lived branch.

Regarding the root system, most of the specimens described to date for *Archaeopteris/Callixylon* possess a four-lobed actinostele. The only exception before this study is one lateral root showing a pentagonal protostele (Meyer-Berthaud et al., 2013), making the specimens assigned to *C. seamrogia* the first to possess a three-lobed-actinostele. The architecture of *Callixylon* roots is then less well-known than that of the aerial parts. In *Callixylon*, the four-lobed organization has been found for different root diameters (3.5 to 90 mm). Their steles mostly measured between 0.5 to 1 mm (Beck, 1953; Andrews et al., 1965; Meyer-Berthaud et al., 2013) with one specimen reaching

about 1.6 mm (inferred from Snigirevskaya, 1984: Pl. 2, Fig 1b). The rooting system of the only known specimen of *Eddya sullivanensis* (Beck, 1967) shows, at the same level, multiple steles of different types that will likely represent individual roots at a later growth stage. These roots possess two types of stele, either a three-lobed actinostele (0.4–0.5 mm long) or a two-lobed one (about 0.4 mm wide). Note that the protoxylem placement is unclear (Beck, 1967; TD pers. obs.). If *Eddya sullivanensis* is indeed a young sporophyte of *Callixylon/Archaeopteris*, then *C. seamrogia* is the second taxon of this group showing roots with a three-lobed actinostele. However, the new species have a stele diameter that is much larger than that of other *Callixylon* roots reported to date, with a diameter reaching about 2.3 mm.

In the root systems of extant plants the number of primary xylem lobes has been observed to vary between species, individuals, and even inside the same plant (Li et al., 2022 and references therein). The number of lobes/protoxylem strands in roots is generally higher in lower order axes (Wardlaw, 1928; Biswas et al., 1997; Hishi and Takeda, 2005; Tawa and Takeda, 2015; Li et al., 2022). Because of this variation observed in extant plants and the absence of other stele types in *Callixylon* fossil roots from the locality, nothing can be inferred regarding the location of the new specimens within a complete root system. It is possible that the difference in the number of lobes/ stele diameter between the new specimens and previously reported *Callixylon* roots is specific to the new species.

Insights about the placements of the new isolated roots within the whole archaeopteridalean root system could potentially be provided by comparison with a morphologically preserved root system. Veenma et al. (2023, fig 6) reported a root system in their “lower Sandeel Bay plant bed”, a couple of meters from where the new specimens were collected. They recognized it as likely belonging to an archaeopterid based on its branching type and density. They interpret it as a horizontal root system with vertical rootlets directly attached to the base of the trunk. However, the diameters of both the vertical roots and the largest horizontal rootlets are in the same range as our new specimens, so it remains impossible to infer where in the root system our specimens were positioned.

2.5.3 *Archaeopteris* and *Callixylon* in Ireland

In Ireland, four uppermost Famennian (Upper Devonian) localities are known to contain *Archaeopteris* fossils: Toe Head (Johnson, 1911; Connery, 1999, 2002; Klavins, 1999), Kerry Head (Bridge et al., 1980; Matten et al., 1980; Decombeix et al., 2022a), Hook Peninsula (Sleeman et al., 1983; Matten, 1995; Klavins, 1999; Decombeix et al., 2023), and the most famous one, the Kiltorcan Old Plant Quarry (Forbes, 1853; Johnson, 1911; Jarvis, 1990). Another locality may

exist: Moll's Gap Quarry; however, it has been reported only by Walsh (1968) with no picture, drawing, or even description, the only sentence found in the literature about these fossils is "*...fragmentary plant debris resembling* Archaeopteris hibernica*...*" (Walsh, 1968: p. 13).

From these localities, four species represented by compressions/impressions of vegetative and fertile parts of *Archaeopteris* have been identified: *A. hibernica* (Forbes, 1853; Johnson, 1911; Matten, 1995), *A. tschermakii* (Johnson, 1911), *A. macilenta* (Klavins, 1999), and *A. roemeriana* (Johnson, 1911; Klavins, 1999). However, except for *A. hibernica*, reports are old and mostly provide no detail about taxonomic placement.

Before our recent reinvestigations (Decombeix et al., 2022a, 2023), only three anatomically preserved specimens of *Archaeopteris/Callixylon* had been reported in Ireland (Matten, 1995; Klavins, 1999). They have all been found in localities of the Hook Peninsula and were mentioned in Matten (1995) and in Klavin's (1999) PhD thesis. The first anatomically preserved *Archaeopteris* specimen of Ireland were illustrated in Matten (1995), represented by a single rachis. However, there is no description of this specimens by Matten (1995), and only a short description by Klavins based on Matten's (1995: Fig. 2B) figure because this specimen seems to have been lost (see Klavins, 1999: p. 143). According to Klavins (1999), this specimen is 1.4 mm x 0.6 mm wide, lacks secondary xylem, and is "*...organized as a ridged cylinder surrounding a pith*" (Klavins, 1999: p. 143). A second anatomically preserved specimen of *Archaeopteris* was found in Sandeel Bay by Klavins (1999); this specimen is 9 x 4.8 mm wide, devoid of secondary xylem, may possess leaf traces, and seems to have approximately eight primary xylem bundles surrounding a central pith (Klavins, 1999: p. 143). Finally, a 3 mm wide *Callixylon* wood fragment was also found in Sandeel Bay by Klavins (1999). This specimen has tracheids 35 μm in radial diameter. In radial view, it shows the typical *Callixylon* groups of pits. These groups are composed of 4–17 pits (10 μm in average diameter) arranged in three rows. Only one ray has been observed, its seriation was not determined (but is likely uni- or biseriate) and it seems to be "*...at least sixteen cells high*" (Klavins, 1999: p. 146).

The two *Archaeopteris* specimens in Matten (1995) and Klavins (1999) are devoid of secondary xylem and have a relatively small stele diameter. This combination suggests that they might represent a higher order of branching (i.e., penultimate branches of Scheckler, 1978; Types II or III of Trivett, 1993) than the new specimens described in the present study. The lack of information about the exact ray structure in the piece of *Callixylon* wood described by Klavins prevents its assignment to the new species *Callixylon seamrogia*. Nevertheless, the two specimens previously described by Klavins (1999) were found in the same locality as the new specimens in this study and thus, we can speculate about their possible conspecificity.

2.6 Conclusions

This study describes five new root and stem specimens of *Callixylon* from the upper Famennian of Ireland. All of the specimens share wood characters that are different from previously described *Callixylon* species. One of the most taxonomically important wood characters of these specimens is the presence of ray tracheids that are numerous, unevenly arranged, and shorter than parenchyma cells in tangential section. The roots have a three-lobed actinostele, making them the first specimen of *Callixylon* roots with this type of stele. In addition, these roots are unique within the genus by their large stele diameters and their numerous protoxylem strands surrounding the stele.

The unique combination of wood characters observed in the roots and stems and the unusual stele anatomy of the roots lead to their assignment to a new species, *Callixylon seamrogia*, therefore increasing the known diversity of *Callixylon* in the latest Devonian.

Using the anatomical characteristic of the stems and of the lateral organs that they emitted, the two stems identified as 'main axes' sensu Scheckler (1978) showing a "Type IV growth" sensu Trivett (1993), with one of the two showing a trace that corresponds to a non-persistent branch emitted apically ('Type-A branches' sensu Meyer-Berthaud et al., 2000).

On the other hand, while this study provides new information on the anatomy of *Callixylon* roots, the underground parts of this genus are still too poorly known to propose hypotheses about the order of root axis that the new three-lobed specimens could represent. This study demonstrates the importance of renewed and continued collecting from historical localities. Additional discoveries of permineralized root specimens and root traces in paleosoils will hopefully provide additional information on archaeopteridalean root architecture.

Chapter 3

Same component, different structure, the asymmetrical wood growth of *Cladoxylon*

Under minor revision in International Journal of Plant Sciences in August 2025 as: Durieux, T., Decombeix, A.-L., Harper, C.J. Reconstructing the architecture of *Cladoxylon taeniatum*, an early Carboniferous non-arborescent cladoxylopsid.

Figure, table, section numbers, and citation style have been modified to fit the manuscript's purpose.

3. Reconstructing the architecture of *Cladoxylon taeniatum*, an early Carboniferous non-arborescent cladoxylopsid

3.1 Abstract

Premise of the research. The cladoxylopsids *s.l.* are an extinct group famous for including taxa that formed the first forests during the Middle Devonian. While different growth models have been proposed for the largest cladoxylopsids, similar analyses have never been conducted on smaller representatives of the group. Here, we propose the first architectural reconstruction of a non-arborescent cladoxylopsid, based on *Cladoxylon taeniatum* specimens from the early Carboniferous of France.

Methodology. About 200 thin-sections, wafers and peels corresponding to 53 anatomically preserved specimens of *Cladoxylon* from the Tournaisian Lydiennes Formation were observed to describe their anatomy and traces emission patterns. Variations in stele anatomy within the most common morphotype were also studied using principal component analysis and hierarchical clustering.

Pivotal results. Four stele morphotypes are recognized based on differences in stele shape, diameter (6.5-30 mm), and secondary growth. One morphotype is assigned to *Cladoxylon mirabile* and the three others to *C. taeniatum*. *C. taeniatum* specimens are reconstructed as stems that bore petiole-like organs with dichotomous ultimate appendages. Variations in stele anatomy among the *C. taeniatum* specimens, combined with previous knowledge on cladoxylopsids growth, suggest an apoxogenesis growth and a determinate development of the secondary xylem for these stems. Two hypotheses on the likely architecture of the whole plant are presented.

Conclusion. This study provides the first reconstruction of the development, organotaxis, and possible habit of *Cladoxylon taeniatum*, which advances our understanding of the architecture of non-arborescent cladoxylopsids.

3.2 Introduction

Vascular plants experienced an important radiation during the Devonian, with the successive diversification of several major clades (e.g. Capel et al., 2021) and the evolution of key morpho-

anatomical features such as wood (Gerrienne et al., 2011; Hoffman and Tomescu, 2013), leaves (Hao and Beck, 1993; Hao and Xue, 2013), deep rooting systems (Algeo et al., 1998; Morris et al., 2015), and seeds (Gerrienne et al., 2004). The Devonian is also a period of increased diversity in terms of habit, from small, often creeping, growth forms in the early Devonian towards more three-dimensionally complex plant communities that included trees with various architectures (Meyer-Berthaud and Decombeix, 2009; Meyer-Berthaud et al., 2010) as well as large non-self-supporting, possibly climbing plants (Speck and Rowe, 2003; Xu et al., 2011; Stein et al., 2012).

The first plants to have evolved the tree habit belong to the cladoxylopsids (Boyer, 1995; Stein et al., 2007; Meyer-Berthaud et al., 2010; Giesen and Berry, 2013; Davies et al., 2024), a group of early euphyllophytes phylogenetically related to ferns and sphenopsids (Stein, 1982a; Stein et al., 1984; Stewart and Rothwell, 1993; Kenrick and Crane, 1997; Xue et al., 2010). Taxa assigned to this group are known from the Early Devonian to the early Carboniferous and have been found in Laurussia, Gondwana, as well as in Kazakhstan, and China (Bertrand, 1935; Galtier, 1970; Lemoigne and Iurina, 1983; Stein and Hueber, 1989; Gerrienne, 1992; Berry and Stein, 2000; Soria et al., 2001; Meyer-Berthaud et al., 2007; Xue et al., 2010; Champreux et al., 2020; Chu et al., 2024). In addition to tree-sized species, the cladoxylopsids also included smaller taxa that shared the same general organization.

Within the cladoxylopsid *s.l.*, taxa can be identified based on morphological characters (e.g., organotaxis) but they are primarily identified based on anatomical characters (Berry and Stein, 2000; Cordi and Stein, 2005; Meyer-Berthaud et al., 2007; see Durieux et al., (2021) for a review of these characters and their phylogenetical significance). Genera with an actinostele are included in the iridopteridales and those with a dissected stele are included in the cladoxylopsids *s.s.*. These cladoxylopsids *s.s*. (referred to as "cladoxylopsids" hereafter) are the group that includes all the Devonian arborescent species. Different growth models have been proposed for the largest cladoxylopsids, based on the analysis of anatomically preserved specimens, i.e. *Pietzschia* (Soria and Meyer-Berthaud, 2004; Meyer-Berthaud et al., 2010) and *Xinicaulis* (Xu et al., 2017), and morphologically preserved specimens, i.e. *Pseudosporochnus* (Berry and Fairon-Demaret, 2002) and *Calamophyton* (Giesen and Berry, 2013). Nevertheless, similar analyses have never been conducted on smaller representatives of the group. The only exception is *Cladoxylon taeniatum* (Bertrand, 1935), a small early Carboniferous representative of the cladoxylopsids that has been the subject of a preliminary study conducted by Soria and collaborators (2006). In this study, the authors assigned axes to three ontogenetic stages, and estimated the biomechanical properties of each of them, leading to the conclusion that *Cladoxylon taeniatum* was likely a non-self-supporting plant. However, this preliminary study did not investigate in detail the architecture of the plant

(*sensu* Barthélémy and Caraglio (2007), i.e. including the development). Here we use the extensive collection of *Cladoxylon* fossils found in the Tournaisian (360 - 345 Ma) Lydiennes Formation of the Montagne Noire in southern France to (1) identify the diversity of *Cladoxylon* species present in the formation, (2) reconstruct the development of *C. taeniatum*, as well as the anatomy and organotaxis of its lateral organs, and (3) propose hypotheses on the architecture of this species.

3.3 Materials and Methods

3.3.1 Fossil material

The Lydiennes Formation is a marine formation with an alternation of radiolarian chert and argillites located in southwestern France (Feist et al., 2021). Outcrops of the formation have yielded anatomically preserved fossil plants that represent a high diversity of taxa (Galtier et al., 1988; Decombeix et al., 2020). The beds containing fossil plants are dated from the early Carboniferous (middle Tournaisian, Tn2a-Tn2b) based on conodont biostratigraphy (Galtier et al., 1988; Feist et al., 2021). The studied specimens come from 4 different localities, near St Nazaire de Ladarez, Coumiac, Puech de la Suque, and close to Pic de Bissous.

The study is based on 53 plant axes that had been prepared using classical thin-section and acetate peels techniques (Joy et al., 1956) and preliminary assigned to the genus *Cladoxylon*. We observed a little over 200 slides (including mounted peels, thin-sections, and wafers), as well as and polished sections of specimens, and imaged all significant specimens with a Keyence VX700 digital microscope at UMR AMAP (Montpellier). All the measurements were taken using the ImageJ (https://imagej.nih.gov/ij/) software. Some characters, i.e. the roundness and surface of xylem ribs, were measured on drawings made from photos of the specimens using a Wacom One pen tablet on Adobe Photoshop version 26.2 (San José, CA, USA). This software has also been used to prepare the plates and figures.

All the prepared material and specimens are deposited at UMR AMAP (Montpellier, France) and are part of the Collection de Paléobotanique, Université de Montpellier, France. Accession numbers of the 53 specimens are MN 204–209, MN 223, MN 268, MN 292, MN 400, MN 719, MN 742, MN 751, MN 759, MN 765–766, MN 809, MN 821, MN 832, MN 837, MN 844, MN 852, MN 876, MN 879, MN 902, MN 904–906, MN 910, MN 918, MN 920–927, MN 943, MN 947, MN 950–954, MN 952 bis, MN 958, MN 958 bis, MN 966, MN 969, MN 969 bis, MN 982, and A 168. The preservation of these specimens is variable, and only 32 were kept for detailed

analysis. Twelve showed details of lateral organ emission, and 13 have been used as a basis to propose the architectural hypotheses (Appendix B.1).

3.3.2 Quantitative analysis of stele anatomy and character definition

To clarify the vocabulary used in the study, we use the term “rib” for peripheral vascular bundles possessing a protoxylem strand, primary xylem, primary phloem, and secondary xylem. “Primary rib” refers to the part of these ribs that corresponds to the primary tissue. “Central vascular bundle” is used for stele vascular bundles that are circular, located at the central part of the stele, and devoid of protoxylem strand (see diagrams in Appendix B.2).

We analyzed the variations observed in the anatomy of the stele between specimens with a principal component analysis (PCA) using 12 continuous variables. We used R 4.2.3 version and the packages “FactoMiner” (Lê et al., 2008), “Factoextra” (Kassambara and Mundt, 2017), “corrplot” (Murdoch and Chow, 1996; Friendly, 2002) to run the PCA. We also used hierarchical clustering to recover different clusters based on the distance scores between specimens resulting from the PCA analysis (Appendix B.3). Only 13 specimens were preserved enough to measure all the different characters of the PCA (see Appendix B.1). Note that two specimens (MN 958 and MN 920) have been included twice (N = 15). In these cases, the goal is to have characters measured at different locations along a same axis, allowing us to verify whether the location in the plant influences the results.

In total 12 characters have been measured on the 13 specimens. Two of them are surfaces, corresponding respectively to the total area of the primary xylem and to that of the secondary xylem. Many specimens are devoid of their most peripheral layers of tissues, so instead of total axes diameters we have focused on vascular tissue (stele) diameters, measured from the peripheral end of one rib to another located at the stele opposite end (character 3). All ribs in an outer position and with mesarch protoxylem strands at the peripheral ends were counted as ribs (character 4). Each of the ribs (i.e. including wood) and primary ribs (i.e. only primary tissues) have been measured from their inner end toward their most peripheral end. The shortest and the longest were then selected, giving characters 5 to 8: maximum and minimum rib length, and maximum and minimum primary ribs length. Finally, to include rib shape in the analyses we use roundness ((4A/(pi*major axis²); A = area; major axis = maximum width of the ellipse) and characters 9 to 12 correspond to the maximum roundness and minimum roundness of ribs and of primary ribs.

3.4 Results

All the specimens share characters typical of *Cladoxylon* but they show variations (1) in the organization of their stele, and (2) in the anatomy of secondary order axes and the way they are produced. We describe below all the different morphotypes encountered for these two features.

3.4.1 Stele organization

The 32 best preserved specimens show differences in both qualitative (stele organization) and quantitative (e.g. diameter, number of ribs, amount of secondary xylem) characters of the steles and 4 morphotypes can be recognized (Figures 3.1, 3.2), one of them including most of the specimens (n=28 [see Appendix B.1]).

Stele morphotype 1 (n = 28, Figures 3.1, 3.2A) – These specimens have steles 3.7 to 10.6 mm wide, with 8 to 14 ribs (Figures 3.1A, 3.1B, 3.2A). All possess ribs with a mesarch protoxylem strand at the tip (Figures 3.1A, B, 3.1D –G). They have 0 to 6 central vascular bundles, which can fuse with or be produced by the inner end of the ribs. Ribs can be "U" to "V"-shaped when two of them are fused at the base (Figure 3.1D), or "Y"-shaped when they are fused more or less centrally (Figure 3.1E). In the same way as the central vascular bundles, the ribs may fuse or divide along the axis without a recognizable pattern. Fusion almost always happens with a neighboring rib but one exception has been observed (in MN 920). None of the specimens shows a central anastomosis of their ribs, i.e., two opposite ribs or more fused together forming a vascular structure crossing the center of the stele.

The specimens typically produce secondary xylem surrounding the primary ribs, nevertheless, two of them (MN 918 and MN 926) have (1) ribs lacking secondary xylem (Figure 3.1G) and (2) ribs with secondary xylem only on one side (Figure 3.1F). There is also a variation in the amount of secondary xylem between specimens, from the two specimens partially lacking secondary xylem towards others with a high amount of secondary xylem all around the ribs, with more growth toward the inner part of the stele (e.g. in Figure 3.1B).

Measurements were conducted on 6 specimens including the largest (MN 268, Figure 3.1B), the smallest (MN 958 bis, Figure 3.1A), and 4 medium-sized ones (MN 204, MN 223, MN 765, MN 876). Protoxylem strands are made of parenchyma cells (10–80 µm, n = 270) at the center surrounded by protoxylem tracheids (10–45 µm, n = 300) (Figures 3.1A, 3.1B, 3.1D–1G). Some longitudinal sections show that parenchyma cells (Figure 3.1H PxP) can be intermixed with protoxylem tracheids (Figure 3.1H arrow), a pattern also observed in transverse sections.

In longitudinal sections, protoxylem tracheids have helical thickenings (Figures 3.1H arrow, 3.1J arrows), parenchyma cells are of various sizes (10–115 µm high, n = 90) and shapes, and their apparent organization in vertical files are only seen in some parts of the strands.
Metaxylem tracheids are polygonal with rounded corners (25–90 µm wide, n = 300) in transverse sections, and bear scalariform to oval pits on their walls (Figures 3.1H, 3.1J).
Secondary xylem tracheids are rectangular to square with rounded corners; they form layers of 2 to 20 tracheids that are 10–70 µm wide tangentially (n = 300) and 10–80 wide radially (n = 300) (Figures 3.1A, 3.1B, 3.1D –1G). Rare putative anticlinal divisions in the secondary xylem can be seen in specimens with a high amount of secondary growth (i.e., MN 268, MN 958). Tracheid pitting consists of multiseriate circular to oval pits with an opposite arrangement (Figures 3.1H, 3.1K). Pitting is not present on the tangential walls (Figure 3.1K). Rays are uniseriate and up to 3 cells high (Figure 3.1K). Ray cells are 7–30 µm wide (n = 170) and 15–110 µm high (n = 70) (Figure 3.1K). No cross-field pitting was observed (Figure 3.1L).
A thin layer of non-aligned elliptical cells (10–40 µm wide, n = 70) surrounds each rib (Figure 3.1C). This layer is in most specimens made of compressed cells or not preserved. Based on its position, the lack of radial alignment of the cells, and the absence of rays, this layer has been identified as the primary phloem (Figure 3.1C Ph).
In two specimens (MN 204 and MN 268) there is a one-cell thick layer surrounding the primary phloem (Figure 3.1C En), composed of thick-walled polygonal cells with a wider diameter parallel to the rib's outline (20–90 µm tangentially, 15–40 µm radially; n = 35). This layer may correspond to the endodermis.
There are two to three cortical layers surrounding these tissues. The differences between them are especially challenging to see in transverse sections (Figures 3.1A, 3.1B). In longitudinal section, an innermost cortical layer surrounds each of the ribs. It is composed of parenchymatous cells that are rectangular, 5–170 µm wide (n= 300) and 30–360 µm high (n = 170), and organized in vertical files (Figure 3.1I iC). Surrounding it, two cortical layers have been identified, starting from wide and elongated cells forming the middle cortex toward narrower cells (some also maybe longer) forming the outer cortex (15–190 µm wide, n = 280; 52–1400 µm high, n = 90), which are interpreted as collenchyma (Figure 3.1I).

The 28 specimens included in this stele morphotype can hardly be differentiated from each other based on qualitative anatomical characters but some variations can be seen inside the sample. To test whether our specimens represent a morpho-anatomical gradient or if distinct groups can be identified, we ran a PCA analysis coupled with a hierarchical clustering on 12 continuous characters measured on 13 of the specimens (see Appendix B.1).

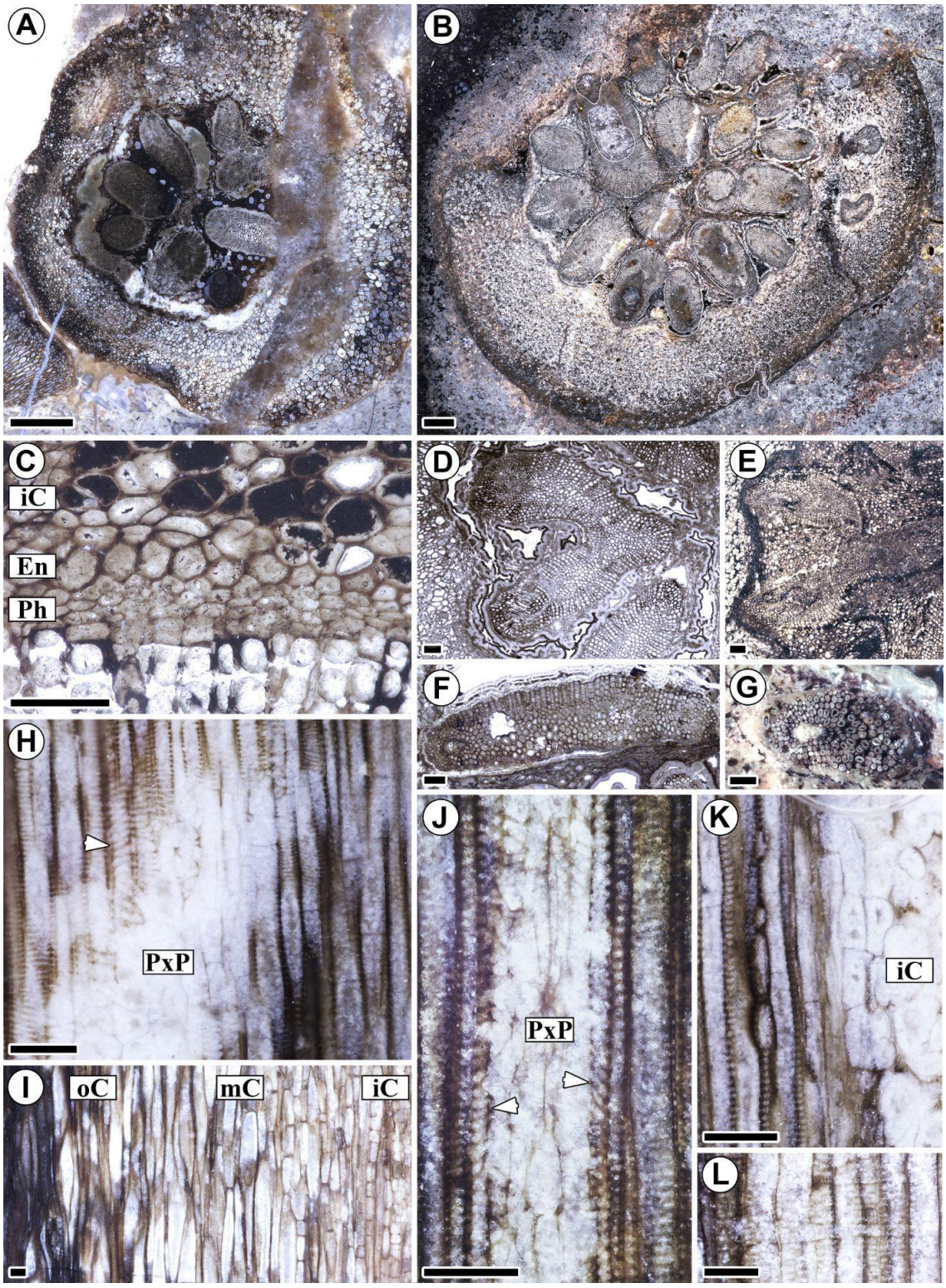

Figure 3.1 Stele morphotype 1 specimens, overview, and anatomical details.

(A) General view of the smallest specimen belonging to stele morphotype 1; scale bar = 1 mm; wafer MN 958bis 12 C. (B) General view of the largest specimens belonging to stele morphotype 1; scale bar = 1 mm; wafer MN 268 AS 1. (C) Details of the tissues surrounding the secondary xylem in transversal view: the primary phloem (Ph), the endodermis (En), and the inner cortex (iC); scale bar = 100 µm; slide MN 204 CS

1. (D) “U”-shaped ribs: scale bar = 200 µm; slide MN 223 AS 01. (E) “Y”-shaped ribs; scale bar = 200 µm; slide MN 953 B sup. (F) Rib with secondary xylem only on one side; scale bar = 200 µm; slide MN 926 AT 01. (G) Rib lacking secondary xylem; scale bar = 200 µm; slide MN 918 A3 I3. (H) Protoxylem strand in longitudinal view showing parenchyma cells (PxP) adjacent to tracheids; arrow pointing at a protoxylem tracheid with a helical thickening; scale bar = 100 µm; slide MN 765 CL2. (I) Three cortical layers in longitudinal view; inner cortex (iC), middle cortex (mC), and outer cortex (oC); scale bar = 100 µm; slide MN 876 AL2. (J) Protoxylem strand in longitudinal view with protoxylem parenchyma (PxP) surrounded by protoxylem tracheids showing a helical thickening (arrows); scale bar = 100 µm; slide MN 876 AL2. (K) Secondary xylem ray and inner cortex (iC) in tangential view; scale bar = 100 µm; slide MN 765 CL3. (L) Secondary xylem ray in radial view; scale bar = 100 µm; slide MN 876.

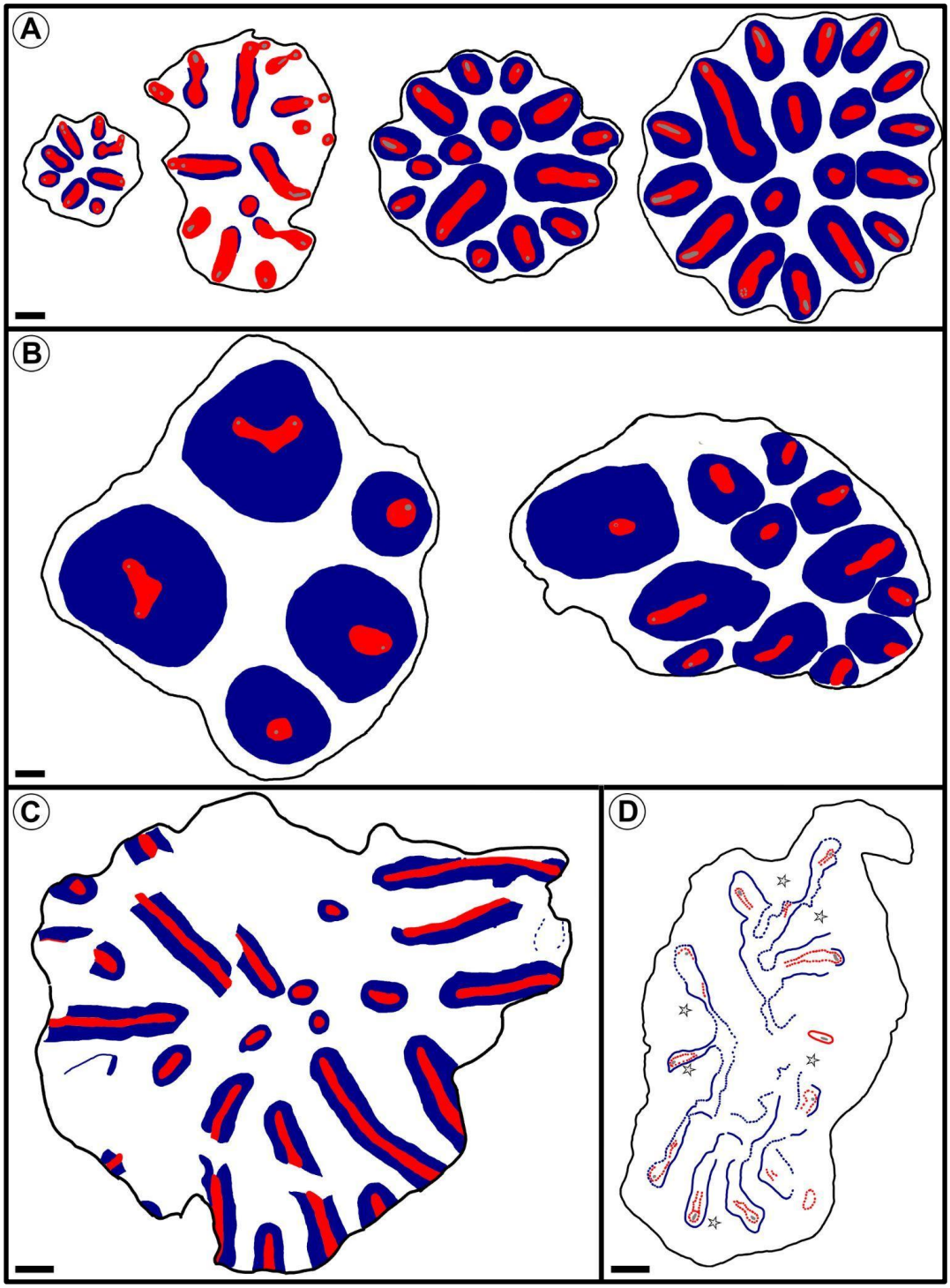

Figure 3.2 Drawing of the different stele morphotypes in transversal view with protoxylem (in grey), primary xylem (in red), secondary xylem (in blue), and stele/specimens limites (in black).

(A) Drawing of stele morphotype 1 specimens; specimens belonging to clusters 1, 2, 3, and 4 of the hierarchical clustering (left to right); scale bar = 1 mm; draws from wafer MN 958bis 12 C, slide MN 918 A3 I3, slide MN 282 B, wafer MN 2969 AS1. (B) Drawing of stele morphotype 2 specimens; scale bar = 1 mm; draws from slide MN 400 DS 2, slide MN 904 D2S1. (C) Drawing of stele morphotype 3 specimen; scale bar = 2 mm; draws from slide MN 921 BT 01. (D) Drawing of stele morphotype 4 specimen with sclerenchymatous tissues represented by white stars; scale bar = 2 mm; draws from slide MN 719.

The first 3 axes of the PCA represent 89.32 % of the total inertia (axis 1: 57.28%; axis 2: 21.97%, axis 3: 10.07%; Appendix A4). The first axis mainly represents characters influenced by the size of the stele (i.e., diameter, number of ribs, ribs and primary ribs length, metaxylem surface, secondary xylem surface) as well as the roundness of the primary ribs (Figures 3.3D, 3.3E). The second axis includes more shape-related characters, i.e., maximum and minimum ribs roundness and the amount of secondary xylem (Figures 3.3D, 3.3F). The third axis is predominantly represented by the maximum roundness of the primary ribs (Figures 3.3E, 3.3F), a character that is independent of secondary growth. Among the chosen characters, there is a positive correlation between the number of ribs, the minimum and maximum length of the primary ribs, and the amount of primary xylem (Figure 3.3D). In addition, the diameter seems to be also positively correlated with the amount of secondary xylem. There is also a positive correlation between the diameter, the number of ribs, and the primary xylem surfaces (Figure 3.3E). Finally, we can also see a positive correlation between the surface of the secondary xylem and the minimal roundness of the ribs (Figure 3.3F).

Using the PCA graph of the specimens (Figures 3.3A), we can see that the first 2 dimensions seem to split the sample into at least 3 groups, one made of only one specimen (MN 268) and the two others made of respectively 6 and 8 specimens. Nevertheless, in plotting axis 1 with axis 3 (Figures 3.3B) and axis 2 with axis 3 (Figures 3.3C), these groups are more overlapping, even if some specimens seem to be isolated. To clarify these grouping patterns, we applied a hierarchical clustering method to our PCA result, in order to group specimens with the most similar steles.

The result of this clustering recovers 4 clusters: cluster 1 includes 2 specimens (MN 958 and MN 958 bis), cluster 2 includes 6 specimens (MN 876, MN 204, MN 918, MN 223, MN 926, MN 920), cluster 3 includes 4 specimens (MN 206, MN 292, MN 844, MN 925), and cluster 4 includes only

MN 268 (Figures 3.3A). Note that specimens that have been measured twice in different locations (i.e., MN 920 and MN 958) are recovered in the same clusters and as the most similar individuals (Appendix B.5).

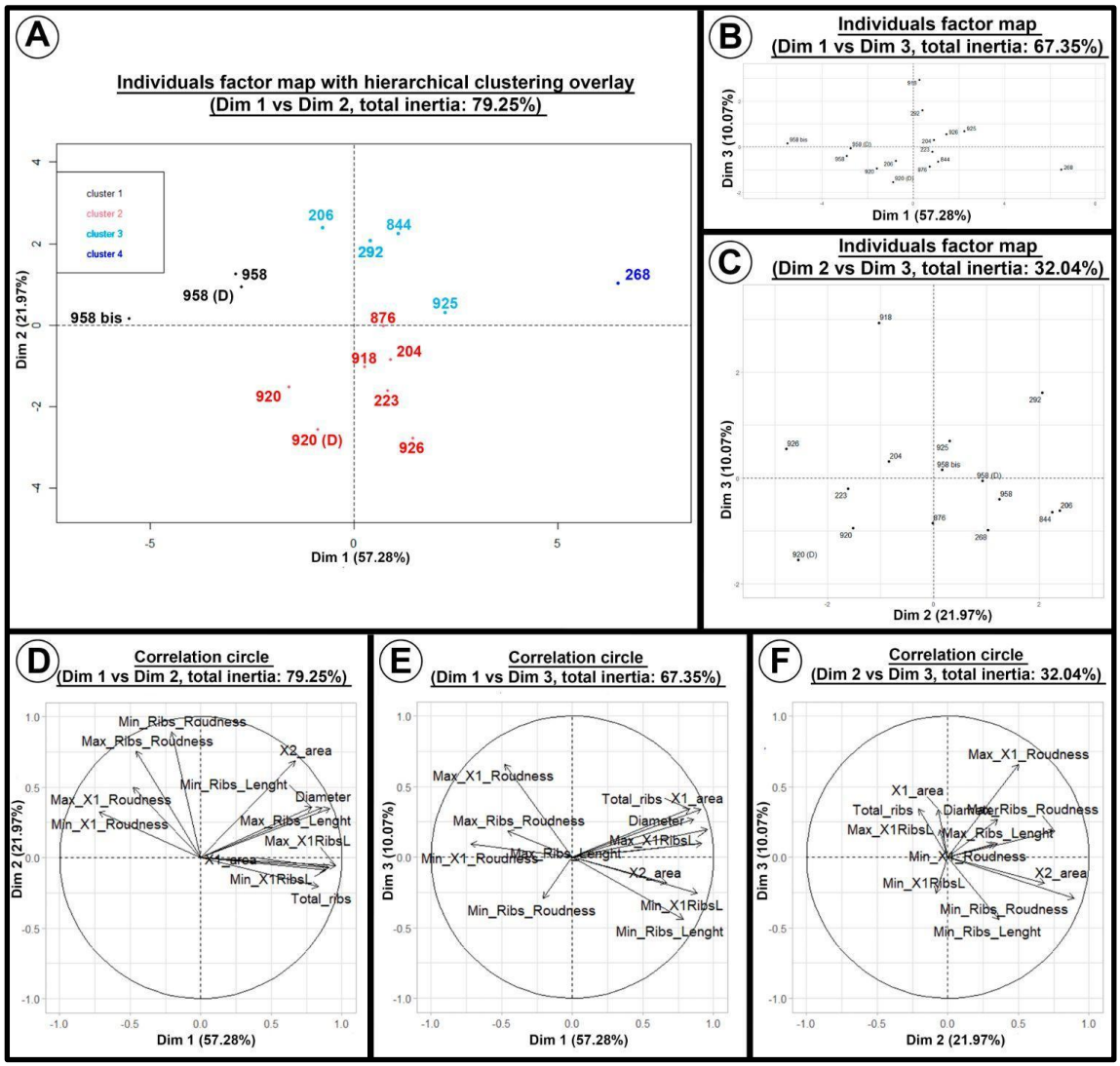

Figure 3.3 Graphical representation of the principal component analysis (PCA) and hierarchical clustering results of stele morphotype 1 specimens.

(A) Individual factor map (dimensions 1 vs 2) with resulting clusters overlay. (B) and (C) individual factor map of dimensions 1 vs 3 and dimension 1 vs 3. (D), (E) and (F) correlation circles of dimensions 1 vs 2, dimensions 1 vs 3, and dimension 1 vs 3.

Stele morphotype 2: MN 400 and MN 904 (Figures 3.2B, 3.4, 3.5A) – Stele morphotype 2 differs from the other stele morphotypes by its secondary tissues, with a high amount of secondary xylem as well as the presence of a well-developed periderm. MN 400 is 14.1 mm in diameter (Figures 3.4A, 3.2B left drawing). Its stele is composed of 7 ribs. Four of them form two "U"-shaped primary ribs resulting from the fusions of 2 ribs by their internal ends (Figure 3.4B). The 3 remaining primary ribs are more or less circular (Figure 3.4C). The amount of secondary xylem gives a circular shape to all the ribs (Figure 3.4A). MN 400 does not possess central vascular bundles, and all the primary ribs possess a mesarch protoxylem strand at their tips (Figures 3.4A–D).

Protoxylem strands are circular and contain poorly preserved large thin-walled cells (or lacunae when the cells are not preserved) surrounded by small tracheids. This corresponds to protoxylem parenchyma cells (10–30 µm wide, n = 21) surrounded by protoxylem tracheids (10–30 µm wide, n = 50) (Figure 3.4D). In longitudinal sections, these tracheids have helical thickenings (Figure 3.4H arrow) and parenchyma cells are poorly preserved but seem to be of various shapes and sizes (Figure 3.4H). Metaxylem tracheids are 20–110 µm wide (n = 49) and are polygonal in shape with rounded corners. In the longitudinal section, these tracheids seem to be mostly scalariform pitted (Figure 3.4H).

The secondary xylem surrounds the primary ribs and is more developed towards the center of the stele (Figure 3.4A). The secondary xylem is up to 40 cells thick. Tracheids are square to rectangular, 20–60 µm wide radially (n = 50) and 15–90 µm wide tangentially (n = 50). Tracheid files are separated by narrow rays (Figures 3.4B–C). Some putative anticlinal divisions in the secondary xylem can be seen and there is no obvious increase in the tangential diameter of the tracheids radially (Figures 3.4A–C). In radial sections, the tracheids have scalariform to multiseriate circular/oval border pits with an opposite arrangement (Figures 3.4I, 4K–L). One 3-cell high ray has been observed (Figure 3.4K) but the preservation does not allow us to see the cross-field pitting. In the tangential section, the rays are uniseriate, and ray cells are 15–40 µm wide (n = 20) and 30–90 µm high (n = 20) (Figure 3.4J).

A layer of thin-walled cells surrounds the secondary xylem. They are 25–105 µm wide (n = 50) and seem to be larger centripetally (Figures 3.4E Ph, 3.4F arrow). Their shape varies from circular to oval with many deformations likely due to secondary growth. In longitudinal sections, these cells are large and elongated (320–640 µm high (n = 5)) (Figures 3.4K, 3.4L, arrows). Based on the position and the characteristics of these cells, the tissue is interpreted as the primary phloem.
In some transverse sections, another layer surrounds the phloem. It is one cell thick and composed of rectangular cells (30–60 µm wide radially and 65–140 µm wide tangentially, n = 31), which may

correspond to an endodermal layer (Figure 3.4E arrow).
A poorly preserved area of compressed cells surrounds the ribs (Figures 3.4A, 3.4F). In longitudinal sections, cells seem to form files of rectangular to square cells of various sizes (25–70 µm high, 35–95 µm wide, n = 50) (Figures 3.4L iC, 3.4M). Based on the cell type and its position inside the stele, this tissue is interpreted as the inner cortex made of parenchyma cells.

Peripherally, the stele is surrounded by a layer of square and radially aligned cells (10–35 µm wide, n = 50) and, more radially, cells of similar size and shape are full of a dark content (Figure 3.4F Pe). In longitudinal sections, these cells are also square and arranged in vertical files (Figure 3.4M Pe). This layer of cells corresponds to parenchymatous cells interpreted as a periderm. In some specimen parts, the last tissue type has been found beyond the periderm. It is composed of poorly preserved cells of various sizes and shapes (30–140 µm, n = 50), and interpreted as a remain of the cortex (Figure 3.4G arrows).

The second specimen assigned to morphotype 2, MN 904 (Figures 3.2B, 3.5A), shares many characteristics with MN 400, i.e. its large amount of secondary xylem, a similar diameter (13.6 mm), the circular outline of some primary ribs, circular protoxylem strands, and a periderm forming the most peripheral layer of the specimen. Nevertheless, MN 904 has more ribs (11) and a central vascular bundle (Figure 3.5A). One of its ribs has secondary xylem in a higher amount toward the outside than toward the inside of the axis.

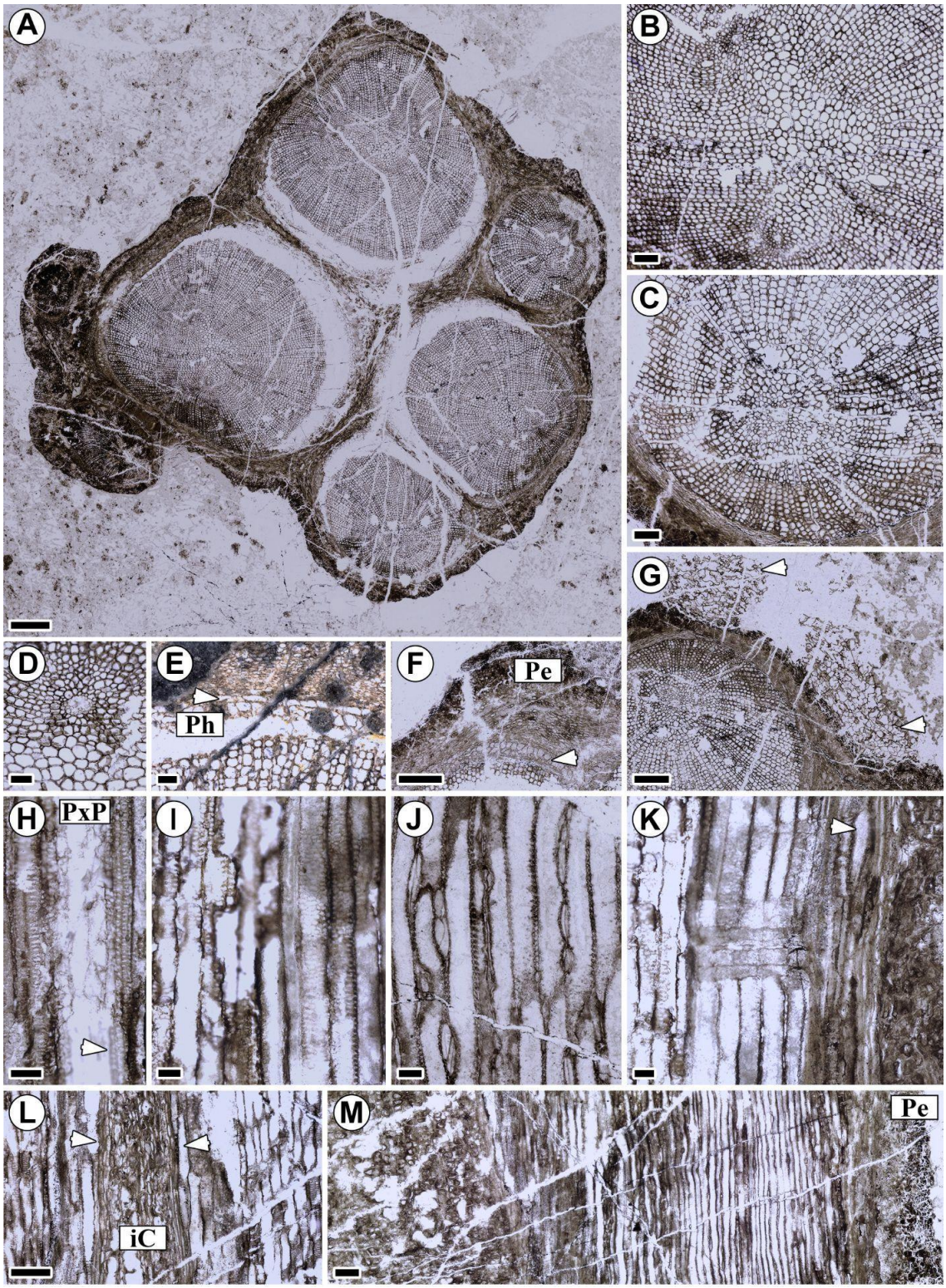

Figure 3.4 Stele morphotype 2 specimens, overview, and anatomical details.

(A) General view of specimen MN 400 with traces attached; scale bar = 1 mm; slide MN 400 DS 01. (B) "U"-shaped ribs; scale bar = 200 µm; slide MN 400 DS 01. (C) Circular rib; scale bar = 200 µm; slide MN 400 AS 01. (D) Detail of a mesarch protoxylem strand showing central parenchyma surrounded by

protoxylem tracheids; scale bar = 100 µm; slide MN 400 AS 02. (E) Details of the tissues surrounding the secondary xylem in transversal view: the primary phloem (Ph), the endodermis (arrow), and the inner cortex; scale bar = 100 µm; polished surface of MN 400 part A. (F) Outermost layers of MN 400 showing large putative phloem cells (arrow), inner cortex, and periderm (Pe); scale bar = 500 µm; slide MN 400 AS 02. (G) Remain of cortical layers (arrows) push by the periderm growth; scale bar = 500 µm; slide MN 400 AS 02. (H) Protoxylem strand in longitudinal view with protoxylem parenchyma (PxP) surrounded by protoxylem tracheids showing a helical thickening (arrow); scale bar = 50 µm; slide MN 400 DL 17. (I) Secondary xylem tracheids in radial view with scalariform to multiseriate circular/oval border pits with an opposite arrangement; scale bar = 50 µm; slide MN 400 DL 15. (J) Secondary xylem rays in tangential view; scale bar = 50 µm; slide MN 400 DL 5. (K) Secondary xylem rays in radial view with putative phloem cell (arrow); scale bar = 50 µm; slide MN 400 DL 5. (L) Longitudinal view of the edges of two ribs separated by the inner cortex (iC) surrounded by large putative phloem cells (arrows); scale bar = 200 µm; slide MN 400 DL 15. (M) Overview of the inner cortex, primary(?) and secondary xylem, and periderm (Pe) in longitudinal view; scale bar = 200 µm; slide MN 400 DL 7.

Stele morphotype 3: MN 921 (Figures 3.2C, 3.5B, 3.5C) – Stele morphotype 3 differs from the other stele morphotypes by its diameter, which is close to 3 times bigger than the biggest specimens assigned to stele morphotype 1, even though the most peripheral part of the stele is lacking. However, the other observed characters are highly similar to those of stele morphotype 1.

MN 921 is the only specimen belonging to this stele morphotype. It is the largest specimen of the sample (29.2 mm) and has the highest number of ribs (16) and central vascular bundles (up to six) (Figures 3.2C, 3.5B). Unfortunately, the specimen's peripheral parts are not preserved, preventing us from observing the tips of the ribs. Its total diameter and information on its protoxylem strands are thus not available. Nevertheless, the central part of the stele is well preserved.

The ribs and the central vascular bundles are composed of metaxylem surrounded by secondary xylem (Figures 3.5B, 3.5C). Metaxylem tracheids are 40–130 µm wide (n = 50) and are polygonal in shape. The secondary xylem is formed by square to rectangular tracheids between 35–80 µm wide radially (n = 53), and 30–80 µm wide tangentially (n = 53). These radial files are separated by narrow rays, and one anticlinal division has been observed.

A layer (mostly always one cell thick) of thick-walled rectangular cells surrounds each of the ribs and central vascular bundles (Figures 3.5B, 3.5C arrow). It can be directly in contact with the secondary xylem or can be separated from it by a non-preserved tissue that may correspond to a phloem layer. These cells are from 25–80 µm wide radially (n = 50), 35–85 µm wide tangentially (n = 50), and are interpreted as an endodermal layer. Surrounding it, is a tissue made of thick-walled cells highly variable in width (30–190 µm, n = 50; Figure 3.5B), which may correspond to the inner part of the cortex. Unfortunately, the outer part of the specimen is not preserved.

The preservation on the specimen's longitudinal section is poor, so the primary xylem has not been recognized. However, a tangential section shows that the secondary xylem is made of tracheids bearing scalariform to circular pits and uniseriate rays with cells 26–47 µm wide and 19–31 µm high (n = 10). In this view, the putative endodermal layer is also recognized based on its thick wall and its location in between the secondary xylem tracheids and parenchymatous tissue. The latter corresponds to the inner cortex with cells 25–117 µm wide and 29–296 µm high (n = 40) organized in vertical files.

Stele morphotype 4: MN 719 (Figures 3.2D, 3.5D-F) – Stele morphotype 4 can is distinguished from the other three morphotypes by the central anastomosis of its ribs, as well as the presence of sclerenchymatous tissue between its ribs. MN 719 is the only specimen belonging to this stele morphotype. It is the second largest specimen of the sample (22.5 mm wide) and has 11 ribs (Figures 3.2D, 3.5D). It is a poorly preserved specimen, but it shows some unique anatomical features. First, it has long ribs that anastomose at the center of the stele giving them a "V"-shaped outline. Second, there is a patch of sclerenchymatous tissue between the ribs, (Figures 3.2D stars, 3.5E arrow). Primary ribs are made of metaxylem tracheids and mesarch protoxylem strands at their tips (Figure 3.5F).
Metaxylem tracheids are 20–50 µm (n = 50) in diameter and the poor preservation of the specimen does not allow us to recognize if the protoxylem strands originally had parenchyma cells surrounded by protoxylem tracheids or have lacunae. Nevertheless, despite its poor preservation, the protoxylem strand seems more elliptical than the round protoxylem of the specimens MN 400 and MN 904.

The secondary xylem is well preserved in some parts of the specimen, and it is made of more or less square tracheids 15–45 µm wide (n = 50). These tracheid files are separated by narrow rays (not observed in longitudinal section) (Figure 3.5F).

The ground tissue proximal to the ribs is highly degraded (likely the inner cortical part), but in the most peripheral part of the specimen, we can see well-preserved cells circular in outline, 20–71 µm wide, which may represent an outer/middle cortex.
Based on the small part where cells are preserved on the longitudinal section, the secondary xylem has pitted tracheids, and the innermost cortex is made of large parenchymatous cells arranged in vertical files. Scalariform pitting has also been observed inside the specimen, however, because of the poor preservation, we cannot conclude on the primary or secondary origin of these tracheids.

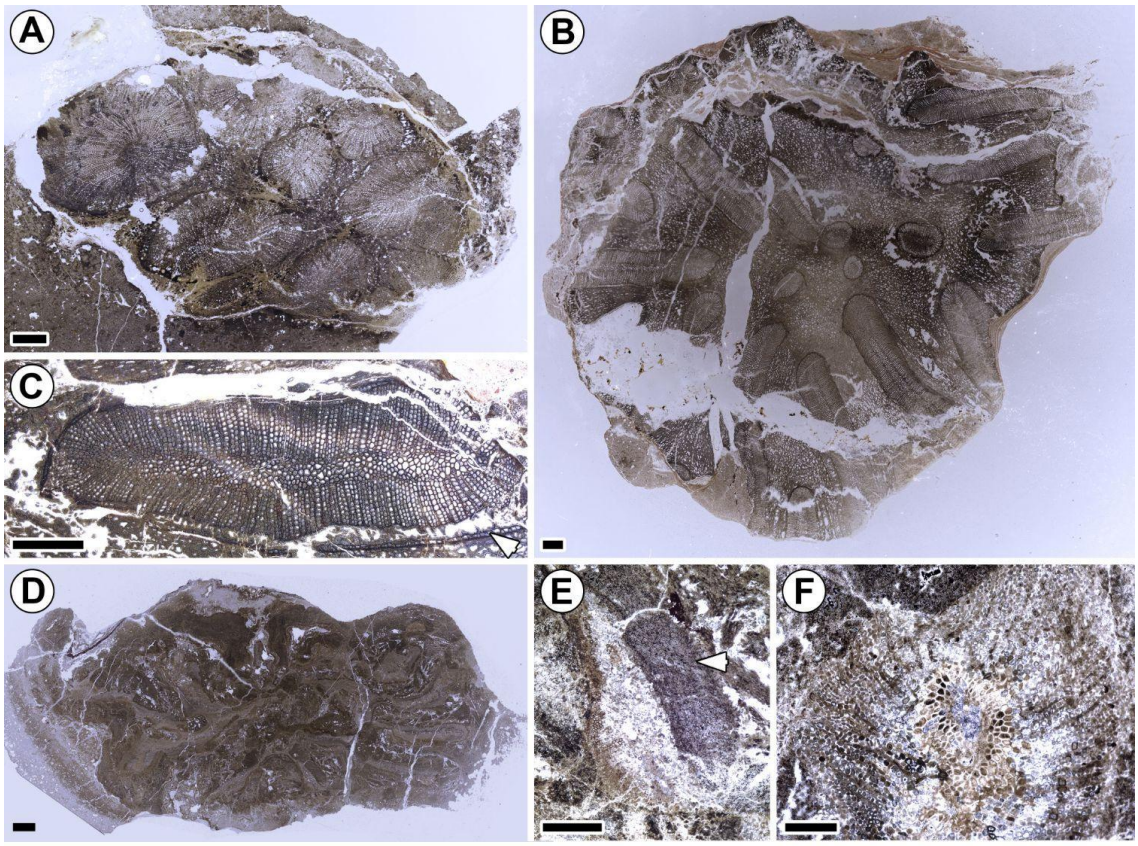

Figure 3.5 Overview of stele morphotypes 2, 3, and 4.

(A) Stele morphotypes 2 (second specimen) overview; scale bar = 1 mm; slide MN 904 D2S1. (B) Stele morphotypes 3 overview; scale bar = 1 mm; slide MN 921 BT 01. (C) Details of an elongated central vascular bundle of the stele morphotype 3 specimen; arrow pointing at the endodermis; scale bar = 1 mm; slide MN 921 AT 01. (D) Stele morphotypes 4 specimen overview; scale bar = 1 mm; slide MN 719. (E) Detail of sclerenchymatous tissues (arrow) located between ribs of stele morphotype 4; scale bar = 500 µm; slide MN 719. (F) Protoxylem strand at the tips of stele morphotype 4 specimen rib; scale bar = 200 µm; slide MN 719.

3.4.2 Anatomy and emission pattern of lateral organs

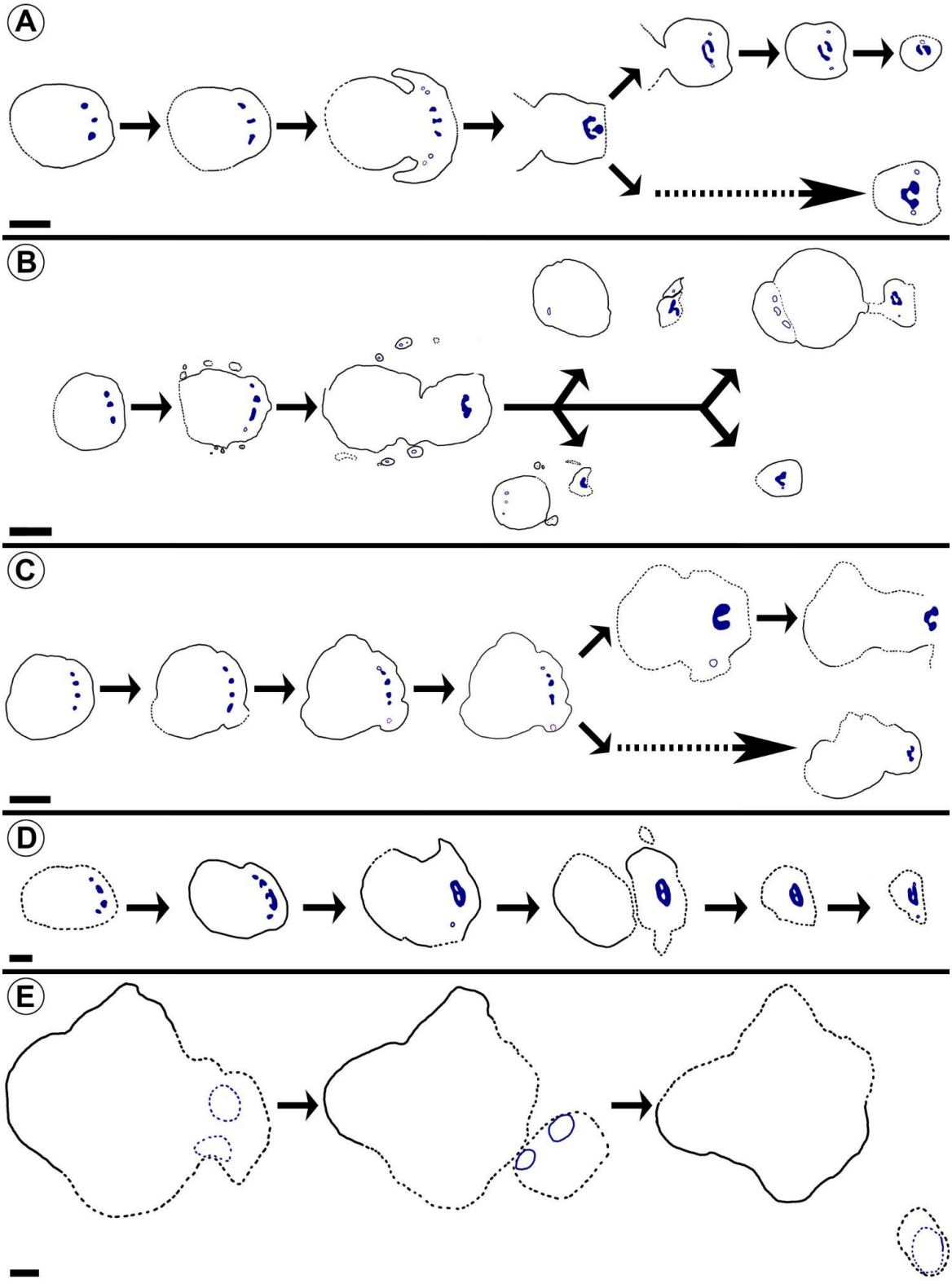

Figure 3.6 Drawings of the five different emission types with the second (traces/lateral organs filled in blue) and third-order axis (empty circle) represented.

(A) Drawings of specimens morphotype 1, showing an emission type 1; scale bar = 5 mm; draw from slides MN 292 BS 1; MN 292 CI; MN 292 DI 3; MN 292 IDS; MN 292 DS 1; MN 292 EI 1; MN 292 ES 1; MN 268 C LO I6. (B) Drawings of specimens morphotype 1, showing an emission type 2; scale bar = 5 mm; draw from slides MN 951 AI 2; MN 951 AS 1; MN 951 BI 7; MN 951 CI S1; MN 925 B inf (specimen polished surface); MN 958 AS 2; MN 920 A2 LO I2. (C) Drawings of specimens morphotype 1, showing an emission type 3; note purple circle represent the third order axis in longitudinal view; scale bar = 5 mm; draw from slides MN 223 BS 06; MN 223 CaI 1; MN 223 CaI 2; MN 223 CaI 3; MN 947 C sup (specimen polished surface); MN 947 CS 2; MN 223 CIoI 1. (D) Drawings of morphotype 1 specimen MN 209 showing an emission type 4; scale bar = 5 mm; draw from slides MN 209 A 01; A (specimen polished surface); MN 209 A 04; MN 209 A 03; MN 209 A 02; MN 209 A 01. (E) Drawings of specimen morphotype 2 showing an emission type 5; scale bar = 5 mm; draw from slides MN 400 DS 01; MN 400 BS 05; MN 400 CS 03.

In the collection, numerous *Cladoxylon* specimens show the emission of a second-order axes. Among them, the length and preservation of 12 specimens allow us to observe this process in detail and to recognize five different emission patterns (Figure 3.6). Four of these five types occur in specimens assigned to stele morphotype 1 (Figures 3.6A–D). The remaining emission type is observed in MN 400, assigned to stele morphotype 2 (Figure 3.6E). Second-order axes may (Figures 3.7A, 3.7I) or may not have secondary xylem (Figures 3.7B, 3.7D–H). In the following section, this character will not be described in detail, but the secondary xylem, if present, is always only located on the abaxial side of the lateral organ (Figures 3.7A, 3.7I).

Emission type 1: symmetrical emission involving 3 ribs of the first order axis (MN 268, MN 292, MN 759, MN 876 [Figure 3.6A]) – In this type, the emission of the second-order axes starts with the production from the tips of three neighboring ribs in the first order axis of three circular strands (Figure 3.6A), one called hereafter “central strand” and two “peripheral” strands. During most of the process, all three strands have a large central protoxylem strand containing big parenchyma cells intermixed with small protoxylem tracheids (Figures 3.7A–B). After the three strands turn free from their emitting ribs, the 2 peripheral strands start to expand tangentially and radially in the direction of the central strand giving them a sub-triangular shape (Figure 3.6A). Then, each one divides into two strands: a pyriform one that will continue to expand toward the central strand, and an elliptical one that is emitted tangentially and corresponds to the vascular trace to a third-order axis (Figures 3.6A, 3.7C). This elliptical trace then divides into two traces, which represent the first dichotomy of the third-order axis (Figures 3.6A, 3.7C). At the same level than this dichotomy, the

central strand expands radially, changing from circular to rectangular and then to an asymmetrical hourglass shape (Figure 3.7B).

The second stage of the emission starts when the former peripheral strands merge with the central one. This produces a “T”-shaped trace with three protoxylem strands located at each end (Figures 3.6A, 3.7D). The upper part of the “T” is more or less curved, with an abaxial concavity (Figure 3.7D). The bottom part of the “T” seems to be emitted radially afterward, but the preservation does not allow us to follow it.

The next stage of trace emission is preserved in two specimens (MN 292 and MN 268), showing different patterns (Figure 3.6A). In MN 292, the curved upper part of the “T” divides at the curvature point. At the same time, two circular third-order traces are emitted tangentially (Figure 3.7D). At this stage, the second-order axis is surrounded by its own cortex, and its vasculature is composed of the two remaining strands facing each other with a light curvature toward the center (Figures 3.6A, 3.7F). The second-order axis is thus devoid of abaxial-adaxial polarity distally.

In MN 268, the transition between the “T”-shaped trace and the following one is not preserved and the resulting vasculature of the second-order axis is different. Distally, the stele of this axis is still “C” to “V”-shaped, looking like two hourglass-shaped strands fused on the adaxial end (Figure 3.7A). Three protoxylem strands are present, one elliptical at the “fusion” zone and one circular at each abaxial end. These last ones will divide to emit third-order axis traces tangentially (Figure 3.7A arrows). We can note that at the stage of a third-order axis trace emission, this specimen shows secondary xylem in its second-order axis vasculature, which is not the case for MN 292.

MN 268 and MN 292 also differ in terms of the angles of their lateral emission. In MN 268, transversal views of lateral appendages can be observed on longitudinal sections from the main axis perspective, however, in MN 292, all emission stages have been observed in sections that are transversal for the main axis. Then, MN 268 emits lateral that are perpendicularly oriented and the one of MN 292 diverges from the first-order axis with a narrower angle.

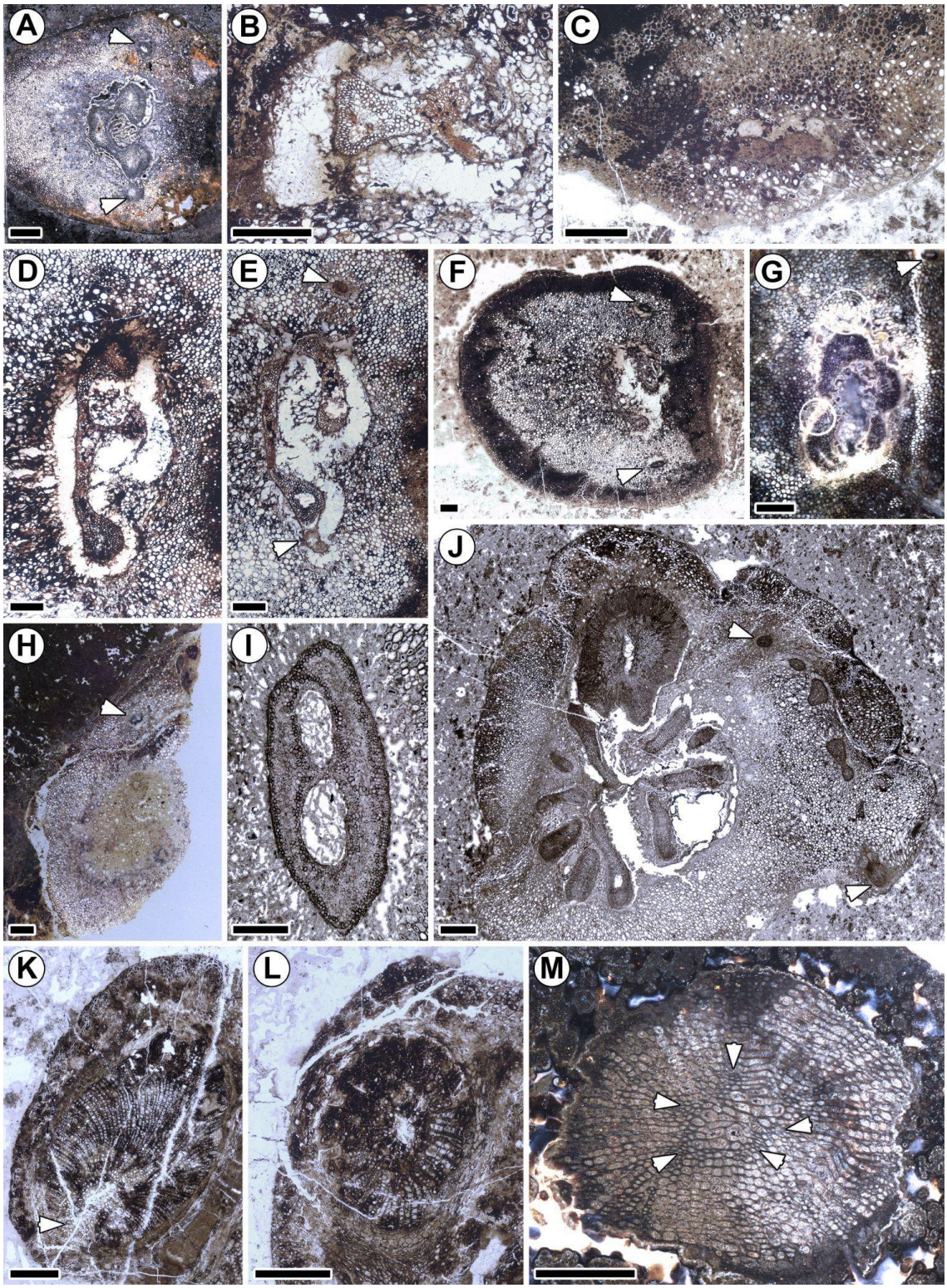
A
B
C
D
E
F
G
J
H
I
K
L
M

Figure 3.7 Details of the lateral emissions in transversal view.

(A) “V”-shaped second-order axis with secondary xylem emitting oppositely third-order axis traces (arrows); this axis is produced by an emission type 1; scale bar = 1 mm; slide MN 268 C LO I6. (B) Asymmetrical hourglass-shaped central strand; this axis is produced by an emission type 1; scale bar = 500 µm; slide MN 292 DI 3. (C) Dichotomy of a third-order axis; scale bar = 500 µm; slide MN 292 EI 4. (D) “T”-shaped second-order axis; this axis is produced by an emission type 1; scale bar = 500 µm; slide MN 292 DI 5. (E) “C”-shaped second-order axis emitting oppositely third-order axis traces (arrows); this axis is produced by an emission type 1; scale bar = 500 µm; slide MN 292 DS 1. (F) Late emission stage of second-order axis with vasculature laking abaxial/adaxial polarity; arrows pointing at the third-order axe traces; this axis is produced by an emission type 1; scale bar = 500 µm; slide MN 292 EI 1. (G) “Butterfly”-shaped second-order axis emitting third-order axis trace (arrow); this axis is produced by an emission type 2; scale bar = 500 µm; slide MN 925 E1 B inf. (H) “V”-shaped second-order axis emitting third-order axis trace (arrow); this axis is produced by an emission type 2; scale bar = 500 µm; slide MN 951 E1 C1 S1. (I) “8”-shaped second-order axis; this axis is produced by specimen MN 209 during its emission type 4; scale bar = 500 µm; slide MN 209 AI 03. (J) Specimen MN 223 during an early stage of emission type 3 with arrows pointing at emission of the first third-order axe traces emits before the second-order axis fusion; note the unusual shape of one of the rib (see Discussion, Secondary growth): scale bar = 1 mm; slide MN 223 CaI 3. (K) Second-order trace showing a mesearch protoxylem strand (arrow) and secondary xylem located only on one side; this trace is produced by an emission type 5; scale bar = 500 µm; slide MN 400 DS 01. (L) Putative root trace lacking central protoxylem strand and secondary xylem surrounding the primary xylem evenly; this trace is produced by a specimen belonging to the stele morphotype 2; scale bar = 500 µm; slide MN 400 DS 01. (M) Root trace with exarch protoxylem strands (arrows) and secondary xylem surrounding the primary xylem evenly; this trace is produced by a specimen belonging to the stele morphotype 2; scale bar = 500 µm; slide MN 904 Fsl.

Emission type 2: asymmetrical emission involving 3 ribs of the first-order axis (MN 920, MN 925, MN 951, MN 958 [Figure 3.6B]) – Three ribs of the first order axis are also implicated in the emission of these second-order axes, but unlike in the symmetrical pattern described previously, the two peripheral strands do not follow the same changes (Figure 3.6B). One divides tangentially in the same way as in the symmetrical emission type, resulting in one strand towards the inside of the axis and the other towards the outside (i.e. similar to a third-order trace in the previous type). The second peripheral strand is emitted tangentially toward the exterior without division, i.e. it seems equivalent to a third-order axis trace in the symmetrical emission process. This peripheral trace remains circular during the process.

At this stage the two other strands increase in diameter, becoming elliptical to pyriform with large central protoxylem strands (Figure 3.6B). These two strands continue to expand tangentially as well as radially and fuse into a single “C”-shaped strand (Figure 3.6B). Distally, this strand divides into a “U” to “V”-shaped strand with three protoxylem poles (Figures 3.6B, 3.7H) or as a

“butterfly-shaped strand”, made of four arched portions (two large ones abaxially and two small ones adaxially) (Figures 3.6B, 3.7G).

The two traces to the third-order axis remain circular to elliptical all along the emission process and have the same pattern but are not emitted exactly with the same timing (Figures 3.6B, 3.7E arrows). On the two specimens with this stage preserved (i.e., MN 925 and MN 958), the peripheral strand that exits laterally seems to be emitted after one produced by the peripheral strand on the other side (Figure 3.6B). The traces to the third-order axes have been seen to be dichotomized to produce a total of four strands.

Emission type 3: symmetrical emission involving 4 ribs of the first-order axis (MN 223 and MN 947 [Figure 3.6C]) – The emission process starts with the emission of strands from four ribs of the first order axis instead of three in the two previous types. The two peripheral strands are circular until they divide tangentially to produce third-order axis traces (Figures 3.6C, 3.7J arrows). The two central strands increase in diameter while staying more or less circular. These two strands will fuse, first with one of the peripheral strands (Figure 3.7J), and then all together (Figure 3.6C). On specimen MN 947, the trace of the second-order axis seems very similar to the “V”-shaped trace coming from the symmetrical emission of MN 268 (Figures 3.6C, 3.7A).

Emission type 4: 8-shaped emission involving 4 ribs of the first order axis (MN 209 [Figure 3.6D]) – Like in the previous type, the emission process starts with the trace emissions from 4 ribs of the first-order axis (Figure 3.6D) but in this case the 2 central strands start their tangential elongation before being free from the ribs (Figure 3.6D). When all the strands turn free there are two circular lateral strands, and 2 central ones that are more tangentially elongated and starting to be different from the others. Both are more or less “C”-shaped, one is small with its concavity facing the other trace, and the second is larger with an adaxial concavity. The emission pattern of the lateral traces is not preserved all along the axis, nevertheless, one of the two traces fuse with the biggest central strands (Figure 3.6D). After this, the central strands combine, resulting in an “8”-shaped strand with the biggest surface of primary xylem and some secondary xylem present at its abaxial face (Figure 3.7I). This 8-shaped strand then emits circular traces in an alternate organotaxis from its tangential ends. Later in the emission process, one of the tangential ends of the strand seems opened, but it is not clear if this corresponds to an actual emission stage or to a preservation artifact (Figure 3.6D).

Emission type 5: non-fused emission involving 2 ribs of the first order axis (MN 400 [Figures 3.6E]) – This emission type is very different from the previous ones and likely vascularized another type of organ. The trace is emitted alternately and originates from two neighboring ribs of the first

order axis that may or may not be fused. The actual early emission of the trace from the primary xylem of the first order axis ribs has not been observed, however, their origin is hypothesized based on the disruption of the secondary xylem and the short distance of the ribs from one of the two strands in the earliest stage observed. The following stages of the trace emission, i.e. the separation of the trace vascular tissues from those of the first order axis, have not been observed due to the poor preservation of this part of the specimen. However, contrary to all the other emission types, the two strands are never fused and will diverge from each other tangentially (Figure 3.6E). These 2 strands have a distinct anatomy. The first strand possesses an elliptical primary xylem (Figure 3.7K) with a single preserved mesarch protoxylem strand (Figure 3.7K arrow). The secondary xylem surrounds only the tangential side of the trace facing the other one (Figure 3.7K). The second one shows a terete primary xylem but contrary to the terete traces of the other specimens, a central position of the protoxylem strand is not observed (Figure 3.7L). Despite its poor preservation, the central part seems composed of large cells centrally with small ones located at the periphery of the primary tissues, making the maturation in this trace likely exarch (Figure 3.7L). The secondary xylem surrounds the primary xylem, giving an overall circular shape to the trace (Figure 3.7L).

In all the specimens observed during this study, there is only one other occurrence of a trace identified as possessing exarch xylem maturation (Figure 3.7M). It is observed in MN 904 (Figure 3.5A), a specimen that belongs to the same stele morphotype as MN 400 (Figure 3.2B). This trace possesses primary tissue that is overall circular with multiple protoxylem strands (up to 5) forming ridges (Figure 3.7M arrows). The secondary xylem that surrounds it is evenly spaced, making this trace circular. Based on the above characters and all the differences between this type of trace emission and the previous ones, we interpreted these lateral organs with exarch maturation as corresponding to roots.

3.5 Discussion

3.5.1 How many *Cladoxylon* species are present in the Lydienne Formation?

The Tournaisian localities in the Montagne Noire are currently the source of the largest known collection of specimens assigned to the genus *Cladoxylon*, however, their taxonomic affinities have never been studied in detail. The following section compares the various morphotypes identified in

this study to known *Cladoxylon* species, allowing us to assess the diversity of the *Cladoxylon* species present in the assemblage.

Cladoxylon is a genus erected by Unger in 1856 with the following diagnosis: “Fleshy trunk, wooden axis made of bundles of simple and composite band-shaped vessels variously divided and assembled together. Parenchymatous cortex marked by discrete filamentous bundles. The name (*Clado*) branch and (*xylon*) wood.” (translated from Latin, Unger, 1856: p. 179). This generic diagnosis has not been amended since. The genus has been recognized as a paraphyletic group belonging to the non-pseudosporochanean cladoxylopsids (also called cladoxylalean cladoxylopsids) by the latest phylogenetic studies, which included 3 species (*C. taeniatum*, *C. radiatum*, and *C. mirabile* [Durieux et al., 2021; Chu et al., 2024]). Based on this original diagnosis combined with the much more detailed description of the genus by Bertrand (1935), all the specimens in our study can be assigned without doubt to *Cladoxylon*. Three had already been described and assigned to *Cladoxylon* by Galtier in 1970 (MN 206, MN 209, MN 223) and four to the species *C. taeniatum* by Decombeix and Galtier in 2021 (MN 400, MN 876, MN 904, MN 925). Note that Böhm (1935) also briefly describes three *Cladoxylon* specimens from the Montagne Noire (Saint-Nazaire-de-Ladarez, “collection Böhm, Faculté des sciences de Montpellier and Faculté des sciences de Lille”), however, we have not been able to identify these specific specimens within the collection.

The taxonomical history of species assigned to *Cladoxylon* includes many synonymizations and exclusions from the genus (e.g. Bertrand, 1935; Schweitzer and Giesen, 1980; Stein and Hueber, 1989; Cordi and Stein, 2005). According to the latest study on *Cladoxylon* (Decombeix and Galtier, 2021), the genus includes today four Tournaisian species from Germany and France *C. mirabile*, *C. radiatum*, *C. solmsii*, and *C. taeniatum*, and two Tournaisian to Visean species from Scotland, *C. waltonii* and *C. edromense*. Specimens comparable to *C. taeniatum* and *C. radiatum* have also been reported from the Late Devonian of Australia (Meyer-Berthaud et al., 2021).

Four additional *Cladoxylon* species found in the literature are excluded in the following comparison: 1) *C. kidstoni* (Solms-Laubach, 1910), because according to Scheckler (1975: p. 36) this specimen “is based upon one fragmentary specimen and is only doubtfully placed in *Cladoxylon*, or even in Cladoxylales”, 2) *C. bakrii* (Mustafa, 1978) because of its Middle Devonian age and its numerous anatomical differences such as its ribs number (up to 46), 3) *C. centrale* (Unger, 1856) because it have never been described in detail or illustrated and Unger (1856: p. 180) was not sure wether it was different from *C. mirabile*, and 4) *C. tanaiticum* (Snigirevsky, 1992; Snigirevsky and Lyubarova, 2021) because of its ribs number (up to 25 ribs and 10 central vascular bundles), lack of secondary xylem, and unusual exarch protoxylem in central bundles (Snigirevsky,

1992). The specimens from the Montagne Noire are thus compared with the six remaining early Carboniferous *Cladoxylon* species.

C. waltonii (Long, 1968) differs from all the Montagne Noire specimens by its stele that can have two aspects: 1) all the ribs are connected through the center or forming a central circular part composed of inner cortex/pith-like tissue, or 2) a horseshoe-shaped actinostele. In addition to this difference, *C. waltonii* produces *Clepsydropsis*-shaped traces from 2 neighboring ribs that fuse at their peripheral ends and do not possess secondary xylem. The horseshoe-shaped stele of *C. waltonii* is similar to another species from the same localities, *C. edromense*, which possesses secondary growth (Long, 1987). Based on these differences, these two species are not represented among the Montagne Noire specimens

C. radiatum (Unger, 1856; Bertrand, 1935) also differs from the Montagne Noire specimens. The central anastomosis seen in this species is shared with one specimen (MN 719) in our sample. However, MN 719 differs from *C. radiatum* by its high amount of secondary xylem and the presence of sclerenchymatous tissues between its ribs. The pattern of emission of lateral organs in *C. radiatum* is also very different from the different types observed in this study: in *C. radiatum* lateral organs are vascularized by eight traces emitted by (at least) four ribs of the first order axis, forming bilateral organs without apparent abaxial-adaxial polarity.

C. solmsii (Bertrand, 1935) differs from the Montagne Noire specimens by the central anastomoses of the ribs in its stele, the shape of its lateral organ vasculature, and its very reduced amount of secondary xylem. Even if the early stage of the emission pattern in *C. solmsii* is similar to some specimens in our sample (i.e. emission type 3), the other differences listed above prevent their assignment to this species.

C. mirabile (Unger, 1856; Bertrand, 1935) also differs from most of the Montagne Noire specimens. However, the central anastomosis of its ribs, combined with the “U” to “V”-shaped ribs and the presence of sclerenchymatous tissue between the ribs are characteristics shared with specimen MN 719 (Figures 3.2D, 3.5D–F). Differences between MN 719 and *C. mirabile* include the presence of an endodermis, a very reduced secondary growth, only present close to the rib tips, and a higher number of ribs in the latter. These differences could however be developmental, so we assign MN 719 (i.e. stele morphotype 4) to *C. mirabile*.

C. taeniatum (Unger, 1856; Bertrand, 1935) and *C. taeniatum* var. *dubium* De Solms (Bertrand, 1935) share numerous characteristics with Montagne Noire specimens assigned to stele morphotype 1 (Figures 3.1, 3.2A) and 3 (Figures 3.2C, 3.5B, 3.5C). *C. dubium* was erected by Unger (1856) based on one incomplete specimen. Later, Solms-Laubach (1896) improved the

species description using new specimens. However, Bertrand (1935) considered this species to represent small specimens of *C. taeniatum*, leading to the creation of the form called *C. taeniatum* var. *dubium* De Solms. From the stele shape point of view, *C. taeniatum* shares with the Montagne Noire specimens a dissected stele with mesarch protoxylem strands at the rib tips, central vascular bundles devoid of protoxylem strands, and fusions between neighboring ribs for most of the specimens ("U" to "V"-shaped). They also share a well-developed secondary xylem surrounding the ribs, protoxylem strands made of parenchyma cells surrounded by protoxylem tracheids, and a similar cortex anatomy. As described above, the emission patterns are variable in the study group, nevertheless, *C. taeniatum* var. *dubium* emission pattern involves 3 or 4 ribs and produces an organ with an abaxial-adaxial polarity, a process similar to specimens from the Montagne Noire (Figures 3.6A–D).

Differences between the studied specimens and *C. taeniatum* are the number of ribs (12 to 24 in *C. taeniatum*, 8-12 in the stele morphotype 1 specimens), and potentially some thickening of cortical layers. However, similarities are too numerous between the stele morphotype 1 specimens and *C. taeniatum* (in particular the form *dubium*) to establish a new species. Then, we assign all the specimens with stele morphotype 1 to the species *C. taeniatum*. Despite the lack of preservation of the rib tips of MN 921 (i.e. stele morphotype 3), the anatomy of the inner part of the ribs, the number of ribs, the central vascular bundle, and the amount of inner cortex suggest that MN 921 also represents a large specimen (for our sample) of *C. taeniatum*.

Stele morphotype 2 (Figures 3.2B, 3.4, 3.5A) specimens are different from all the previously mentioned species based both on stele organization, on secondary growth differences, and on lateral emission patterns. However, we choose to not erect a new species for them based on the fact that they might represent a different ontogenetic stage of *C. taeniatum* (see below). This possibility was already raised in the study of Soria and collaborators (2006) and Decombeix and Galtier (2021), who considered them to be *C. taeniatum* axes with a periderm and a large amount of secondary xylem. We also agree with Bertrand (1935) in his identification of *C. taeniatum* var. *dubium* as a small *C. taeniatum* (see ***Primary growth*** *– Primary vascular system*).

At least two species of *Cladoxylon*, *C. mirabile* and *C. taeniatum*, and different "forms" of *C. taeniatum,* likely corresponding to different ontogenetic stages, have thus been identified in the Montagne Noire assemblage. These taxa have also been found in the German locality of Saalfeld (Unger, 1856) and in equivalent deposits of Kahlleite quarry, 25 kms from Unger's historical locality (Meyer-Berthaud and Rowe, 1996; Decombeix et al., 2005; Decombeix and Galtier, 2021). This similarity is not surprising since these localities have outcrops of the same age, were close paleogeographically, and share most of their taxonomic diversity (Scott et al., 1984).

3.5.2 Organotaxis and growth of *Cladoxylon taeniatum*

As mentioned above*, Cladoxylon taeniatum* has been known for a long time based on specimens coming from Saalfeld (Germany, Bertrand [1935]), Kahlleite quarry, and the Montagne Noire (Galtier, 1970; Decombeix and Galtier, 2021). However, its organotaxis has not been studied in detail and no hypothesis about the growth of the plant has been put forward. In the present study, the number and morpho-anatomical diversity of specimens assignable to *C. taeniatum* allow us to analyze the nature and organotaxis of its lateral organs, and to propose hypotheses about the primary and secondary growth of the plant.

Organotaxis – The only study detailing the organotaxis of *Cladoxylon* was conducted by Bertrand (1935) (see Figure 6 of Cross and Hoskins [1951] for a drawing showing the relationship between the different organs). Similarities with our finding are that *Cladoxylon* is a morpho-genus corresponding to stems, defined by their radially symmetrical stele and the production of lateral organs emitted from multiple ribs. However, the anatomy of the lateral organs and the number of axis orders are different in the present study. For Bertrand (1935), *Cladoxylon* possesses lateral organs (second-order axis) called *Hierogramma* and *Syncardia*. They possess a dissected stele made of ribs (respectively 8 to 10 for *Hierogramma* and 4 to 6 for *Syncardia*) with mesarch protoxylem strands, a small amount of secondary xylem (when present), and a bilateral symmetry (Bertrand, 1935). *Hierogramma* can isotomously dichotomize or emit another order of *Hierogramma* axes. *Hierogramma* and *Cladoxylon* can both produce *Clepsydropsis* as a second or third-order axis ("primary rachis" in Bertrand [1935]) bearing the ultimate appendages. *Clepsydropsis* are produced from circular traces that will elongate distally, forming organs with a bipolar symmetry looking like a primary rib with a mesarch protoxylem strand at each end. Two other orders of axes (4th and 5th) are attached to the *Clepsydropsis* in a distichous way (secondary and third order rachis for Bertrand [1935]). The 4th-order ones possess an elliptical vasculature, and the 5th are circular and can also be emitted by the 4th-order axis.

In the present study, specimens identified as *Cladoxylon taeniatum* are recognized as first-order axes characterized by a radially symmetrical dissected stele made of numerous ribs. These first order axes produce traces resulting from the fusion of 3 of 4 strands that vascularize second-order axes with abaxial-adaxial polarity, which themselves bear third-order axes (Figures 3.7A, 3.7D, 3.7E, 3.7G-–I). The latter ones are vascularized by a trace emitted from the tangential ends of the second-order axis, which is circular to elliptical and dichotomizes (Figure 3.7C). We also recognized another type of third-order axis, sharing the same organotaxis and anatomy as the first type, but produced very proximally, i.e. before the fusion of the strands of the second-order axis trace (Figures 3.6A–D).

Our reconstructed organotaxis is thus different from Bertrand's because 1) no second-order axis dichotomy was observed, 2) second order axes do not produce an axis with the same vasculature but only simple terete traces, 3) no fully developed *Hierogramma* type organs have been observed, 4) no *Clepsydropsis* type organs have been observed. We conclude that the model established by Bertrand for *Cladoxylon* does not apply to *C. taeniatum*. We reconstruct *C. taeniatum* as a stem/last order of branch that bears petiole-like (i.e. possessing an abaxial-adaxial polarity and lacking laminar tissue) second-order axes in a spiral. These second-order axes bear third-order axes, interpreted as ultimate appendages, in alternate to opposite arrangement. Third-order axes produced in the most proximal parts of the second-order axes likely correspond to the aphlebia already reported in *Cladoxylon* by Bertrand (1935) and Galtier (1970).

Primary growth – *Primary vascular system* – All the specimens are represented by short axes (between 2 and 10 cm in length) and did not show any clear anatomical differences between their basal and their apical parts, which makes the primary growth of *Cladoxylon* challenging to reconstruct. Nevertheless, our PCA analysis using multiple specimens with stele morphotype 1, all assigned to *C. taeniatum*, provides insight into its primary growth. First, the positive correlation between the number of ribs and the surface of primary xylem (Figures 3.3D–E) suggests that the total amount of primary xylem is more influenced by the number of ribs in the axis than by the amount of tissue in each rib. Second, there is a positive correlation between these two characters and the stele diameter, i.e. larger axes have more ribs and more primary xylem (Figures 3.3D–E). These characters are also recovered by the PCA as being highly represented in the first axis that explained by itself 57.28% of the inertia, so the hierarchical clustering might recover clusters influenced by these characters. Three interpretations can be given for the variations in diameter and number of ribs seen in the sample.

The first hypothesis is that the specimens might represent different organs or axes' orders. For example, *Polypetalophyton wufengensis* (Li and Cui, 1995; Hilton et al., 2003), *Pseudosporochnus hueberi* (Stein and Hueber, 1989), *Pietzschia shulleri* (Soria and Meyer-Berthaud, 2005) are cladoxylopsids species showing different number of ribs depending on the studied order of axes. The different clusters recovered by our analyses could thus represent different axis orders.

The second hypothesis is that the sample represents the natural variation of the species (polymorphy), and that the correlation between the number of ribs and the diameter corresponds to a sample composed of both small and large plants, each with a fixed number of ribs. One point supporting this is the lack of variation in the number of ribs (i.e. a 'definitive' division or a fusion of ribs) within a same specimen as observed in the cladoxylopsid species *Pietzschia schulleri* and *P. polyupsilon* (Soria and Meyer-Berthaud, 2003, 2005). The clusters recovered in our analyses

could thus represent different individuals from the same polymorphic species, small plants with few ribs and larger ones with more ribs.

A last hypothesis is that the specimens represent different ontogenetic stages (Figure 3.8), and that the correlation between diameter, number of ribs, and amount of primary xylem reflects *Cladoxylon taeniatum* growth. A relationship between the diameter and the number of ribs has already been reported in some *Cladoxylon* species (Mustafa, 1978; Long, 1968), and seems to be present in most cladoxylopsids, with larger axes most likely to exhibit the highest number of ribs. It is even more interesting for this hypothesis that, in some cases, this variation is observed inside a same axis. An increase in number of ribs towards the apex has been reported in *Pietzschia levis* for a specimen in epidogenetic phase of growth (Soria and Meyer-Berthaud, 2004) and in the trunk of *Xinicaulis lignescens* (Xu et al., 2017). Conversely, a decrease toward the apex has been reported in 1) a branch of *Pseudosporochnus nodulus* (Stein and Hueber, 1989), 2) the only specimen of *C. bakrii* (Mustafa, 1978), and 3) specimens of *Pietzschia levis* in apoxogenetic phase of growth (Soria et al., 2001; Soria and Meyer-Berthaud, 2004). This variation reported in *P. levis* does not apply to all the genera because in *P. polyupsilon* and *P. schulleri* (Soria and Meyer-Berthaud, 2003; 2005) the apoxogenetic phase is marked by a decrease of the amount of primary xylem per ribs, but not of the number of ribs. *Polypetalophyton* (Hilton et al., 2003) might also show this variation based on the statement that the number of ribs is "up to 12" and its decrease of the axis width apically (Hilton et al., 2003: p. 795). Nevertheless, it is unclear in the description if the variation in the number of ribs happens along the same axis or in different specimens identified as axes of the same order. These examples show that variations in rib number in cladoxylopsids can correspond to different ontogenetic stages of a same plant.

Three hypotheses can thus be invoked to explain the observed morpho-anatomical diversity in our *Cladoxylon taeniatum* assemblage, i.e. 1) the specimens represent different types of axes, 2) the specimens represent a same type of axis with a variable anatomy (polymorphy), and 3) the specimens represent different ontogenetic stages of a same type of axis. The first hypothesis is less likely since we showed previously that there is a clear sequence of different organs from a stem/last order of branch towards ultimate appendages and no evidence of an axis producing a lateral with the same anatomy (see ***Organotaxis*** and Figures 3.6A–D). The polymorphic hypothesis does not necessarily conflict with the 2 others, and we cannot exclude that *C. taeniatum* is a polymorphic species. However, it would imply a large amount of variation for a single species. We thus favor the ontogenetic hypothesis, which is the most consistent with the observed correlation between the amount of primary vs. secondary growth (Figure 3.8A) observed in the specimens (details in ***Ontogenetical interpretations of the Montagne Noire specimens***). We conclude that the

Cladoxylon taeniatum specimens of the Montagne Noire assemblage most likely represent different ontogenetic stages of a same plant.

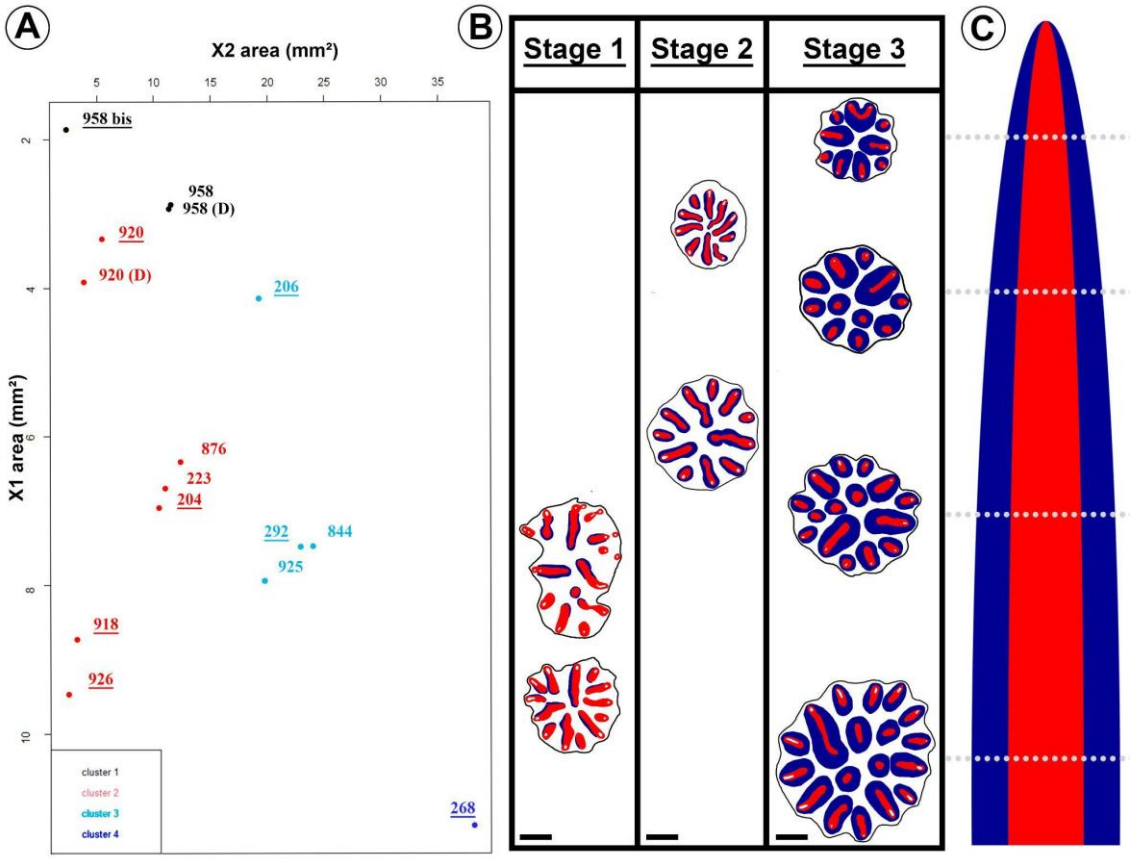

Figure 3.8 Illustration of *Cladoxylon taeniatum* apoxogenesis and its different secondary growth stages.

Color code for (B) and (C): protoxylem in grey, primary xylem in red, secondary xylem in blue, and stele/specimens limits in black. (A) Stele morphotype 1 specimens included in the PCA display on the graph showing the amount of secondary xylem on the X-axis and primary xylem on the Y-axis; colors according to their respective cluster from the hierarchical clustering; specimen numbers underlined have their stele represented in (B). (B) Table with the specimen steles drawings representing each hypothesized stages of secondary growth; scale bar = 2mm. (C) Representation of a plant in apoxogenetic phase of growth with virtual placement of the specimens showing stage 3 secondary growth of (B) (grey dashed line).

Primary growth – *Endodermis* – A layer of cells identified in four specimens of *Cladoxylon* (MN 204, MN 268, MN 400, and MN 921) belonging to three different stele morphotypes (1, 2, and 3) has been identified as an endodermis based on cell shapes and on its position (Figures 3.1C En, 3.4E arrow, 3.5C arrow). The endodermis is a layer of cells surrounding the pericycle and the vascular tissues. It is mostly known in seed plant roots but has also been observed in roots and

aerial parts of multiple seed plants, ferns, and lycophytes (Bond, 1931; Warmbrodt and Evert, 1979; Lersten, 1997; Seago, 2020). This layer has different functions, including acting as a selective barrier between the nutrients and water diffusing from the soil and the stele, protecting the vascular system from pathogens, and containing cell materials allowing gravitropic and phototropic responses (Geldner [2013] and reference therein). An endodermis has previously been reported in other cladoxylopsids, e.g., in *Polyxylon australe* (Meyer-Berthaud et al., 2007), *Keraphyton mawsonia* (Champreux et al., 2020), specimens of *C. mirabile* and *C. taeniatum* studied by Bertrand (1935; TD, pers. obs.), and specimens of *Cladoxylon* from Australia studied by Meyer-Berthaud and collaborators (2021). The presence of an endodermis in several *Cladoxylon* specimens from the Montagne Noire is then not surprising. However, the majority of the specimens seem to be devoid of this tissue, which can be explained by 1) the preservation (i.e. the specimens with degraded phloem are also devoid of endodermis), and 2) a potentially different composition of the endodermal cell wall changing the preservation potential. The first hypothesis is consistent with the endodermal layer found in MN 204 and MN 400 because they are specimens with well-preserved soft tissues such as phloem cells (Figure 3.1C Ph). On the other hand, MN 921 and MN 268 lack these phloem layers and the endodermal cells are still recognizable (Figure 3.5C). These differences of preservation of an endodermal layer between specimens thus suggest that it might have a different cell-wall thickening inducing this unequal likelihood of tissue preservation.

Three stages of endodermal development have been identified in extant (seed) plants (review by Geldner [2013]), which have been defined based on 1) Casparian strip establishment, 2) suberin deposition on the secondary walls of the endodermal cells, and 3) lignification of the cell wall. These changes in the endodermal cell walls towards a composition more likely to be preserved might create a difference in the endodermis preservation potential. In extant plants the presence of the three stages is highly variable depending on the species and the organ (e.g. the third stage is still unknown in pteridophytes and rare in stem and leaf [Lersten, 1997]).

Three of the 4 specimens with visible endodermis belong to the biggest representatives of *Cladoxylon* from our sample, following the tendency to find endodermal layers in relatively "big" cladoxylopsids. In *Polyxylon*, only *P. elegans* is devoid of endodermal cells with "thickened in narrow side" (Meyer-Berthaud et al., 2007: Table 1), and it represents the smallest species of the genus. *Keraphyton* (Champreux et al., 2020) has been assigned to the iridopteridales, making it the biggest species of the clade and the only one with an endodermis reported. *C. taeniatum* and *C. mirabile* specimens from Saalfeld possessing an endodermis are also large specimens that are bigger than all the Montagne Noire specimens. In our view, these large specimens represent basal parts (i.e. the oldest parts) of the plants showing a final/advanced stage of endodermis

development. In this way, large cladoxylopsids, despite poor preservation of soft tissues possess lignified/suberised endodermal cells that are more likely to be preserved. In addition, the presence of a putative endodermis in *Pietzchia levis* (Soria et al., 2001; and TD pers obs) associated with its adventitious roots might confirm this hypothesis by supporting the presence of this tissue in a basal part of the plant.
An interesting point to consider for the understanding of *Cladoxylon*'s anatomy is that the endodermis represents the innermost layer of cortical cells (Enstone et al., 2003), making its surrounding tissue the inner part of the cortex based on its position. This leads to two conclusions 1) the pith-like tissue of *Cladoxylon* (and likely all the other cladoxylopsids with a dissected stele) is then cortical, and 2) the stele of *Cladoxylon* can be qualified as an eustele or a plectostele, and more precisely might represent an *eustelic boundary eustele* as defined by Tomescu (2021).

Secondary growth – *Secondary xylem* – The secondary xylem of the *Cladoxylon taeniatum* specimens is located all around the primary xylem, whether it is in the ribs or in the central vascular bundles. Nevertheless, there are some variations in the distribution of the secondary xylem around the ribs between specimens. We can distinguish 3 types of secondary xylem distribution (Figure 3.8B). The first one is represented by two specimens (MN 918 and MN 926) where, in the same stele, some ribs are devoid of secondary xylem while others have some. In this case, the secondary growth is located at the inner end (MN 918) or on a specific side of the ribs (MN 926). In the second type, all ribs have secondary xylem that is evenly distributed around the primary xylem (e.g. MN 204, MN 223, MN 918, MN 920, MN 925).
The third type is represented by specimens with an uneven distribution of the secondary growth in each of the ribs. In these specimens, the secondary xylem is more developed toward the center, a feature particularly obvious when specimens possess a high amount of secondary growth (e.g. MN 206, MN 292, MN 844, MN 876, MN 947, MN 958, MN 400).

We interpret these 3 types of distributions as 3 stages of secondary growth (Figure 3.8B) 1) the initiation, starting from the center part of the stele or on one side of the ribs, 2) secondary growth develops evenly, and 3) secondary growth continues only toward the inside ends of the ribs. Because of the even distribution observed in the second stage, the difference in the amount of the secondary growth around the ribs in the third stage is more likely due to a variation in growth rate around the ribs than to a lag linked to the location of the initiation.

In addition to the previously described 3 stages, special cases of secondary growth only concerning one rib of the stele have been recognized in two specimens (i.e., MN 223 and MN 904 [Figures 3.2B right drawing, 3.5A, 3.7J]). In both, a rib shows an increase of secondary growth on its external end (i.e. toward the outside). This variation happens only on one rib in the stele, and the

other ribs seem to be either, in the second stage (MN 223) or a third stage of growth (MN 904). We thus hypothesize that this variation is more likely to be due to a punctual variation of the growth, e.g. induced by a biomechanical stress. In the case of MN 223, this unusual secondary growth is also coupled with an unusual primary growth of the same rib that is unique in the sample from the Montagne Noire.

Cladoxylon taeniatum specimens in the assemblage all lack secondary phloem, suggesting that the vascular cambium was unifacial, a non-surprising finding since specimens of this species (Decombeix and Galtier, 2021) and several other woody cladoxylopsids have already been reported as possessing this type of cambium (Tomescu and Groover, 2019; Decombeix et al., 2019a). The specimens also show that secondary vascular growth in *C. taeniatum* was likely determinate. Indeed, it is characterized by few occurrences of anticlinal divisions, and is constrained by two factors: first, the space between the different ribs, as witnessed by the lack of contact between the secondary xylem of two ribs, and second by the highly thickened endodermal layer in the specimens with a large amount of secondary xylem. In the case of indeterminate growth, once the endodermal layer starts to be lignified and unable to keep dividing (i.e. in MN 400), one would expect it to break apart under the mechanical pressure from the expanding secondary vascular tissues.

Secondary growth – *Periderm* – Another type of secondary growth, the periderm, has already been reported in some *Cladoxylon taeniatum* specimens from the Montagne Noire (MN 400, MN 876, MN 904). A detailed description of this tissue, a discussion on its implication on the growth habit of *C. taeniatum*, and a comparison with other cladoxylopsids can then be found in Decombeix and Galtier (2021). Nevertheless, two new observations have been made: 1) the identification of an endodermis in *C. taeniatum* specimens, and 2) the important similarity between the inner cortical cells and the others cells found at the center of the stele or in between the rib. Based on this, the periderm growth is hypothesized to have been initiated between the inner and middle cortex.

3.5.3 Reconstructing the architecture of *Cladoxylon taeniatum*

Insights from the 2006 biomechanical study – The preliminary study about the habit of *C. taeniatum* conducted by Soria and collaborators (2006) identified three ontogenetic stages. The first one is defined by a stele possessing eight ribs with an alternation of short or elongated ones, a central parenchymatous pith, and tree distinct cortical layers. The second stage is defined by a similar stele, but with 10 ribs, slightly more secondary xylem developed predominantly towards the center, and a new cell layer corresponding to the periderm initiation. The oldest stage is highly different, it has an elliptical cross-section, a lot of secondary xylem, a well-developed periderm,

and lacks cortical layers. It also only possesses eight ribs that are fused two by two. Using the above ontogenetic stages, the authors applied the biomechanical reconstruction method developed by Rowe and Speck [1998] for isolated fossil axes. They showed that the transition from the first to the second stage gives a signal suggesting that the young parts of the plant were self-supporting (i.e. basipetal increase of Young's modulus). The change from the second to the older stage however indicates that the older stages were likely less rigid (i.e. basipetal decrease of Young's modulus). This decrease is due to 1) the replacement in the outermost part of the axis of the collenchymatous cortex by layers of periderm cells with thinner walls, and 2) the development of a secondary xylem toward the inside of the stele, i.e. not in a mechanically important position. The authors conclude that *Cladoxylon taeniatum* was comparable to "non-self-supporting plants such as lianas" (Soria et al., 2006: p. 4).

A lianescent habit of *Cladoxylon* had previously been put forward by Snigirevsky (1992) based on an observation of a *C. tanaiticum* crawling around a *Callixylon* stem/branch. However, because of the lack of detail on this finding to date (only a drawing and a short description) and the numerous anatomical differences between this *Cladoxylon* species and the specimens described in this study, we do not think that the habit of *C. taeniatum* can be inferred from that of *C. tanaiticum*.
In our opinion there is currently no strong evidence supporting a lianescent habit for *Cladoxylon taeniatum* because (1) there is no evidence of attachment organs in *Cladoxylon taeniatum*, (2) being non-self-supporting does not automatically imply a lianescent habit, and (3) the three stages for which Young's modulus have been calculated by Soria et al. (2006) might not correspond to the same type of axis (see the rhizomatous hypothesis below).

Ontogenetical interpretations of the Montagne Noire specimens – The different ontogenetic stages defined by Soria and collaborators (2006), are aligned with the ontogenetical hypothesis, our preferred hypothesis for explaining the observed stele diversity in the specimens of *C. taeniatum* in the present study. Using the characters correlation from the specimens of *C. taeniatum* included in the PCA analysis, we have shown that the number of ribs is highly correlated with the amount of primary growth and the diameter. In addition, another interesting correlation is the fact that the amount of primary and secondary vascular tissues varies together independently of the diameter (Figure 3.8A). Note that MN 918 and MN 926 seem to highly weaken this correlation (0.46 with them, 0.83 without) but we interpret this as being due to their early stage of secondary growth (see *Primary vascular system* above [Figure 3.8B]). The correlation between the amount of primary and secondary growth can be used to identify the different growth phases defined by Eggert (1961) without information about the location of the different specimens in the plant, as has been done previously for example for *Armoricaphyton chateaupannens* (Gerrienne and Gensel, 2016). Indeed,

from the base to the apex of the plant 1) during an apoxogenetic phase of growth the amount of secondary and primary tissues might decrease together (i.e. a positive correlation), 2) during an epidogenetic phase the amount of secondary tissue decrease and primary growth increase (i.e. a negative correlation), and 3) during a menetogenic phase, secondary tissues decrease but primary tissues remain the same (i.e. no correlation). Using this framework, the positive correlation between the surface of the primary and secondary xylem recovered in our analysis might be testimony of an apoxogenetic phase of growth in *C. taeniatum*. Furthermore, the different groups recovered from our hierarchical clustering analysis fit well with different parts of a same axis order undergoing an apoxogenetic phase of growth (Figure 3.8). In this paradigm, 1) cluster 4 corresponds to the most basal part of the plant with a lot of primary and secondary xylem, 2) cluster 2 and 3 specimens might represent the same position in the axis (based on their amount of primary xylem) but with different amounts of secondary xylem (specimen from cluster 2 represent younger plants than cluster 3), and 3) specimens from cluster 1 represent the most apical parts, with the smallest amount of primary xylem. Although cluster 1 specimens possess a small amount of primary xylem, their secondary xylem seems to be in stage 3 (i.e. secondary xylem surrounds unevenly the ribs) meaning that they might represent fully developed apical part of the plants (Figure 3.8). The stele morphotype 3 specimen (MN 921) was not included in the cluster analysis, but it is identified as *C. taeniatum* and is the largest of the sample with the highest number of ribs. This characteristic suggest that it might represent a (very) basal part of the plant at the beginning of the apoxogenetic phase of growth (Figure 3.9).

The extant bracken fern *Pteridium aquilinum* provides an analogy to this interpretation of *C. taeniatum* ontogeny. *In P. aquilinum* an underground rhizome produces rachises with a radially symmetrical stele composed of several vascular bundles (Brodersen et al., 2012) that can be considered as analogous to *Cladoxylon* primary ribs. The decreases in diameter from the base toward the apex of the rachis in *P. aquilinum* is correlated with a decrease in both the amount of primary xylem and the number of vascular bundles (Brodersen et al., 2012), which is comparable to our ontogenetical hypothesis for *C. taeniatum* axes.

Since all plants possess at the beginning of their development an epidogenetic phase of growth (Gerrienne and Gensel, 2016), this also has to be the case for *C. taeniatum*. Insights into this growth phase in the sample is more limited than for apoxogenesis, but may be provided by specimens MN 400 and MN 904 (i.e. stele morphotype 2), both characterized by an extensive amount of secondary xylem for a small amount of primary xylem. MN 400 has more secondary xylem (68.6 mm^2 vs. 53.9 mm^2 for MN 904) but less primary xylem (5.3 mm^2 vs. 5.5 mm^2) and less ribs (7 vs. 11). The comparison of the two specimens thus shows a putative negative

correlation between primary and secondary growth of stele morphotype 2 specimens, a feature that might correspond to an epidogenetic phase happening in the basalmost part of *C. taeniatum* (Figure 3.9). In any case, a basal location of these specimens within the plant is consistent with their well-developed periderm, thick-walled endodermis, and emission of laterals organs interpreted as roots (Figures 3.7L–M).

3.5.4 *Cladoxylon taeniatum* architecture and comparison with other cladoxylopsids

The Montagne Noire specimens allow us to put forward updated hypotheses on the architecture of *C. taeniatum*. First, using the different specimens that show lateral organ emission, we have shown that *C. taeniatum* stems possesses petiole-like organs that are emitted in spiral and bear opposite to alternate dichotomous ultimate appendages. Second, based on the correlation between the amount of primary *vs* secondary xylem, we have shown that *C. taeniatum* possesses an apoxogenetic phase of growth (Figure 3.8). Third, its secondary xylem growth seems determinate and follows a pattern of development around the ribs leading to an unequal distribution with more secondary xylem toward the center of the axis (Figure 3.8B). Four, specimens with stele morphotype 2 (MN 400 and MN 904) correspond to basal parts of the plant with a lot of secondary vs. primary growth, root traces, and may be interpreted as corresponding to an epidogenetic phase and/or to less rigid portions of axes.
Based on this information, we can hypothesize 2 different habits for *C. taeniatum* (Figure 3.9):

1) a *Pietzschia*-type habit, where *C. taeniatum* is a monocaulous, self-supporting to semi-self-supporting species with a determinate growth, undergoing a basal epidogenesis followed by an apoxogenesis phase of growth. In this hypothesis, morphotype 2 specimens (MN400 and 904) are interpreted as representing the epidogenetic phase of the stem. The monocaulous part of the hypothesis is based on the fact that no *Cladoxylon* dichotomizing or emitting a lateral axis looking like another *Cladoxylon* has not been found among the 53 Montagne Noire specimens. The *Pietzschia*-type habit is based on the identification of similar growth phases. Indeed, the apoxogenetic growth exhibited by the *C. taeniatum* specimens makes them more similar to the growth model proposed for *Pietzschia* (Soria and Meyer-Berthaud, 2004; Meyer-Berthaud et al., 2010) -but with secondary growth involved- than to the models proposed for *Pseudosporochnus* (Berry and Fairon-Demaret, 2002) or *Calamophyton* (Giensen and Berry, 2013). This hypothesis is also consistent with the phylogenetic position of *Cladoxylon* that belongs with *Pietzschia* to the non-pseudosporachnealean (Meyer-Berthaud et al., 2007) monophyletic group (or cladoxylalean cladoxylopsids of Durieux et al. [2021]). A notable difference is that *Pietzschia* possesses a mantle of adventitious roots in its basal part, while MN 400 and MN 904 only show evidence of isolated roots.

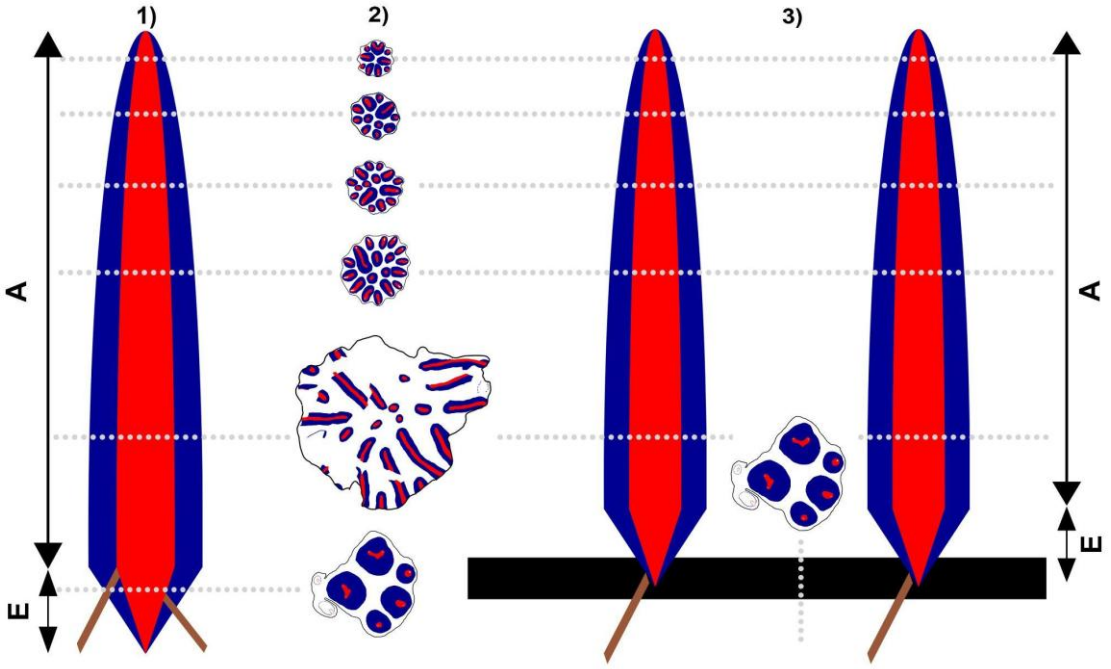

Figure 3.9 Illustration of the two hypothesized habits of *Cladoxylon taeniatum*.

Color code protoxylem in grey, primary xylem in red, secondary xylem in blue, and stele/specimens limits in black line. The *Pietzschia* habit hypothesis is represented in 1) and the creeping hypothesis in 3). Grey dashed lines represent the virtual placement of the specimens' stele drawings (2), brown rectangles represent roots, and the black rectangle the putative creeping part. “A” and “E” mapped plant parts that are respectively in apoxogenetic and epidogenetic phases of growth.

2) a rhizomatous habit, where *C. taeniatum* is interpreted as composed of underground or creeping non-self-supporting axes (rhizomes) that bear self-supporting stems. In this hypothesis, morphotype 2 specimens are interpreted as representing the rhizomes of *C. taeniatum* while the other specimens represent the self-supporting stems. The interpretation of morphotype 2 specimens as creeping axes is based on the preliminary biomechanical study of Soria and collaborators (2006), and on the occurrence in this morphotype of root traces (Figures 3.7L–M) and a mesarch trace (Figure 3.7K) with different angle of emission produced at a same node (Figure 3.6E). A similar emission process is observed in extant ferns with an emission at the same node of a leaf and a root (a stem-born root in the literature) originating from the same apical cell (Hou and Hill, 2002; Hou and Blancaflor, 2009; Aragón-Raygoza et al., 2020). In addition, the repartition of the secondary xylem around the traces is different with the mesarch trace showing this tissue only on one side and the root been surrounding evenly. This might indicate that this trace, as for the other traces, needs a

biomechanical support. A comparable hypothesis was first discussed by Solms-Laubach (1896) and there is at least one example of a rhizomatous cladoxylopsid, i.e., *Metacladoxylon tetraxylum* (Wang and Geng, 1997). However, in the absence of evidence of a *C. taeniatum* stem produced by a morphotype 2 specimen, this hypothesis is not entirely supported at this stage.

3.6 Conclusion

The majority of *Cladoxylon* specimens found in the Montagne Noire deposits belong to *C. taeniatum*, but *C. mirabile* is also likely present. The architecture *of Cladoxylon taeniatum* is reconstructed as characterized by a putative basal phase of epidogenesis and a phase of apoxogenetic growth involving a diminution of the number of ribs that is similar to *Pietzschia levis's* growth pattern (Soria et al., 2001; Soria and Meyer-Berthaud, 2004). However, unlike *Pietzschia*, *C. taeniatum* growth involved secondary growth of two type of tissues, the secondary xylem and the periderm. In term of organotaxis, *C. taeniatum's* basal parts emit alternately traces for aerial organs and roots at the same node, and the more apical parts emit in a spiral petiole-like organs bearing alternate to opposite dichotomous ultimate appendages. These advances in the understanding of *Cladoxylon taeniatum* lead to two hypotheses about its habit: (1) a monocaulous self-supporting to semi-self-supporting plant like *Pietzschia*, or (2) a plant with rhizomatous axes emitting self-supporting stems with a *Pietzschia* growth type (Figure 3.9).This is the first reconstruction of the architecture of a non-arborescent cladoxylopsid and an important addition to our understanding of the diversification of plant's habits during the late Devonian-early Carboniferous period.

Chapter 4

Woody plants and palaeoenvironements: a new group crossing the Devonian-Carboniferous boundary

Published as: Durieux, T., Decombeix, A.-L., and Harper, C.J. 2024. Re-investigation of *Stauroxylon beckii*, a possible aneurophytalean progymnosperm from the Mississippian of France. International Journal of Plant Sciences, 729412. https://doi.org/10.1086/729412

Figure, table, section numbers, and citation style have been modified to fit the manuscript's purpose.

4. Re-investigation of *Stauroxylon beckii*, a possible aneurophytalean progymnosperm from the Mississippian of France.

4.1 Abstract

Premise of the Research. The fossil record shows that seed plants appeared during the Devonian and started to become dominant in the Mississippian. However, the identity of their closest relatives remains uncertain with three candidates: Stenokoleales, Archeopteridalean progymnosperms, and Aneurophytalean progymnosperms. To clarify the relationships of these groups, it is necessary to document as many Devonian-Missisippian taxa as possible and increase taxon sampling in phylogenetic analyses. In this context, *Stauroxylon beckii* Galtier 1970 from Mississippian deposits of France is particularly interesting because of its similarities with both seed plants and some of their potential closest relatives. Here, we provide an updated description of *Stauroxylon* and discuss its affinities using morpho-anatomical comparisons and phylogenetic analyses.

Methodology. The holotype of *Stauroxylon beckii* and a new specimen from the same formation are described using thin-sections, cellulose acetate peels, and polished surfaces. The morpho-anatomy of the specimens is compared to that of early seed plants and their putative relatives. *Stauroxylon* is also included in phylogenetic analyses of the Radiotopses based on Toledo et al, 2021's matrix.

Pivotal Results. Stauroxylon beckii possess a cruciform protostele with protoxylem strands at the tips of the ribs, a central protoxylem strand, and produces second and third order axes in perpendicular planes. The new specimen differs by characters interpreted as developmental differences or intraspecific plasticity (organotaxis, secondary growth) and is also assigned to *Stauroxylon beckii*. Both comparative approaches and phylogenetic analyses place *Stauroxylon* within the Aneurophytalean progymnosperms, a group previously only known in the Devonian. The inclusion of *Stauroxylon* strengthens previously established relationships within the radiatopsids. *Stauroxylon* also displays structural fingerprints important for leaf and pith evolution.

Conclusions. Stauroxylon is interpreted as a Mississippian representative of the Aneurophytales. It provides new information on the relationships and morpho-anatomical diversity of early seed plants and their closest relatives.

4.2 Introduction

Understanding the early stages of seed plant evolution in the Devonian and Carboniferous and the identity of their sister group are key research topics in paleobotany. The first occurrence of fossil seeds and vegetative remains with a possible seed plant affinity is a Middle-Late Devonian event (May and Matten, 1983; Rothwell et al., 1989; Gerrienne et al., 2004), and the candidates for their closest relatives are taxa that appeared during the Devonian and disappeared at, or soon after, the end of this period. Three groups have been proposed in the literature, all sharing important morpho-anatomical features with the early seed plants, (1) the Archaeopteridalean and (2) Aneurophytalean progymnosperms and the (3) Stenokoleales, (Matten and Banks, 1969; Rothwell and Erwin, 1987; Beck and Stein, 1993; Galtier and Meyer-Berthaud, 1996; Toledo et al., 2018, 2021).

The progymnosperms include three different orders (Beck, 1960c; Beck and Wight, 1988), the Devonian Archaeopteridales and Aneurophytales (Rothwell and Serbet, 1994; Gerrienne et al., 2016; Toledo et al., 2021) and the Carboniferous Protopityales (Beck, 1976; Decombeix et al., 2015). The progymnosperms have been grouped with the seed plants within the Lignophyte division of Crane (1985: "unnamed group" p.720; Doyle and Donoghue, 1986) based on the shared possession of a bifacial vascular cambium producing both secondary xylem and secondary phloem. Unlike seed plants, the progymnosperms all reproduced by spores, with both homosporous and heterosporous representatives (Beck and Wight, 1988). It is still debated (1) whether the progymnosperms are a monophyletic group or a grade, and (2) which one of the three orders is the most closely related to the seed plants. The Protopityales, represented by the single genus *Protopitys*, are unknown in the Devonian, making them too young to be considered good candidates. Arguments to place the Aneurophytales as the closest relatives of early seed plants are mostly related to characters of the stele anatomy (Rothwell and Erwin, 1987), whereas for the Archaeopteridales the evidence is partly based on the reproduction (Beck, 1981).

The Stenokoleales (Matten and Banks, 1966; Beck and Stein, 1993) are an enigmatic Devonian-early Carboniferous family for which only information on the anatomy of main axes and first-orders laterals is known. The anatomy of their distal parts (vegetative or reproductive) and their external morphology remain unknown (Galtier, 2010). Stenokoleales are represented by three genera: *Stenokoleos* (Hoskins and Cross, 1951), *Crossia* (Beck and Stein, 1993), and *Brabantophyton* (Momont et al., 2016a, 2016b). Their stele anatomy is relatively similar to that of the earliest seed plants (Beck and Stein, 1993) and both *Brabantophyton* and *Crossia* possess secondary xylem (Beck and Stein, 1993; Momont et al., 2016a, 2016b) which led some authors (i.e.

Matten and Banks, 1969; Galtier and Meyer-Berthaud, 1996; Momont, 2015; Toledo et al., 2018) to suggest a close relationship with the seed plants.

While the Devonian saw the origin of the seed plants, the early Carboniferous (Mississippian) is the period that witnesses the first major diversification of this group (Galtier, 1988: fig 3.1). Among their possible sister groups, the last Stenokoleales are early Mississippian in age (Cross and Hoskins, 1951; Beck, 1960b). The Archaeopteridalean progymnosperms may have crossed the Devonian/Carboniferous boundary (although this is contingent to a revised dating of some "early Tournaisian" deposits, (Cross and Hoskins, 1951; Beck, 1981; Beck and Wight, 1988) but there are no Aneurophytalean progymnosperm reported in the Carboniferous. One possible and intriguing exception however is *Stauroxylon beckii,* an anatomically preserved plant from middle Tournaisian (early Mississippian, *ca*. 350 Ma) deposits of the Montagne Noire region in southern France. The original description of *Stauroxylon* (Galtier, 1970) was in French and this taxon has rarely been mentioned in the literature afterwards, despite having an interesting combination of characters, including a cross-shaped actinostele with 5 permanent strands of mesarch protoxylem, and relatively well-developped secondary xylem. Despite a good understanding of the specimen's unique stem anatomy and lateral organs emission, the lack of reproductive structures prevented its assignment to a well-defined group. Galtier (1970) compared *Stauroxylon* with the seed plant *Tetrastichia* (Gordon, 1938; Dunn and Rothwell, 2012), the Aneurophytalean progymnosperm *Tetraxylopteris* (Beck, 1957; Scheckler and Banks, 1971a), the Archaeopteridalean progymnosperm *Actinoxylon* (Matten, 1968), and the Stenokoleale *Stenokoleos* (Hoskins and Cross, 1951; Beck, 1960b; Matten and Banks, 1969; Beck and Stein, 1993). Galtier (1970) also noted some similarities with the Iridopteridales and Cladoxylales, extinct relatives of the ferns *s.l.* (i.e. Moniliformopses, Kenrick and Crane, 1997; Durieux et al., 2021). Galtier (1970) concluded that *Stauroxylon* was probably a progymnosperm, likely a representative of the Aneurophytales. This hypothesis was later shared by Beck (1976) and by Stein (1982b).

Despite its intriguing possible affinities with Devonian Aneurophytales and its well-understood stem anatomy, *Stauroxylon* was never included in phylogenetic analyses. In the current stage of our knowledge, it however seems important to test its relationships, especially since Toledo et al. (2021) showed that the phylogenetic signal between Aneurophytales, Archeopteridales, and Stenokoleales can change under different taxon sampling. It is therefore important to include and test the phylogenetic relationships of *Stauroxylon* in these analyses. In this context, we present here a re-investigation of *Stauroxylon beckii* using the original description of Galtier (1970), new observations and measurements of the holotype, and data from a new specimen from the same deposit. We combine a classical comparative approach and the first inclusion of *Stauroxylon* in a

phylogenetic analysis to discuss its affinities in the light of our current understanding of Stenokoleales, progymnosperms, and early seed plants.

4.3 Material and Methods

4.3.1 Geological context, fossil preparation and imaging

The holotype of *Stauroxylon beckii* (Galtier, 1970) was found in the Lydienne formation, south-east of the village of St Nazaire de Ladarez in southern France (Hérault).

The Lydiennes Formation corresponds to sedimentary deposits in a shallow sea and consists of alternating beds of argilites and radiolarian cherts containing phosphatic nodules. Horizons containing plant fossils are considered middle Tournaisian in age (Tn2a–Tn2b) based on conodonts (Galtier et al., 1988; Feist et al., 2021). More than 500 specimens representing at least 30 plant taxa have been collected to date in the Lydiennes Formation (Galtier et al., 1988; Decombeix et al., 2020), constituting one of the most diverse plant assemblage of that time period.

The holotype (MN218) was initially analyzed by Galtier (1970) by observing polished surfaces, taking a picture using reflected light with a Ultropak Leitz device, then griding down the polished surface, and repeating the process. This technique is highly destructive because only the photographs remain. On the other hand, it can lead to better observations of the different levels of the plant than using peels or thin-sections. As a result of the destruction of part of the material, some of our reinvestigation is based on the black and white photographs taken by Galtier (1970), via the original 35 mm negative films scanned using a scanner Epson Perfection V850 Pro.

A second specimen (MN 297) found in the Lydienne Formation near Coumiac (Feist et al., 2021: fig 1), had been partially prepared by Galtier who had made 2 thin-sections and 28 acetate peels. For the current study, 72 additional peels were prepared according to standard cellulose acetate peel techniques (Joy et al., 1956; accession numbers: MN 297 B top 2-32, MN 297 C Bot 3-33, MN 297 GL 1-12).

Images from both specimens were taken with a Keyence VX7000 digital microscope at UMR AMAP, France. Some photos were taken with the peel still on the specimen to improve contrast. Images were processed minimally (e.g. brightness and contrast) and converted to greyscale to allow a better comparison with the original images of the holotype taken by Galtier (1970) using Adobe

Photoshop version 7.0 (San José, CA, USA). All measurements were made with ImageJ (https://imagej.nih.gov/ij/). Cell diameter measurements are given for the widest dimension unless specified otherwise.

Specimens, slides, peels, and films are part of the Collections de Paléobotanique of Université de Montpellier and are deposited at UMR AMAP, under accession numbers MN 218 (holotype) and MN 297.

4.3.2 Phylogenetic analyses

The phylogenetic analyses, Bremer support, and bootstrapping were conducted using the methodology and the morphological matrix of Toledo et al. (2021:cf. S4: Parsimony analyses). Phylogenetic analyses with parsimony as the optimal criterion were conducted using TNT 1.5 (Goloboff and Catalano, 2016) in Windows 10. The matrix (Appendix C.3) used corresponds to the TEA ++ version of Toledo et al. (2021) and includes 50 characters, 9 of them continuous and the others discrete, and 32 taxa, 31 scored by Toledo et al. (2021) and *Stauroxylon beckii*. We scored *Stauroxylon beckii* as a plant possessing a bilateral organotaxis domain *sensu* Toledo et al. (2021). One character in *Tetrastichia bupatides* (C33 = ?) became polymorphic ([1 & 2], i.e. sparganum and dictyoxylon outer cortex) and one in *Laceya hibernica* has been re-scored (Character 1 was corrected from 0.093 -exact same as *T. longii* just above it- to 0.134). Character 4 has also been modified in all the taxa since values for *Stauroxylon* were outside the range of the other taxa, leading to a different value of standardization of this character.

4.4 Results

4.4.1 Holotype (MN 218), Figures 4.1–6

General aspect – *Stauroxylon beckii* is preserved in a 6 cm long phosphatic nodule. The main axis is about 9 mm in diameter. In cross-section, *S. beckii* displays a central cross-shaped actinostele surrounded by secondary xylem and cortex, with conspicuous traces to lateral organs (Figure 4.1A). The distance between the tips of two opposite ribs of the actinostele is 5 to 6.4 mm. This distance between the tips of the ribs and the general diameter of the axis do not vary much and are relatively uniform along the preserved length of the specimen.

Primary xylem – The primary xylem is composed of polygonal metaxylem tracheids (Figure 4.1A) and parenchyma at the level of the protoxylem (Figures 4.1B, 4.1C, 4.1D). The protoxylem strands are located at the rib tips, with an additional strand in the center of the stele. There are no strands in the midplanes of the ribs (Figures 4.1B, 4.1C, 4.4).

The protoxylem strands have a mesarch maturation and are composed of protoxylem tracheids surrounding parenchyma cells. In cross section, the protoxylem strands at the tip of the ribs are elliptical (about 3 times wider radially than tangentially), 0.25–0.7 mm long and about 0.1 mm wide (Figure 4.1B), or circular with a diameter about of 160–260 µm (Figures 4.1C, 4.1D). Under the circular strands, there is also a poorly preserved tangentially elongated zone of the same cell type (Figures 4.1C, 4.1D, at arrowhead) that may also be part of the protoxylem strands. The size and shape of strands may vary during the emission of vascular traces, but it is observed in 5 out of 6 of the cross sections.

The central strand is slightly ellipsoidial, but primarily circular and is about 0.2 mm in diameter (Figure 4.2A), however, in most sections, the edges of the strand are not clear. Nevertheless, in some instances it appears much larger, about 0.3 to 0.4 mm (see variation in Figure 4.4). At the base of the specimen, the central strand is four-lobed (Figure 4.2B) and approximately 0.4 mm in diameter. In longitudinal section, the central strand corresponds to an area of parenchymatous cells and tracheids with reticulate to scalariform pitting (Figure 4.2C). Unlike in the strands located at the rib tips, protoxylem and parenchyma cells are highly intermixed within this central strand. Protoxylem tracheids are 12–34 µm in diameter (n=50). In longitudinal section, the protoxylem tracheid walls bears reticulate to scalariform pits (Figures 4.2C, 4.2D). In the center of the strand, cells with thin walls and polygonal to round shapes are interpreted as parenchyma (Figure 4.2E). They are wider (14–61 µm, n=50) than the protoxylem tracheids (Figure 4.2E) and of various heights (24–120 µm, n=20). Metaxylem tracheids are polygonal, usually larger in their radial dimension, and bigger toward the center of the stele (Figure 4.1A), leading to cells with disparate sizes ranging in diameter from 14 to 136 µm (n=400). Moreover, these tracheids (which can be partially observed in longitudinal section) are > 3 mm in length according to Galtier (1970). The walls are pitted on all faces. The smallest tracheids have scalariform pitting (Figure 4.2F), while larger ones have bi- to multiseriate pits that are circular to elliptical in shape and 9–16 µm in diameter (N = 20). These pits are alternate to opposite (Figure 4.2G). No parenchyma cells were observed in the metaxylem.

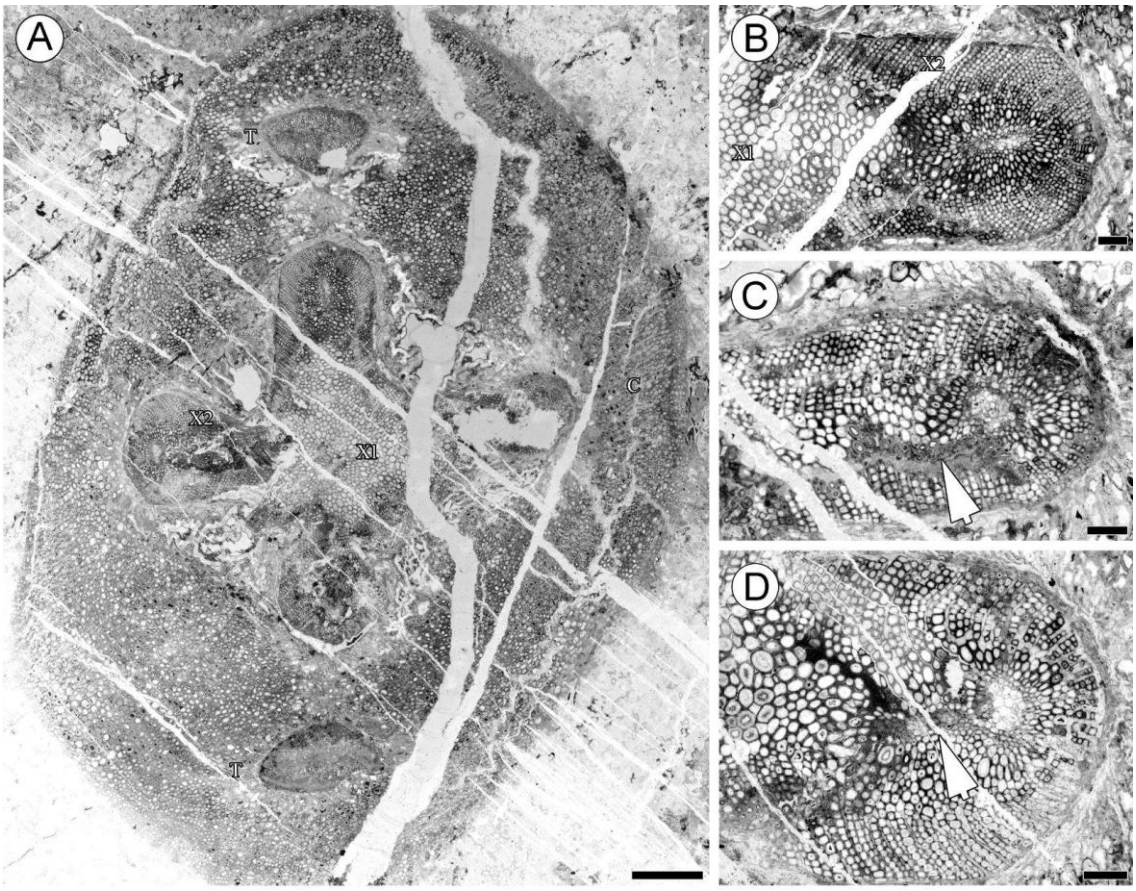

Figure 4.1 *Stauroxylon beckii*, holotype. General aspect and primary xylem organization.

(A) Cross section of main axis showing a cruciform actinostele, secondary xylem, and two opposite traces; scale bar = 1 mm; slide MN218-AI 01; C: Cortex, T: Traces, X1: Metaxylem, X2: Secondary xylem. (B) Buttonhole-shaped protoxylem strand at the tip of a rib; that rib corresponds to the upper rib in A and the right rib of Figures 4.4C, 4.5C; scale bar = 200 µm; slide MN 218-AI 01. (C) Circular protoxylem strand at the tip of another rib (bottom rib of Figures 4.4B, 4.5B) with a badly preserved zone which may be part of the protoxylem strand (arrowhead); scale bar = 200 µm; slide MN 218-BS 02. (D) Circular protoxylem strand at the tip of a rib (upper rib of Figures 4.4B, 4.5B) with a badly preserved zone which may be part of the protoxylem strand (arrowhead); scale bar = 200 µm; slide MN 218-BS 02.

Secondary xylem – The secondary xylem is 0.15–0.55 mm in thickness (Figure 4.1A), and composed of tracheids and rays. In cross section, the tracheids are rectangular to hexagonal, with smaller diameters than those of the metaxylem (15–50 µm, n=50). In longitudinal section, walls are pitted on all faces, typically with scalariform pits (Figure 4.2H), but a few displays circular bordered pits (Figure 4.2I). The rays are numerous and parenchymatous. In cross section, they separate 1-8 files of tracheids, but most commonly 2. The innermost ray cells, at the contact with the metaxylem, are larger (Figures 4.1B, 4.1C, 4.1D). In tangential section, the rays are usually uniseriate and 1–3 cells high (Figure 4.3A). Ray cells are higher than wide (75–35 µm x 15–40 µm,

n=12). In radial section, ray cells are rectangular and longer than high (75 µm in height, 150 µm in length, n=1, Figure 4.3B). Cross-field pitting was not observed.

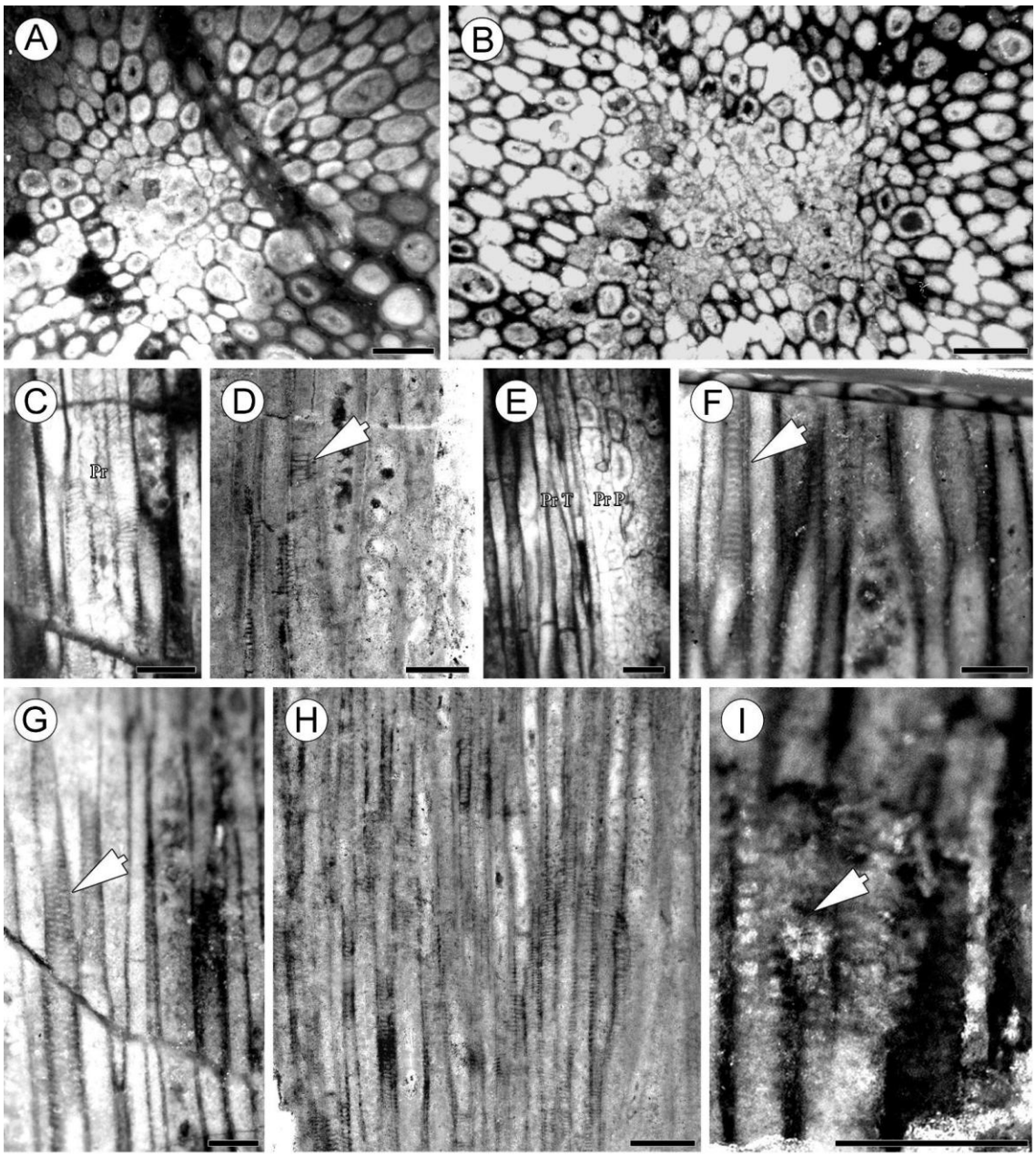

Figure 4.2 *Stauroxylon beckii* holotype. Primary and secondary xylem anatomy.

(A) Central circular protoxylem strand in cross section; scale bar = 100 µm; scan Galtier's film n° 134 (Figure 4 plate 49, Galtier 1970) section MN 218- BL 18. (B) Central four-lobed protoxylem strand in cross section; scale bar = 100 µm; scan Galtier's film n° 104 (Figure 1 plate 50, Galtier 1970) section MN 218-BI. (C) Central protoxylem strand in longitudinal section close to the level of Figure 4.1A; scale bar = 100 µm; scan Galtier's film n° 133 (Figure 5 plate 49, Galtier 1970) section MN 218-BL 17; Pr: Protoxylem strand.

(D) Reticulate (arrowhead) to scalariform pits of the protoxylem; scale bar = 100 µm; slide MN 218-AL 01. (E) Buttonhole-shaped protoxylem strand in longitudinal section; the parenchyma cell (Pr P: Protoxylem parenchyma) in the right part of the picture and the 3 small tracheids just toward them corresponding to the protoxylem (Pr T); scale bar = 100 µm; scan Galtier's film n° 135 (Figure 5 plate 50, Galtier 1970) section MN 218-BL 18. (F) Scalariform pits on the wall of a small metaxylem tracheid (arrowhead); scale bar = 100 µm; longitudinal section with peel on the specimen 218. (G) Metaxylem tracheid with multiseriate pits (arrowhead); scale bar = 100 µm; longitudinal section with peel on the specimen 218. (H) Secondary xylem tracheids with scalariform pits; scale bar = 100 µm; slide MN 218-AL 01. (I) Secondary xylem with poorly preserved bordered pits (arrowhead); scale bar = 100 µm; longitudinal section with peel on the specimen 218.

Phloem – The phloem tissue is reduced (Figure 4.3E) and rarely preserved. When it is present the cells are poorly preserved. In cross section, the phloem is one to three cells thick and composed of small polygonal cells with thin walls that are 19–58 µm wide (n=20) (Figure 4.3D). Thin-walled phloem cells that are narrow and elongated in longitudinal section may represent sieve cells (Figure 4.3C, at arrowhead). There are no conspicuous fibers. Phloem cells seem to be radially aligned (Figure 4.3D, at arrowhead) suggesting a secondary origin but phloem rays have not been identified.

Cortex – Distal to the phloem, two different cortical zones can be distinguished. They are not easily identifiable in cross section (Figure 4.3F) but are relatively clear in longitudinal view (Figure 4.3G). From the center of the stem towards its periphery, the first zone is about 1 mm thick, the second is larger (about 2–4mm) and better preserved.

The first cortical layer is composed of large polygonal cells (40–190 µm wide) with thickened walls. In longitudinal section these cells are more or less rectangular (43–170 µm high and 66–188 µm wide, n=20) and arranged in vertical files (Figure 4.3G, at black star).

The second cortical layer (Figures 4.3F, 4.3G) is formed by cells that are round in cross section, with thickened walls and a highly variable diameter (35–141 µm, n=20). In longitudinal section, these cells are elongated (0.3–1.2 mm long, n=20) and thus easy to distinguish from those of the first zone (Figure 4.3G).

A third zone composed of smaller cells can be distinguished in some parts of the specimen (Figure 4.3G), but cells are not clearly different from that the second zone, so we consider this as a simple variation in size of cells from the outer cortical zone.

The axis was likely eroded before fossilization and the epidermis is missing, as could be the most external part of the cortex.

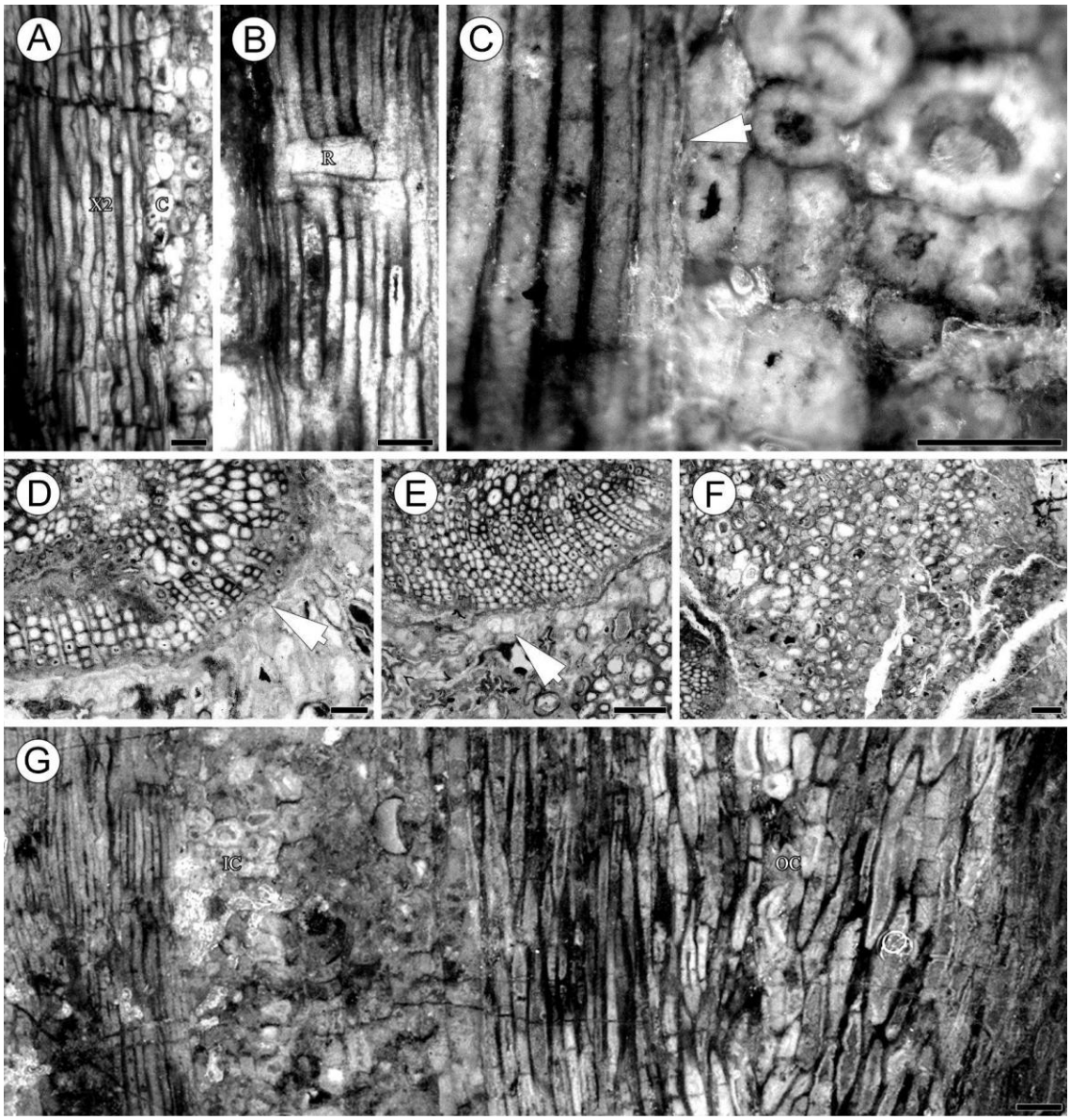

Figure 4.3 *Stauroxylon beckii*, holotype. Secondary xylem and cortex.

(A) Tangential section showing secondary xylem with short uniseriate rays and the inner cortex; scale bar = 100 µm; scan Galtier's film n° 124 (Figure 6 plate 51, Galtier 1970) section MN 218-BL 09; C: Cortex, X2: Secondary xylem. (B) Radial section showing secondary xylem with one ray (R); note the pitting on the radial walls of tracheids; scale bar = 100 µm; scan Galtier's film n°140 (Figure 1 plate 51, Galtier 1970) section MN 218-BL 22-23. (C) Putative phloem sieve cell (arrowhead) in longitudinal section; scale bar = 100 µm; longitudinal section with peel on the specimen 2018. (D) Phloem cells in transversal view; note the arrowhead pointing to three aligned cells, scale bar = 100 µm; slide MN 218-BS 02. (E) Transverse section showing the proximity of inner cortex cell (arrowhead) and the secondary xylem; scale bar = 200 µm; slide MN 218-AI 02. (F) Transverse section of the cortex; scale bar = 200 µm; slide MN 218-AI 02. (G) Longitudinal section of showing the inner cortex (IC) and the outer cortex (OC); scale bar = 200 µm; longitudinal section with peel on the specimen 218.

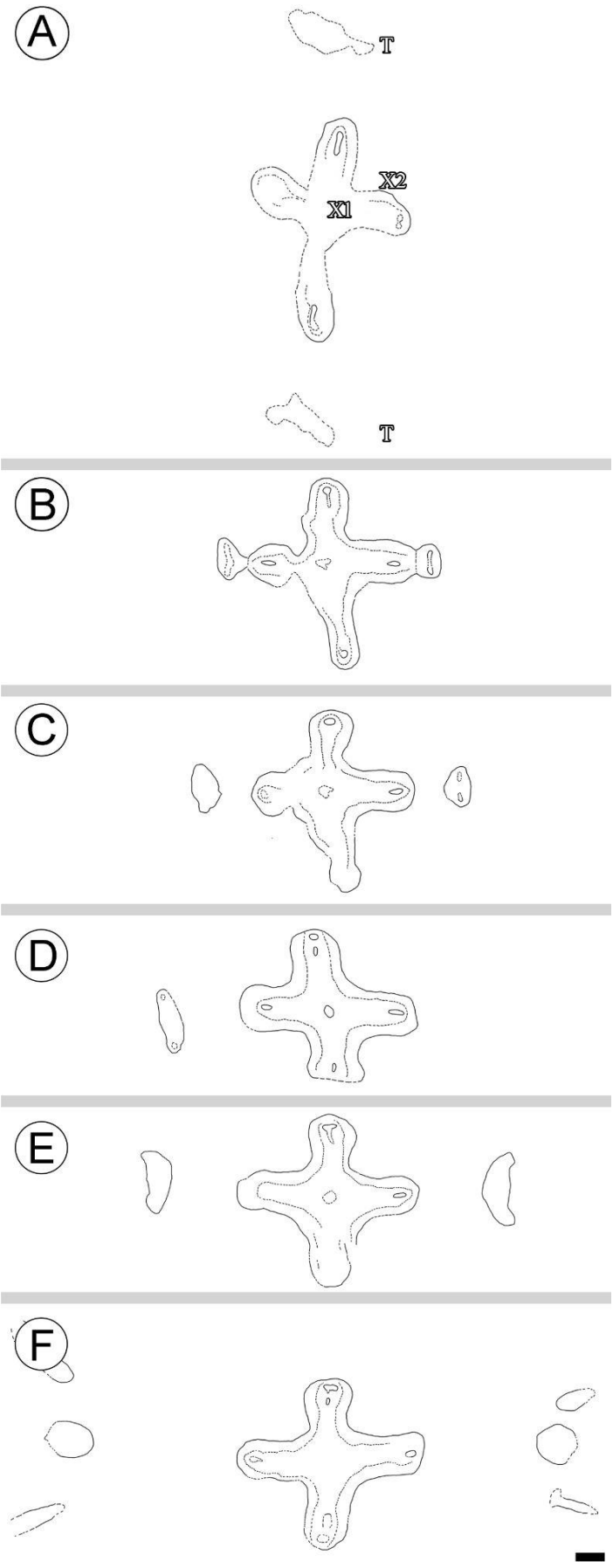

Traces to lateral organs- The central protoxylem strand is not involved in the emission of lateral traces (Figure 4.4). The emission of vascular traces to lateral organs departing from the tips of the ribs occurs according to a decussate opposite organotaxis (Figures 4.4, 4.5). Two traces are emitted at a same level, from two opposite ribs of the primary xylem (Figures 4.4A, 4.5A). At the following node, the other two ribs emit traces (Figures 4.4B–F, 4.5B–F). During the emission, the two opposite traces diverge from the main axis stele at the same speed (Figure 4.4). Internodes are estimated to be about 18 mm.

Figure 4.4 *Stauroxylon beckii*, holotype. Camera lucida drawings of serial transverse sections showing lateral traces emission; scale bar = 1 mm.

(A) Slide MN218-BS 04. (B) Slide MN 218-BS 02. (C) Slide MN 218-BS 01. (D) Slide MN 218-AS 02. (E) Slide MN 218-AI 01. (F) Slide MN 218-AI 02; C: Cortex, T: Traces, X1: Metaxylem, X2: Secondary xylem.

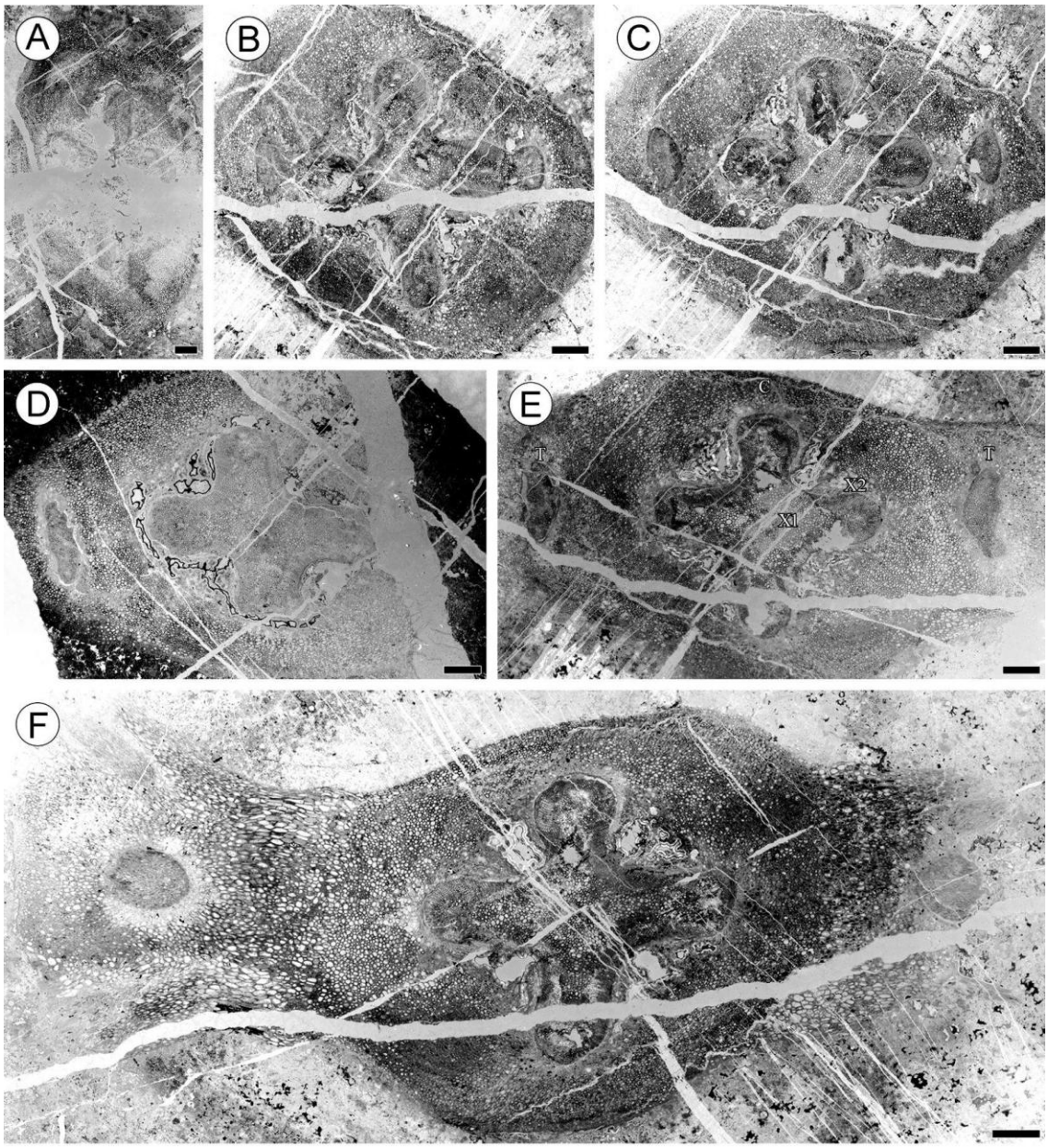

Figure 4.5 *Stauroxylon beckii*, holotype. Transverse sections corresponding to the drawings on Figure 4.4; scale bar = 1 mm.

(A) Slide MN 218-BS 04. (B) Slide MN 218-BS 02. (C) Slide MN 218-BS 01. (D) Slide MN 218-AS 02. (E) Slide MN 218-AI 01; C: Cortex, T: Traces, X1: Metaxylem, X2: Secondary xylem. (F) Slide MN 218-AI 02.

The detailed mechanism of a lateral organ emission is presented in the drawings on Figure 4.4 and the corresponding pictures in Figures 4.5 and 4.6. First, the protoxylem strand at the tip of a rib, which normally has the aspect of a radially elongated lenticular shape with a circle at one end, henceforth referred to as 'buttonhole' shaped (Figure 4.1B), expands towards the outside (Figures 4.1C, 4.1D). A tangential division then gives the strand an overall T-shape (Figure 4.6A). The radial expansion continues until it has crossed the secondary xylem layer of the main axis (Figure

4.6B). At that point, the strand that will belong to the departing trace disconnects from the more internal strand, which becomes very reduced (0.2 mm long) (Figure 4.6B). The protoxylem strand of the stele keeps going straight up and will divide again to produce another second order traces further up. The protoxylem strand of the departing trace continues its tangential elongation (0.75 mm), leading to the formation of two oval strands, which are still linked at the center of the trace (Figure 4.6C).

In the subsequent stages, the tissues representing the exiting organ individualize completely (Figures 4.6D–F) and it becomes triangular (Figure 4.6D), with the apex pointing towards the main axis (the two traces are about 1–4 mm wide by 0.97 mm high and 1.8 mm wide by 1 mm high; Figure 4.6D). The tangentially stretched protoxylem seems to form two opposite oval (tangentially elongated) strands with an unclear boundary at the center of the trace making it difficult to establish if these two strands are independent or not (Figures 4.6D, 4.6E). At this level the extremity of the rib of the main axis is at a resting phase; the secondary xylem surrounds the metaxylem again and the rib protoxylem strand is buttonhole shaped. The outgoing trace remains devoid of secondary xylem.

During its trajectory in the cortex, the outgoing trace keeps increasing tangentially (2.2–2.5 mm), it expands at its two lateral extremities (Figure 4.6E), producing an arc shaped, adaxially concave trace (2.5 mm wide) with the protoxylem not particularly abaxial or adaxial but still mesarch. At a higher level, the trace emits two secondary traces perpendicular to the previous plane of branching (Figure 4.6F). This results in three traces: the circular second order axis (about 1.3 mm wide) accompanied by two small traces of the third order axes, which are emitted in an opposite arrangement in the same plane. The vascularization of these third order axes (Figure 4.6F, at arrowhead) are viewed in longitudinal section due to the oblique trajectory in the second order axis but they are likely circular in cross section. The vascularization of the second order axes changes from a bilateral symmetry with an adaxial/abaxial polarity in the first stage of emission (triangular and arc shaped) (Figures 4.4C–E, 4.5C–E, 4.6D, 4.6E) toward a radial symmetry after the secondary emission (Figures 4.4F, 4.5F, 4.6F). Due to erosion of the specimen, it is not possible to observe the second and third order axes detached from the main axis and the preservation does not allow to see the location and the number of protoxylem strands in the last stage of the emission.

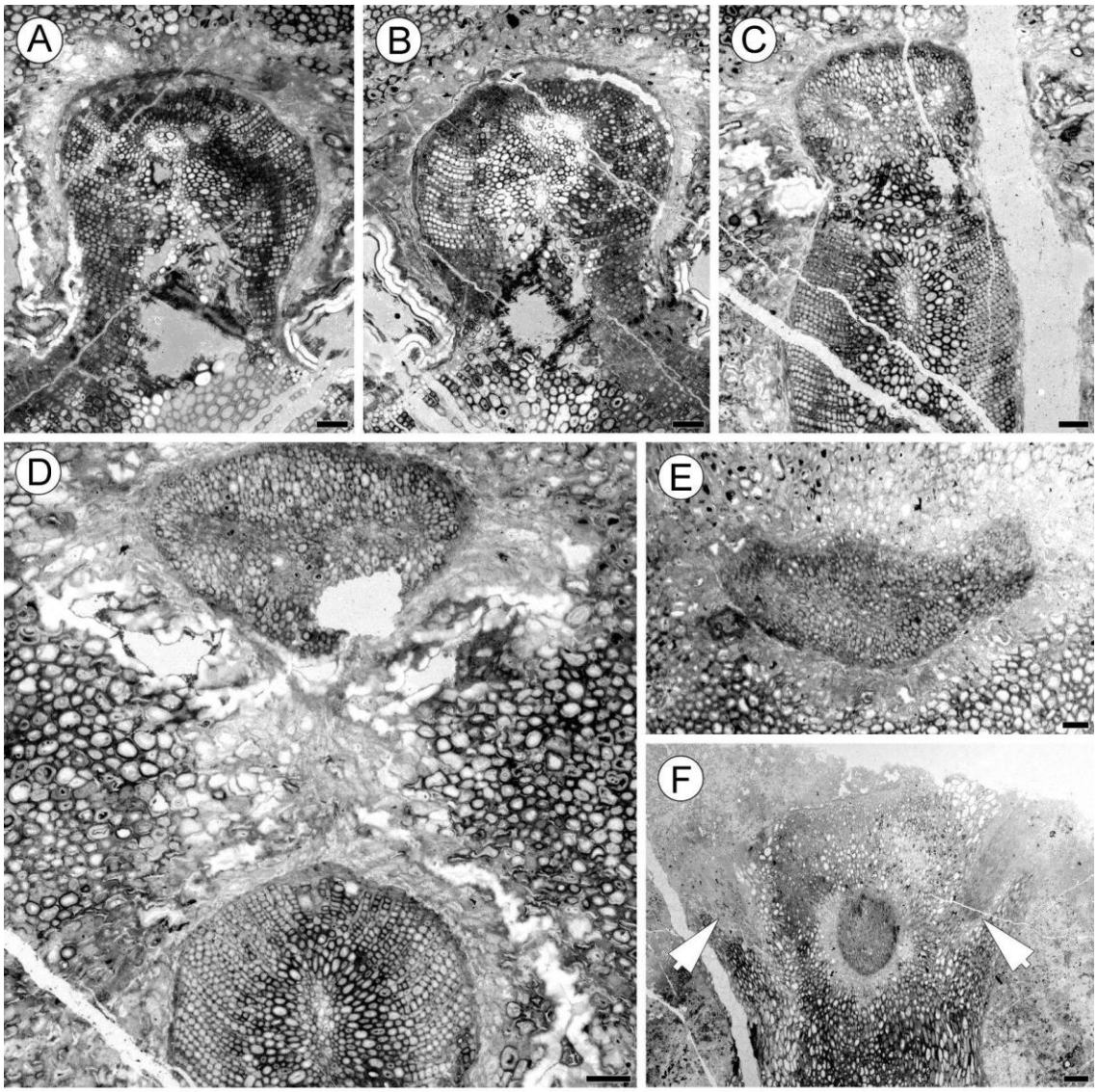

Figure 4.6 *Stauroxylon beckii,* holotype. Anatomy of trace emission.

(A) T-shaped protoxylem strand; that strand corresponds to the upper rib in Figures 4.4E, 4.5E; scale bar = 200 µm; slide MN 218-AI 02. (B) Radial division of the protoxylem strand; that strand corresponds to the upper rib in Figures 4.4F, 4.5F and the secondary xylem stop surrounding the upper part of the rib; scale bar = 200 µm; slide MN 218-AI 01. (C) Last stage of emission before the trace detaches from the stele; that trace corresponds to the right rib in Figures 4.4B, 4.5B; scale bar = 200 µm; slide MN 218-AI 02. (D) Triangular shaped trace; the protoxylem strand is not abaxially or adaxially placed, this trace is emitted by the right rib of Figures 4.4C, 4.5C, and a similar trace is emitted by the opposite rib; scale bar = 200 µm; slide MN 218-BS 01. (E) Arc-shaped trace; the protoxylem strand is not abaxially or adaxially placed, this trace is emitted by the right ribs of Figures 4.4E, 4.5E, and a similar trace is emitted by the opposite rib; scale bar = 200 µm; slide MN 218-AI 01. (F) Circular trace with two opposite third order axis traces; arrowheads mark the base of the third order traces. This trace is emitted by the left ribs of Figures 4.4F, 4.5F, and a similar trace is emitted by the opposite rib; scale bar = 500 µm; slide MN 218-AI 01.

4.4.2 Specimen MN 297 (Figures 4.7–4.11)

General aspect - The specimen is preserved in a cone-shaped phosphatic nodule that is about 4.5 cm long and up to 3 cm wide. The specimen has a cross-shaped actinostele, 4.2 to 4.5 mm from one rib tip to the other (Figure 4.7A). There is no secondary xylem present. The dimensions of the axis do not vary along the nodule, but the overall shape of the stele is twisted in some parts.

Primary xylem - The primary xylem is composed of polygonal metaxylem tracheids without intermixed xylem parenchyma (Figures 4.7A–4.7D) and of protoxylem strands located at the center (Figures 4.7C, 4.7D, 4.9) and at the tips of the ribs (Figures 4.7B, 4.7H, 4.9). The mesarch strands at the rib tips are buttonhole shaped, highly elongated and thin (0.3 to 0.8 mm long and 0.05–0.1 mm wide, n=11). They are composed of large parenchyma cells (one cell in width, most of the time) about 28 to 72 µm in diameter (n=30) surrounded by protoxylem tracheids 16–35 µm in diameter, (n=30, Figure 4.7B).

The central protoxylem strand is more or less circular and composed of a mix of protoxylem tracheids and parenchyma. It can be composed either mainly of parenchymatous cells (Figure 4.7C) or of protoxylem tracheids (Figure 4.7D). It is about 0.2–0.3 mm wide (n= 7) with no clear boundary with the surrounding metaxylem. There are no protoxylem strands in the midplane of the ribs.
In cross section, metaxylem tracheids are wider at the center of the stele (17 to 94 µm) than at the rib tips (15 to 43 µm, n=200). The radial diameter of the tracheids at the center of the stele (18 to 94 µm, n=200) is wider than the tangential diameter (17 to 73 µm, n=200), which is not the case for tracheids at the rib's tips. In longitudinal section, the pitting pattern is often poorly preserved. It consists of rounded to scalariform pits about 4.5 to 7 µm wide (n=10) for the metaxylem (Figures 4.7E, 4.7F) and annular thickenings for the protoxylem (Figure 4.7G). The tracheids pitting was also observed inside a departing trace (Figure 4.7H, at arrowhead). Longitudinal sections confirm the parenchymatous nature of the cells at the center of the protoxylem strands (Figure 4.7G).

Phloem - Outside the primary xylem some putative phloem cells have been observed. Their identification is based on their location directly in contact with the primary xylem and their thin walls distinct from those of primary xylem and cortical cells (Figure 4.8A). In transverse section, these putative phloem cells are oval and elongated tangentially (18–26.5 µm radially, 10.5–18 µm tangentially, n=4). They could not be observed in longitudinal section.

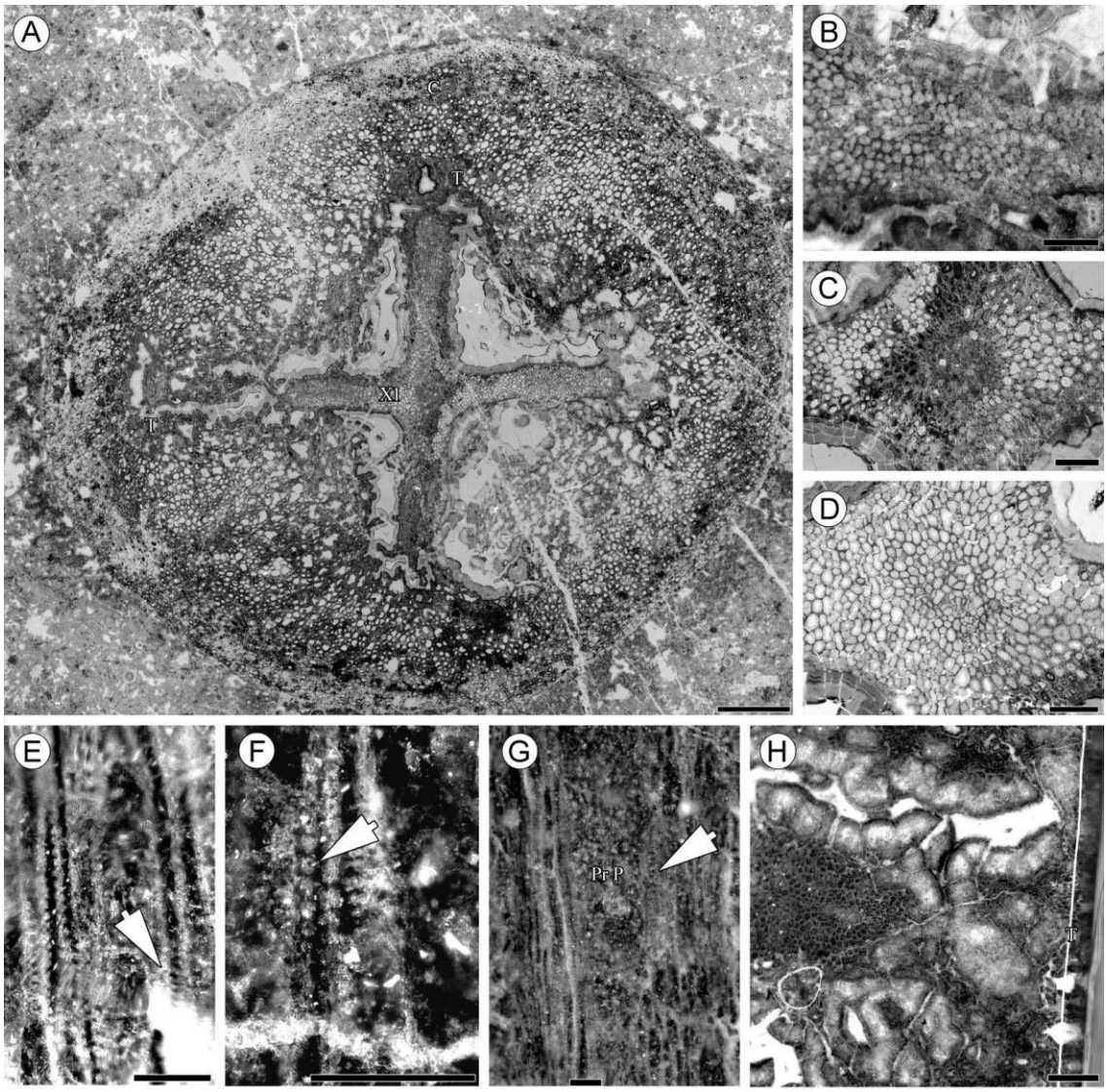

Figure 4.7 *Stauroxylon beckii*, specimen MN297.

(A) Cross section of main axis showing the cruciform actinostele and traces; scale bar = 1 mm; slide MN 297-EI 01; C: Cortex, T: Traces, X1: Metaxylem. (B) Buttonhole-shaped protoxylem strand at the tip of a rib; scale bar = 200 µm; specimen MN 297-B top. (C) Circular central protoxylem strand mainly parenchymatous; scale bar = 200 µm; slide MN 297-EI 01. (D) Central protoxylem strand mainly composed of protoxylem tracheids; scale bar = 200 µm; slide MN 297-FI 01. (E, F) Metaxylem tracheids with round to scalariform pitting (arrows); scale bar = 50 µm; longitudinal section with peel on the specimen MN 297-GL. (G) Protoxylem strand in longitudinal section; note the parenchymatous nature of the inner cells (Pr P) and the annular pitting pattern of the protoxylem tracheids (arrows); scale bar = 50 µm; longitudinal section with peel on the specimen MN 297-GL. (H) Transversal view of the trace (arrowhead); this trace shows the pitting pattern (Figures 4.7E, 4.7F, 4.7G), parenchyma and sclerenchymatous cells (Figures 4.7G, 4.8C) in longitudinal section; scale bar = 200 µm; section with peel on the specimen MN 297-G bot.

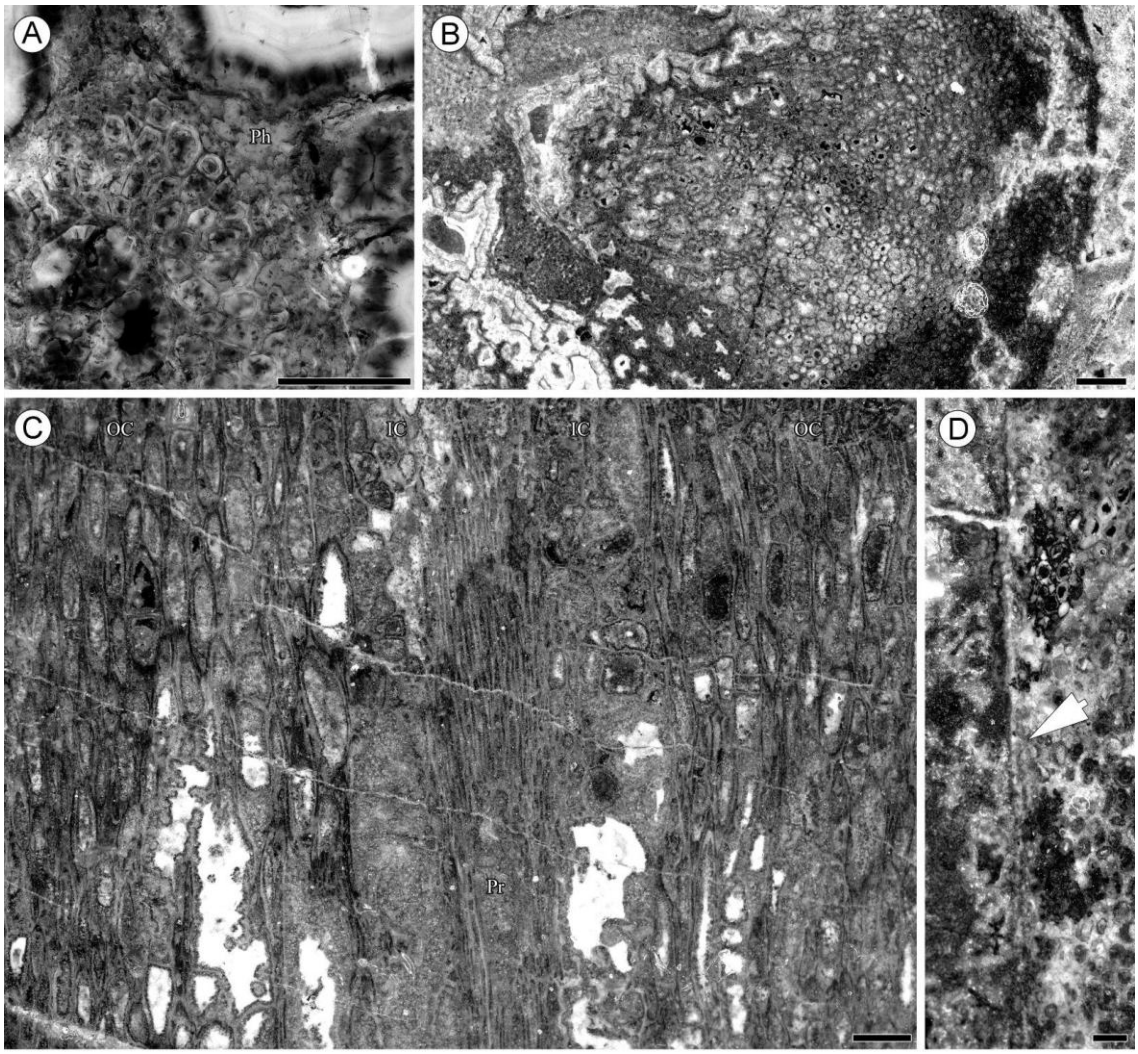

Figure 4.8 *Stauroxylon beckii*, specimen MN297.

(A) Primary phloem (Ph) in transversal section; scale bar = 100 µm; slide MN 297-EI 01. (B) Cortex overview in transversal section; scale bar = 400 µm; section with peel on the specimen MN 297-A3. (C) Longitudinal section with outer cortex (OC), inner cortex (IC), and the metaxylem with parenchymatous protoxylem strand (Pr); note this longitudinal view of the metaxylem is through the trace of Figures 4.7H; scale bar = 200 µm; longitudinal section with peel on the specimen MN 297-GL 12. (D) Epidermal layer (arrows); scale bar = 100 µm; section with peel on the specimen MN 297-C bot 14.

Cortex - The cortex can be separated in two parts. The inner cortex is composed of a few large parenchymatous cells (61–162.5 µm wide, n=22). The outer cortex is composed of smaller cells with thickened walls, polygonal to round-shaped in cross section (46–153 µm wide, n=30) (Figure 4.8B). In longitudinal section, the two zones are more conspicuous. The inner cortex contains square to rectangular parenchymatous cells 66–184 µm high (n = 22) (Figure 4.8C), while the outer

cortex contains elongated cells (220–820 µm high, n=30) of collenchymatous or sclerenchymatous nature (Figure 4.8C).

A final outer layer with a badly preserved single layer of cells is found in some part of the specimen and presumably corresponds to the epidermis (Figure 4.8D). Its cells are oval in transverse section and about 20 to 35 µm (n=5).

Traces to lateral organs – The trace emission pattern can be followed vertically from one extended trace at the bottom of the specimen towards a similar one from the same rib at the top of the specimen. Between these two emissions from a same rib, the specimen emits traces from the 3 other ribs in a more or less simultaneously, giving a triangular shape to the whole specimen. In these two patterns (i.e. 1 vs 3. simultaneous emissions), the mechanism of trace emission from each rib looks similar. It starts with the tangential division of parenchyma cells at the radial tip of the buttonhole strand (Figure 4.11A). Then, the inflated tip of the protoxylem strand detaches radially from the other part. This emitted strand is circular and made of a few big parenchyma cells (Figure 4.11B). The trace is also circular when it detaches from the rib of the main axis, with a large, rectangular, central protoxylem strand (Figure 4.11C). It then divides tangentially, becoming oval with still a large band of protoxylem in its midplane (Figure 4.11D) that may split to form two mesarch strands (Figure 4.11E). Later this oval trace emits two secondary traces tangentially. They are poorly preserved but seem to be initially terete (Figure 4.11F, at arrowhead) and the second order axis becomes more or less circular after emitting them.

While the mechanism of individual trace production is simple, the unusual organotaxis of this specimen combined with the bad preservation of some portions, make a clear understanding of the general pattern challenging. It seems to be composed of two different phases. First, one second order axis is emitted from a rib of the main axis (Figures 4.9A, 4.9F–I, 4.10A, 4.10E, right rib). This second order axis emits two secondary traces tangentially (Figures 4.9I, 4.10E, 4.11F right rib). During this first phase, three other second order axes are emitted almost simultaneously from the three other ribs of the main axis, but they remain close to the stele until the first trace is completely free. That is the beginning of the second phase (Figures 4.9B–E), where the three traces start moving out, giving a triangular outline to the specimen. During this second phase, the trace located opposite the one emitted during the first phase is the first to be farthest from the stele. Its change to a more circular shape (Figure 4.9E, left emission) after an initial tangentially elongated shape suggests that it may have produced a secondary trace that could not be observed due to poor preservation. The two other second order axes seem to remain tangentially elongated for a longer time (Figures 4.9D–E, upper and bottom emission).

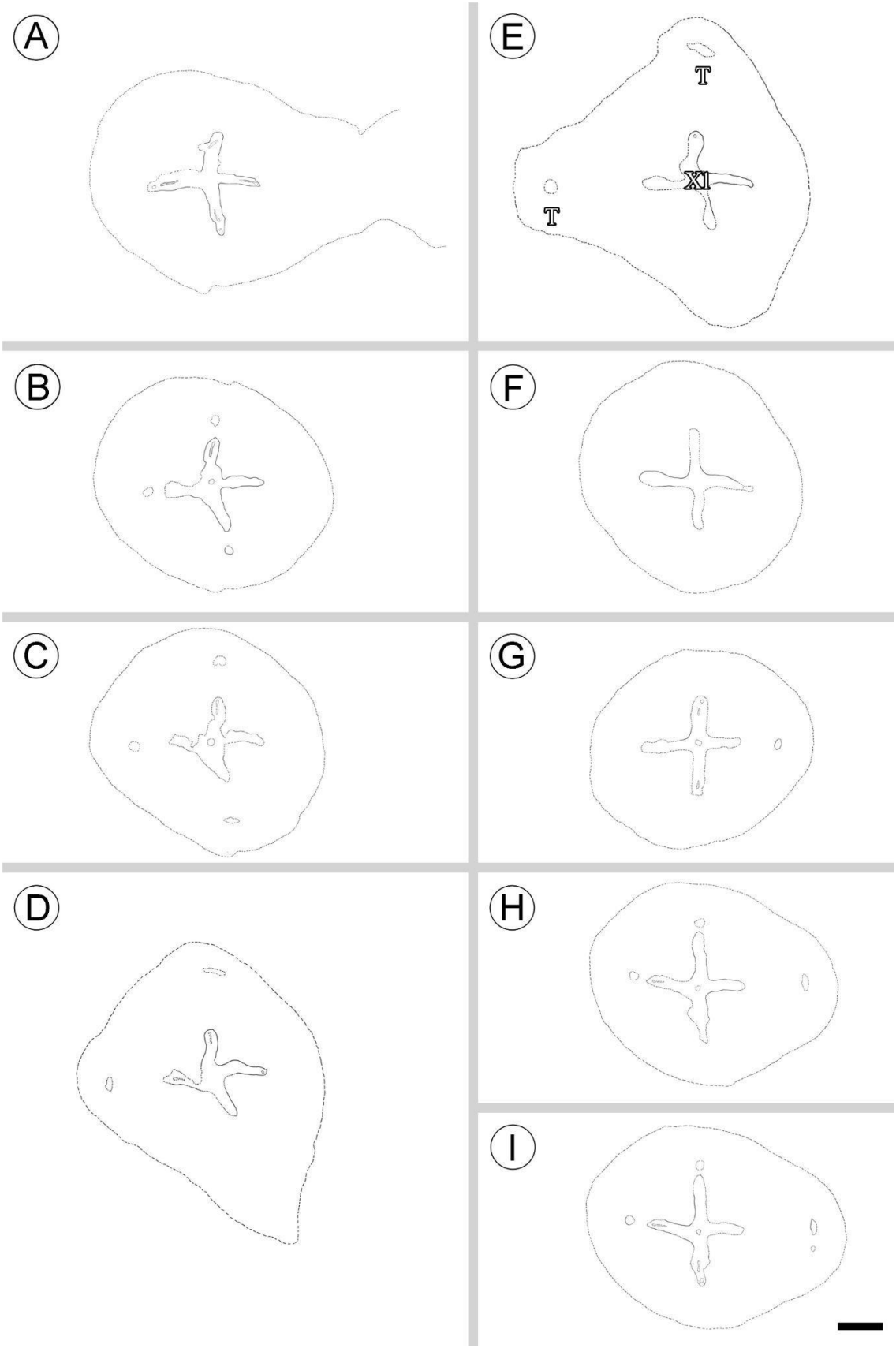
A
E
T
XI
T
B
F
C
G
D
H
I

Figure 4.9 *Stauroxylon beckii*, specimen MN297. Camera lucida drawings of serial transverse sections showing lateral traces emission; scale bar = 2 mm.

(A) Polished section MN297-A3. (B) Polished section MN297-A2. (C) Polished section MN297-A1. (D) Polished section MN297-Btop 16. (E) Polished section MN297-Cbot 16; T: Traces, X1: Metaxylem. (F) Polished section MN297-C. (G) Slide MN297- DS 01. (H) Polished section MN297-E. (I) Slide MN297-FI 01.

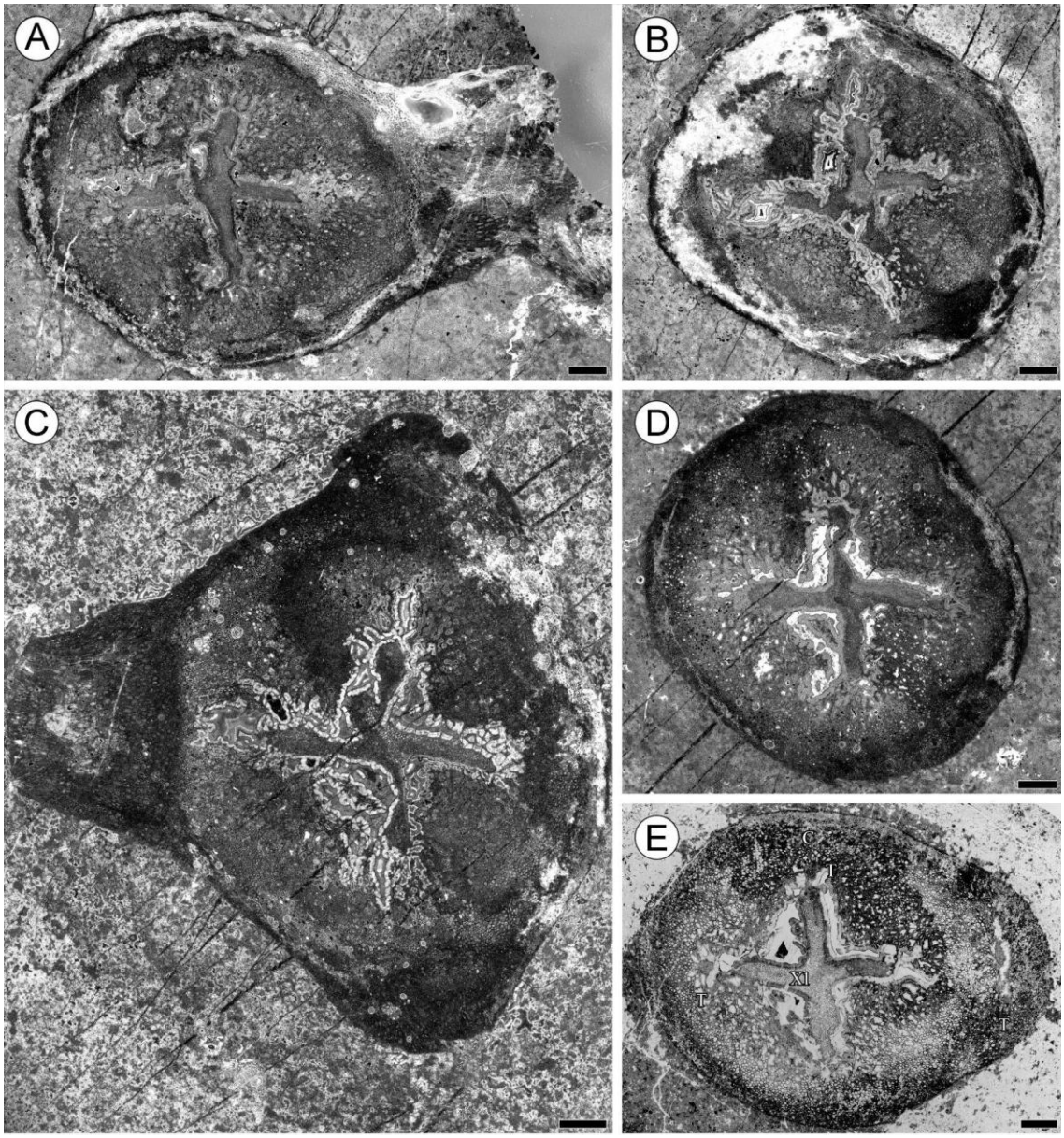

Figure 4.10 *Stauroxylon beckii*, specimen MN297. Transverse sections corresponding to the drawings on Figure 4.9; scale bar = 1 mm.

(A) Polished section MN297-A3, drawing in Figure 4.10A. (B) Polished section MN297-A1, drawing in Figure 4.10C. (C) Polished section MN297-Cbot 16, drawing in Figure 4.10E. (D) Polished section MN297-C, drawing in Figure 4.10F. (E) Slide MN297-FI 01, drawing in Figure 4.10I; C: Cortex, T: Traces, X1: Metaxylem.

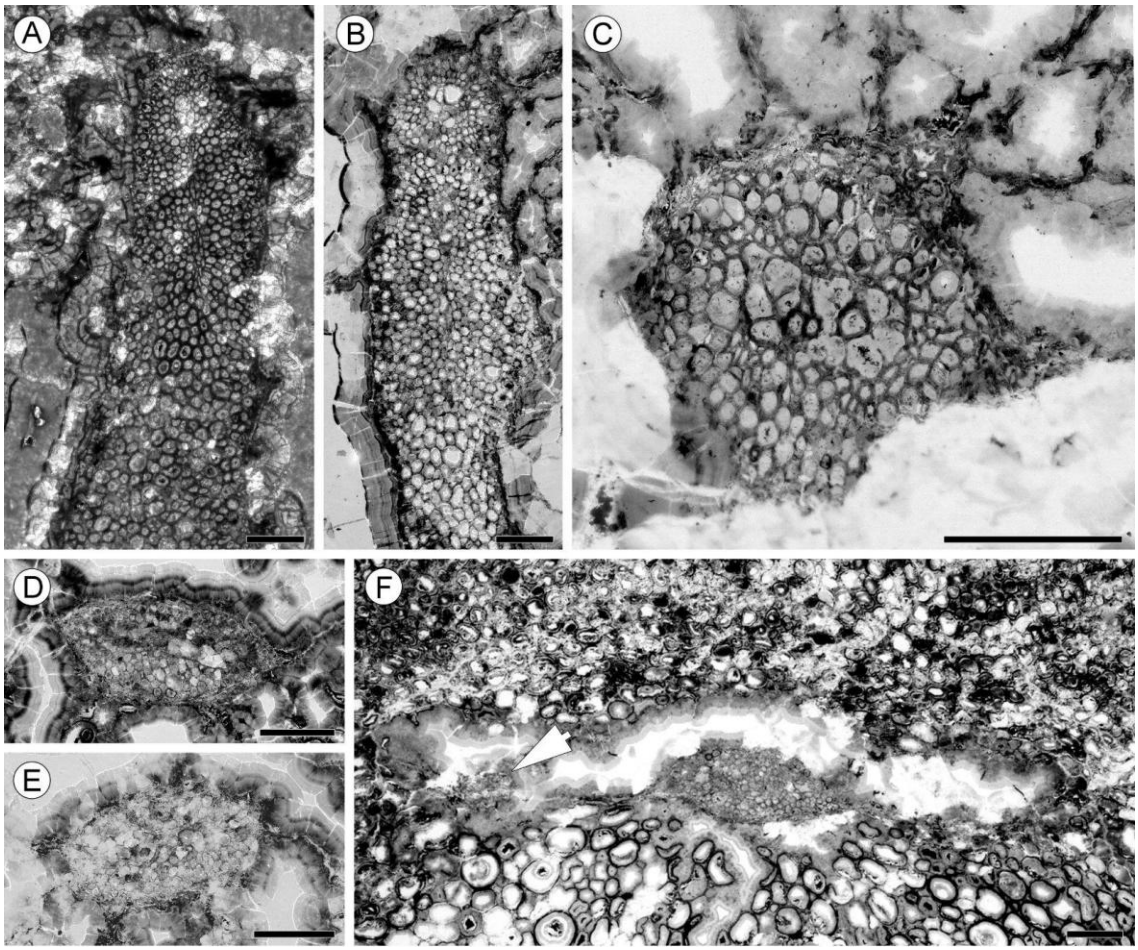

Figure 4.11 *Stauroxylon beckii*, specimen MN297. Anatomy of trace emission; scale bar = 200 µm.

(A) Buttonhole-shaped protoxylem tangentially widened at the tip; peel MN297-FS1. (B) Radial division of the protoxylem strand, with around detaching strand; slide MN 297-EI 01. (C) Circular trace with a large rectangular central protoxylem strand; this trace is emitted by the left rib of Figures 4.10H, 4.11E; slide MN 297-FI 01. (D) Tangentially elongated oval trace; the central protoxylem strand form a central band; slide MN 297-EI 01. (E) Tangentially elongated oval trace; the central protoxylem strand looks split in two mesarch strands and this trace is emitted by the right rib of Figure 4.10G; slide MN 297-DS 01. (F) Oval trace with two opposite third order axis traces; arrowhead mark the basis of the only third order trace preserved, and this trace is emitted by the right ribs of Figures 4.10I, 4.11E; slide MN 297-FI 01.

4.4.3 Systematic palaeobotany

The diagnoses have been translated from Galtier (1970). Crossed text correspond to information that was deleted from the original diagnose and bolded text to information that was added.

Division: Tracheophyta Cavalier-Smith, 1998

Subdivision: Euphyllophytina Kenrick and Crane, 1997

Infradivision: Radiatopses Kenrick and Crane, 1997

Order: Aneurophytales Beck, 1957

Genus: *Stauroxylon* Galtier 1970 Emended Durieux, Decombeix, Harper and Galtier.

Generic diagnosis: anatomically preserved axis bearing opposite decussate ~~branches~~ ~~(~~2nd order axes~~)~~: the latter bear, ~~apparently in a similar fashion, third order axes~~ **two opposite third order axis in a perpendicular plane to the previous level of branching**. The main axis has a cross-shaped protostele (actinostele). Primary xylem has 5 mesarch strands of protoxylem: a central strand and one at the extremity of each rib. **The metaxylem tracheids are larger in their radial dimension, and bigger at the center of the stele.**

Each trace to a second order axis is emitted by a single rib. Outgoing trace triangular **proximally**, produced after tangential division of trace's protoxylem strand, **becoming arc-shaped and adaxially concave before** dividing in three mesarch strands apparently circular and with a radial structure: two small traces (third order axes) surround the strand of the second order axis. Secondary xylem **sometimes present** ~~only~~ at the level of the central stele of the main axis. Protoxylem with parenchymatous elements. Inner ~~bark~~ **cortex** parenchymatous. ~~Middle and outer (?)~~ **Outer** ~~bark~~ **cortex** collenchymatous or sclerenchymatous.

Type species: *S. beckii* Galtier 1970 Emended Durieux, Decombeix, Harper and Galtier

Specific diagnosis: similar to the genus. Main axis circular to elliptical, 9 mm of average diameter. ~~Main branch~~ **Second order axis** 4 mm at the base. Free second and third order axes not preserved. Stele of the main axis cross-shaped: 6 mm in diameter. Central protoxylem larger at the base (0.4 mm). Protoxylem of the ribs buttonhole shaped (0.35 x 0.1 mm).
Metaxylem tracheids **20 to 140 µm wide** with circular or elliptical, bi to multiseriate or scalariform pitting. Secondary xylem (~~0.3–0.5mm thick)~~ **up to at least 0.5 mm when present**. Tracheids smaller **(10 to 50 µm)** than those of the metaxylem, with scalariform pits on all walls.
Rays small **and numerous**, uni to biseriate, of reduced height **(1– 3 cells).**
Inner ~~bark~~ **cortex** (0.6 mm wide) with parenchymatous cells **(40 to 190 µm wide).**
~~Middle and outer~~ Outer ~~bark~~ **cortex** (1–3 mm) collenchymatous ~~or~~ **to** sclerenchymatous with fusiform cells, highly variable in diameter **(50 to 150 µm wide).**
Outgoing trace first triangular (1.3 then 2.2 mm tangentially), producing two small opposite circular strands (0.5 mm) going to the two third order axes
Vascularisation of the ~~primary ramification~~ **second order axis** more or less circular (1.1 x 1.5 mm in diameter)
Internode 18 mm.

Holotype: ~~specimen G 218 Coll. Lab. Paléobotanique, Fac. Sciences, Montpellier~~. **Specimen MN 218 (ex number G 218), Collections de paléobotanique, Université de Montpellier, France.**

Formation: ~~nodule in the~~ Lydienne Formation ~~near St. Nazaire de Ladarez~~, Hérault, France.

Age: Early Carboniferous. ~~Visean~~ **Tournaisian**

4.4.4 Phylogenetic analyses

The analysis using the Toledo et al. matrix TEA ++ without continuous characters resulted in 208 most parsimonious trees (length 110, RI = 0.587, CI = 0.436). The strict consensus tree does not have a lot of resolution (Figure 4.12A). Nevertheless, it recovers *Armoricaphyton* as sister to all the other taxa of the analysis, which are included in a large polytomy with only 3 clades resolved. One contains the two Archaeopteridalean genera, *Archaeopteris* and *Actinoxylon.* The second clade (named *Cairoa*'s clade hereafter) includes *Cairoa* in the first derived position and *Stauroxylon* sister to the Aneurophytalean progymnosperms *Proteokalon – Tetraxylopteris*. The last clade includes the early seed plant *Tristichia tripos* sister to a polytomy that includes all the other early seed plants. The rest of the polytomy includes the Stenokoleales, the remaining Aneurophytales, and plants with unclear affinities (e.g. *Yiduxylon*, *Gothanophyton*, *Kenricrana*)

The synapomorphies recovered in the three clades are (1) the presence of a parenchymatous zone at the center of the stele (C49 = 1) for the *Archaeopteris-Actinoxylon* clade, (2) more than 1 distinct order of branching in the radial organographic domain (C11 = <1) for the *Cairoa* group, (3) a sub-opposite organotaxis (C12 = 2) for the group of *Stauroxylon* sister to *Proteokalon* - *Tetraxylopteris*, and (4) the presence of scattered sclerenchyma in the inner cortex (C29 = 1) for the early seed plant group.

The 50% majority rule tree (Appendix C.1) adds resolution. *Kenricrana* and *Gothanophyton* are included in a polytomy sister to all the other taxa except *Armoricaphyton*. The rest of the taxa form a polytomy, including (1) a clade with all the *Stenokoleos* species, (2) three unresolved species: the Aneurophytale *Triloboxylon arnoldii*, and two Stenokoleales species (i.e. *Brabantophyton, Crossia*), and (3) a clade including the rest of the taxa. This last group is made of a polytomy including a clade containing the early seed plants, and the *Cairoa* clade. In addition, *Langoxylon* is sister to *Archaeopteris* - *Actinoxylon* (Archeopteridales hereafter). *Triloboxylon ashlandicum* is grouped with *Rellimia*, and *Wilhowia phocarum* (Gensel, 1984; 2022) with *Reimannia*.

Additional synapomorphies in the 50% majority rule tree (Appendix C.1) include the absence of a central protoxylem strand in Archeopteridales (also shared by the most derived seed plants in the

analysis, i.e. *Laceya* and *Tetrastichia*, C17 = 0), and the absence of secondary xylem in the *Stenokoleos* clade.

The analysis using the same matrix with continuous characters results in a single most parsimonious tree (length 128.797, RI = 0.556, CI = 0.424) (Figure 4.12B). This fully recovered tree adds resolution to numerous polytomies seen in the other analyses but breaks up the monophyly of *Stenokoleos* in a grade that includes *Wilhowia phocarum* as sister to *Stenokoleos holmesii*. However, in this tree, the previously defined groups are all recovered. The Stenokoleales (from *Stenokoleos simplex*'s group towards *Brabantophyton* - *Crossia* clade) form a grade. *Triloboxylon arnoldii* is basal to *Yiduxylon* (Wang and Liu, 2015), which is the taxa sister to a clade including all the other progymnosperms and the early seed plants. Within this clade, the Aneurophytales are resolved as a monophyletic group (excluding *Triloboxylon arnoldii*) that is sister to the Archeopteridales + early seed plants clade.

The Aneurophytales are supported by the presence of terete ultimate appendages (C37 = 1) and the absence of bilaterality, except in *Stauroxylon* (C10 = 0). The synapomorphy of the sister clade of the Aneurophytales, including the Archeopteridales - early seed plant clade is a heterosporous life cycle (note this character is known in only two of the analyzed species; C9 = 1). The group including all the progymnosperms and the early seed plants is supported by a trace divergence pattern involving only one vascular bundle (C42 = 0).

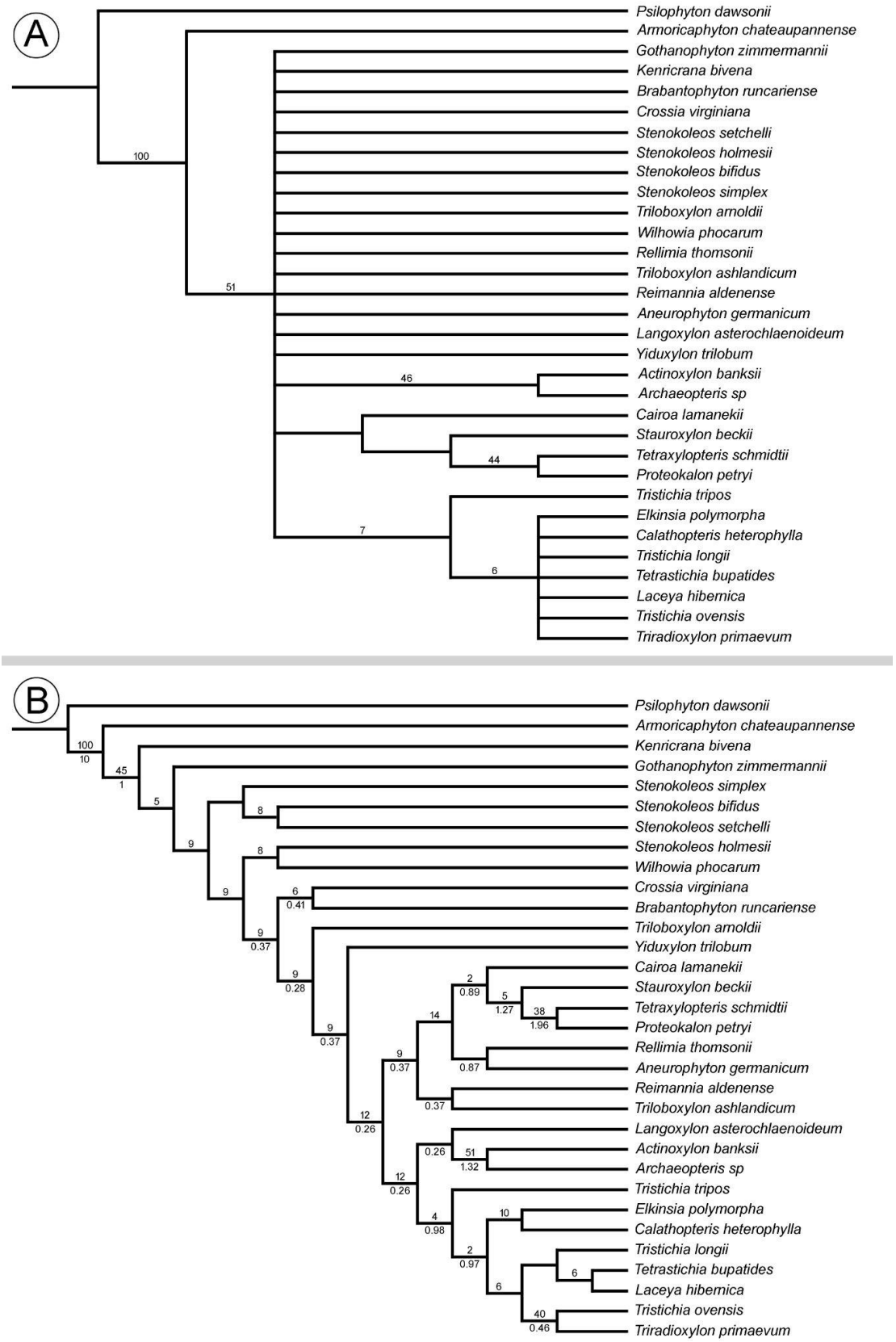

Figure 4.12 Strict consensus trees of the phylogenetic analyses; numbers at node are bootstrap value ≥2 above and Bremer support ≥0.2 below.

(A) Analysis with discrete characters only (32 taxa, 41 characters, 208 most parsimonious trees, length 110, RI = 0.587, CI = 0.436) (B) Analysis with discrete and continuous characters (32 taxa, 50 characters, 1 most parsimonious tree, length 128.797, RI = 0.556, CI = 0.424).

4.5 Discussion

4.5.1 Stauroxylon material known to date

Comparison of MN 297 with the holotype – The new specimen MN297 shares many features with the holotype of *Stauroxylon*, especially the organization of its primary vascular system. These similarities include the shape of the actinostele and the location of the protoxylem strands. Both specimens also have protoxylem strands that are buttonhole-shaped with parenchyma at the center and that have comparable sizes even if some strands can be narrower in MN297. The two specimens also share an heterogenous size of metaxylem tracheids, with larger cells at the center and smaller at the rib tips, and both possess radially elongated central tracheids. The cortex of the two specimens has a comparable organization, with an inner part composed of large rectangular cells with thin walls and an outer part composed of smaller cells with thick walls that are elongated longitudinally. Regarding the pattern of trace emission, both specimens produce a single trace to second order axes from a rib tip, and terete traces to third order axis. The two specimens have a central strand that does not divide or seem to be not involved in the production of traces to second order axes. They also display a transition from bilaterality to radial polarity in the same axis order (second order).

On the other hand, there are two conspicuous differences between the specimens. First MN297 does not possess secondary xylem like the holotype. Second, the organotaxis of the second order axes is different: it is clearly opposite-decussate in the holotype, while in MN297 it is more irregular, with a level where three traces are produced at the same node. The early stage of emission is also a bit different, with the formation of a round shape directly after the individualization of the trace in the specimen 297.

Despite these differences, the two specimens are found in the same formation and share several characters of the primary body that are considered systematically significant. It is also interesting to note that no other contemporaneous taxon -from the same formation or elsewhere- has a comparable organization of the stele and lateral organs. In this context, we consider that the observed differences are not enough to warrant the creation of a new taxon for MN297 and we choose to assign it to *Stauroxylon beckii*. The absence of secondary xylem in the new specimen can be explained by the fact that it represents a different part of the plant or developmental stage (as

seen in Aneurophytales and Archeopteridales; Scheckler, 1976, 1978). Similarly, a different organotaxis between plants from the same species and even on the same plant can occur during the plant development (Peaucelle et al., 2007), inside the same order of axes (Guédon et al., 2013) and also between axes from different order of branching (e.g., *Actinoxylon*, *Tetraxylopteris*, *Triloboxylon*, *Elkinsia*). The limited length of both the holotype and MN297 prevents us from fully appreciating the regularity of the organotaxis.

Other putative fossils of Stauroxylon - *Stauroxylon beckii* now include two anatomically preserved stems showing the base of lateral organs. One additional specimen (MN896) may exist but it is crushed and extremely difficult to compare with confidence to MN218 and MN297. Other fossils that could potentially belong to this species include an anatomically preserved root from the Lydienne formation (Decombeix et al., 2017) and a compression from coeval deposits of Germany (Meyer-Berthaud and Rowe, 1997). For the root, the affinities have been suggested to be either with *Stauroxylon* or with *Protopitys* based on the secondary xylem tracheids pitting pattern (Decombeix et al., 2017). The compression has a main axis with a diameter and internode length comparable to those of the anatomically preserved holotype, opposite decussate second order axes, and 3 dimensional ultimate appendages (Meyer-Berthaud and Rowe, 1997). However, one important character that is not found in the compression is the quick secondary emission leading to third order branching. The new information on *Stauroxylon* gathered in the present study does not allow us to support or reject the affinities of these two other fossils with *Stauroxylon*, even if the compression possesses many important characters in common with the holotype.

4.5.2 Anatomical comparisons with other Late Devonian-early Carboniferous taxa

Stauroxylon is characterized by an actinostele with a central protoxylem strand and secondary vascular tissues. Devonian-Carboniferous plants with comparable features are the Stenokoleales, the early seed plants, and the Aneurophytalean progymnosperms, presented hereafter from the less to the most similar to *Stauroxylo*n.

Stenokoleales – The Stenokoleales appear in the Middle Devonian and became extinct during the earliest Mississippian (Beck and Stein, 1993). They include 3 genera: *Stenokoleos* (Hoskins and Cross, 1951), *Crossia* (Beck and Stein, 1993), and *Brabantophyton* (Momont et al., 2016a, 2016b). *Stenokoleos* includes 4 species: *S. setchelli* (Hoskins and Cross, 1951), *S. simplex* (Beck, 1960b), *S. bifidus* (Matten and Banks, 1969), and *S. holmesii* (Matten, 1992). The two other genera are

monospecific, with the species *Crossia virginiana* (Beck and Stein, 1993) and *Brabantophyton runcariense* (Momont et al., 2016b).

Stenokoleos shares with *Stauroxylon* the presence of an actinostele with mesarch maturation and a central strand. However, the stele of *Stenokoleos* is very different from that of *Stauroxylon*, consisting of 3 or 4 primary xylem ribs that bifurcate at least once. This bifurcation is related to the emission of traces to lateral organs that consist of two traces diverging from a single rib (note that is not known for *S. setchelli* [Momont et al., 2016b]). Nevertheless, *S. bifidus* can also produce a single trace showing an abaxial concavity but, in contrast to *Stauroxylon*, protoxylem strands are numerous and the trace is not triangular at first, but arc shaped (Matten and Banks, 1969). None of the known specimens of *Stenokoleos* has a decussate organotaxis or secondary xylem.

Brabantophyton and *Crossia* share with *Stauroxylon* the presence of an actinostele with mesarch maturation and a central strand, as well as the presence of secondary xylem. Both genera are however highly different from *Stauroxylon*. Their actinostele possess 3 primary ribs that are divided, with numerous protoxylem along each ribs, and traces to second order axes emitted in pairs. In summary, all the representatives of the Stenokoleales known to date differ significantly from *Stauroxylon* in regard to their overall stele organization and their trace emission pattern.

Early seeds plants – The second group of plants that *Stauroxylon* shows morpho-anatomical similarities with is the early seeds plants, an observation already made by Galtier (1970) when he compared his specimen to *Tetrastichia bupatides*.

The late Devonian-early Mississippian actinostelic seed plants have been assigned to several families: the Calamopityaceae, the Buteoxylonaceae, and the Lyginopteridaceae. Some authors also recognize the Elkinsiaceae (Rothwell et al., 1989) and the Tetrastichiaceae (Rothwell et al., 2022). The delimitation of these families is unclear (especially the Lyginopteridaceae [Dunn, 2006]) and their relationships have not been studied from a phylogenetic point of view, likely because of the high amount of missing information and the challenging homologies.

The three genera of Calamopityaceae that possess an actinostele (*Galtiera*, *Bostonia*, and *Stenomyelon)* are highly different from *Stauroxylon*. Those plants do not have a central protoxylem strand, and they possess abundant secondary xylem, a complex trace emission pattern, a spiral phyllotaxis, pitting restricted to the radial wall of secondary xylem tracheids, and *Kalymma*-type petioles, in which one or two traces divide to form four to eight vascular bundles (Stein and Beck, 1978, 1992; Meyer-Berthaud, 1984; Beck and Stein, 1987; Galtier, 1988; Meyer-Berthaud and Stein, 1995). Except for the presence of an actinostele in some taxa, the Calamopityaceae have thus few morpho-anatomical characters in common with *Stauroxylon*.

The Buteoxylonaceae includes 3 monospecific genera (C*alathopteris*, *Buteoxylon*, and *Triradioxylon*) (Galtier, 1988). *Calathopteris heterophylla* (Long, 1976) and *Buteoxylon gordonianum* (Barnard and Long, 1973) have a protostele, but they are very different from that of *Stauroxylon*. They possess a "mixed pith" with abundant parenchyma, no central protoxylem, and have a ⅖ phyllotaxy with U-shaped (papilionoid) traces in *Calathopteris* and T-shaped traces in *Buteoxylon*. *Triradioxylon primaevum* shows more similarities with *Stauroxylon,* in particular regarding the location of the protoxylem strands, which are located at the tips of ribs with one or more strands located at the center of the stele (Barnard and Long, 1975). Differences include the presence of a 3 ribbed actinostele, a high amount of secondary xylem with multiseriate and high rays, and a ⅓ phyllotaxis of the fronds with a papilionoid (Y- or T-shaped) trace (Barnard and Long, 1975).

The Lyginopteridaceae include numerous species of late Devonian-Carboniferous age, typically with a *Lyginorachis* type petiole, in which an undivided basal trace that can be butterfly- to U-shaped with multiple abaxial protoxylem strands (May and Matten, 1983; Galtier, 1988). Among the taxa with an actinostele, the less similar to *Stauroxylon* is *Kerryoxylon hexalobatum* (Matten et al., 1984) which possess a six-ribbed actinostele with no central strand, no secondary xylem, and helically born petioles.

Laceya hibernica described by Matten et al. (1984) has a 3 ribbed actinostele with protoxylem strands only at the rib tips, manoxylic wood with rays up to 6 cells wide, a ⅓ phyllotaxy, and U-shaped traces.

Tristichia species also have a 3 ribbed actinostele, possess manoxylic wood (Dunn, 2006), and a ⅓ phyllotaxis. Their traces are bilobed to papilionoid, with sometimes two bilobed bundle traces as reported by Galtier and Meyer-Berthaud (1996). One species has been described from the Lydienne Formation (*Tristichia longii* [Galtier, 1977]) but the species most similar to *Stauroxylon* is *Tristichia ovensii* (Long, 1961), with a comparable location of the protoxylem strands and a similar shape of one of its early trace emission (Long, 1961: Plate II Figure 17-19, Galtier and Meyer-Berthaud, 1996: Figure 2 H-I). On the other hand, the shape of the stele, the role of the central protoxylem strand in trace emission, and the shape of the trace itself, make *T. ovensii* clearly different from *Stauroxylon*.

Similarities with *Elkinsia polymorpha* described by Rothwell et al. (1989) and by Serbet and Rothwell (1992) and included by some authors in a separate family (i.e. Elkinsiaceae, Rothwell et al., 1989) include the presence of an actinostele with a central protoxylem and pycnoxylic wood.

Differences include a 3 ribbed actinostele, the presence of midribprotoxylem strands, and a ⅓ phyllotaxy with variable trace emission (C-shaped, papilionoid, two or four bundles)

Tetrastichia bupatides, also included by some authors in a separate family (i.e. Tetrastichiaceae, Rothwell et al., 2022), is the only early seed plant sharing the 4 ribbed actinostele and an opposite/decussate phyllotaxy (for some specimens) with *Stauroxylon*. Differences include a manoxylic wood, a variable number of xylem ribs in its stele, highly diverse trace formation from butterfly shaped, U- or T-shaped, row or gentle arc (Gordon, 1938; Dunn and Rothwell, 2012; Rothwell et al., 2022). In addition, the trace of *Tetrastichia* when it is close to becoming individualized (see stage D and E of fig 6 Dunn and Rothwell [2012]) has 4 then 8 abaxial protoxylem strand and is surrounded by secondary xylem, which is different from *Stauroxylon*.

The previous comparisons illustrate how, while several taxa of early seed plants show similarities with *Stauroxylon*, none of them share all the important characters. A difference with most of the taxa is the absence of a central protoxylem strand. Another interesting difference is the anatomy of the traces to second order axes in *Stauroxylon* vs. leaf traces of the seed plants. In *Stauroxylon* the concavity of the trace faces the stele and the protoxylem strand is not abaxial or adaxial. Even if some early stages of leaf trace emission in seed plants can have a comparable overall shape (i.e. arc-shaped), they have their concavity towards the outer part of the stem and their protoxylem in an abaxial position (Sanders et al., 2009; Galtier, 2010; Corvez et al., 2012; Momont et al., 2016b).

Aneurophytalean progymnosperms – The Aneurophytales were defined as an order of progymnosperms by Beck (1957). They are only known in the Devonian, from the late Eifelian to the Frasnian (372–393 Ma) and had a large geographic distribution (Hammond and Berry, 2005; Meyer-Berthaud et al., 2016). Occurrences of *Rhabdbosporites langii*, a spore found *in situ* in the sporangia of *Tetraxylopteris schmidtii* (Bonamo and Banks, 1967) and *Rellimia thomsonii* (Leclercq and Bonamo, 1971, 1973), suggests a worldwide distribution of the Aneurophytales (Gerrienne et al., 2010).
Anatomically, these plants possess in all their orders of branching an actinostele with 3 to 4 ribs, a central protoxylem strand and at least one protoxylem strand at the tip of each rib (Stein, 1993). When present, other protoxylem strands are located along the midplane of the ribs. Their ultimate appendages are vascularized by a terete strand. Aneurophytales are the first plants to possess secondary vascular tissues produced by a bifacial cambium (Stein, 1993), their secondary phloem contains a lot of thick-walled fibers, and their outer cortex contains a network of thick-walled sclerenchyma cells (Beck, 1976). Aneurophytales have complex pseudomonopodial three-dimensional branching systems, dichotomized ultimate appendages arranged in a spiral or in an opposite-decussate pattern. They are homosporous plants (Gerrienne et al., 2010).

Most Aneurophytales (*Cairoa*, *Triloboxylon* [Matten and Banks, 1966; Stein and Beck, 1983]), *Rellimia*, *Aneurophyton*, and *Reimannia* (Matten, 1973) differ from *Stauroxylon* by possessing a three-ribbed actinostele. *Proteokalon* does not have the same number of ribs in its stele depending on the order of branching, so its axes can have either a four-ribbed or three-ribbed actinostele (Scheckler and Banks, 1971b). *Tetraxylopteris* is the only genera to possess a cruciform actinostele similar to *Stauroxylon* in all orders of axes.

Despite important similarities, *Tetraxylopteris* possesses protoxylem strands along the midplane of its ribs (9 strands in total), which is not the case for *Stauroxylon* (5 strands in total). In this regard, *Stauroxylon* is more similar to *Aneurophyton germanicum*, which has one central protoxylem and one strand at the tips of each of its three ribs (Serlin and Banks, 1978, but see in Scheckler and Banks, 1971b).

In the Aneurophytales, the ultimate appendages traces are terete (Scheckler and Banks, 1971a; Beck and Wight, 1988), and those to the last order of axis are at least three-lobed (Momont, 2015). Thus, the trace emission of *Stauroxylon,* which is triangular to arc shaped with an abaxial/adaxial polarity and becomes more oval-shaped distally (Figures 4.4C-F), resembles neither that of a next order axis nor that of an ultimate appendage in an Aneurophytales. However, the trace to third order organs and the distal part of the second order axis in *Stauroxylon* are terete, similarly to the ultimate appendages of the Aneurophytales. The opposite taxis of ultimate appendages are present among the Aneurophytales in *Tetraxylopteris*, *Proteokalon* and *Cairoa*, leading to a highly similar emission pattern of the secondary trace in *Tetraxylopteris* and *Cairoa* in comparison to *Stauroxylon*, as can be seen on Beck (1957)'s drawing of *Tetraxylopteris* (especially C and G) and on Stein (1982b)'s drawing of *Cairoa*. (Text Figure 2 10, 12). However, *Proteokalon* and *Cairoa* hava a 3-ribbed actinostele when they produce their ultimate appendages and *Tetraxylopteris* still have is cruciform actinostele, and in all of them the branching order that give rise to terete traces does not became terete itself after emitting these traces.

Despite this difference, Aneurophytales species especially *Tetraxylopteris* and *Cairoa* share with *Stauroxylon* the same type of stele with the same arrangement of protoxylem strands, pycnoxylic wood, and a similar organotaxis with the same pattern of secondary trace emission (last order of branching emitting ultimate appendages). These similarities suggest that *Stauroxylon* could be a derived member of the Aneurophytales.

4.5.3 Phylogenetic analyses

The phylogenetic analyses recover a monophyletic group including *Cairoa* sister to *Stauroxylon* (*Proteokalon* - *Tetraxylopteris*) in all the analyses, which is consistent with the conclusion of the above comparative approach suggesting that *Stauroxylon* is closer to the Aneurophytales.

The inclusion of *Stauroxylon* did not change any relationship already shown by Toledo et al. (2021) under the taxon sampling TEA ++, i.e. Stenokoleales as a basal grade, and Aneurophytales as the sister group of the Archaeopteridales - seed plant clade. The implication of these results about taxa placement inside groups, characters evolution, and the tree instability are therefore already described by Toledo et al. (2021). The inclusion of *Stauroxylon* in the matrix decreased the number of maximum parsimonious trees (from 334 to 208) and the resolution of a new group in the analyses without continuous characters. This shows that the inclusion of relatively young taxa (Mississippian in this case) can increase the resolution without changing any phylogenetic relationships. We also noted that the relationships of *Wilhowia phocarum* changed between the two types of analyses. When only discrete characters are used *Wilhowia phocarum* is found closely related to the progymnosperms in the 50 % majority rule tree (Appendix C.1), but when the continuous characters are used it belong to the grade of the Stenokoleales (Figure 4.12B). This observation, already seen in trees of Toledo et al. (2018, Appendix 7 vs Figure 1), suggests that the inclusion of this taxon could significantly impact the accuracy of our analyses. Excluding *Wilhowia phocarum* from our analysis with discrete characters (Appendix C.2A) decreases the number of most parsimonious trees from 208 to 89, and leads to two new groups in the strict consensus tree, monophyletic Aneurophytales and *Stenokoleos holmesii* as the sister taxa to *S. bifidus*. When excluding *Wilhowia phocarum* plant from our analysis with continuous characters (Appendix C.2B), the Stenokololeales appear as a monophyletic group including *Crossia* and *Brabantophyton,* which is consistent with previous classification of these plants (Beck and Stein, 1993; Momont et al., 2016b). This Stenokoleales group is also recovered in Toledo et al. (2021) in using 2 different taxon sampling (TEA and TEA+). On the other hand, the phylogenetic position of *Stauroxylon* is independent from the taxon sampling (with or without *Wilhowia phocarum* and from the type of characters used (Figure 4.12; Appendices C.1, C.2). Those results tend to show the solidity of the taxonomic placement of *Stauroxylon* in the Aneurophytales.

4.5.4 Evolutionary considerations

Leaf evolution – From a leaf evolution point of view, *Stauroxylon* is interesting because its laterals possess bilateral and abaxial/adaxial polarity at the earliest stage of the trace emission but rapidly

become terete distally. This is similar to the situation in the early seed plant *Elkinsia* (Serbet and Rothwell, 1992) but in *Stauroxylon*, this phase of polarity is much more reduced and the abaxial/adaxial polarity seems to be independent of the protoxylem location (i.e. triangular and arc-shaped with protoxylem at the center of the trace). In *Elkinsia*, laterals (i.e. fronds in this case) are terete only distally (Serbet and Rothwell, 1992; Sanders et al., 2009) and the abaxial/adaxial polarity is shown by the abaxial position of protoxylem strands. The polarity of the laterals of *Stauroxylon* could represent an early stage of development towards the abaxial/adaxial polarity of the seed plants, or as implied by its phylogenetic placement in the Aneurophytalean progymnosperms, as another independent evolution of incomplete abaxial/adaxial identity in Lignophytes.

Stele evolution – Stauroxylon is also interesting because it possesses wider metaxylem tracheids at the center of the stele than in the ribs, and its central protoxylem strand varies in cell composition, size, and shape. Those variations inside metaxylem and central protoxylem strand is interesting in the context of the discussion on pith evolution and the "*delayed and shortened protoxylem differentiation* hypothesis" put forward by Tomescu and McQueen (2022). This hypothesis involved a modification of the timing of growth and differentiation of the central tracheids leading to the transition from protoxylem/metaxylem toward a central pith. Tomescu and McQueen (2022) also highlight the fact that their hypothesis can be coupled with one of the two hypotheses of Stein (1993) call the hyperinduction scenario when "pith is considered to differentiate in response to the highest auxin concentrations". In this hypothesis, auxin induces (at least in part) the shortening of the differentiation phase and the increase of the growth period for protoxylem tracheids in *Leptocentroxyla* leading to paedomorphic metaxylem tracheids (i.e. tracheids with reduce wall thickness and "simpler thickening" but with same diameter with the surrounding ones) (Tomescu and McQueen, 2022). Auxin flow influencing the timing of growth and differentiation in this way could explain the proto/metaxylem tracheids arrangement of *Stauroxylon*. The parenchymatous center of the central protoxylem strand (Figures 4.2A, 4.7C) would be linked to a high concentration of auxin (acting as an inhibitor in this case) in the stele. Then with the distance from the center, the concentration decreases leading to the differentiation of tissues starting with the protoxylem tracheids (at "the highest non-inhibitory auxin concentrations" Tomescu and McQueen, 2022). Surrounding it, the metaxylem, made of large tracheids close to the center, and the most peripherical tissues of this sequence, the narrower metaxylem tracheids in the ribs. These differences of metaxylem tracheids size can be due to the positive influence of auxin (as seen in secondary xylem tracheids of *Pinus* (Larson, 1969; see also Aloni, 2021 chap 13 for a review and also the counterargument). We can note that the impact of auxin on the tracheids can also be functioning the other way around with the diameter of the conducting cells increasing with the

diminution of the auxin concentration (Aloni, 2021), which in this case is more in line with the hypoinduction hypothesis of Stein (1993). The differences of metaxylem tracheids diameter depending on their position as well as the interchangeability of central protoxylem tracheids toward parenchyma cells, as seen in *Stauroxylon,* tend to confirm the hypothesis of a transition from the central protoxylem strand toward pith formation induce by different auxin concentrations (Stein, 1993; Tomescu and McQueen, 2022).

4.6 Conclusions

· We redescribe the anatomy of *Stauroxylon beckii*, an early Mississippian plant first described in 1970, based on a reinvestigation of the holotype and on an additional specimen that shows a different organotaxis and lacks secondary growth.

· Classical comparative approaches and phylogenetic analyses suggest a placement in the Aneurophytales, making *Stauroxylon* the youngest representative of this group of progymnosperms previously restricted to the Devonian.

· This discovery highlights once again the high potential of anatomically preserved fossils to understand plant affinities by preserving key diagnostic characters.

· Phylogenetic analyses of radiotopsid recover Stenokoleales as a basal grade sister to the monophyletic Aneurophytales, which are the sister group of the Archeopteridales – seed plants clade. This result is similar to Toledo et al. (2021)'s with the highest taxon sampling and the inclusion of *Stauroxylon* increases the strength of previously recovered relationships.

· *Stauroxylon* is interpreted as displaying structural fingerprints of early stages of leaf and pith evolution: (1) the presence of lateral organs combining an abaxial/adaxial polarity without an adaxial/abaxial placement of the protoxylem strand proximally, (2) size variations of metaxylem tracheids, and a central protoxylem strand variability in terms of size and cell type composition.

Data availability

All data that support the findings of this study are included in this article and its appendices. The original versions of Figures 4.1-4.3, 4.5, 4.6-4.8, and 10-11 (in color) are deposited in Figshares (DOI: https://doi.org/10.6084/m9.figshare.24959736). The fossils, associated slides, and peels are deposited in the Collections de paléobotanique, Université de Montpellier, under specimen numbers MN218 and MN297.

Chapter 5

Co-evolution of woody plants and wood-degrading microorganisms: another exquisite example of common human-linked bias

Published as: Durieux, T., Harper, C.J., Decombeix, A.-L., Krings, M. (2025). A rare permineralized *Sphenophyllum* (Sphenophyta, Sphenophyllales) stem containing abundant fungal remains from the Permian of Autun, central France. Review of Palaeobotany and Palynology, 105416. https://doi.org/10.1016/j.revpalbo.2025.105416

Figure, table, section numbers, and citation style have been modified to fit the manuscript's purpose.

5. A rare permineralized *Sphenophyllum* (Sphenophyta, Sphenophyllales) stem containing abundant fungal remains from the Permian of Autun, central France.

5.1 Abstract

Present-day sphenophytes, i.e. the species of the genus *Equisetum*, are hosts to a variety of fungi. Although the Sphenophyta have a long evolutionary history and were far more diverse in the past than they are today, little is known about fungi associated with the fossil representatives of this group of free-sporing vascular plants. A permineralized *Sphenophyllum* stem from the early Permian Autun Basin in France contains several types of fungal remains in the xylem and periderm, including a *Perexiflasca*-like chytrid thallus, blastic inflations of hyphal tips resembling simple glomoid spores, basidiomycete hyphae with clamp connections, and compact, three-dimensional hyphal structures of unknown function and systematic affinity. Cell wall appositions in the periderm are evidence that at least one of the fungi colonized the stem while it was alive. A taphonomic peculiarity are trace fossils of hyphae in tracheids filled with an amber-colored to brown substance, perhaps a type of gum. This is only the second report of fungi from the aerial parts of a fossil sphenophyte. It adds to the growing body of evidence that diverse fungal communities were associated with the iconic plants of the Carboniferous and early Permian coal swamp forests.

5.2 Introduction

Fungi are important ecosystem constituents that interact with plants in a wide spectrum of ways. They can be either endophytes, mutualists, parasites or pathogens, and, as saprotrophs, they are among the most important decomposers of dead plant material (e.g. Zeilinger et al., 2016; Geetha and Dathar, 2022; Priyashantha et al., 2023). Fungal interactions with plants in modern ecosystems have long been the subject of intense research, and much is therefore known about their importance for plant performance and ecosystem functioning (Dighton and White, 2017; Case et al., 2025). Although it is assumed that fungi have interacted with plants in very similar ways in the geological

past since at least the Early Devonian, relatively little is known about such interactions in most fossil ecosystems (Taylor et al., 2015; Harper and Krings, 2021).

One of the first scholars to document fossil fungi more systematically and to hypothesize about fungal interactions with fossil plants was French paleobotanist Bernard Renault, who studied permineralized Carboniferous and early Permian floras from various rock deposits in central France (Galtier, 2016). Renault's success in detailing the fungi associated with some of these plants (Renault and Bertrand, 1885; Renault, 1893; 1895a; 1895b; 1896a; 1896b; 1900; 1903) can be attributed to the excellent preservation of the fossils and his ability to produce high quality thin sections (Taylor and Krings, 2010). Since Renault's groundbreaking work, many additional fungi and fungus-like organisms, as well as various fungal associations with plants, have been described from the Carboniferous and Permian of France (Krings et al., 2007; 2009a; 2009b; 2009c; 2010b; 2010c; 2010d; 2010e; 2011a; 2011b; 2012a; 2023; Dotzler et al., 2008; 2011; Taylor et al., 2012; Harper et al., 2016a; Strullu-Derrien et al., 2021), including the only record to date of fungi associated with the aerial parts of a fossil sphenophyte (Dotzler et al., 2011).

Previous records of fungi associated with fossil sphenophytes (Sphenophyta) include unidentified hyphal fragments and spores in the cortical tissues of Pennsylvanian calamitalean roots from North America (Agashe and Tilak, 1970), and *Cashhickia acuminata* T.N. Taylor et al., a root endophyte of Pennsylvanian calamites from France (Taylor et al., 2012). The scarcity of documented evidence of fungi colonizing fossil sphenophytes is somewhat surprising since present-day members of the genus *Equisetum* L. are hosts to a wide variety of fungi (e.g. Holm and Holm, 1981; Koske et al., 1985; Dhillion, 1993; Künkele et al., 2005; Lechat and Baral, 2008; Hodson et al. 2009; Aly et al., 2010; Li et al., 2010; Parkash and Dhungana, 2011; Suwannarach et al., 2013; Baral and Haelewaters, 2015; Abd-Elsalam et al., 2016; Haelewaters et al., 2018; Giesemann et al., 2020; Xu et al., 2020).

Here, we describe a permineralized *Sphenophyllum* stem from the early Permian of the Autun Basin in central France. Several different types of fungal hyphae and reproductive units occur in all parts of the primary and secondary xylem, and in the periderm. A host reaction in the form of cell wall appositions in periderm cells is evidence that at least one of the fungi colonized the stem while it was alive. A taphonomic particularity is the in-situ preservation of undistorted hyphae as trace fossils in tracheids filled with an amber-colored to brown substance. This discovery adds to our knowledge of fungal associations with sphenophytes in late Paleozoic ecosystems.

5.3 Geological setting, material, and methods

The fungal remains described in this study are all present in a single cross section of an almost perfectly preserved, permineralized *Sphenophyllum* Brongniart stem. The slide containing the cross section belongs to the historical 'collection Roche' (Box D, without number), a set of more than 2000 thin sections prepared during the late 19th and early 20th centuries by Auguste Roche, a friend, co-worker, and biographer of Bernard Renault (Galtier, 2016), that is today housed at the Muséum d'histoire naturelle d'Autun. Parts of the section were previously illustrated by Decombeix et al. (2019a: fig. 6F) and Decombeix and Galtier (2021: fig. 7B). The information on the original label is sparse; however, we are fairly confident that the specimen comes from the Autun Basin in central France and was collected in the vicinity of the city of Autun.

In the Autun Basin, there are several fossil sites known for their great diversity of impression/compression fossils and permineralizations of early Permian plants. To date, more than 70 different fossil-species (in 40 genera) of anatomically preserved plants have been described from there (see Broutin et al., 1999; Galtier et al., 2011), including *Sphenophyllum* (Renault, 1873, 1876, 1878, 1896b). Specimens of the latter taxon come from deposits that Renault called "zone 4". The exact locations where these specimens were found are not known, although Renault himself gives the names "Champs de Borgis" and "Champ de la Justice" for some of them (Renault, 1896b: pp. 505/506; see also Broutin et al., 1999). According to Broutin et al. (1999: fig. 3) and Pellenard et al. (2017: fig. 1b), "zone 4" is late Autunian (an approximate equivalent of the Sakmarian) in age and comprised of the Surmoulin and Millery formations (Figure 5.1). The fact that some 75% of the 2212 slides in the 'collection Roche' contain fossils from the Autun Basin and from this period of geologic time (Galtier, 1980, 2016) suggests that the *Sphenophyllum* specimen colonized by fungi is early Permian in age and originates from either the Surmoulin or Millery Formation. Because silicified plants in the Autun Basin are so far only known only from the Igornay, Muse, and Millery formations (Galtier, 1980), the specimen from the collection Roche most likely comes from the Millery Formation.

Digital images were taken with a Keyence VX7000 digital microscope and an Olympus BX 51 transmitted light microscope equipped with a Sony XCD-U100CR digital camera at UMR AMAP in Montpellier, France, and with a Leica DM LB2 transmitted light microscope equipped with a Jenoptik Gryphax Naos camera at SNSB-BSPG in Munich, Germany. Images were processed in Adobe Photoshop CS6 for brightness and contrast, and images of the same specimen were recorded at multiple focal planes and stacked into a single image. To make it easier to find the slide in the box, it was marked with a white dot with the letter "S".

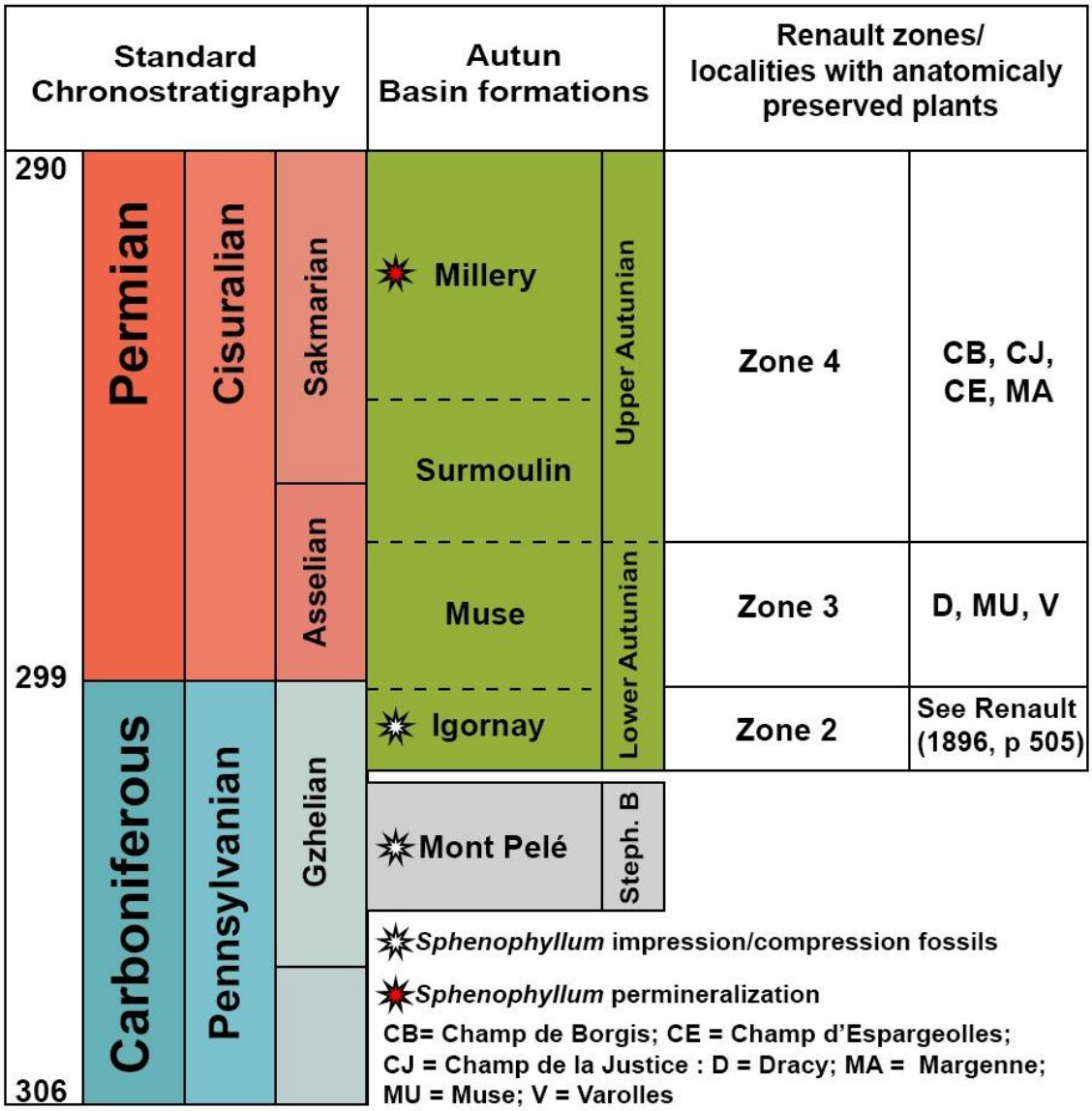

Figure 5.1 Correlation of stratigraphic zones used by Renault (1873; 1876; 1878; 1896b) with the standard chronostratigraphy and the continental European Autunian [based in part on Broutin et al. (1999: fig. 3) and Pellenard et al. (2017: fig. 1b)].

5.4. Results

5.4.1 The host

The *Sphenophyllum* stem, in which the fungal remains are located, is roughly roundish in cross section and has a diameter of approximately 10 mm (Figure 5.2, 1). The primary xylem is more or less triangular in outline, with three concave sides (Figure 5.2 1, 2); the protoxylem is located at the tips of the three arms (arrows in Figure 5.2, 2). Protoxylem tracheids have a diameter of 10–30 µm,

while the tracheids of the primary xylem are 23–136 µm in diameter. The primary xylem is surrounded by a secondary xylem up to 4 mm thick.

The secondary xylem consists of regular radial rows of cells, is divided into three fascicular segments opposite the protoxylem strands, and three interfascicular segments opposite the sides of the metaxylem (Figure 5.2, 2). The tracheids of the fascicular secondary xylem are square to rectangular in cross section, with rounded corners or nearly oval to circular, and have radial diameters of 31–207 µm and tangential diameters of 19–185 µm; tracheids towards the periphery usually are larger than those closer to the center. The tracheids of the interfascicular secondary xylem are also square to almost circular in cross section, but significantly larger on average (radial diameter 47–292 µm, tangential diameter 97–277 µm). In addition, the radial rows show a less pronounced increase in diameter of the tracheids towards the periphery. A small area of the stem shows partially destroyed tracheids, in which parts of the longitudinal cell walls are visible (Figure 5.2, 4). The walls show what appear to be densely spaced circular to hexagonal bordered pits 8–12 µm wide. In some rows of the fascicular secondary xylem, a pronounced alteration of tracheids with small and large diameters can be observed (Figure 5.2, 7), which does not occur in the interfascicular secondary xylem, with one exception. Cichan and Taylor (1984) attribute this pattern to the fact that the apparently smaller tracheids are cut near their tips, while the larger tracheids are cut in a central area. Between the secondary xylem tracheids are small parenchymatous cells (14–53 µm wide), either singly or in groups of two to more than 15 cells (Figure 5.2, 5). In many cases, similar parenchymatous cells also line the rays, which extend through the xylem into the phloem (Figure 5.2, 7, 8). The ray cells are usually radially elongated (arrows in Figure 5.2, 8). All cells of the protoxylem and primary xylem are filled with an amber-colored to (dark) brown substance of unknown origin and composition (Figure 5.2, 1, 2). Many cells of the inner region of the secondary xylem also have such a filling, although some are only partially filled (e.g. Figure 5.3, 17; Figure 5.5, 1).

The vascular cylinder is surrounded by a 0.2–0.5 mm thick, poorly preserved layer (Figure 5.2, 3), which probably represents the phloem and inner cortex. A periderm c. 1.2 mm thick is the best preserved extraxylary tissue of the stem (Figure 5.2, 1, 3, 6). Periderm cells are rectangular, 16–63 µm in radial diameter, and 60–179 µm in tangential diameter. The periderm is stratified and consists of alternating layers of cells with and without black content (Figure 5.2, 6). The tissues outside the periderm were no longer present at the time of fossilization or are not preserved.

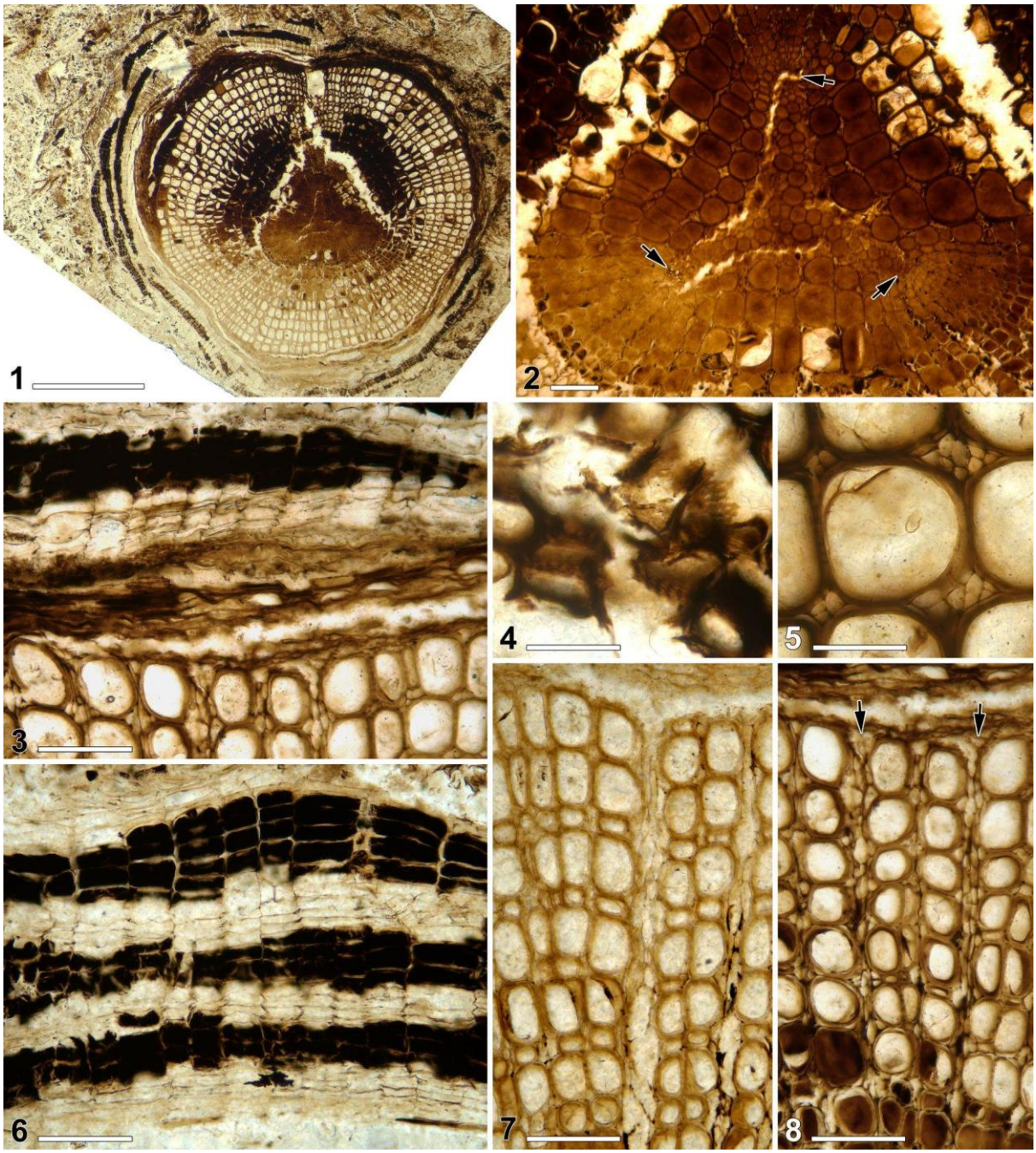

Figure 5.2 *Sphenophyllum* stem (in cross-section view) from the collection Roche, Autun.

1. Overview of specimen. 2. Triangular primary xylem and inner portion of the fascicular and interfascicular secondary xylem; arrows indicate exarch protoxylem. 3. Peripheral secondary xylem, poorly preserved extraxylary tissues (probably phloem and inner cortex), and well-preserved periderm. 4. Partially destroyed secondary xylem tracheids showing pits. 5. Secondary xylem tracheids and clusters of small parenchyma cells. 6. Periderm cells with and without black content. 7. Fascicular secondary xylem showing alternation of narrow and wide tracheids. 8. Radial parenchymatous system (arrows), with radially elongated ray cells. Scale bars: 1 = 2 mm; 2, 3, 6–8 = 200 µm; 4, 5 = 100 µm.

5.4.2 Fungal remains

Evidence for colonization by fungi is abundant and diverse in this *Sphenophyllum* stem. Fungal remains are present in all parts of the stem, but colonization appears to have been much more massive in the primary and secondary xylem (more than 85% of the tracheids show some evidence of colonization) than in the extraxylary tissues (less than 20% of the cells with evidence of colonization). However, the extent of colonization of the protoxylem, xylem parenchyma, and rays is generally difficult to assess due to the small size of the cells. The vast majority of fungal remains are found in the lumen of their host cells, but some are also found in the cell walls. Certain hyphae are preserved as trace fossils in tracheids filled with an amber-colored to brown substance.

5.4.2.1 Hyphae

Body fossils of four different types of hyphae regularly occur in the primary and secondary xylem (Figures 5.3, III); however, they are – with one exception (see below) – better preserved and much easier to recognize in the cells not filled with an amber-colored to brown substance (see Figure 5.2, 1).

The first hyphal type (*type 1*) is thick-walled (Figure 5.3, 1–3; Figure 5.5, 1), usually (but not always) occurs singly in the host cells, and typically extends in longitudinal direction (i.e. parallel to the long axis of the host plant), as a result of which these hyphae can be seen almost exclusively as cross-sections (arrows in Figure 5.3, 1; Figure 5.5, 1). The hyphae are between 7.5 and 16 µm wide, and many appear to have stratified walls (Figure 5.3, 3). The outer wall layer(s) in many cases have a granular texture, but this could be an artifact of preservation or reflect partial degradation of the wall prior to fossilization.

The second type of hypha (*type 2*) is thin-walled, regularly branched at angles of less than 90° (Figure 5.3, 6), between 1.5 and 3.5 µm wide, and sparsely and irregularly septate (e.g. arrow in Figure 5.3, 6). These hyphae extend in all directions, and occur both in the lumen of the tracheids and in the tracheid walls. When penetrating the wall of a host cell, the diameter of the hypha typically is not reduced (Figure 5.3, 7, 8); no evidence was found of special structures (e.g. appressorium-like swellings) that could have either released enzymes to chemically alter the host cell walls or generated hydrostatic force to push the hyphae through the walls. In some cases, the hyphae not only appear to grow straight through host cell walls, but even extend and spread inside the walls (Figure 5.3, 9). Some of the *type-2* hyphae form large, terminal inflations, which presumably represent chlamydospores, as they are separated at the base by a septum from the

subtending hypha (arrow in Figure 5.3, 11). Evidence that *type-2* hyphae are produced by *type-1* hyphae is provided in the form of organic connections of both types of hyphae (Figure 5.3, 10).

A third type of hypha (*type 3*) is fine as hair (usually less than 1.5 µm wide) and can only be viewed reasonably well in the cells filled with amber-colored to brown substance under inverted light (Figure 5.3, 12–15). These hyphae are rarely branched and traverse from tracheid to tracheid without changing their structure when passing through a host cell wall. Some of the hyphae are fragmented and, in some cases, also filled with black, opaque material, so that they appear as interrupted lines (Figure 5.3, 14, 15).

The fourth hyphal type (*type 4*) is narrow to wide (2 to more than 10 µm wide), thin-walled, almost colorless or light-brown, and aseptate or sparsely septate (Figure 5.3, 16). Some hyphae are more or less tubular, others are not uniformly wide. Still others consist of a series of closely spaced ellipsoidal to spherical inflations of very different sizes (up to 25 µm or more in diameter), whereby the entire hypha resembles a string of pearls (Figure 5.3, 17, 18); lateral inflations in the form of greatly enlarged short branches also occur. In some tracheids, the *type-4* hyphae form peculiar, usually compact three-dimensional structures, which may fill the entire host cell lumen (at least in cross section; Figure 5.4, 1–5) and consist of densely packed, irregularly septate or pseudo-septate (arrows in Figure 5.4, 1), more or less tubular hyphal segments and variously shaped and sized sac-like inflations, some of which are distorted or collapsed. A few of the inflations in these structures have a granular-appearing content (Figure 5.4, 4); others contain small spheroidal bodies (up to 6 µm in diameter) of unknown nature (arrow in Figure 5.4, 4).

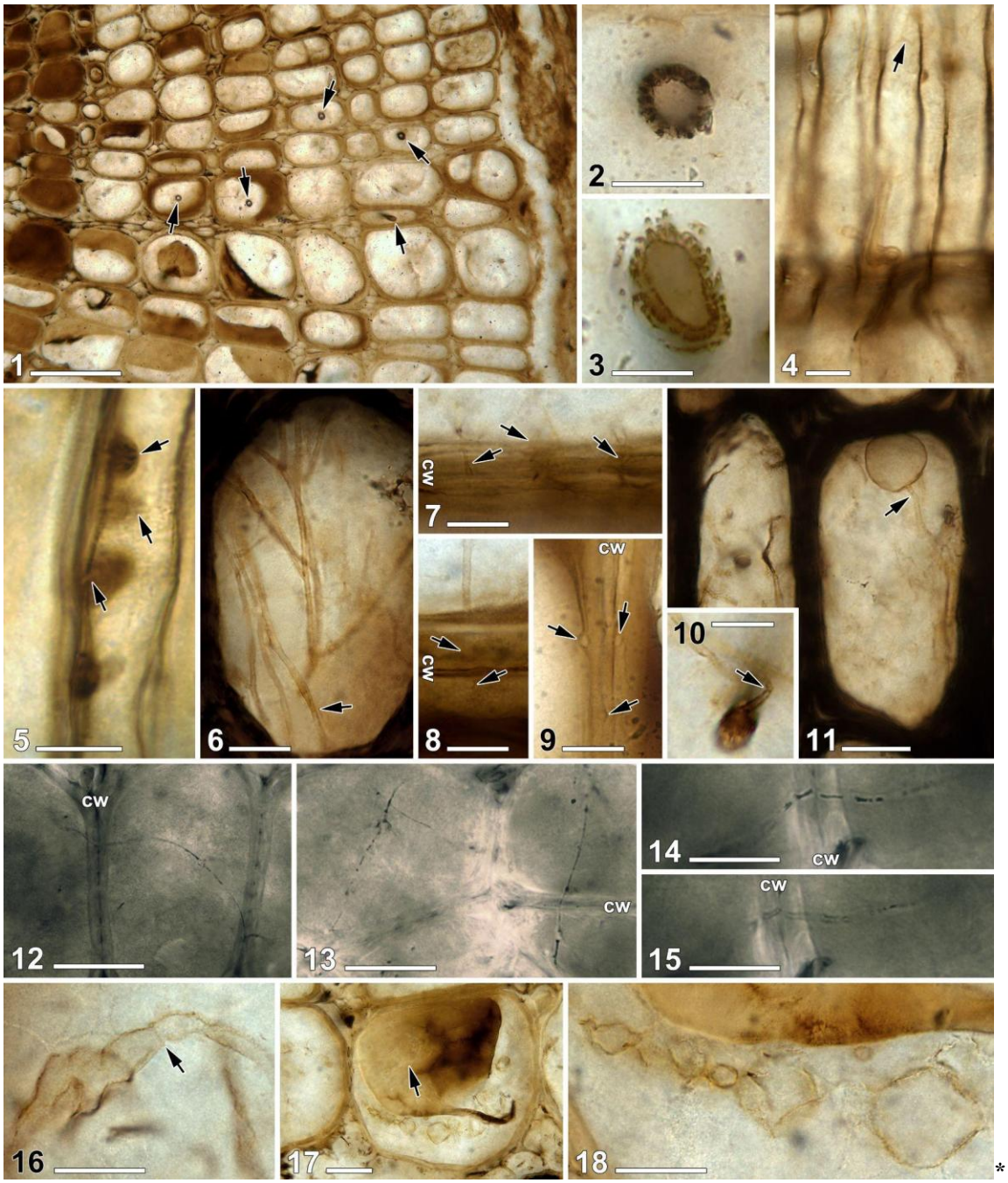

Figure 5.3 Fungal remains in xylem and periderm – Hyphae, reproductive units, and cell wall appositions.

1.Secondary xylem tracheids containing type-1 hyphae (arrows). 2, 3. Close-ups of type-1 hyphae in cross-section view; note granular texture of outer wall layer and stratified wall in the specimen shown in Figure 5.3, 2. 4. Hypha and putative reproductive unit with a thin subtending hypha (arrow) in periderm cells. 5. Periderm cell with cell wall appositions in longitudinal-section view; arrows show penetration hyphae in the center of the appositions. 6. Branched type-2 hyphae in secondary xylem tracheid; arrow shows septum. 7, 8. Type-2 hyphae (arrows) passing through a host cell wall (cw). 9. Type-2 hyphae (in cross-section view; arrows) extending inside a host cell wall (cw). 10. Type-1 hypha giving off a type-2 hypha (arrow). 11. Type-

2 hypha with terminal inflation, presumably a chlamydospore; arrow shows septum. 12–15. Type-3 hyphae (inverted light) passing through host tracheids and tracheid walls (cw); note fragmented hyphae filled with black contents in Figure 5.3, 14. 16. Type-4 hypha with a septum (arrow). 17. Cell partially filled with an amber-colored to brown substance; note trace fossil hyphae in the filled part (arrow) and body fossil type-4 hypha in the unfilled part. 18. Detail of Figure 5.3, 17, focusing on type-4 hypha with closely spaced irregular swellings. Scale bars: 1 = 200 µm; 12, 13, 17 = 50 µm; 11 = 30 µm; 2, 6–10, 14–16, 18 = 20 µm; 3–5 = 10 µm.

5.4.2.2 Reproductive units

In addition to the hyphae, various types of reproductive units are also found in the cells of the xylem. One of them is spherical, 40–55 µm in diameter, thin-walled, and usually rests on, or is somehow connected to, the host cell wall (Figure 5.4, 6–8); subtending hyphae have not been observed, with one possible exception (arrow in Figure 5.4, 8), but some specimens are closely associated with *type-2* hyphae in the host cell wall on which they rest (arrow in Figure 5.4, 6). Other spheroidal reproductive units in xylem cells are smaller, 25–35 µm in diameter, and have a relatively thick wall (Figure 5.4, 10); a fragment of the subtending hypha is still present in some of them. In addition, a single specimen of a minute thallus (less than 20 µm in diameter) comprised of a central cavity with a discharge tube surrounded by what appears to be a prominent sheath has been found attached to a host cell wall (Figure 5.4, 12). Finally, a large, ovoid glomeromycotan spore (c. 160 µm long and 125 µm wide) is located in between the secondary xylem and the periderm (Figure 5.4, 13); a short segment of the subtending hypha is still attached (Figure 5.4, 14), suggesting that the spore is glomoid.

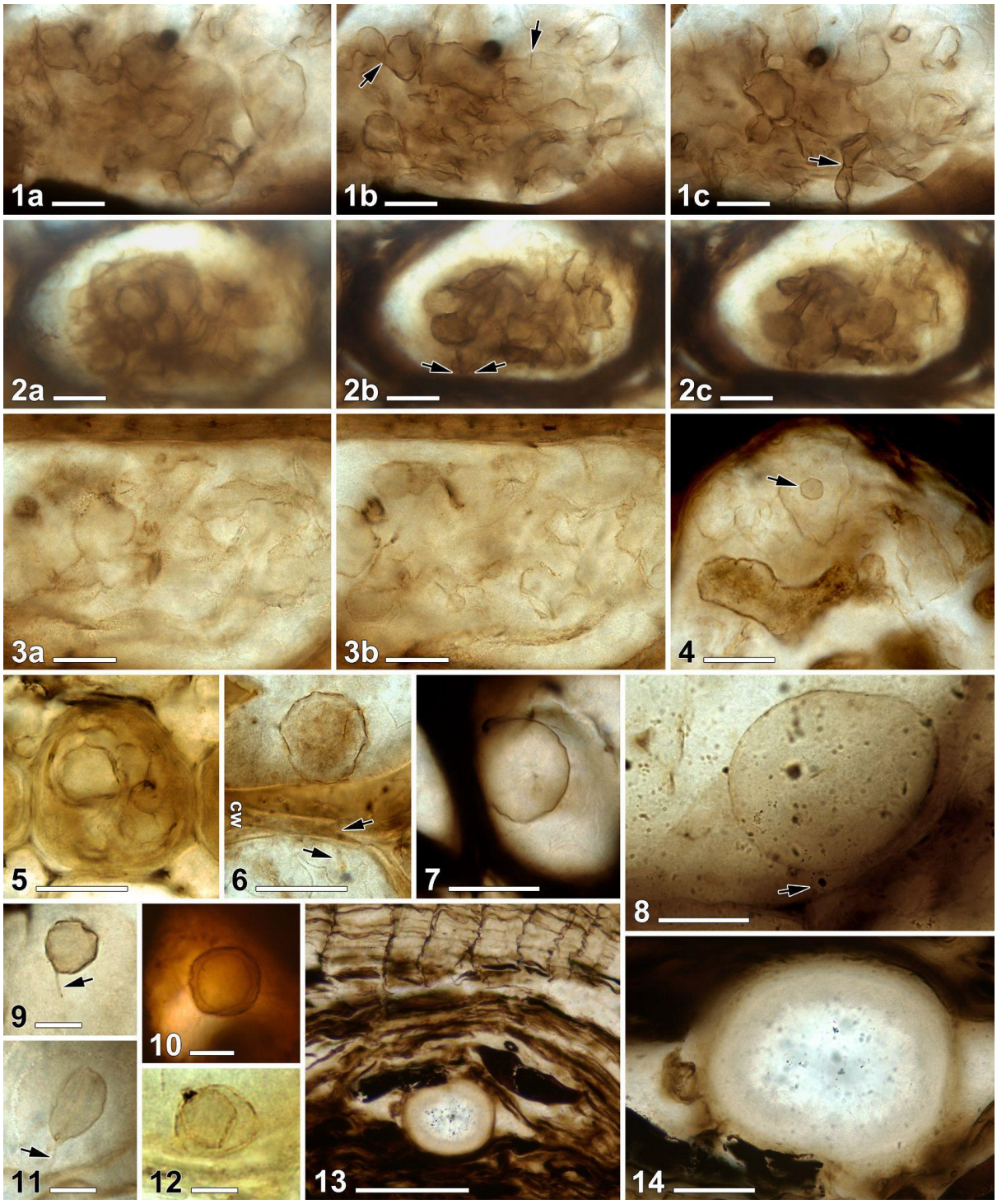

Figure 5.4 Fungal remains in xylem – Type-4 hyphae and fungal reproductive units.

1–3. Complex three-dimensional structures formed by type-4 hyphae, each shown in several focal planes; arrows in Figure 5.4, 1b, c point to septa, arrows in Figure 5.4, 2 show entry site of fungus. 4. Three-dimensional structure containing a spheroidal body of unknown nature (arrow) in a swelling. 5. Three-dimensional structure that almost completely occludes a tracheid. 6. Spherical reproductive unit lying on a

tracheid wall (cw) and closely associated with a type-2 hypha extending through the wall (arrows). 7, 8. Spheroidal to ovoid reproductive units lying on tracheid cell walls; arrow in Figure 5.4, 8 indicates short segment of putative subtending hypha. 9, 11. Simple reproductive units in periderm cells, with fragment of subtenting hypha (arrows) still attached. 10. Thick-walled (or sheathed) reproductive unit or propagule in lumen of a tracheid. 12. *Perexiflasca*-like thallus attached to a tracheid wall. 13, 14. Large glomoid spore in poorly preserved extraxylary tissue between secondary xylem and periderm. Scale bars: 13 = 200 µm; 5–7, 14 = 50 µm; 1–4, 8, 10 = 20 µm; 9, 11, 12 = 10 µm.

5.4.2.3 Fungal trace fossils

Many of the tracheids filled with an amber-colored to brown substance show almost perfectly preserved fungal hyphae, which do not seem to have changed at all in shape and course due to desiccation and biological degradation prior to fossilization and the process of fossilization itself (Figure 5.5, 3–11). These hyphae are not body fossils, but trace fossils in the form of hollows in the solidified amber-colored to brown substance; only vestiges, if any, of the actual hyphal walls are preserved (e.g. Figure 5.5, 2). However, body fossils of hyphae (predominantly *types 2* and *3*) also occur in some of the filled tracheids, in a few cases together with trace fossils. There are also tracheids that are only partially filled with the amber-colored to brown substance (Figure 5.3, 1). The filled part in some of these cells contain fungal trace fossils, while the unfilled part contains body fossils (Figure 5.3, 17; Figure 5.5, 1).

Trace fossil hyphae can only be vaguely recognized under the microscope and can only be properly brought out with the help of various color gradients and photo filters in Photoshop (e.g., compare Figure 5.3, 17 [arrow; no color gradient nor photo filter applied] with Figure 5.5, 3–11). From the images processed in this way, one can see that the hyphae are between 1 and 6.8 µm wide, tubular or somewhat irregular, and unbranched (Figure 5.5, 3) or irregularly branched (Figure 5.5, 5, 6, 11), with the branches usually (but not always) being narrower than the hyphae from which they are given off (Figure 5.5, 5). When penetrating the wall of a host cell, the diameter of the hypha is in most cases slightly to greatly reduced (Figure 5.5, 3 [arrow] + inset, 4, 6, 7) but returns to its normal width immediately after exiting the wall. Some hyphae form a pear-shaped, appressorium-like swelling (up to 5.5 µm wide) before entering a host cell wall (arrow in Figure 5.5, 7), and others have a series of consecutive constrictions at some distance before entering the wall (Figure 5.5, 8). Of particular interest are hyphal formations which are almost certainly clamp connections (arrows in Figure 5.5, 4, 5 + inset), some of which appear to possess an open slit (black arrow in the inset in Figure 5.5, 4) between the hyphal septum (lower white arrow in the inset in Figure 5.5, 4) and the clamp. A few spherical or ovoid intercalary hyphal swellings (Figure 5.5, 9) and reproductive units (Figure 5.5, 10) have also been preserved in this way.

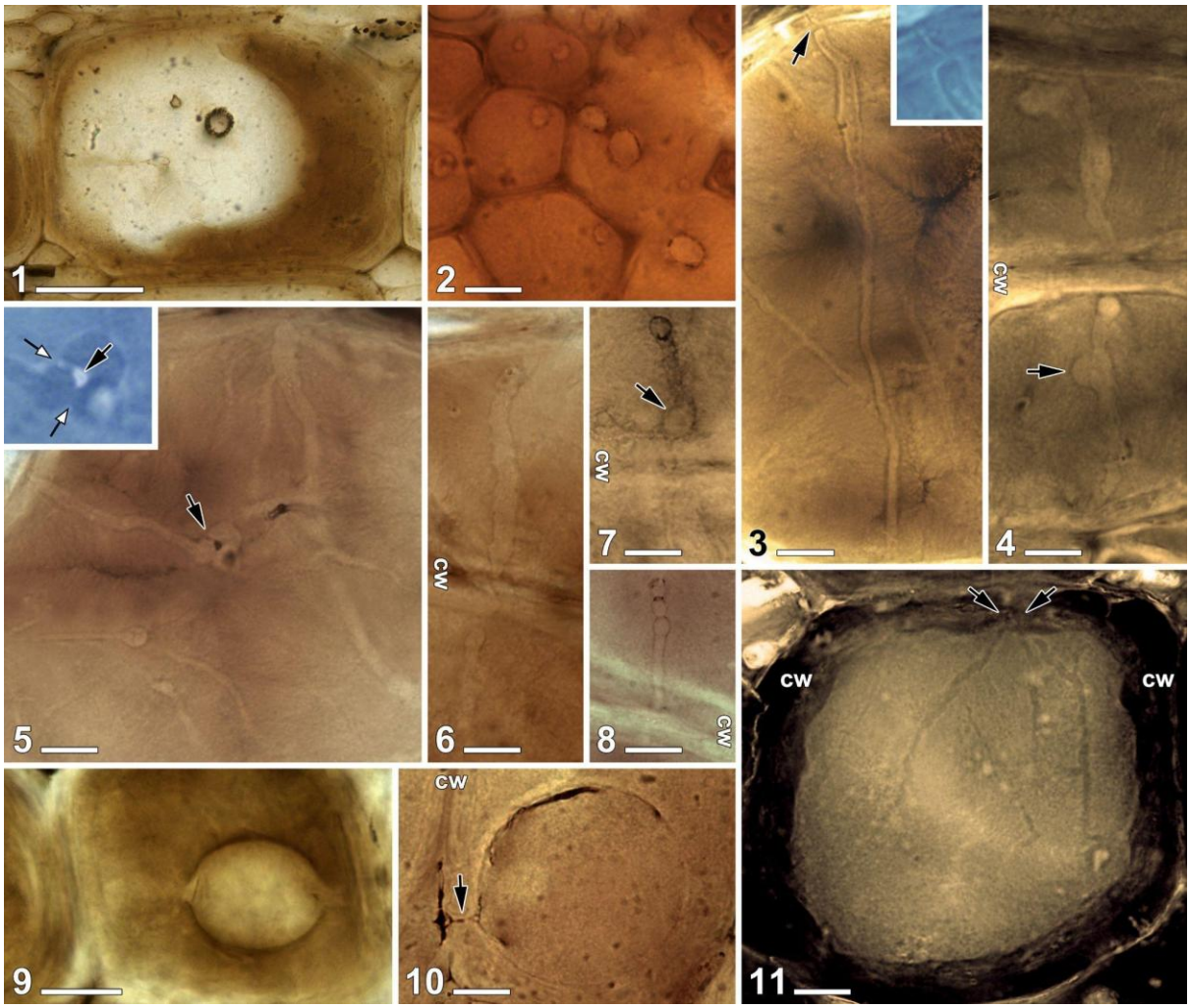

Figure 5.5 Fungal remains in xylem – Trace fossils in cells filled with an amber-colored to brown substance.

1. Partially filled tracheid containing body fossils of type-1 and type-2 hyphae in the unfilled part and trace fossil hyphae in the filled part. 2. Hyphae with only vestiges of the hyphal walls still preserved. 3. Hypha passing through a cell wall into the lumen of a tracheid; note hyphal diameter greatly reduced in cell wall, but returning to normal width after exiting the wall (arrow + inset in inverted light). 4, 5. Branched hyphae with clamp connections (arrows); inset (inverted light) in Figure 5.5, 5: close-up of clamp connection with open slit between hyphal septum (lower white arrow) and clamp (black arrow); upper white arrow indicates second septum. 6. Irregularly branched hypha showing a reduction in diameter before entering a tracheid wall (cw). 7. Hypha forming an appressorium-like swelling (arrow) before passing through a tracheid wall (cw). 8. Hypha with a series of consecutive constrictions before entering a tracheid wall (cw). 9. Large intercalary hyphal swelling. 10. Ovoid reproductive unit with subtending hypha (arrow) attached to tracheid wall (cw). 11. Bundle of hyphae (arrows) passing through a tracheid wall (cw) and into the cell lumen. Scale bars: 1 = 50 µm; 9 = 20 µm; 2–8, 10, 11 = 10 µm.

5.4.2.4 Fungal remains in the periderm

Fungal remains are also found in the periderm, but in much lower frequency than in the xylem. Relatively wide (2–2.5 µm wide) and narrow (less than 1.5 µm wide) tubular hyphae similar to *type 2* and *type 3* were observed in several cells (Figure 5.3, 4, 5), as well as various thin-walled spheroidal or ovoid reproductive units (probably chlamydospores) up to 12 µm in diameter (arrow in Figure 5.3, 4; Figure 5.4, 9, 11), the latter in most cases with a short segment of the subtending hypha still attached (arrows in Figure 5.4, 9, 11). In some (less than 10%) periderm cells, conical cell wall appositions up to 6 µm long and proximally 6.5 µm wide have formed in response to the entry of narrow hyphae. In many of these formations the penetrating hypha can be seen in the center of the apposition (arrows in Figure 5.3, 5).

5.5 Discussion

It is widely believed that the fungi of the Carboniferous and early Permian coal swamp forests formed a wide variety of associations and interactions with the plants that lived in these ecosystems (Cross and Phillips, 1990; Krings et al., 2012b; Nelsen et al., 2016; Naranjo-Ortiz and Gabaldón, 2019; Harper and Krings, 2021). Because many of these plants were large, long-lived, and complex in their morphology and internal organization (Taylor et al., 2009; Wilson et al., 2017), they provided numerous contact sites and ecologically different habitats for fungal biotrophs and saprotrophs. It is therefore not surprising that diverse assemblages of fungal remains have been discovered within a number of structurally preserved Carboniferous–early Permian plants. For example, different types of hyphae, reproductive units, and propagules (spores), as well as evidence of a host response in the form of conical cell wall appositions, co-occur in Carboniferous lycophyte xylem and periderm from France and Great Britain (Krings et al., 2007; 2009b; 2010a), and similarly diverse assemblages have been found in Carboniferous cordaite and seed fern foliage (Krings et al., 2011b; 2014). The best-preserved fungal community to date has been described from the root mantle of a *Psaronius gimmii* M. Barthel et al. stem from the lower Permian of Germany (Barthel et al., 2010; Krings et al., 2017b). The majority of these discoveries were made in historical thin sections of plant fossils described in the late 19th and first half of the 20th century. In principle, this is also the case for the fungal assemblage presented in this study in a *Sphenophyllum* stem from the Autun Basin, except that neither the fungi nor the host plant had been comprehensively described before.

5.5.1 Host: affinities and comparisons

The genus *Sphenophyllum* was originally established based on impression and compression fossils (e.g., Brongniart in 1822; 1828; Coemans and Kickx, 1864; Williamson, 1892), but Renault (1873; 1876; 1878) accommodated in this taxon also permineralized stems characterized by (i) a triangular primary xylem; (ii) an exarch protoxylem; and (iii) a fascicular and interfascicular secondary xylem (for details, refer to Batenburg, 1982; Rößler et al., 2021). The affiliation of the stem cross section described in this study to *Sphenophyllum* is undoubted based on these characters.

Seven species of structurally preserved *Sphenophyllum* stems have been formally described from Europe and North America, namely *S. insigne* Williamson et Scott (Williamson, 1874; Williamson and Scott, 1894), *S. plurifoliatum* Williamson et Scott (Williamson, 1874; Williamson and Scott, 1894), *S. stephanense* Renault (= S. *quadrifolium* Renault, *S. renaultii* Phillips [Renault, 1873; 1876; Phillips, 1959; Boureau, 1964; Doubinger et al., 1995]), *S. gilkinetii* Leclerq (Leclercq, 1924), *S. perforatum* Koopmans (Koopmans, 1928), *S. minus* Koopmans (Koopmans, 1928), and *S. constrictum* Phillips (Phillips, 1959). However, *S. gilkinetii*, *S. minus*, and *S. perforatum* are very similar to *S. plurifoliatum*, and therefore cannot be considered as separate species (e.g., Baxter, 1948; Phillips, 1959; Schabilion and Baxter, 1971). In addition, *S. constrictum* has been found in physical connection with *S. plurifoliatum* (Good, 1973), leaving three “good” species for permineralized *Sphenophyllum* stems. However, *S. insigne* has protoxylem lacunae and rays crossing the entire thickness of the interfascicular secondary xylem (Williamson and Scott, 1894; Baxter,1948; Rößler et al., 2021), while the stem described here lacks evidence of protoxylem lacunae, and its rays do not cross the entire secondary xylem. *Sphenophyllum stephanense* is vaguely defined. The main characters are the number of leaves per node and the pattern of leaf emission (Renault, 1878), which cannot be determined on the fossil discussed here due to the inherent limitations of the specimen. The third species, *S. plurifoliatum* (Williamson, 1874; Williamson and Scott, 1894), has secondary xylem with parenchyma between cells connected by elongated cells that rarely cross the entire thickness of the secondary xylem, true phloem, and an internal periderm layer that can form regular scale-bark (i.e. banded aspect of the periderm [Eggert and Gaunt, 1973; Decombeix and Galtier, 2021]). Tracheids in this species are on average 160 µm in diameter (Cichan, 1985a). The species appears to be highly variable, however, which has led to the majority of anatomically preserved large specimens of *Sphenophyllum* found in North America, Europe, and Russia being assigned to this taxon (Good, 1973). The cross section described in this study seems to be more closely related to *S. plurifoliatum* than any other permineralized *Sphenophyllum* stem.

Sphenophyllum plurifoliatum has been hitherto unknown from the Autun Basin, Grand-Croix, and the Montagne Noire, the three French regions where anatomically preserved specimens of *Sphenophyllum* have been found (Galtier, 2008; Terreaux De Felice et al., 2019). If the stem described here is indeed *S. plurifoliatum*, then it would be of interest not only as a host for a well-preserved fungal community, but also because it would represent the first record of this species from France.

5.5.2 Fungal remains

5.5.2.1 Affinities and comparisons

There is only one report to date of fungi associated with the aerial parts of a fossil sphenophyte, namely *Sphenophyllum* leaves from the Upper Pennsylvanian Grand'Croix chert of France that house several types of fungal remains, including putative chytrid zoosporangia, propagules, and mycelia with intercalary swellings (Dotzler et al., 2011). However, none of these fossils morphologically match the fungal remains described in his study.

Interpreting the systematic affinities of the fungal remains in the *Sphenophyllum* stem from Autun is difficult, if not impossible in some cases, because, with one possible exception (see below), they are not complete organisms, but individual parts or life history stages of organisms. For the same reason, it is not possible to determine the exact number of biological species represented in the assemblage. The different fungal remains are most certainly not all separate species. Conversely, it is also possible that the more common remains represent several morphologically similar species. For some of the fungal remains, however, we can make cautious assumptions about their systematic placement based on morphological characteristics and comparisons with other fossil and present-day fungi.

The *type-1* and *type-2* hyphae (Figure 5.3, 1–11; Figure 5.5, 10), as well as the terminal hyphal inflations physically connected to (Figure 5.3, 11), or closely associated with (Figure 5.4, 6, 7), some of the *type-2* hyphae, belong to the same fungal species, perhaps a member of the Glomeromycota (arbuscular mycorrhizal fungi) or zygomycete fungi if the hyphal inflations are actually sporangia or spores. One of the few structural features by which fossil zygomycete fungi can be reliably distinguished from Glomeromycota is the sexual stage of the life cycle, which occurs in the former through zygosporogenesis after gametangial fusion, but is unknown in the latter (Krings et al., 2013). The fossils discussed here cannot be identified as a zygomycete fungus, as there is no evidence of zygosporangium-gametangia complexes. The occurrence terminally on a tubular hypha rather suggests that the inflations are glomoid chlamydospores (e.g. compare the

fossils to Magurno et al., 2024: figs. 1A, B, F, 2B), which have formed asexually by blastic inflation and thickening of a hyphal tip. Likewise, the single large ovoid spore located in the ill-preserved tissue between the xylem and the periderm (Figure 5.4, 13, 14) probably also belongs to the Glomeromycota. However, there is no evidence to date that *Sphenophyllum* and glomeromycotan fungi formed mycorrhizal symbioses, as is known for some other coal swamp plants, including marattialean ferns (Wagner and Taylor, 1982), arborescent lycophytes (Krings et al., 2011c), and cordaites (Strullu-Derrien et al., 2009).

The affinities of the *type-3* (Figure 5.3, 12–15) and *type-4* hyphae (Figure 5.3, 16–18) remain unknown. However, the latter are interesting because of the catenulate hyphal swellings (Figure 5.3, 18) and the peculiar three-dimensional structures formed in some host cells (Figure 5.4, 1–5). Although they have a very different structure and are much larger, the latter structures are still somewhat reminiscent of the coralloid structures found in root cortical cells of the early Permian *Psaronius gimmii* (Krings et al., 2017b), which are assumed to have been produced by a member of the fungus-like Oomycetes (Peronosporomycetes). It has been hypothesized that these structures in *P. gimmii* were effective as some type of physiological interface. They may have functioned as haustoria, which form inside a living host cell as a branch of an extracellular (or intercellular) hypha or thallus (Bushnell, 1972; Szabo and Bushnell, 2001; Judelson and Ah-Fong, 2019; Mapuranga et al., 2022). However, the tracheids in which the fossil structures occur are not living cells (at maturity), and there is no evidence of intercellular *type-4* hyphae in the *Sphenophyllum* stem. Alternatively, the three-dimensional structures could be irregularly swollen sporangia, similar to those of the present-day oomycete *Pythium catenulatum* V.D. Matthews (Androusse et al., 2007: figs. 10–15), or comparable to the sporangia of *Pythium torulosum* Coker et Patterson and *Pythium kashmirense* Paul, among other taxa, which all consist of inflated branched outgrowths of the mycelium forming toruloid complexes of varying size (Coker and Patterson 1927: figs. 2–4; van der Plaats-Niterink, 1981: figs. 3b, 84b; Paul and Bala, 2008: fig. 1c). In addition, a few of the fossil swellings have a granular-appearing content and look very similar to the immature sporangia of some present-day oomycetes (e.g. compare Figure 5.4, 4 with Salmaninezhad et al., 2024: fig. 5e). Nevertheless, the location of the structures in tracheids renders this option rather unlikely. Yet another possibility is that these structures served as storage sites, perhaps in a similar manner as vesicles in present-day Glomeromycota (e.g. Herrmann, 1995; Walker et al., 2018). Vesicles are structures in which these fungi store energy as lipids for use in times of limited resources. Moreover, by accumulating phosphorus in these structures, they may have an important resource that they can make available to the plant host if phosphorus is scarce (Helgason and Fitter, 2009; Olsson et al., 2011; Bach et al., 2018). However, there is currently no direct evidence that the *type-4* hyphae belong to the Oomycetes or the Glomeromycota.

Some of the hyphae preserved as trace fossils show structures that are almost certainly clamp connections (Figure 5.5, 4, 5 + inset). Clamp connections are hyphal protrusions known exclusively in Basidiomycota that develop during cell division to maintain the binucleate (dikaryon) condition (Furtado, 1966; Oberwinkler, 2012). More recently, it has been hypothesized that they are also effective as screening devices for the quality of nuclei, with both nuclei continuously testing each other for fusion capability (Aanen et al., 2023). Clamp connections are classified based on, among other features, the ratio of clamp size to hyphal diameter (Stalpers, 1978; Buchalo et al., 1983, 2011). The structures described here can be identified as large clamps, in which the hypha and the clamp have approximately the same width. A recent phylogenomic analysis suggests that the subphyla of the Basidiomycota diverged in the Ordovician, in a time range of 490–443 million years (He et al., 2024). However, the oldest fossil evidence of hyphae with clamp connections comes from the Mississippian of France (in *Botryopteris antiqua* Kidston; Krings et al., 2011a) and the Pennsylvanian of North America (in *Zygopteris illinoiensis* (Andrews) Baxter; Dennis 1969, 1970). Slightly younger, early Permian hyphae with clamp connections have been reported from Germany (in *Psaronius gimmii*; Krings et al*.,* 2017b) and China (in *Shanxioxylon* sp.; Wan et al*.,* 2017). So far there has been no fossil evidence of Basidiomycota in association with sphenophytes.

Finally, a minute but nonetheless noteworthy fossil in the stem is shown in Figure 5.4, 12. Based on morphology, this fossil can be attributed with confidence to the fossil-genus *Perexiflasca* M. Krings et al, first described from the Lower Devonian Rhynie cherts of Scotland (Taylor et al., 1992; Krings et al., 2017a; Krings and Harper, 2019). *Perexiflasca* occurs singly or in clusters of up to more than 100 specimens attached to the walls of plant cells and large fungal spores. The fossil has been interpreted as a sheathed zoosporangium of a eucarpic, monocentric chytrid-like organism (Krings et al., 2017a). There are also two Carboniferous microfossils that correspond to the morphology of *Perexiflasca*, one from the Mississippian and one from the Pennsylvanian of France (Krings et al., 2009b, 2011b). Krings and Harper (2019) point out that the occurrence of *Perexiflasca*-like fossils in the Devonian, Mississippian, and Pennsylvanian may provide a very rare opportunity to study microbial life through deep time. The specimen described here adds the first early Permian record to this inventory.

5.5.2.2 Formation of trace fossils

Trace fossils of fungal structures in permineralized plants have, to our knowledge, never been reported. Their abundance in the *Sphenopyllum* stem from Autun therefore raises the question of how they originated. Almost all fungal body fossils in this stem show at least some degree of structural change compared to their in vivo state, e.g. in the form of fragmentation, collapse, shrinkage, displacement within the host cell, or partial decay. The almost perfect preservation of

certain hyphae as trace fossils exclusively in tracheids that are filled with an amber-colored to brown substance indicates that this substance may have played a role in trace fossil formation. We speculate that the amber-colored to brown substance was already present in the cells during the lifetime of the fungi and, at some point, it solidified and enshrined every fungal structure in these cells. In this way, the original shape and course of the hyphae could have been preserved even after the decay of the hyphal walls. The fact that body fossils of hyphae also occur in some of the filled cells might be due to the intrusion of other fungi into the cells containing the already solidified substance at a later stage. However, it is more likely that the hyphae later to become body fossils were in the cells at the same time as those that became trace fossils, but that they are different fungi whose hyphal walls are differently resistant to decay. Support for this hypothesis is the fact that no evidence of hyphae with clamp connections was found in any of the cells that are not filled with the amber-colored to brown substance.

All these considerations naturally raise the question of what the special substance in the filled cells might be. Plants produce a variety of occlusions in their vascular tissues in response to biotic and abiotic stresses, which can be divided into two main categories, namely tyloses on the one hand and gels or gums on the other (Sun et al., 2008; De Micco et al., 2016). Both are produced by the parenchyma cells in the xylem. Tyloses are outgrowths of parenchyma cells into the lumen of neighboring conducting cells, while gels (or gums) are amorphous substances secreted by parenchyma cells that fill the conducting cells (Sun et al., 2008). Although tyloses are known in plants from the Late Devonian (Decombeix et al., 2023), and have been observed in sphenophytes since the Carboniferous, they have not yet been found in *Sphenophyllum* (Decombeix et al., 2022b). Plants today can produce either only tyloses, or only gel, or both, and this can also vary depending on the time of year when colonization with the pathogen begins (Sun et al., 2008). No tyloses were observed in the *Sphenophyllum* stem described here, despite extensive fungal colonization, but the occluding material in this case may have been a gel, as it has a uniform texture and shows an outline when the cell is only partially filled (Figure 5.5, 1). Hyphae in a present-day plant vessel filled with gel have been illustrated by Mutawila et al. (2011: fig. 1D), but these hyphae appear to have grown through the gel, rather than being enshrined by the gel. To our knowledge, there is no published report of hyphae trapped inside a gel. The amber-colored or brown substance in the fossil is therefore probably a solidified gel, but more analyses (e.g. geochemical) are needed to understand this phenomenon in detail.

5.5.2.3 Nature of the associations

The nature of the biological relationship between the various fungi and the host plant remains largely unknown in detail, as both the host and the fungi are only incompletely preserved. The

fungi could be either biotrophs or saprotrophs. The only evidence of a biotrophic (parasitic) relationship occurs in the form of small conical cell wall appositions found in several of the periderm cells (Figure 5.3, 5). Cell wall appositions (also called lignotubers, papillae, or Röhrentüpfel, among other terms; see Leroux et al., 2011) are inwardly directed projections consisting of newly synthesized wall material that are formed by living plant cells (but also by certain fungal spores, where they are called callosities; see Swart, 1975; Purin and Rillig, 2008) in response to invading fungi or some other biotic cause. They encase the infection hyphae or filaments and, in this way, prevent or at least decelerate the penetration of the parasite (e.g. Pearce, 1996; Schulze-Lefert, 2004; Collinge, 2009). This type of host reaction has previously been documented in several Carboniferous–early Permian plant lineages, including arborescent lycophytes (Krings et al. 2009b; 2010a), marattialean and filicalean ferns (Krings et al., 2011a; 2017b), gymnosperms (Stubblefield et al., 1984), and calamitalean sphenophytes (Taylor et al., 2012). The cell wall appositions described here are the first evidence in sphenophyllalean sphenophytes.

The nutritional mode of the fungi in the xylem is far more difficult to assess. There is no evidence of a host response nor of any particular fungal features that might indicate a relationship with a living host, perhaps with the exception of the compact three-dimensional structures formed by the *type-4* hyphae (Figure 5.4, 1–5), if one assumes that these structures are indeed functionally similar to haustoria. Harper and Krings (2021) state that a distribution pattern of fungi in an intact host that reflects forced invasion and a consistent pathway of colonization (e.g. along the vascular bundles or rays), or that is restricted to specific parts or tissue types of the host, is indicative of colonization of a living host, whereas colonization of dead and decaying plant parts is more likely to result in random fungal distribution. The numerous fungal remains, likely from multiple fungal species, throughout the primary and secondary xylem of the *Sphenophyllum* stem, as well as evidence of incipient mechanical destruction and degradation of the stem, would therefore be indicative of post mortem colonization by saprotrophic fungi. However, a reliable evaluation of fungal distribution on the basis of a single cross section is not possible. For example, the section does not provide any information about where and how the fungi have entered the stem and how they have spread from there.

5.6 Conclusions

A thin section from the collection Roche in Autun, France, of a permineralized early Permian *Sphenophyllum* stem in cross section from the Autun Basin shows the presence of a variety of fungi, including a *Perexiflasca*-like chytrid, greatly inflated hyphal tips resembling glomoid spores, hyphae with clamp connections, and three-dimensional hyphal formations of unknown function and affinity. Cell wall appositions in periderm cells are evidence that at least one of the fungi colonized the stem while it was alive. Most of the fungal remains are body fossils, but some hyphae in tracheids filled with an amber-colored to brown substance, perhaps a type of gel or gum, appear as trace fossils. There are a number of comprehensive descriptions of structurally preserved *Sphenophyllum* stems in the literature (e.g., Renault, 1873, 1876, 1878, 1896b; Williamson and Scott, 1894; Baxter, 1948; Reed, 1949; Snigirevskaya, 1959; Schabilion and Baxter, 1971; Good and Taylor, 1972; Eggert and Gaunt, 1973; Good 1973; Cichan and Taylor, 1982; Wang et al., 2009; Terreaux De Felice et al., 2019; Rößler et al., 2021), but none that also report on the presence of fungi. Whether fungi were observed but not described, or whether there are no fungal remains in all these specimens, remains to be clarified. The present study is a good example of how worthwhile it can be to revisit old collections and reanalyze specimens that, one should assume, have already been intensively studied. The fact that the fungi in the *Sphenophyllum* stem from Autun have not been described is all the more surprising given that the specimen was prepared by Auguste Roche, a close collaborator of Bernard Renault, who was a pioneer in the study not only of structurally preserved *Sphenophyllum*, but also of fossil fungi. Our discovery contributes to the knowledge of fungal associations in Carboniferous-early Permian sphenophytes, a group of free-sporing vascular plants that today comprises only a single genus, *Equisetum*, with less than 20 species of herbaceous perennials, but was then much more diverse, both in terms of species number and growth habits (Husby, 2013). Because sphenophyte cell walls are characterized by an uncommon polysaccharide composition and the deposition of silica (e.g. Perry and Fraser, 1991; Fry et al., 2008), it would be especially interesting to find out how similar or dissimilar the fungal communities associated with fossil representatives of this group of plants are compared to the fungal communities in other plants of the same habitats. We therefore hope that in the course of further research on structurally preserved plants, more specimens of *Sphenophyllum* and other sphenophytes colonized by fungi will be discovered and described, which may lead to a more complete documentation of fungal relationships in this group of plants over time.

Chapter 6
Conclusions and future research directions

6.1 General conclusions

Three studies on anatomically preserved specimens dating from the Devonian-Carboniferous were conducted during this thesis. Their results have contributed to reassessing the taxonomical and anatomical diversity of the woody plants from this period and give another example of a plant group surviving to the Hangenberg event.

6.1.1 Taxonomical diversity

The taxonomical diversity has been increased through the description of a new species (Chapter 2), *Callixylon seamrogia*, which adds to the Devonian-Carboniferous plant diversity as a whole.
The study focuses on the description and growth of *Cladoxylon taeniatum* (Chapter 3), which also leads to the identification of *Cladoxylon mirabile* in the French locality of the Montagne Noire (Hérault, France). This species has been previously reported exclusively in Saalfed (Germany), this finding increases the taxonomical diversity of the French Tournaisian flora. In addition, the studies representing Chapters 3 and 4 of this thesis also reassess the taxonomical diversity at the genus and order levels, respectively.
The study of the growth of *Cladoxylon taeniatum* confirms the previous hypothesis about the conspecificity between the latter species and *C. dubium* (Bertrand, 1935), decreasing the taxonomical diversity within the genus.
The taxonomical diversity of the aneurophytales has also been increased by including *Stauroxylon beckii* within it, using phylogenetic and classical comparison methods (Chapter 4). The studies on *S. beckii* and *C. taeniatum* show again how the reexamination of taxa and specimens known for a long time can, in the light of new knowledge (e.g. here on the phylogeny of radiotopsids and the growth of Cladoxylopsids), lead to re-assessing the plant diversity.

6.1.2 Anatomical diversity

The main finding of this thesis, in terms of anatomical diversity, is to describe a new wood growth pattern within the Devonian-Carboniferous euphyllophytes. This pattern has been described in the study of *Cladoxylon taeniatum*, which has been reconstructed as possessing an uneven growth of its wood around its ribs. The wood composition being similar to other coeval woody plants, this finding shows how a new pattern of wood development can evolve from the same cell composition (Chapter 3). In addition, another specimen has been described in the study of *Stauroxylon beckii*. This new specimen, shows a different organotaxis and lacks wood, which adds to the anatomical

diversity at the species level.
The study of *Callixylon seamrogia* (Chapter 2) increased the anatomical diversity of the genus by showing a unique combination of ray tracheid characters and root stele (i.e. the first three-lobed actinostele of the genus). These actinosteles are also unique in the placement of their numerous putative exarch protoxylem strands that are located all around them. To my knowledge, this character makes it the only actinosteles with this specificity in either fossil or extant plants.

6.1.3 Hangenberg event and woody plants

The three studies increase the taxonomical and anatomical diversity of the Late Devonian (Chapter 2) and early Carboniferous floras (Chapters 3 and 4). These findings can be included in future studies comparing the anatomical and taxonomical diversity between these two periods. In addition, in this thesis, new evidence of a group (i.e. the Aneurophytales) crossing the Devonian-Carboniferous boundary has been recovered through the study of *Stauroxylon beckii* (Chapter 4).
The first definition of the term mass extinction is provided by Sepkosky in 1986 (p 278) as "any substantial increase in the amount of extinction (i.e., lineage termination) suffered by more than one geographically widespread higher taxon during a relatively short interval of geologic time, resulting in an at least temporary decline in their standing diversity." Mass extinctions are then defined based on temporal, quantitative, and geographical criteria, which have already been used together when Newell (1952) used for the first time the term "mass extinction," marking the "beginning of scientific analysis of mass extinction" (Bambach, 2006, p 129). However, beyond the bias linked to the determination of taxonomical diversity in the terrestrial fossil record (especially important in plant studies [see Cleal et al., 2021]), either this definition or the following ones will suffer from the "vagueness" of their terms or, on the contrary, the imposition of arbitrary thresholds. For example, how much is a "substantial increase"? Or if you have stated that you need 75% of extinction to define an event as a mass extinction, how do you characterise an event with 74% extinction? (see Linke and Clements [2024] for a review).

Despite these limitations, studies aiming to determine if past floras experience the same patterns of extinction as fauna have been conducted and have mainly led to the conclusion that plants are typically less impacted by mass extinction events (McElwain and Punyasena, 2007; Cleal and Cascales-Miñana, 2014; Nowak et al., 2019; Cleal et al., 2021). The Hangenberg event is not part of the classical "5 big mass extinctions" and has only relatively recently been recognised as a major extinction event. The debate on its impact on plants is still ongoing (Cleal and Cascales-Miñana, 2014; Kaiser et al., 2015; Prestianni et al., 2016; Marshall et al., 2020; Capel et al., 2021), in part due to limited data. However, Chapter 4 of this thesis provides further evidence of a new order

crossing the boundary (i.e., the Aneurophytales) that adds to the arguments in favour of a reduced impact of this event on plants, at least at a high taxonomic level. Future studies on new localities and specimens discovered during the fieldtrips conducted for this thesis (see Chapter 1, Part XX) have the potential to advance significantly the discussion on the subject, by providing new information on plant diversity on each side of the event.

6.1.4 Plant-microorganism interaction

This work has included fieldtrips in Irish localities that led to new fossil discoveries such as the stem and roots of *Callixylon seamrogia* presented in Chapter 2. These localities hold well-preserved anatomical specimens, nevertheless, no definitive evidence of interactions with microorganisms like fungi has been identified so far. Similar conclusions can be made from the French specimens of the Montagne Noire presented in Chapters 3 and 4, and more importantly, from decades of study beforehand on the hundreds of specimens currently collected (e.g. Böhm, 1935; Galtier, 1970, 1977; Galtier and Holmes, 1982; Meyer-Berthaud, 1984; Rowe and Galtier, 1989; Phillips and Galtier, 2005; Decombeix et al., 2006, 2008, 2017, 2019b; Masselter et al., 2009).

However, it can be noted that our team describes the oldest evidence of tyloses in one of the *Callixylon* specimens found in Sandeel beach locality in Hook Head (Ireland, County Wexford [Decombeix et al., 2023]). Tyloses are anatomical evidence of a plant's mechanisms aiming to protect the vascular system from embolism or pathogen infections (such as fungi, for example). This finding shows that this locality possesses the preservation potential to observe interaction and sub-cellular structures inside plant cells. This, in turn, has and will lead to a continuous awareness of recognizing and describing fossil fungi, which has been the main topic in the last chapter of this thesis. In this part (Chapter 5), the study of a single slide of a plant recognized as *Sphenophyllum* leads to 1) the first evidence of fungal remains inside a sphenophyte stem, 2) the first report of fungal structure preserved as traces fossils, which providing a prime example of human bias in the study fossil fungi.

6.1.5 Insight into Devonian-Carboniferous plant characters' evolution and architecture

In addition to these findings, the studies presented in Chapters 2, 3, and 4 provide new information about the architecture of Devonian-Carboniferous plants and the evolution of their characters/organs.

In Chapter 2, the studies' specimens of *Callixylon seamrogia* include stems that, according to architectural models, have been recognized as main axes with one emitting a non-persistent branch apically. In this case, the anatomy of the Irish specimens can be compared to preexisting architectural models. However, this study also reported the first *Callixylon* roots showing 3 lobed-actinosteles. This, as well as its unusual protoxylem placement, can lead to future studies about the architecture of archaeopteridalean roots that have, for now, been scarce.
The study on *Cladoxylon taeniatum* has led to hypotheses about a new plant architecture within the Cladoxylopsids. This study provides the first growth model for a non-arborescent Cladoxylopsid, and an identification of the different axes order of *C. taeniatum*, as well as their organotaxis, i.e. stem emitting in spiral petiole-like organs bearing alternately dichotomous ultimate appendages. Although the habit part of the architectural model is still uncertain, the preferred hypothesis is that this plant might have a creeping habit. In any case, this finding adds to the understanding of the architecture of the Devonian-Carboniferous plants.

In terms of characters/organs' evolution, the study of *Stauroxylon beckii* gives insight into the leaf evolution. This species is assigned to the aneurophytales and possesses lateral organs that seem to show bilateral symmetry and an early stage of adaxial-abaxial polarity. These characters have been part of the defining character of the megaphyll (see Tomescu [2009]) but were previously unknown in the aneurophytales. *Stauroxylon beckii,* then, represents another evidence of independent (and incomplete) evolution of the leaf within the lignophytes (Chapter 4).
This work has also uncovered new insights into stele evolution.
First, *Stauroxylon beckii* possesses a large central protoxylem strand and metaxylem tracheids bigger at the center than in the lobes. This primary xylem anatomy might consist of a new structural fingerprint that tends to confirm the hypothesis of a pith formation from central protoxylem strands induced by auxin concentration (Stein, 1993; Tomescu and McQueen, 2022; Chapter 4). The pith evolution has been "*central to understanding the evolution of stelar architecture*" (Tomescu, 2021: p. 11), the above statement about *S. beckii* makes it an important species for a better understanding of stele evolution.
Second, the report of an endodermal layer around each vascular bundle of *Cladoxylon taeniatum* makes its stele classified as an eustelic boundary eustele using the classification recently put forward by Tomescu (2021). This finding led to the reinterpretation of tissue previously recognized as a pith in cladoxylopsids as cortical in nature (Chapter 3), suggesting that the previous hypothesis on the stele and pith evolution in this group may need partial revision.

6.1.6 Thesis findings

In this thesis, four different studies have been conducted that have contributed to 1) the increase of the taxonomical and anatomical diversity of the Devonian-Carboniferous plants, 2) the hypothesis in favor of a reduced impact of the Hangenberg event on plants in giving new evidence of a group crossing the Devonian-Carboniferous boundary, and 3) the hypothesis explaining the “lack” of evidence of wood-degrading fungi before the late Carboniferous by the bias in studying the fossil record of fungi in giving a prime example on how even with a preserved and prepare evidence, it can be forgotten. These results are aligned with the aims of this work, and in addition, the description of the different specimens in the broader context of plant evolution and architecture led to additional findings, 1) a new architectural model of an early Carboniferous plant has been proposed, 2) another independent evolution of a terminal organ toward a leaf structure has been recovered, and 3) support on preexisting hypothesis on stele evolution have been provided.

6.2 Future directions

During this thesis, numerous fossil specimens have been found in Irish localities, and only a part has been observed/prepared/studied. Future works will then focus on these specimens, giving a better idea of the Irish Late Devonian diversity. In addition, new localities holding anatomically and/or morphologically preserved specimens have been found around the already reported one of Sandeel Beach (Hook Head, County Wexford). Upcoming research will contribute to an even better understanding of Ireland's Late Devonian flora by describing and dating these new localities and comparing them with the Sandeel Beach locality and will potentially lead to the discovery of early Carboniferous localities. This combined with comparisons with floras from the late Famennian and the early Carboniferous of the US (Read, 1936; Cross and Hoskin, 1951; Hoskin and Cross, 1951), Australia (Meyer-Berthaud et al., 2021), Argentina (Prestianni et al., 2015; 2022), France (Chapter 3 and 4 and references therein), and Germany (Unger, 1856; Bertrand, 1935; Galtier and Meyer-Berthaud, 1996) will help to define the impact of the Hangenberg event on plants. In addition, anatomically preserved flora from this period being rare, these future studies will also increase our knowledge of Devonian plants and their evolution as a whole.

This work participates in the sampling effort of fossil fungi that will and has to be continued to unravel the timing of wood degradation, in association with other methods, such as using biomarkers and isotopes. In addition, this work also reaffirms the need to continue working on old collections that can provide the opportunity to reinvestigate species known for decades and can lead to (re)discovery of « unique » specimens. For example, this work allows the discovery of a new preservation type for fungi.

During this thesis, large-scale analyses of the phylogenetic relationship and the anatomical diversity of the Devonian-Carboniferous woody plants have not been conducted, and this despite the attempt to create a database encompassing all the characters important for plant descriptions. During the data acquisition process, it became evident that the current inconsistency in the nomenclature of fossil plant characters, combined with the absence of standardized measurement methods, led to significant challenges. In most cases, even essential information, such as the number of cells or structures measured, is missing, making it difficult to establish a reliable foundation for large-scale analyses, e.g. comparing the morphospace of species from the Late Devonian with the ones of the early Carboniferous. On the other hand, even if the above problems are fixed, the selection of relevant characters for running large phylogenetic analyses will need deeper work on their hypothesized homology before being selected. Future studies will then have to respond to these issues to get 1) strong hypotheses about the evolution of the wood thanks to a more accurate phylogeny of the tracheophytes/euphyllophytes, and 2) information on the impact of the Hangenberg event on these plants using potential anatomical differences between Late Devonian and early Carboniferous plants. Such a study can also be done on non-woody plants and/or expanded to include all plant taxa to analyse weather plants with this tissue are impacted differently by past environemental changes.

More generally, I see numerous works that can lead to a better understanding of the Devonian-Carboniferous floras. First, there is a need to restudy historical collections, especially the specimens that have been used as a basis for key genera and species that are still used today, but do not have a formal/relevant diagnosis (e.g. *Archaeopteris*, *Cladoxylon* [see Chapter 3], *Pietzschia*). The old literature on these plants leads to uncertainty because of unprecise descriptions, lack of clear definition of relevant characters, and difficulty in accessing the original publications, which together give extra and unnecessary work to researchers. Second, the Palaeobotany community as a whole needs to establish a nomenclature of characters that everyone will use to have the most complete descriptions possible and avoid misunderstanding. Toward the same wish of uniformity, the community should establish a guideline for how to measure quantitative characters. Third, if the two previous points are completed, it will be easier to start to establish a common database with a strong basis in terms of taxonomy, completeness of relevant characters, and reliability of measurements. Such a database will facilitate relevant large-scale studies on taxonomical relationships, character evolution, paleogeographic distributions, and existence of mass extinction events.

7. References

Aanen, D.K., Van 't Padje, A., Auxier, B., 2023. Longevity of fungal mycelia and nuclear quality checks: a new hypothesis for the role of clamp connections in dikaryons. Microbiology and Molecular Biology Reviews 87, e00022-21. https://doi.org/10.1128/mmbr.00022-21

Abd-Elsalam, K.A., Tibpromma, S., Wanasinghe, D.N., Camporesi, E., Hyde, K.D., 2016. *Equiseticola* gen. nov. (Phaeosphaeriaceae), from *Equisetum* sp. in Italy. Phytotaxa 284, 169–180. https://doi.org/10.11646/phytotaxa.284.3.2

Agashe, S.N., Tilak, S.T., 1970. Occurrence of fungal elements in the bark of arborescent calamite roots from the American Carboniferous. Bulletin of the Torrey Botanical Club 97, 216–218. https://doi.org/10.2307/2483460

Algeo, Thomas.J., Scheckler, S.E., Scott, A.C., 1998. Terrestrial-marine teleconnections in the Devonian: links between the evolution of land plants, weathering processes, and marine anoxic events [and Discussion]. Philosophical Transactions of the Royal Society of London. Series B: Biological Sciences 353, 113–130. https://doi.org/10.1098/rstb.1998.0195

Algeo, T.J., Berner, R.A., Maynard, J.B., Scheckler, S.E., 1995. Late Devonian oceanic anoxic events and biotic crises: "rooted" in the evolution of vascular land plants? GSA today 5, 64–66.

Algeo, T.J., Scheckler, S.E., 2010. Land plant evolution and weathering rate changes in the Devonian. Journal of Earth Science 21, 75–78.

Algeo, T.J., Shen, J., 2023. Theory and classification of mass extinction causation. National Science Review 11, nwad237. https://doi.org/10.1093/nsr/nwad237

Aloni, R., 2021. The control of tracheid size, vessel widening and density along the plant axis, in: Vascular Differentiation and Plant Hormones. Springer International Publishing, Cham. https://doi.org/10.1007/978-3-030-53202-4

Aly, A.H., Debbab, A., Kjer, J., Proksch, P., 2010. Fungal endophytes from higher plants: a prolific source of phytochemicals and other bioactive natural products. Fungal Diversity 41, 1–16. https://doi.org/10.1007/s13225-010-0034-4

Anderson, H.M., Hiller, N., Gess, R.W., 1995. *Archaeopteris* (Progymnospermopsida) from the Devonian of southern Africa. Botanical Journal of the Linnean Society 117, 305–320. https://doi.org/10.1111/j.1095-8339.1995.tb02593.x

Andrews, H.N., Phillips, T.L., 1968. *Rhacophyton* from the Upper Devonian of West Virginia. Journal of the Linnean Society of London, Botany 61, 37–64. https://doi.org/10.1111/j.1095-8339.1968.tb00102.x

Andrews, H.N., Phillips, T.L., Radforth, N.W., 1965. Paleobotanical studies in artic Canada: I. *Archaeopteris* from Ellesmere island. Canadian Journal of Botany 43, 545–556. https://doi.org/10.1139/b65-060

Androusse, A., Aissami, A., Rahouti, M., Lahlou, H., BenN Abdellah, S., Seigle Murandi, F., 2007. First record of three species of *Pythium* from Moroccan waters. Acta Botanica Malacitana 32, 35–40. https://doi.org/10.24310/abm.v32i0.7027

Aragón-Raygoza, A., Vasco, A., Blilou, I., Herrera-Estrella, L., Cruz-Ramírez, A., 2020. Development and cell cycle activity of the root apical meristem in the fern *Ceratopteris richardii*. Genes 11, 1455. https://doi.org/10.3390/genes11121455

Arnold, C.A., 1940. Structure and relationships of some Middle Devonian plants from western New York. American Journal of Botany 27, 57–63. https://doi.org/10.1002/j.1537-2197.1940.tb14215.x

Arnold, C.A., 1934. *Callixylon whiteanum* Sp. Nov., From the Woodford Chert of Oklahoma. Botanical Gazette 96, 180–185. https://doi.org/10.1086/334454

Arnold, C.A., 1930. The genus *Callixylon* from the Upper Devonian of central and western New York Papers of the Michigan Academy of Science, Arts and Letters 11, 1–50.

Bambach, R.K., 2006. Phanerozoic biodiversity mass extinctions. Annual Review of Earth and Planetary Sciences 34, 127–155. https://doi.org/10.1146/annurev.earth.33.092203.122654Bach, E.M., Narvaez-Rivera, G., Murray, K., Bauer, J.T., Hofmockel, K.S., 2018. The dynamic life of arbuscular mycorrhizal fungal symbionts. Ecology 99, 978–980. https://doi.org/10.1002/ecy.2096

Baral, H.-O., Haelewaters, D., 2015. *Rommelaarsia flavovirens* gen. et sp. nov. (Helotiales), a new discomycete on *Equisetum* with a peculiar asexual state. Ascomycete.org 7, 321–330.

Barnard, P.D.W., Long, A.G., 1975. *Triradioxylon*, a new genus of lower Carboniferous petrified stems and petioles together with a review of the classification of early *Pterophytina*. Transactions of the Royal Society of Edinburgh 69, 231–250.

Barnard, P.D.W., Long, A.G., 1973. On the structure of a petrified stem and some associated seeds from the lower Carboniferous rocks of east Lothian, Scotland. Transactions of the Royal Society of Edinburgh 69, 91–108. https://doi.org/10.1017/S008045680001499X

Bar-On, Y.M., Phillips, R., Milo, R., 2018. The biomass distribution on Earth. Proceedings of the National Academy of Sciences 115, 6506-6511. https://doi.org/10.1073/pnas.1711842115

Barthel, M., Krings, M., Rößler, R., 2010. Die schwarzen Psaronien von Manebach, ihre Epiphyten, Parasiten und Pilze. Semana 25, 41–60.

Barthélémy, D., Caraglio, Y., 2007. Plant architecture: a dynamic, multilevel and comprehensive approach to plant form, structure and ontogeny. Annals of Botany 99, 375–407. https://doi.org/10.1093/aob/mcl260

Bateman, R.M., Crane, P.R., DiMichele, W.A., Kenrick, P.R., Rowe, N.P., Speck, T., Stein, W.E., 1998. Early evolution of land plants: phylogeny, physiology, and ecology of the primary terrestrial radiation. Annual Review of Ecology and Systematics 29, 263–292. https://doi.org/10.1146/annurev.ecolsys.29.1.263

Batenburg, L.H., 1982. “Compression species” and “petrifaction species” of *Sphenophyllum* compared. Review of Palaeobotany and Palynology 36, 335–359. https://doi.org/10.1016/0034-6667(82)90028-8

Baxter, R.W., 1948. A study of the vegetative anatomy of the genus *Sphenophyllum* from american coal balls. Annals of the Missouri Botanical Garden 35, 209–231. https://doi.org/10.2307/2394531

Beck, C.B., 1981. *Archaeopteris* and its role in vascular plant evolution, in: Paleobotany, Paleoecology, and Evolution. New York: Praeger, 1981., New York, pp. 193–230.

Beck, C.B., 1976. Current status of the Progymnospermopsida. Review of Palaeobotany and Palynology 21, 5–23. https://doi.org/10.1016/0034-6667(76)90020-8

Beck, C.B., 1967. *Eddya sullivanensis*, gen. et sp. nov., a plant of gymnospermic morphology from the Upper Devonian of New York. Palaeontographica Abteilung B 121, 1–22.

Beck, C.B., 1964. Predominance of *Archaeopteris* in Upper Devonian flora of western Catskills and adjacent Pennsylvania. Botanical Gazette 125, 126–128. https://doi.org/10.1086/336257

Beck, C.B., 1962a. Reconstructions of *Archaeopteris*, and further consideration of its phylogenetic position. American Journal of Botany 49, 373–382. https://doi.org/10.1002/j.1537-2197.1962.tb14953.x

Beck, C.B., 1962b. Plants of the New Albany Shale. II. *Callixylon arnoldii* Sp. Nov. Brittonia 14, 322. https://doi.org/10.2307/2805249

Beck, C.B., 1960a. Connection between *Archaeopteris* and *Callixylon*. Science, New Series 131, 1524–1525. https://doi.org/10.1126/science.131.3412.1524

Beck, C.B., 1960b. Studies of New Albany Shale plants. I. *Stenokoleos simplex* comb. nov. American Journal of Botany 47, 115–124. https://doi.org/10.1002/j.1537-2197.1960.tb07103.x

Beck, C.B., 1960c. The identity of *Archaeopteris* and *Callixylon*. Brittonia 12, 351–368. https://doi.org/10.2307/2805124

Beck, C.B., 1957. *Tetraxylopteris schmidtii* gen. et sp. nov., a probable pteridosperm precursor from the Devonian of New York. American Journal of Botany 44, 350–367. https://doi.org/10.1002/j.1537-2197.1957.tb10551.x

Beck, C.B., 1953. A new root species of *Callixylon*. American Journal of Botany 40, 226–233. https://doi.org/10.2307/2438659

Beck, C.B., Stein, W.E., 1993. *Crossia virginiana* gen. et sp. nov., a new member of the Stenokoleales from the Middle Devonian of Southwestern Virginia. Palaeontographica Abt. B, Palaeophytologie 229, 115–134.

Beck, C.B., Stein, W.E., 1987. *Galteria bostonensis*, gen. et sp. nov., a protostelic calamopityacean from the New Albany shale of Kentucky. Canadian Journal of Botany 65, 348–361. https://doi.org/10.1139/b87-045

Beck, C.B., Wight, D.C., 1988. Progymnosperms, in: Origin and Evolution of Gymnosperms. Columbia University Press, New York, pp. 1–84.

Berry, C., 2008. The Middle Devonian plant collections of Francois Stockmans reconsidered. Geologica Belgica 12, 25–30.

Berry, C.M., Fairon-Demaret, M., 2002. The architecture of *Pseudosporochnus nodosus* Leclercq et Banks: a Middle Devonian cladoxylopsid from Belgium. International Journal of Plant Sciences163, 699–713. https://doi.org/10.1086/342037

Berry, C.M., Stein, W.E., 2000. A new Iridopteridalean from the Devonian of Venezuela. International Journal of Plant Sciences 161, 807–827. https://doi.org/10.1086/314295

Bertrand, P., 1935. Contribution à l'étude des cladoxylées de Saalfeld. Palaeontographica Abteilung B: Palaeophytologie 80, 101–179.

Böhm, R., 1935. Etude sur la flore de l'horizon à lydiennes de la base du Carbonifère de la Montagne Noire. Faculté des Sciences de Montpellier, Montpellier.

Bonamo, P.M., Banks, H.P., 1967. *Tetraxylopteris schmidtii*: its fertile parts and its relationships within the aneurophytales. American Journal of Botany 54, 755–768. https://doi.org/10.1002/j.1537-2197.1967.tb10697.x

Bond, G., 1931. XXVIII.—The stem-endodermis in the genus *Piper*. Transactions of the Royal Society of Edinburgh 56, 695–724. https://doi.org/10.1017/S0080456800016549

Boureau, E., 1964. Traité de Paléobotanique tome III. Sphenophyta Noeggerathiophyta. Masson.

Boyer, J.S., 1995. Reexamination of *Eospermatopteris eriana* (Dawson) Goldring from the Upper Middle Devonian (=Givetian) flora at Gilboa, New York. Ph.D. Southern Illinois University. 61p.

Bridge, J.S., Van Veen, P.M., Matten, L.C., 1980. Aspects of the sedimentology, palynology and palaeobotany of the Upper Devonian of southern Kerry Head, Co. Kerry, Ireland. Geological Journal 15, 143–170. https://doi.org/10.1002/gj.3350150208

Brodersen, C.R., Roark, L.C., Pittermann, J., 2012. The physiological implications of primary xylem organization in two ferns. Plant, Cell and Environment 35, 1898–1911. https://doi.org/doi: 10.1111/j.1365-3040.2012.02524.x

Brongniart, A., 1828. Prodrome d'une histoire des végétaux fossiles. Levrault.

Brongniart, A., 1822. Sur la classification et la distribution des végétaux fossiles. Imprimerie de A. Belin.

Broutin, J., Châteauneuf, J.-J., Galtier, J., Ronchi, A., 1999. L'Autunien d'Autun reste-t-il une référence pour les dépots continentaux du Permien inférieur d'Europe? Apport des données paléobotaniques. Geologie de la France 17–31.

Buchalo, A.S., Wasser, S.P., Mykhaylova, O.B., Bilay, V.T., Lomberg, M.L., 2011. Taxonomical significance of microstructures in pure cultures of macromycetes. Presented at the

Proceedings of the 7th International Conference on Mushroom Biology and Mushroom Products, Institut National de la Recherche Agronomique (INRA) Paris, pp. 50–57.

Buchalo, A.S., Zakordonec, O.A., Šašek, V., 1983. Scanning electron microscopic study of clamp connections in higher Basidiomycetes. Folia Microbiologica 28, 420–423. https://doi.org/10.1007/BF02879493

Burdon, J.J., 1983. *Trifolium Repens* L. The Journal of Ecology 71, 307. https://doi.org/10.2307/2259979

Bushnell, W.R., 1972. Physiology of Fungal Haustoria. Annual Review of Phytopathology 10, 151–176. https://doi.org/10.1146/annurev.py.10.090172.001055

Capel, E., Cleal, C.J., Gerrienne, P., Servais, T., Cascales-Miñana, B., 2021. A factor analysis approach to modelling the early diversification of terrestrial vegetation. Palaeogeography, Palaeoclimatology, Palaeoecology 566, 110170. https://doi.org/10.1016/j.palaeo.2020.110170

Caplan, M.L., Bustin, R.M., 1999. Devonian–Carboniferous Hangenberg mass extinction event, widespread organic-rich mudrock and anoxia: causes and consequences. Palaeogeography, Palaeoclimatology, Palaeoecology 148, 187–207. https://doi.org/10.1016/S0031-0182(98)00218-1

Carmichael, S.K., Waters, J.A., Batchelor, C.J., Coleman, D.M., Suttner, T.J., Kido, E., Moore, L.M., Chadimová, L., 2016. Climate instability and tipping points in the Late Devonian: detection of the Hangenberg event in an open oceanic island arc in the Central Asian Orogenic Belt. Gondwana Research 32, 213–231. https://doi.org/10.1016/j.gr.2015.02.009

Case, N.T., Gurr, S.J., Fisher, M.C., Blehert, D.S., Boone, C., Casadevall, A., Chowdhary, A., Cuomo, C.A., Currie, C.R., Denning, D.W., Ene, I.V., Fritz-Laylin, L.K., Gerstein, A.C., Gow, N.A.R., Gusa, A., Iliev, I.D., James, T.Y., Jin, H., Kahmann, R., Klein, B.S., Kronstad, J.W., Ost, K.S., Peay, K.G., Shapiro, R.S., Sheppard, D.C., Shlezinger, N., Stajich, J.E., Stukenbrock, E.H., Taylor, J.W., Wright, G.D., Cowen, L.E., Heitman, J., Segre, J.A., 2025. Fungal impacts on Earth's ecosystems. Nature 638, 49–57. https://doi.org/10.1038/s41586-024-08419-4

Cavalier-Smith, T., 1998. A revised six-kingdom system of life. Biological Reviews 73, 203–266. doi: 10.1017/s0006323198005167. PMID: 9809012.

Chaloner, W.G., 1972. Devonian plants from fair Isle, Scotland. Review of Palaeobotany and Palynology 14, 49–61. https://doi.org/10.1016/0034-6667(72)90007-3

Champreux, A., Meyer-Berthaud, B., Decombeix, A.-L., 2020. *Keraphyton* gen. nov., a new Late Devonian fern-like plant from Australia. PeerJ 8, e9321. https://doi.org/10.7717/peerj.9321

Chitaley, S., Cai, C., 2001. Permineralized *Callixylon* woods from the Late Devonian Cleveland Shale of Ohio, U.S.A. and that of Kettle Point, Ontario, Canada. Review of Palaeobotany and Palynology 114, 127–144. https://doi.org/10.1016/S0034-6667(00)00073-7

Christoudias, T., Kirkby, J., Stolzenburg, D., Pozzer, A., Sommer, E., Brasseur, G.P., Kulmala, M., Lelieveld, J., 2024. Earth's atmosphere protects the biosphere from nearby supernovae. Communications Earth & Environment 5, 326. https://doi.org/10.1038/s43247-024-01490-9

Chu, J., Durieux, T., Tomescu, A.M.F., 2024. An early cladoxylopsid with complex vascular architecture: *Paracladoxylon kespekianum* gen. et sp. nov. from the Lower Devonian (Emsian) of Quebec, Canada. American Journal of Botany 111, e16418. https://doi.org/10.1002/ajb2.16418

Cichan, M.A., 1985a. Vascular cambium and wood development in Carboniferous plants. II. *Sphenophyllum plurifoliatum* Williamson and Scott (Sphenophyllales). Botanical Gazette 146, 395–403. https://doi.org/10.1086/337539

Cichan, M.A., 1985b. Vascular cambium and wood development in Carboniferous plants. I. Lepidodendrales. American Journal of Botany 72, 1163–1176. https://doi.org/10.1002/j.1537-2197.1985.tb08369.x

Cichan, M.A., 1984. Vascular cambium and wood development in selected Carboniferous plants Ph.D.. Ohio State University. 237p.

Cichan, M.A., Taylor, T.N., 1990. Evolution of cambium in geologic time–a reappraisal, in: The Vascular Cambium. Wiley New York, Taunton, Somerset, England, pp. 213–228.

Cichan, M.A., Taylor, T.N., 1984. A method for determining tracheid lengths in petrified wood by analysis of cross section. Annals of Botany 53, 219–226. https://doi.org/10.1093/oxfordjournals.aob.a086683

Cichan, M.A., Taylor, T.N., 1982. Vascular cambium development in *Sphenophyllum*: A Carboniferous arthrophyte. IAWA Journal 3, 155–160. https://doi.org/10.1163/22941932-90000830

Cleal, C.J., Cascales-Miñana, B., 2014. Composition and dynamics of the great Phanerozoic Evolutionary Floras. Lethaia 47, 469–484. https://doi.org/10.1111/let.12070

Cleal, C., Pardoe, H.S., Berry, C.M., Cascales-Miñana, B., Davis, B.A.S., Diez, J.B., Filipova-Marinova, M.V., Giesecke, T., Hilton, J., Ivanov, D., Kustatscher, E., Leroy, S.A.G., McElwain, J.C., Opluštil, S., Popa, M.E., Seyfullah, L.J., Stolle, E., Thomas, B.A., Uhl, D., 2021. Palaeobotanical experiences of plant diversity in deep time. 1: How well can we identify past plant diversity in the fossil record? Palaeogeography, Palaeoclimatology, Palaeoecology 576, 110481. https://doi.org/10.1016/j.palaeo.2021.110481Coemans, E., Kickx, M.J.-J., 1864. Monographie des *Sphenophyllum* d'Europe. Bulletins de l'Académie Royale des Sciences, des Lettres et des Beaux-Art de Belgique 18, 134–163.

Coker, W.C., Patterson, P.M., 1927. A new species of *Pythium*. Journal of the Elisha Mitchell Scientific Society, 42, 247–250. http://www.jstor.org/stable/24332015

Collinge, D.B., 2009. Cell wall appositions: the first line of defence. Journal of Experimental Botany 60, 351–352. https://doi.org/10.1093/jxb/erp001

Connery, T., 2002. An integrated study of the palaeobotany, palynology and sedimentology of the Late Devonian plant bearing horizons in the Toe Head Sandstone Formation at Toe Head, west Cork, Ireland. Ph.D. University College Cork, Ireland. 371 p.

Connery, T., 1999. Plant fossils from the Late Devonian Toe Head Sandstone Formation, west Cork, Ireland: a preliminary report, in: Acta Palaeobotanica. Presented at the 5th European Palaeobotanical and Palynological Conference, KraKow, Poland, pp. 21–25.

Cordi, J., Stein, W.E., 2005. The anatomy of *Rotoxylon dawsonii* comb. nov. (*Cladoxylon dawsonii*) from the Upper Devonian of New York State. International Journal of Plant Sciences 166, 1029–1045. https://doi.org/10.1086/432630

Cornet, L., Gerrienne, P., Meyer-Berthaud, B., Prestianni, C., 2012. A Middle Devonian *Callixylon* (Archaeopteridales) from Ronquières, Belgium. Review of Palaeobotany and Palynology 183, 1–8. https://doi.org/10.1016/j.revpalbo.2012.07.004

Corvez, A., Barriel, V., Dubuisson, J.-Y., 2012. Diversity and evolution of the megaphyll in euphyllophytes: phylogenetic hypotheses and the problem of foliar organ definition. Comptes Rendus Palevol 11, 403–418. https://doi.org/10.1016/j.crpv.2012.05.003

Crane, P.R., 1985. Phylogenetic analysis of seed plants and the origin of angiosperms. Annals of the Missouri Botanical Garden 72, 716–793. https://doi.org/10.2307/2399221

Crang, R., Lyons-Sobaski, S., Wise, R., 2018. Parenchyma, collenchyma, and sclerenchyma, in: Plant Anatomy. Springer International Publishing, Cham, pp. 181–213. https://doi.org/10.1007/978-3-319-77315-5_6

Crepet, W.L., Niklas, K.J., 2018. Early tracheophyte phylogeny, in: Transformative Paleobotany. Elsevier, pp. 69–92. https://doi.org/10.1016/B978-0-12-813012-4.00005-X

Cross, A.T., Hoskins, J.H., 1951. Paleobotany of the Devonian-Mississippian Black Shales. Journal of Paleontology 25, 713–728. https://www.jstor.org/stable/1299812

Cross, A.T., Phillips, T.L., 1990. Coal-forming plants through time in North America. International Journal of Coal Geology 16, 1–46. https://doi.org/10.1016/0166-5162(90)90012-N

D'Antonio, M.P., Boyce, C.K., 2021. Secondary phloem in arborescent lycopsids. New Phytologist 232, 967–972. https://doi.org/10.1111/nph.17641

Davies, N.S., McMahon, W.J., Berry, C.M., 2024. Earth's earliest forest: fossilized trees and vegetation-induced sedimentary structures from the Middle Devonian (Eifelian) Hangman Sandstone Formation, Somerset and Devon, SW England. Journal of the Geological Society 181, jgs2023-204. https://doi.org/10.1144/jgs2023-204

Dawson, J.W., 1871. The fossil plants of the Devonian and upper Silurian formations of Canada. Dawson Bros.

De Micco, V., Balzano, A., Wheeler, E.A., Baas, P., 2016. Tyloses and gums: a review of structure, function and occurrence of vessel occlusions. IAWA Journal 37, 186–205. https://doi.org/10.1163/22941932-20160130

Decombeix, A.-L., Galtier, J., 2021. Periderm production in the Mississippian cladoxylopsid *Cladoxylon taeniatum* and a review of periderm occurrence in Paleozoic plants. International Journal of Plant Sciences 182, 430–444. https://doi.org/10.1086/714284

Decombeix, A., Meyer-Berthaud, B., 2013. A *Callixylon* (Archaeopteridales, Progymnospermopsida) trunk with preserved secondary phloem from the Late Devonian of Morocco. American Journal of Botany 100, 2219–2230. https://doi.org/10.3732/ajb.1300167

Decombeix, A.-L., Harper, C.J., Prestianni, C., Durieux, T., Ramel, M., Krings, M., 2023. Fossil evidence of tylosis formation in Late Devonian plants. Nature Plants 9, 695–698. https://doi.org/10.1038/s41477-023-01394-0

Decombeix, A.-L., Durieux, T., Harper, C.J., Meyer-Berthaud, B., Prestianni, C., Ramel, M., Horajska-Shaikh, M., 2022a. Reinvestigating the Late Devonian plant bearing localities of Co. Kerry and Co. Wexford, Ireland, in: 11th European Palaeobotany and Palynology Conference. Stockholm, Sweden.

Decombeix, A.-L., Harper, C.J., Galtier, J., Meyer-Berthaud, B., Krings, M., 2022b. Tyloses in fossil plants: New data from a Mississippian tree, with a review of previous records. Botany Letters 169, 510–526. https://doi.org/10.1080/23818107.2022.2099461

Decombeix, A.-L., Galtier, J., Meyer-Berthaud, B., Prestianni, C., Rowe, N.P., Harper, C.J., 2020. A review of the early Mississippian anatomically preserved flora from Montagne Noire, in: Botany 2020 - Virtual Botany Conference. Virtual, United States.

Decombeix, A.-L., Boura, A., Tomescu, A.M.F., 2019a. Plant hydraulic architecture through time: lessons and questions on the evolution of vascular systems. IAWA Journal 40, 387–420. https://doi.org/10.1163/22941932-40190254

Decombeix, A.-L., Galtier, J., Meyer-Berthaud, B., Prestianni, C., Harper, C.J., Terreaux de Félice, H., 2019b. Anatomically preserved plants from the Tournaisian of the Montagne Noire (France): an exceptional window into early Mississippian floras, in: 19th International Congress on the Carboniferous and Permian (XIX ICCP 2019). cologne, Germany.

Decombeix, A.-L., Letellier, D., Meyer-Berthaud, B., 2017. Whose roots are these? Linking anatomically preserved Lignophyte roots and stems from the early Carboniferous of Montagne Noire, France. International Journal of Plant Sciences 178, 42–56. https://doi.org/10.1086/689029

Decombeix, A.-L., Galtier, J., Prestianni, C., 2015. The early Carboniferous progymnosperm *Protopitys*: new data on vegetative and fertile structures, and on its geographic and stratigraphic distribution. Historical Biology 27, 345–354. https://doi.org/10.1080/08912963.2014.905554

Decombeix, A.-L., Galtier, J., Meyer-Berthaud, B., 2014. Secondary phloem in early Carboniferous seed plants: anatomical diversity and evolutionary implications. International Journal of Plant Sciences 175, 891–910. https://doi.org/10.1086/677650

Decombeix, A. -L., Meyer-Berthaud, B., Galtier, J., 2008. Diversity of Mississippian arborescent Lignophytes: A new species of *Eristophyton* from the Middle Tournaisian of France. International Journal of Plant Sciences 169, 1116–1127. https://doi.org/10.1086/590455

Decombeix, A.-L., Galtier, J., Meyer-Berthaud, B., 2006. *Faironia difasciculata*, a new gymnosperm from the early Carboniferous (Mississippian) of Montagne Noire, France. Review of Palaeobotany and Palynology 142, 79–92. https://doi.org/10.1016/j.revpalbo.2006.03.020

Decombeix, A.-L., Meyer-Berthaud, B., Rowe, N., Galtier, J., 2005. Diversity of large woody lignophytes preceding the extinction of *Archaeopteris*: New data from the middle Tournaisian of Thuringia (Germany). Review of Palaeobotany and Palynology 137, 69–82. https://doi.org/10.1016/j.revpalbo.2005.08.006

Dennis, R.L., 1974. Studies of Paleozoic ferns: *Zygopteris* from the middle and late Pensylvanian of the United States. Palaeontographica Abteilung B, Palaeophytologie 148, 95–136.

Dennis, R.L., 1970. A middle Pennsylvanian basidiomycete mycelium with clamp connections. Mycologia 62, 578–584. https://doi.org/10.1080/00275514.1970.12018997

Dennis, R.L., 1969. Fossil mycelium with clamp connections from the middle Pennsylvanian. Science 163, 670–671. https://doi.org/10.1126/science.163.3868.670

Dhillion, S.S., 1993. Vesicular-arbuscular mycorrhizas of *Equisetum* species in Norway and the U.S.A.: occurrence and mycotrophy. Mycological Research 97, 656–660. https://doi.org/10.1016/S0953-7562(09)80142-1

Dighton, J., White, J.F. (Eds.), 2017. The fungal Community its organization and role in the ecosystem, 4th ed. CRC Press, Boca Raton, FL. https://doi.org/10.1201/9781315119496-22

Donoghue, M.J., 2005. Key innovations, convergence, and success: macroevolutionary lessons from plant phylogeny. Paleobiology 31, 77–93. https://doi.org/10.1666/0094-8373(2005)031[0077:KICASM]2.0.CO;2

Dotzler, N., Taylor, T.N., Galtier, J., Krings, M., 2011. *Sphenophyllum* (Sphenophyllales) leaves colonized by fungi from the Upper Pennsylvanian Grand-Croix cherts of central France. Zitteliana 51, 3–8.

Dotzler, N., Krings, M., Agerer, R., Galtier, J., Taylor, T.N., 2008. *Combresomyces cornifer* gen. sp. nov., an endophytic peronosporomycete in *Lepidodendron* from the Carboniferous of central France. Mycological Research 112, 1107–1114. https://doi.org/10.1016/j.mycres.2008.03.003

Doubinger, J., Vetter, P., Langiaux, J., Galtier, J., Broutin, J., 1995. La flore fossile du bassin houiller de Saint-Étienne. Éd. du Muséum.

Doyle, J.A., Donoghue, M.J., 1986. Seed plant phylogeny and the origin of angiosperms: an experimental cladistic approach. The Botanical Review 52, 321–431. https://doi.org/10.1007/BF02861082

Driese, S.G., Mora, C.I., Elick, J.M., 1997. Morphology and taphonomy of root and stump casts of the earliest trees (Middle to Late Devonian), Pennsylvania and New York, U.S.A. PALAIOS 12, 524. https://doi.org/10.2307/3515409

Dunn, M.T., 2006. A review of permineralized seed fern stems of the Upper Paleozoic. The Journal of the Torrey Botanical Society 133, 20–32. https://doi.org/10.3159/1095-5674(2006)133[20:AROPSF]2.0.CO;2

Dunn, M.T., Rothwell, G.W., 2012. Phenotypic plasticity of the hydrasperman seed fern *Tetrastichia bupatides* Gordon (Lyginopteridaceae). International Journal of Plant Sciences 173, 823–834. https://doi.org/10.1086/666661

Durieux, T., Harper, C.J., Decombeix, A.-L., Krings, M., 2025a. A rare permineralized *Sphenophyllum* (Sphenophyta, Sphenophyllales) stem containing abundant fungal remains from the Permian of Autun, central France. Review of Palaeobotany and Palynology 343, 105416. https://doi.org/10.1016/j.revpalbo.2025.105416

Durieux, T., Decombeix, A.-L., Harper, C.J., Ramel, M., Mays, C., Prestianni, C., 2025b. *Callixylon seamrogia* sp. nov., a new species from the uppermost Famennian (Upper Devonian) of Ireland. Review of Palaeobotany and Palynology 334, 105256. https://doi.org/10.1016/j.revpalbo.2024.105256

Durieux, T., Decombeix, A.-L., Harper, C., Galtier, J., 2024. Re-investigation of *Stauroxylon beckii*, a possible aneurophytalean progymnosperm from the Mississippian of France. International Journal of Plant Sciences 729412. https://doi.org/10.1086/729412

Durieux, T., Lopez, M.A., Bronson, A.W., Tomescu, A.M.F., 2021. A new phylogeny of the cladoxylopsid plexus: contribution of an early cladoxylopsid from the Lower Devonian (Emsian) of Quebec. American Journal of Botany 108, 2066–2095. https://doi.org/10.1002/ajb2.1752

Eggert, D.A., 1961. The ontogeny of Carboniferous arborescent Lycopsida. Palaeontographica Abteilung B 43–92.

Eggert, D.A., Gaunt, D.D., 1973. Phloem of *Sphenophyllum*. American Journal of Botany 60, 755–770. https://doi.org/10.1002/j.1537-2197.1973.tb07588.x

Enstone, D.E., Peterson, C.A., Ma, F., 2003. Root endodermis and exodermis: structure, function, and responses to the environment. Journal of Plant Growth Regulation 21, 335–351. https://doi.org/10.1007/s00344-003-0002-2

Esau, K., 1977. Anatomy of seed plant. 2nd Edition, John Wiley & Sons Ltd. ed. New York.

Esteban, L.G., De Palacios, P., Gasson, P., García-Iruela, A., García-Fernández, F., García-Esteban, L., 2024. Hardwoods: anatomy and functionality of their elements—A short review. Forests 15, 1162. https://doi.org/10.3390/f15071162

Feist, R., Cornée, J.-J., Corradini, C., Hartenfels, S., Aretz, M., Girard, C., 2021. The Devonian–Carboniferous boundary in the stratotype area (SE Montagne Noire, France). Palaeobiodiversity and Palaeoenvironments 101, 295–311. https://doi.org/10.1007/s12549-019-00402-6

Fields, B.D., Melott, A.L., Ellis, J., Ertel, A.F., Fry, B.J., Lieberman, B.S., Liu, Z., Miller, J.A., Thomas, B.C., 2020. Supernova triggers for end-Devonian extinctions. Proceedings of the National Academy of Sciences U.S.A. 117, 21008–21010. https://doi.org/10.1073/pnas.2013774117

Floudas, D., Binder, M., Riley, R., Barry, K., Blanchette, R.A., Henrissat, B., Martínez, A.T., Otillar, R., Spatafora, J.W., Yadav, J.S., Aerts, A., Benoit, I., Boyd, A., Carlson, A., Copeland, A., Coutinho, P.M., de Vries, R.P., Ferreira, P., Findley, K., Foster, B., Gaskell, J., Glotzer, D., Górecki, P., Heitman, J., Hesse, C., Hori, C., Igarashi, K., Jurgens, J.A., Kallen, N., Kersten, P., Kohler, A., Kües, U., Kumar, T.K.A., Kuo, A., LaButti, K., Larrondo, L.F., Lindquist, E., Ling, A., Lombard, V., Lucas, S., Lundell, T., Martin, R., McLaughlin, D.J., Morgenstern, I., Morin, E., Murat, C., Nagy, L.G., Nolan, M., Ohm, R.A., Patyshakuliyeva, A., Rokas, A., Ruiz-Dueñas, F.J., Sabat, G., Salamov, A., Samejima, M., Schmutz, J., Slot, J.C., St. John, F., Stenlid, J., Sun, H., Sun, S., Syed, K., Tsang, A., Wiebenga, A., Young, D., Pisabarro, A., Eastwood, D.C., Martin, F., Cullen, D., Grigoriev, I.V., Hibbett, D.S., 2012. The Paleozoic origin of enzymatic lignin decomposition reconstructed from 31 fungal genomes. Science 336, 1715–1719. https://doi.org/10.1126/science.1221748

Forbes, E., 1853. On the fossils of the Yellow Sandstone of the south of Ireland, in: Rep. Br. Assoc. Adv. Sci.(22nd Meet.). Presented at the 22nd Meeting of the British Association for the Advancement of Science, Belfast, p. 43.

Friendly, M., 2002. Corrgrams: exploratory displays for correlation matrices. The American Statistician 56, 316–324. https://doi.org/10.1198/000313002533

Fry, S.C., Nesselrode, B.H.W.A., Miller, J.G., Mewburn, B.R., 2008. Mixed-linkage (1→3,1→4)-β- d -glucan is a major hemicellulose of *Equisetum* (horsetail) cell walls. New Phytologist 179, 104–115. https://doi.org/10.1111/j.1469-8137.2008.02435.x

Furtado, J.S., 1966. Significance of the clamp-connection in the basidiomycetes. Persoonia 4, 125–144.

Galtier, J., 2016. Bernard Renault (1836-1904) illustre paléobotaniste bourguignon et son héritage scientifique. Revue scientifique Bourgogne-Nature 23.

Galtier, J., 2010. The origins and early evolution of the megaphyllous leaf. International Journal of Plant Sciences 171, 641–661. https://doi.org/10.1086/653130

Galtier, J., 2008. A new look at the permineralized flora of Grand-Croix (Late Pennsylvanian, Saint-Etienne Basin, France). Review of Palaeobotany and Palynology 152, 129–140. https://doi.org/10.1016/j.revpalbo.2008.04.007

Galtier, J., 1988. Morphology and phylogenetic relationships of early pteridosperms, in: Origin and Evolution of Gymnosperms. Columbia University Press, New York, pp. 135–176.

Galtier, J., 1980. Les végétaux silicifiés du Permian d'Autun: analyse quantitative et interprétation possible. Bulletin trimestriel de la Société d'histoire naturelle et des amis du Muséum d'Autun 35–40.

Galtier, J., 1977. *Tristichia longii*, nouvelle pteridospermale probable du Carbonifère de la Montagne Noire. Comptes rendus hebdomadaires des séances de l'Académie des sciences. D, Sciences naturelles 284, 2215–2218.

Galtier, J., 1970. Recherches sur les végétaux à structure conservée du Carbonifère inférieur Français. Faculté des Sciences de Montpellier, Montpellier.

Galtier, J., Holmes, J.C., 1982. New observations on the branching of Carboniferous ferns and pteridosperms. Annals of Botany 49, 737–746. https://doi.org/10.1093/oxfordjournals.aob.a086303

Galtier, J., Meyer-Berthaud, B., 1996. The early seed plant *Tristichia tripos* (Unger) comb. nov. from the lower Carboniferous of Saalfeld, Thuringia. Review of Palaeobotany and Palynology 93, 299–315. https://doi.org/10.1016/0034-6667(95)00131-X

Galtier, J., Ronchi, A., Broutin, J., 2011. Early Permian silicified floras from the Perdasdefogu Basin (SE Sardinia): comparison and bio-chronostratigraphic correlation with the floras of the Autun Basin (Massif central, France). Geodiversitas 33, 43–69. https://doi.org/10.5252/g2011n1a4

Galtier, J., Meyer-Berthaud, B., Rowe, N.P., 1988. Tournaisian plants from the “lydiennes” formation of the Montagne Noire (France). Courier Forschungsinstitut Senckenberg 100, 109–117.

Geetha, K., Dathar, V., 2022. Plant–fungal interactions, in: Shukla, A.C. (Ed.), applied mycology, fungal biology. Springer International Publishing, Cham, pp. 271–285. https://doi.org/10.1007/978-3-030-90649-8_13

Geldner, N., 2013. The endodermis. Annual Review of Plant Biology 64, 531–558. https://doi.org/10.1146/annurev-arplant-050312-120050

Gensel, P.G., 2022. Partially permineralized adpressions of *Wilhowia phocarum* Gensel gen. et sp. nov., a new basal euphyllophyte from the Lower Devonian Battery Point Formation, north shore of Gaspé Bay, Quebec, Canada. International Journal of Plant Sciences 183, 604–629. https://doi.org/10.1086/721263

Gensel, P.G., 2018. Early Devonian woody plants and implications for the early evolution of vascular cambia, in: Transformative Paleobotany. Elsevier, pp. 21–33. https://doi.org/10.1016/B978-0-12-813012-4.00002-4

Gensel, P.G., 1984. A new Lower Devonian plant and the early evolution of leaves. Nature 309, 785–787. https://doi.org/10.1038/309785a0

Gerrienne, P., 1992. The Emsian plants from Fooz-Wépion (Belgium). III. *Foozia minuta* gen. et spec. nov., a new taxon with probable cladoxylalean affinities. Review of Palaeobotany and Palynology 74, 139–157. https://doi.org/10.1016/0034-6667(92)90142-4

Gerrienne, P., Gensel, P.G., 2016. New data about anatomy, branching, and inferred growth patterns in the Early Devonian plant *Armoricaphyton chateaupannense*, Montjean-sur-Loire, France. Review of Palaeobotany and Palynology 224, 38–53. https://doi.org/10.1016/j.revpalbo.2015.07.014

Gerrienne, P., Servais, T., Vecoli, M., 2016. Plant evolution and terrestrialization during Palaeozoic times—The phylogenetic context. Review of Palaeobotany and Palynology 227, 4–18. https://doi.org/10.1016/j.revpalbo.2016.01.004

Gerrienne, P., Gensel, P.G., Strullu-Derrien, C., Lardeux, H., Steemans, P., Prestianni, C., 2011. A simple type of wood in two early Devonian plants. Science 333, 837–837. https://doi.org/10.1126/science.1208882

Gerrienne, P., Meyer-Berthaud, B., Lardeux, H., Régnault, S., 2010. First record of *Rellimia* Leclercq & Bonamo (aneurophytales) from Gondwana, with comments on the earliest lignophytes. Geological Society, London, Special Publications 339, 81–92. https://doi.org/10.1144/SP339.8

Gerrienne, P., Meyer-Berthaud, B., Fairon-Demaret, M., Streel, M., Steemans, P., 2004. *Runcaria*, a Middle Devonian seed plant precursor. Science 306, 856–858. https://doi.org/10.1126/science.1102491

Giesemann, P., Eichenberg, D., Stöckel, M., Seifert, L.F., Gomes, S.I.F., Merckx, V.S.F.T., Gebauer, G., 2020. Dark septate endophytes and arbuscular mycorrhizal fungi (*Paris* -morphotype) affect the stable isotope composition of 'classically' non-mycorrhizal plants. Functional Ecology 34, 2453–2466. https://doi.org/10.1111/1365-2435.13673

Giesen, P., Berry, C.M., 2013. Reconstruction and growth of the early tree *Calamophyton* (Pseudosporochnales, Cladoxylopsida) based on exceptionally complete specimens from Lindlar, Germany (Mid-Devonian): Organic connection of *Calamophyton* branches and *Duisbergia* trunks. International Journal of Plant Sciences 174, 665–686. https://doi.org/10.1086/669913

Goloboff, P.A., Catalano, S.A., 2016. TNT version 1.5, including a full implementation of phylogenetic morphometrics. Cladistics 32, 221–238. https://doi.org/10.1111/cla.12160

Good, C.W., 1973. Studies of *Sphenophyllum* shoots; species delimitation within the taxon *Sphenophyllum*. American Journal of Botany 60, 929–939. https://doi.org/10.1002/j.1537-2197.1973.tb05992.x

Good, C.W., Taylor, T.N., 1972. The ontogeny of Carboniferous articulates: the apex of *Sphenophyllum*. American Journal of Botany 59, 617–626. https://doi.org/10.1002/j.1537-2197.1972.tb10136.x

Gordon, W., T., 1938. On *Tetrastichia bupatides* - a Carboniferous pteridosperm from east Lothian. Transactions of the Royal Society of Edinburgh 59, 321–370.

Grgas, D., Rukavina, M., Bešlo, D., Štefanac, T., Crnek, V., Šikić, T., Habuda-Stanić, M., Landeka Dragičević, T., 2023. The bacterial degradation of lignin—A review. Water 15, 1272. https://doi.org/10.3390/w15071272

Guédon, Y., Refahi, Y., Besnard, F., Farcot, E., Godin, C., Vernoux, T., 2013. Pattern identification and characterization reveal permutations of organs as a key genetically controlled property of post-meristematic phyllotaxis. Journal of Theoretical Biology 338, 94–110. https://doi.org/10.1016/j.jtbi.2013.07.026

Guo, X., Retallack, G.J., Lü, B., He, L., Wang, R., Song, H., 2019. Paleosols in Devonian red-beds from northwest China and their paleoclimatic characteristics. Sedimentary Geology 379, 16–24. https://doi.org/10.1016/j.sedgeo.2018.11.001

Haelewaters, D., Filippova, N.V., Baral, H.-O., 2018. A new species of *Stamnaria* (Leotiomycetes, Helotiales) from Western Siberia. MycoKeys 32, 49–63. https://doi.org/10.3897/mycokeys.32.23277

Halbwachs, H., Harper, C.J., Krings, M., 2021. Fossil Ascomycota and Basidiomycota, with notes on fossil lichens and nematophytes, in: Encyclopedia of Mycology. Elsevier, pp. 378–395. https://doi.org/10.1016/B978-0-12-819990-9.00048-2

Hammond, S.E., Berry, C.M., 2005. A new species of *Tetraxylopteris* (Aneurophytales) from the Devonian of Venezuela. Botanical Journal of the Linnean Society 148, 275–303. https://doi.org/10.1111/j.1095-8339.2005.00418.x

Hao, S., Xue, J., 2013. Earliest record of megaphylls and leafy structures, and their initial diversification. Chinese Science Bulletin 58, 2784–2793. https://doi.org/10.1007/s11434-013-5799-x

Hao, S.-G., Beck, C.B., 1993. Further observations on *Eophyllophyton bellum* from the Lower Devonian (Siegenian) of Yunnan, China. Palaeontographica Abteilung B, Palaophytologie 230, 27–41.

Harper, C.J., Krings, M., 2021. Fungi as parasites: a conspectus of the fossil record, in: De Baets, K., Huntley, J.W. (Eds.), The Evolution and Fossil Record of Parasitism, Topics in Geobiology. Springer International Publishing, Cham, pp. 69–108. https://doi.org/10.1007/978-3-030-42484-8_3

Harper, C.J., Krings, M., Galtier, J., Taylor, T.N., 2016a. A microfossil with suggested affinities to the peronosporomycetes (Oomycota) from the Carboniferous (c. 330 Ma) of France. Nova Hedwigia 103, 315–326. https://doi.org/10.1127/nova_hedwigia/2016/0352

Harper, C.J., Taylor, T.N., Krings, M., Taylor, E.L., 2016b. Structurally preserved fungi from Antarctica: diversity and interactions in late Palaeozoic and Mesozoic polar forest ecosystems. Antarctic Science 28, 153–173. https://doi.org/10.1017/S0954102016000018

Harris, B.J., Clark, J.W., Schrempf, D., Szöllősi, G.J., Donoghue, P.C.J., Hetherington, A.M., Williams, T.A., 2022. Divergent evolutionary trajectories of bryophytes and tracheophytes from a complex common ancestor of land plants. Nature Ecology & Evolution 6, 1634–1643. https://doi.org/10.1038/s41559-022-01885-x

He, M.-Q., Cao, B., Liu, F., Boekhout, T., Denchev, T.T., Schoutteten, N., Denchev, C.M., Kemler, M., Gorjón, S.P., Begerow, D., Valenzuela, R., Davoodian, N., Niskanen, T., Vizzini, A., Redhead, S.A., Ramírez-Cruz, V., Papp, V., Dudka, V.A., Dutta, A.K., García-Sandoval, R., Liu, X.-Z., Kijpornyongpan, T., Savchenko, A., Tedersoo, L., Theelen, B., Trierveiler-Pereira, L., Wu, F., Zamora, J.C., Zeng, X.-Y., Zhou, L.-W., Liu, S.-L., Ghobad-Nejhad, M., Giachini, A.J., Li, G.-J., Kakishima, M., Olariaga, I., Haelewaters, D., Sulistyo, B., Sugiyama, J., Svantesson, S., Yurkov, A., Alvarado, P., Antonín, V., Da Silva, A.F., Druzhinina, I., Gibertoni, T.B., Guzmán-Dávalos, L., Justo, A., Karunarathna, S.C., Galappaththi, M.C.A., Toome-Heller, M., Hosoya, T., Liimatainen, K., Márquez, R., Mešić, A., Moncalvo, J.-M., Nagy, L.G., Varga, T., Orihara, T., Raymundo, T., Salcedo, I., Silva-Filho, A.G.S., Tkalčec, Z., Wartchow, F., Zhao, C.-L., Bau, T., Cabarroi-Hernández, M., Cortés-Pérez, A., Decock, C., De Lange, R., Weiss, M., Menolli, N., Nilsson, R.H., Fan, Y.-G., Verbeken, A., Gafforov, Y., Meiras-Ottoni, A., Mendes-Alvarenga, R.L., Zeng, N.-K., Wu, Q., Hyde, K.D., Kirk, P.M., Zhao, R.-L., 2024. Phylogenomics, divergence times and notes of orders in Basidiomycota. Fungal Diversity 126, 127–406. https://doi.org/10.1007/s13225-024-00535-w

Helgason, T., Fitter, A.H., 2009. Natural selection and the evolutionary ecology of the arbuscular mycorrhizal fungi (Phylum Glomeromycota). Journal of Experimental Botany 60, 2465–2480. https://doi.org/10.1093/jxb/erp144

Herrmann, W.M., 1995. Tripartite symbiotic associations in nitrogen-fixing plants of Mount Changbai Nature Reserve in northeast China. Ph.D. Ludwig-Maximilian-Universität München, Fakultät für Biologie (Botanik).

Hilton, J., Geng, B., Kenrick, P., 2003. A novel Late Devonian (Frasnian) woody cladoxylopsid from China. International Journal of Plant Sciences 164, 793–805. https://doi.org/10.1086/376815

Hodson, E., Shahid, F., Basinger, J., Kaminskyj, S., 2009. Fungal endorhizal associates of *Equisetum* species from Western and Arctic Canada. Mycological Progress 8, 19–27. https://doi.org/10.1007/s11557-008-0574-0

Hoffman, L.A., Tomescu, A.M.F., 2013. An early origin of secondary growth: *Franhueberia gerriennei* gen. et sp. nov. from the Lower Devonian of Gaspé (Quebec, Canada). American Journal of Botany 100, 754–763. https://doi.org/10.3732/ajb.1300024

Holm, L., Holm, K., 1981. Nordic equiseticolous pyrenomycetes. Nordic Journal of Botany 1, 109–119. https://doi.org/10.1111/j.1756-1051.1981.tb01041.x

Holman, A.I., Poropat, S.F., Greenwood, P.F., Bhandari, R., Tripp, M., Hopper, P., Schimmelmann, A., Brosnan, L., Rickard, W.D.A., Wolkenstein, K., Grice, K., 2024. Significance of lignin and fungal markers in the Devonian (407 Ma) Rhynie Chert. Geobiology 22. https://doi.org/10.1111/gbi.12616

Hoskins, J.H., Cross, A.T., 1951. The structure and classification of four plants from the New Albany Shale. American Midland Naturalist 46, 684–716. https://doi.org/10.2307/2421811

Hou, G., Blancaflor, E.B., 2009. Fern root development, in: Beeckman, T. (Ed.), Root Development. Wiley-Blackwell, Oxford, UK, pp. 192–208. https://doi.org/10.1002/9781444310023.ch8

Hou, G., Hill, J.P., 2002. Heteroblastic root development in *Ceratopteris richardii* (Parkeriaceae). International Journal of Plant Sciences 163, 341–351. https://doi.org/10.1086/339156

Husby, C., 2013. Biology and functional ecology of *Equisetum* with emphasis on the giant horsetails. The Botanical Review 79, 147–177. https://doi.org/10.1007/s12229-012-9113-4

Janusz, G., Pawlik, A., Sulej, J., Świderska-Burek, U., Jarosz-Wilkołazka, A., Paszczyński, A., 2017. Lignin degradation: microorganisms, enzymes involved, genomes analysis and evolution. FEMS Microbiology Reviews 41, 941–962. https://doi.org/10.1093/femsre/fux049

Jarvis, E., 1990. New palynological data on the age of the Kiltorcan Flora of Co. Kilkenny, Ireland. Journal of Micropalaeontology 9, 87–94. https://doi.org/10.1144/jm.9.1.87

Jarvis, M.C., 2012. Sclerenchyma, in: Encyclopedia of Life Sciences. Chichester. https://doi.org/10.1002/9780470015902.a0002082.pub2

Johnson, T., 1911. Is *Archaeopteris* a pteridosperm. Scientific Proceedings of the Royal Dublin Society 114–136.

Joy, K.W., Willis, A.J., Lacey, W.S., 1956. A rapid cellulose peel technique in Palaeobotany. Annals of Botany 20, 635–637. https://doi.org/10.1093/oxfordjournals.aob.a083546

Judelson, H.S., Ah-Fong, A.M.V., 2019. Exchanges at the plant-oomycete interface that influence disease. Plant Physiology 179, 1198–1211. https://doi.org/10.1104/pp.18.00979

Kaiser, S.I., Aretz, M., Becker, R.T., 2016. The global Hangenberg Crisis (Devonian–Carboniferous transition): review of a first-order mass extinction. Geological Society, London, Special Publications 423, 387–437. https://doi.org/10.1144/SP423.9

Kassambara, A., Mundt, F., 2017. Package 'factoextra.' Extract and visualize the results of multivariate data analyses 76.

Kenrick, P., Crane, P.R., 1997. The origin and early diversification of land plants, First edition. ed. Smithsonian Institution Scholarly Press, Washington and London.

Kidston, R., Lang, W.H., 1917. On Old Red Sandstone plants showing structure from the Rhynie Chert Bed Aberdeenshire. Part 1: *Rhynia gwynne-vaughani*, Kidston and Lang. Transactions of the Royal Society of Edinburgh 51, 761–784.

Kirk, T.K., Farrell, R.L., 1987. Enzymatic "combustion": the microbial degradation of lignin. Annual Review of Microbiology 41, 465–505. https://doi.org/10.1146/annurev.mi.41.100187.002341

Klavins, S.D., 2004. Re-interpretation of *Wexfordia hookense* from the upper Devonian of Ireland as an arborescent lycophyte. Botanical Journal of the Linnean Society 144, 275–287. https://doi.org/10.1111/j.1095-8339.2003.00242.x

Klavins, S.D., 1999. Systematics and paleoecology of three Late Devonian floras of southern Ireland. Ph.D. Southern Illinois University, USA. 216 p.

Koopmans, R.G., 1928. Researches on the Flora of the Coal-balls from the" Finefrau-Nebenbank" Horizon in the Province of Limburg (The Netherlands). N. V. Bock, Heerlen.

Koske, R.E., Friese, C.F., Olexia, P.D., Hauke, R.L., 1985. Vesicular-arbuscular mycorrhizas in *Equisetum*. Transactions of the British Mycological Society 85, 350–353. https://doi.org/10.1016/S0007-1536(85)80202-3

Kräusel, R., Weyland, H., 1937. Pflanzenreste aus dem Devon. X. Zwei Pflanzenfunde im Oberdevon der Eifel. Senckenberg. 19, 338–355.

Kräusel, R., Weyland, H., 1929. Beiträge zur Kenntnis der Devonflora III. Abhandlungen der Senckenbergischen Naturforschenden Gesellschaft 41, 315–360.

Krings, M., Harper, C.J., 2019. A new species of *Perexiflasca*, enigmatic microfossils with suggested affinities to Chytridiomycota (Fungi) from the Lower Devonian Rhynie and Windyfield cherts. Geobios 56, 107–114. https://doi.org/10.1016/j.geobios.2019.07.007

Krings, M., Harper, C.J., Decombeix, A.-L., Galtier, J., 2023. The core of *Sporocarpon asteroides*, an enigmatic fungal fossil from the Carboniferous. Neues Jahrbuch für Geologie und Paläontologie 309, 111–122. https://doi.org/10.1127/njgpa/2023/1153

Krings, M., Harper, C.J., Taylor, E.L., 2017a. Fungi and fungal interactions in the Rhynie chert: a review of the evidence, with the description of *Perexiflasca tayloriana* gen. et sp. nov.†. Philosophical Transactions of the Royal Society B: Biological Sciences 373, 20160500. https://doi.org/10.1098/rstb.2016.0500

Krings, M., Harper, C.J., White, J.F., Barthel, M., Heinrichs, J., Taylor, E.L., Taylor, T.N., 2017b. Fungi in a *Psaronius* root mantle from the Rotliegend (Asselian, Lower Permian/Cisuralian) of Thuringia, Germany. Review of Palaeobotany and Palynology 239, 14–30. https://doi.org/10.1016/j.revpalbo.2016.12.004

Krings, M., Taylor, T.N., Harper, C.J., 2017c. Early fungi evidence from the fossil record, in: Dighton, J., White, J.F. (Eds.), Mycology. CRC Press, CRC Press Taylor & Francis Group 6000 Broken Sound Parkway NW, Suite 300 Boca Raton, FL 33487-2742, pp. 37–52. https://doi.org/10.1201/9781315119496-4

Krings, M., Taylor, T.N., Dotzler, N., 2014. Microorganisms associated with the seed fern *Lyginopteris oldhamia* (Binney) H. Potonié (Lyginopteridales) from the Carboniferous of Great Britain. Palaeontographica Abteilung B 290, 109–125. https://doi.org/10.1127/palb/290/2014/109

Krings, M., Taylor, T.N., Dotzler, N., 2013. Fossil evidence of the zygomycetous fungi. Persoonia 30, 1–10. https://doi.org/10.3767/003158513X664819

Krings, M., Galtier, J., Taylor, T.N., Dotzler, N., 2012a. Microbial endophytes and pollen chamber contents in a fossil seed from the Upper Pennsylvanian Grand-Croix cherts, France. Geologica et Palaeontologica 44, 93–99.

Krings, M., Taylor, T.N., Dotzler, N., 2012b. Fungal endophytes as a driving force in land plant evolution: Evidence from the fossil record, in: Southworth, D. (Ed.), Biocomplexity of Plant–Fungal Interactions. Wiley, pp. 5–27. https://doi.org/10.1002/9781118314364.ch1

Krings, Michael, Dotzler, N., Galtier, J., Taylor, T.N., 2011a. Oldest fossil basidiomycete clamp connections. Mycoscience 52, 18–23. https://doi.org/10.1007/S10267-010-0065-4

Krings, M., Taylor, T.N., Dotzler, N., Galtier, J., 2011b. Fungal remains in cordaite (Cordaitales) leaves from the Upper Pennsylvanian of central France. Bulletin of Geosciences 86 777–784. https://doi.org/10.3140/bull.geosci.1278

Krings, Michael, Taylor, T.N., Taylor, E.L., Dotzler, N., Walker, C., 2011c. Arbuscular mycorrhizal-like fungi in Carboniferous arborescent lycopsids. New Phytologist 191, 311–314. https://doi.org/10.1111/j.1469-8137.2011.03752.x

Krings, M., Dotzler, N., Taylor, T.N., Galtier, J., 2010a. A fungal community in plant tissue from the Lower Coal Measures (Langsettian, Lower Pennsylvanian) of Great Britain. Bulletin of Geosciences 85, 679–690. https://doi.org/10.3140/bull.geosci.1209

Krings, Michael, Taylor, T.N., Galtier, J., Dotzler, N., 2010b. Microproblematic endophytes and epiphytes of fern pinnules from the Upper Pennsylvanian of France. Geobios 43, 503–510. https://doi.org/10.1016/j.geobios.2010.02.002

Krings, Michael, Taylor, T.N., Galtier, J., Dotzler, N., 2010c. A fossil peronosporomycete oogonium with an unusual surface ornament from the Carboniferous of France. Fungal Biology 114, 446–450. https://doi.org/10.1016/j.funbio.2010.03.006

Krings, Michael, Dotzler, N., Taylor, T.N., Galtier, J., 2010d. Microfungi from the upper Visean (Mississippian) of central France: structure and development of the sporocarp *Mycocarpon cinctum* nov. sp. Zitteliana 50, 127–135.

Krings, Michael, Taylor, T.N., Dotzler, N., Decombeix, A.-L., 2010e. *Galtierella biscalithecae* nov. gen. et sp., a Late Pennsylvanian endophytic water mold (Peronosporomycetes) from France. Comptes Rendus Palevol 9, 5–11. https://doi.org/10.1016/j.crpv.2009.10.002

Krings, M., Galtier, J., Taylor, T.N., Dotzler, N., 2009a. Chytrid-like microfungi in *Biscalitheca cf. musata (Zygopteridales)* from the Upper Pennsylvanian Grand-Croix cherts (Saint-Etienne Basin, France). Review of Palaeobotany and Palynology 157, 309–316. https://doi.org/10.1016/j.revpalbo.2009.06.001

Krings, M., Dotzler, N., Galtier, J., Taylor, T.N., 2009b. Microfungi from the upper Visean (Mississippian) of central France: Chytridiomycota and chytrid-like remains of uncertain affinity. Review of Palaeobotany and Palynology 156, 319–328. https://doi.org/10.1016/j.revpalbo.2009.03.011

Krings, M., Dotzler, N., Taylor, T.N., Galtier, J., 2009c. A late Pennsylvanian fungal leaf endophyte from Grand-Croix, France. Review of Palaeobotany and Palynology 156, 449–453. https://doi.org/10.1016/j.revpalbo.2009.04.010

Krings, M., Dotzler, N., Taylor, T.N., Galtier, J., 2007. A microfungal assemblage in *Lepidodendron* from the upper Visean (Carboniferous) of central France. Comptes Rendus Palevol 6, 431–436. https://doi.org/10.1016/j.crpv.2007.09.008

Künkele, U., Lohmeyer, T.R., Baral, H.O., 2005. *Stamnaria americana*, ein in Auwäldern vermutlich häufiger, aber aus Deutschland bisher nicht berichteter Parasit an *Equisetum hyemale*. Mycologica Bavarica 7, 3–20.

Larson, P.R., 1969. Wood formation and the concept of wood quality. Yale School of Forestry & Environmental Studies Bulletin Series 1–54.

Lê, S., Josse, J., Husson, F., 2008. **FactoMineR** : An *R* package for multivariate analysis. Journal of Statistical Software 25. https://doi.org/10.18637/jss.v025.i01

Lechat, C., Baral, H.-O., 2008. A new species of *ljuhya* on *Equisetum hyemale* and its *Acremonium* anamorph, with notes on *Hydropisphaera arenula*. Österreichische Zeitschrift für Pilzkunde17, 15–24.

Leclercq, S., 1924. Observations nouvelles sur la structure anatomique de quelques végétaux du Houiller belge. Bulletins de la classe des sciences, 5eme série, tome 10 352–354.

Leclercq, S., Bonamo, P.M., 1973. *Rellimia thomsonii*, a new name for *Milleria* (*Protopteridium*) *thomsonii* Lang 1926 emend. Leclercq and Bonamo 1971. Taxon 435–437. https://doi.org/10.2307/1219330

Leclercq, S., Bonamo, P., M., 1971. A study of the fructification of *Milleria* (*Protopteridium*) *thomsonii* Lang from the Middle Devonian of Belgium. Palaeontographica Abteilung B 136, 83–114.

Lemoigne, Y., Iurina, A., 1983. *Xenocladia medullosina* Ch. A. Arnold (1940) 1952 du Dévonien Moyen du Kazakhstan (URSS). Geobios 16, 513–547. https://doi.org/10.1016/S0016-6995(83)80034-5

Lemoigne, Y., Iurina, A., Snigirevskaya, N., 1983. Révision du genre *Callixylon* Zalessky 1911 (*Archaeopteris*) du Dévonien. Palaeontographica Abteilung B 81–120.

Leroux, O., Leroux, F., Bagniewska-Zadworna, A., Knox, J.P., Claeys, M., Bals, S., Viane, R.L.L., 2011. Ultrastructure and composition of cell wall appositions in the roots of *Asplenium* (Polypodiales). Micron 42, 863–870. https://doi.org/10.1016/j.micron.2011.06.002

Lersten, N.R., 1997. Occurrence of endodermis with a casparian strip in stem and leaf. The Botanical Review 63, 265–272. https://doi.org/10.1007/BF02857952

Li, C.-S., Cui, J.-Z., 1995. Atlas of fossil plant anatomy in China. Science Press, Beiging, china.

Li, H.-Y., Zhao, C.-A., Liu, C.-J., Xu, X.-F., 2010. Endophytic fungi diversity of aquatic/riparian plants and their antifungal activity in vitro. The Journal of Microbiology 48, 1–6. https://doi.org/10.1007/s12275-009-0163-1

Li, Z., Wang, S., Wang, W., Gu, J., Wang, Y., 2022. The hierarchy of protoxylem groupings in primary root and their plasticity to nitrogen addition in three tree species. Frontiers in Plant Science 13, 903318. https://doi.org/10.3389/fpls.2022.903318

Linke, L., Clements, C.F., 2024. A sixth mass extinction? How linguistic uncertainty shapes our understanding of the biodiversity crisis. Ecology and Evolution 14, e70653. https://doi.org/10.1002/ece3.70653

Liu, B.-C., Wang, K., Zong, R.-W., Bai, J., Wang, Yao, Yang, N., Wang, Yi, Xu, H.-H., 2024. A new Late Devonian plant assemblage in west Junggar, Xinjiang, China and its floral evolution during the Devonian. Review of Palaeobotany and Palynology 325, 105112. https://doi.org/10.1016/j.revpalbo.2024.105112

Long, A.G., 1987. Observations on *Eristophyton zalessky*, *Lyginorachis waltonii* Calder, and *Cladoxylon edromense* sp. nov. from the lower Carboniferous Cementstone Group of Scotland. Transactions of the Royal Society of Edinburgh 78, 73–84. https://doi.org/10.1017/S0263593300010993

Long, A.G., 1976. *Calathopteris heterophylla* gen. et sp. nov., a lower Carboniferous bearing two kinds of petioles. Transactions of the Royal Society of Edinburgh 64, 477–489. https://doi.org/10.1017/S0080456800012928

Long, A.G., 1968. Some specimens of *Cladoxylon* from the Calciferous Sandstone Series of Berwickshire. Transactions of the Royal Society of Edinburgh 68, 45–61. https://doi.org/10.1017/S0080456800014538

Long, A.G., 1961. *Tristichia ovensii* gen. et sp. nov. : A protostelic lower Carboniferous pteridosperm from Berwickshire and East Lothian, with an account of some associated seeds and cupules. Transactions of the Royal Society of Edinburgh 64, 477–489. https://doi.org/10.1017/S0080456800100468

Lucas, S.G., 2021. Nonmarine mass extinctions. Paleontological Research 25. https://doi.org/10.2517/2021PR004

MacCarthy, I., Higgs, K.T., 2013. Hook Head Peninsula, County Wexford: Cambrian, Devonian and Carboniferous sedimentary rocks, in: Geology of Ireland: A Field Guide. Collins Press, pp. 307–334.

Machado, S.R., Rodella, R.A., Angyalossy, V., Marcati, C.R., 2007. Structural variations in root and stem wood of *Styrax* (Stryracaceae) from brazilian forest and cerrado. IAWA Journal 28, 173–188. https://doi.org/10.1163/22941932-90001632

Mackie, W., 1914. The rock series of Craigbeg and Ord Hill, Rhynie, Aberdeenshire. Transactions of the Edinburgh Geological Society 10, 205–236. https://doi.org/10.1144/transed.10.2.205

Magurno, F., Uszok, S., Bierza, K., Bakr, J., Kende, Z., Bessa De Queiroz, M., Casieri, L., 2024. *Glomus mongioiense*, a new species of arbuscular mycorrhizal fungi from Italian Alps and the phylogeny-spoiling issue of ribosomal variants in the *Glomus* genus. Agronomy 14, 1350. https://doi.org/10.3390/agronomy14071350

Mapuranga, J., Zhang, L., Zhang, N., Yang, W., 2022. The haustorium: The root of biotrophic fungal pathogens. Frontiers in Plant Science 13, 963705. https://doi.org/10.3389/fpls.2022.963705

Marcelle, H., 1951. *Callixylon velinense* nov. sp. : Un bois à structure conservée du Dévonien de Belgique. barb 37, 908–920. https://doi.org/10.3406/barb.1951.70720

Marshall, J.E.A., Lakin, J., Troth, I., Wallace-Johnson, S.M., 2020. UV-B radiation was the Devonian-Carboniferous boundary terrestrial extinction kill mechanism. Sciences Advances 6, 1–8. DOI: 10.1126/sciadv.aba0768

Masselter, T., Rowe, N., Galtier, J., Speck, T., 2009. Secondary growth and deformation of stem tissues in the lower Carboniferous seed fern *Calamopitys*. International Journal of Plant Sciences 170, 1228–1239. https://doi.org/10.1086/605877

Matten, L.C., 1995. The megafossil flora from the uppermost Devonian of Hook Head, County Wexford, Ireland, in: Birbal Sahni Centenary Volume. Presented at the Proceedings fo the International Conference on Global Environment and Diversification of Plants through Geological time., Society of Indian Plant Taxonomists, Allahabad, India., pp. 167–173.

Matten, L.C., 1992. Studies on Devonian plants from New York State: *Stenokoleos holmesii* n. sp. from the Cairo flora (Givetian) with an alternative model for lyginopterid seed fern evolution. Courier Forschungsinstitut Senckenberg 147, 75–85.

Matten, L.C., 1989. A petrified lycopod from the uppermost Devonian of Hook Head, County Wexford, Ireland. Botanical Gazette 150, 323–336. https://doi.org/10.1086/337778

Matten, L.C., 1973. The Cairo flora (Givetian) from eastern New York. I. *Reimannia*, terete axes, and *Cairoa lamanekii* gen. et sp. n. American Journal of Botany 60, 619–630. https://doi.org/10.2307/2441439

Matten, L.C., 1968. *Actinoxylon banksii* gen. et sp. nov.: a progymnosperm from the Middle Devonian of New York. American Journal of Botany 55, 773–782. https://doi.org/10.1002/j.1537-2197.1968.tb07435.x

Matten, L.C., Banks, H.P., 1969. *Stenokoleos bifidus* sp. n. in the Upper Devonian of New York State. American Journal of Botany 56, 880–891. https://doi.org/10.1002/j.1537-2197.1969.tb09738.x

Matten, L.C., Banks, H.P., 1966. *Triloboxylon ashlandicum* gen. and sp. n. from the Upper Devonian of New York. American Journal of Botany 53, 1020–1028. https://doi.org/10.1002/j.1537-2197.1968.tb07435.x

Matten, L.C., Tanner, W.R., Lacey, W.S., 1984. Additions to the silicified Upper Devonian/lower Carboniferous flora from Ballyheigue, Ireland. Review of Palaeobotany and Palynology 43, 303–320. https://doi.org/10.1016/0034-6667(84)90002-2

Matten, L.C., Lacey, W.S., May, B.I., Lucas, R.C., 1980. A megafossil flora from the uppermost Devonian near Ballyheigue, Co. Kerry, Ireland. Review of Palaeobotany and Palynology 29, 241–251. https://doi.org/10.1016/0034-6667(80)90061-5

May, B.I., Matten, L.C., 1983. A probable pteridosperm from the uppermost Devonian near Ballyheigue, Co. Kerry, Ireland. Botanical Journal of the Linnean Society 86, 103–123. https://doi.org/10.1111/j.1095-8339.1983.tb00719.x

McElrone, A.J., Pockman, W.T., Martínez-Vilalta, J., Jackson, R.B., 2004. Variation in xylem structure and function in stems and roots of trees to 20 m depth. New Phytologist 163, 507–517. https://doi.org/10.1111/j.1469-8137.2004.01127.x

McElwain, J.C., Punyasena, S.W., 2007. Mass extinction events and the plant fossil record. Trends in Ecology & Evolution 22, 548–557. https://doi.org/10.1016/j.tree.2007.09.003McLaren, D.J., Goodfellow, W.D., 1990. Geological and biological consequences of giant impacts. Annual Review of Earth and Planetary Sciences 18, 123–171. https://doi.org/10.1146/annurev.ea.18.050190.001011

Meyer-Berthaud, B., 1984. *Stenomyelon* from the upper Tournaisian of the Montagne Noire (France). Canadian Journal of Botany 62, 2297–2307. https://doi.org/10.1139/b84-313

Meyer-Berthaud, B., Decombeix, A.-L., 2009. L'évolution des premiers arbres: les stratégies dévoniennes. Comptes Rendus Palevol 8, 155–165. https://doi.org/10.1016/j.crpv.2008.08.002

Meyer-Berthaud, B., Rowe, N.P., 1997. A lower Carboniferous plant assemblage from Thuringia (Germany): compressions. Review of Palaeobotany and Palynology 97, 361–379. https://doi.org/10.1016/S0034-6667(96)00075-9

Meyer-Berthaud, B., Rowe, N.P., 1996. New mid-Tournaisian plant assemblages from Germany, in: 5th International Organization of Palaeobotany Conference, Santa Barbara, California, USA.

Meyer-Berthaud, B., Stein, W.E., 1995. A reinvestigation of *Stenomyelon* from the late Tournaisian of Scotland. International Journal of Plant Sciences 156, 863–895. https://doi.org/10.1086/297311

Meyer-Berthaud, B., Decombeix, A.-L., Girard, C., Steemans, P., Blanchard, R., Champreux, A., Evreïnoff, M., 2021. A Late Devonian plant assemblage from New South Wales, Australia: diversity and specificity. Review of Palaeobotany and Palynology 295, 104535. https://doi.org/10.1016/j.revpalbo.2021.104535

Meyer-Berthaud, B., Decombeix, A.-L., Dunstone, R., Gerrienne, P., Momont, N., Young, G., 2016. *Tetraxylopteris* Beck emend. Hammond and Berry (2005), the first aneurophytalean genus recorded in Australia. Review of Palaeobotany and Palynology 224, 54–65. https://doi.org/10.1016/j.revpalbo.2015.09.006

Meyer-Berthaud, B., Decombeix, A.-L., Ermacora, X., 2013. Archaeopterid root anatomy and architecture: new information from permineralized specimens of Famennian age from Anti-Atlas (Morocco). International Journal of Plant Sciences 174, 364–381. https://doi.org/10.1086/668685

Meyer-Berthaud, B., Soria, A., Decombeix, A.-L., 2010. The land plant cover in the Devonian: a reassessment of the evolution of the tree habit. Geological Society, London, Special Publications 339, 59–70. https://doi.org/10.1144/SP339.6

Meyer-Berthaud, B., Soria, A., Young, G.C., 2007. Reconsidering differences between Cladoxylopsida and Iridopteridales: evidence from *Polyxylon australe* (Upper Devonian, New South Wales, Australia). International Journal of Plant Sciences 168, 1085–1097. https://doi.org/10.1086/518841

Meyer-Berthaud, B., Scheckler, S.E., Bousquet, J., 2000. The development of *Archaeopteris*: new evolutionary characters from the structural analysis of an early Famennian trunk from southeast Morocco. American Journal of Botany 87, 456–468. https://doi.org/10.2307/2656589

Meyer-Berthaud, B., Scheckler, S.E., Wendt, J., 1999. *Archaeopteris* is the earliest known modern tree. Nature 398, 700–701. https://doi.org/10.1038/19516

Mintz, J.S., Driese, S.G., White, J.D., 2010. Environmental and ecological variability of Middle Devonian (Givetian) forests in Appalachian basin paleosols, New York, United States. PALAIOS 25, 85–96. https://doi.org/10.2110/palo.2009.p09-086r

Momont, N., 2015. Investigation of basal lignophyte: the aneurophytales and stenokoleales reexamined. Ph.D. Université de Liège. 356p.

Momont, N., Decombeix, A.-L., Gerrienne, P., Prestianni, C., 2016a. New information, including anatomy of the secondary xylem, on the genus *Brabantophyton* (Stenokoleales) from Ronquières (Middle Devonian, Belgium). Review of Palaeobotany and Palynology 234, 44–60. https://doi.org/10.1016/j.revpalbo.2016.08.009

Momont, N., Gerrienne, P., Prestianni, C., 2016b. *Brabantophyton*, a new genus with stenokolealean affinities from a Middle to earliest Upper Devonian locality from Belgium. Review of Palaeobotany and Palynology 227, 77–96. https://doi.org/10.1016/j.revpalbo.2015.10.009

Morris, J.L., Leake, J.R., Stein, W.E., Berry, C.M., Marshall, J.E.A., Wellman, C.H., Milton, J.A., Hillier, S., Mannolini, F., Quirk, J., Beerling, D.J., 2015. Investigating Devonian trees as geo-engineers of past climates: linking palaeosols to palaeobotany and experimental geobiology. Palaeontology 58, 787–801. https://doi.org/10.1111/pala.12185

Murdoch, D.J., Chow, E.D., 1996. A graphical display of large correlation matrices. The American Statistician 50, 178–180. https://doi.org/10.2307/2684435

Mustafa, H., 1978. Beiträge zur Devonflora. III. Argum Palaeobot 5, 91–132.

Mutawila, C., Fourie, P.H., Halleen, F., Mostert, L., 2011. Histo-pathology study of the growth of *Trichoderma harzianum*, *Phaeomoniella chlamydospora* and *Eutypa lata* on grapevine pruning wounds. Phytopathologia Mediterranea 50, 46–60 https://www.jstor.org/stable/26458710

Myrow, P.M., Ramezani, J., Hanson, A.E., Bowring, S.A., Racki, G., Rakociński, M., 2014. High-precision U–Pb age and duration of the latest Devonian (Famennian) Hangenberg event, and its implications. Terra Nova 26, 222–229. https://doi.org/10.1111/ter.12090

Naranjo-Ortiz, M.A., Gabaldón, T., 2019. Fungal evolution: major ecological adaptations and evolutionary transitions. Biological Reviews 94, 1443–1476. https://doi.org/10.1111/brv.12510

Nelsen, M.P., DiMichele, W.A., Peters, S.E., Boyce, C.K., 2016. Delayed fungal evolution did not cause the Paleozoic peak in coal production. Proceedings of the National Academy of Sciences113, 2442–2447. https://doi.org/10.1073/pnas.1517943113

Newell, N.D., 1952. Periodicity in invertebrate evolution. Journal of Paleontology 26, 371–385. https://www.jstor.org/stable/1299949

Nowak, H., Schneebeli-Hermann, E., Kustatscher, E., 2019. No mass extinction for land plants at the Permian–Triassic transition. Nature Communications 10, 384. https://doi.org/10.1038/s41467-018-07945-w

Oberwinkler, F., 2012. Evolutionary trends in Basidiomycota. Stapfia 96, 45–104.

Olsson, P.A., Hammer, E.C., Pallon, J., Van Aarle, I.M., Wallander, H., 2011. Elemental composition in vesicles of an arbuscular mycorrhizal fungus, as revealed by PIXE analysis. Fungal Biology 115, 643–648. https://doi.org/10.1016/j.funbio.2011.03.008

Orlova, O.A., Jurina, A.L., 2011. Genus *Callixylon* Zalessky (Archaeopteridophyta): Main criteria for distinguishing its species and revision of its species composition. Paleontological Journal 45, 580–589. https://doi.org/10.1134/S0031030111050108

Parkash, V., Dhungana, P., 2011. Endophytic and symbiotic mycotrophy in *Equisetum arvense* L.: a medicinal spore- dispersing vascular sporophyte. International Journal of Current Research and Review 3, 33–42.

Paul, B., Bala, K., 2008. A new species of *Pythium* with inflated sporangia and coiled antheridia, isolated from India. FEMS Microbiology Letters 282, 251–257. https://doi.org/10.1111/j.1574-6968.2008.01138.x

Pearce, R.B., 1996. Antimicrobial defences in the wood of living trees. New Phytolologist 132, 203–233. https://doi.org/10.1111/j.1469-8137.1996.tb01842.x

Peaucelle, A., Morin, H., Traas, J., Laufs, P., 2007. Plants expressing a *miR164* -resistant *CUC2* gene reveal the importance of post-meristematic maintenance of phyllotaxy in *Arabidopsis*. Development 134, 1045–1050. https://doi.org/10.1242/dev.02774

Pellenard, P., Gand, G., Schmitz, M., Galtier, J., Broutin, J., Stéyer, J.-S., 2017. High-precision U-Pb zircon ages for explosive volcanism calibrating the NW European continental Autunian stratotype. Gondwana Research 51, 118–136. https://doi.org/10.1016/j.gr.2017.07.014

Perry, C.C., Fraser, M.A., 1991. Silica deposition and ultrastructure in the cell wall of *Equisetum arvense*: the importance of cell wall structures and flow control in biosilicification? Philosophical Transactions of the Royal Society of London. Series B: Biological Sciences 334, 149–157. https://doi.org/10.1098/rstb.1991.0104

Pfeiler, K.C., Tomescu, A.M.F., 2023. Mosaic assembly of regulatory programs for vascular cambial growth: a view from the Early Devonian. New Phytologist 240, 529–541. https://doi.org/10.1111/nph.19146

Pfeiler, K.C., Tomescu, A.M.F., 2021. An Early Devonian actinostelic euphyllophyte with secondary growth from the Emsian of Gaspé (Canada) and the importance of tracheid wall

thickening patterns in early euphyllophyte systematics. Papers in Palaeontology 7, 1081–1095. https://doi.org/10.1002/spp2.1335

Phillips, T.L., 1959. A new Sphenophyllalean shoot system from the Pennsylvanian. Annals of the Missouri Botanical Garden 46, 1–17. https://doi.org/10.2307/2394565

Phillips, T.L., Galtier, J., 2005. Evolutionary and ecological perspectives of Late Paleozoic ferns. Review of Palaeobotany and Palynology 135, 165–203. https://doi.org/10.1016/j.revpalbo.2005.03.006

Phillips, T.L., Leisman, G.A., 1966. *Paurodendron*, a rhizomorphic lycopod. American Journal of Botany 53, 1086–1100. https://doi.org/10.1002/j.1537-2197.1966.tb06876.x

Pisarzowska, A., Rakociński, M., Marynowski, L., Szczerba, M., Thoby, M., Paszkowski, M., Perri, M.C., Spalletta, C., Schönlaub, H.-P., Kowalik, N., Gereke, M., 2020. Large environmental disturbances caused by magmatic activity during the Late Devonian Hangenberg Crisis. Global and Planetary Change 190, 103155. https://doi.org/10.1016/j.gloplacha.2020.103155

Prestianni, C., Rustán, J.J., Balseiro, D., Vaccari, E., Sterren, A.F., Steemans, P., Rubinstein, C., Astini, R.A., 2015. Early seed plants from Western Gondwana: Paleobiogeographical and ecological implications based on Tournaisian (Lower Carboniferous) records from Argentina. Palaeogeography, Palaeoclimatology, Palaeoecology 417, 210–219. https://doi.org/10.1016/j.palaeo.2014.10.039

Prestianni, C., Sautois, M., Denayer, J., 2016. Disrupted continental environments around the Devonian-Carboniferous Boundary: introduction of the tener event. Geologica Belgica 19, 135–145. https://doi.org/10.20341/gb.2016.013

Prestianni, C., Rustán, J.J., Balseiro, D., Vaccari, N.E., 2022. *Porongodendron minitensis* gen. nov. sp. nov. a new lycopsid from the Mississippian of Argentina with adaptations to tundra-like conditions. Botany Letters 169, 527–539. https://doi.org/10.1080/23818107.2022.2101515

Priyashantha, A., Dai, D.-Q., Bhat, D., Stephenson, S., Promputtha, I., Kaushik, P., Tibpromma, S., Karunarathna, S., 2023. Plant–fungi interactions: Where it goes? Biology 12, 809. https://doi.org/10.3390/biology12060809

Purin, S., Rillig, M.C., 2008. Parasitism of arbuscular mycorrhizal fungi: reviewing the evidence. FEMS Microbiology Letters 279, 8–14. https://doi.org/10.1111/j.1574-6968.2007.01007.x

Qie, W., Zhang, J., Luo, G., Algeo, T.J., Chen, B., Xiang, L., Liang, K., Liu, X., Pogge Von Strandmann, P.A.E., Chen, J., Wang, X., 2023. Enhanced continental weathering as a trigger for the end-Devonian Hangenberg Crisis. Geophysical Research Letters 50, e2022GL102640. https://doi.org/10.1029/2022GL102640

Rakociński, M., Marynowski, L., Pisarzowska, A., Bełdowski, J., Siedlewicz, G., Zatoń, M., Perri, M.C., Spalletta, C., Schönlaub, H.P., 2020. Volcanic related methylmercury poisoning as the possible driver of the end-Devonian Mass Extinction. Scientific Reports 10, 7344. https://doi.org/10.1038/s41598-020-64104-2

Raup, D.M., Sepkoski, J.J., 1982. Mass extinctions in the marine fossil record. Science 215, 1501–1503. https://doi.org/10.1126/science.215.4539.1501

Read, C.B., 1936. A Devonian Flora from Kentucky. Journal of Paleontology 10, 215–227. https://www.jstor.org/stable/1298452

Reed, F.D., 1949. Notes on the anatomy of two Carboniferous plants *Sphenophyllum* and *Psaronius*. Botanical Gazette 110, 501–510. https://doi.org/10.1086/335550

Renault, B., 1903. Sur quelques nouveaux champignons et algues fossiles, de l'époque houillere. Comptes rendus hebdomadaires des séances de l'Académie des sciences. Paris 136, 904–907.

Renault, B., 1900. Sur quelques microorganismes des combustibles fossiles 4, 865–1169.

Renault, B., 1896a. Bassin houiller et permien d'Autun et d'Épinac. Fascicule IV: : Flore fossile, deuxième partie, Études des Gîtes Minéraux de la France. Imprimerie National, Paris.

Renault, B., 1896b. Notice sur les travaux scientifiques de M. Bernard Renault. Dejussieu Père et fils.

Renault, B., 1895a. Parasites des écorces de Lépidodendrons. Le Naturaliste 9, 77–78.

Renault, B., 1895b. Sur quelques *Micrococcus* du Stéphanien, terrain houiller supérieur. Comptes rendus hebdomadaires des séances de l'Académie des sciences. Paris 120, 217–220.

Renault, B., 1893. Sur quelques nouveaux parasites des Lépidodendrons. Bulletin de la Société d'histoire naturelle d'Autun, Procès-verbaux des séances 1893 1894, 168–178.

Renault, B., 1878. Recherches sur la structure et les affinités botaniques des végétaux silicifiés requeillis aux environs d'Autun et de St. Étienne, Publication de la Société éduenne. ed. Imprimerie Dejussieu père et fils, Autun.

Renault, B., 1876. Végétaux silicifiés d'Autun et de Saint- Etienne. Nouvelles recherches sur la structure des *Sphenophyllum* et sur leurs affinités botaniques. Annales des sciences naturelles. Botanique (6ème série) 277–311.

Renault, B., 1873. Recherches sur l'organisation des *Sphenophyllum* et des *Annularia*. Annales des sciences naturelles. Botanique (5ème série) 1–22.

Renault, B., Bertrand, C.-E., 1885. *Grilletia spherospermii*, Chytridiacée fossile du terrain houiller supérieur. Gauthier-Villars.

Rößler, R., Decombeix, A.-L., Galtier, J., Neregato, R., Niemirowska, S., Noll, R., 2021. The limits of life revealed in a silicified micro-ecosystem: *Sphenophyllum* stems, leaves, and roots trapped inside an arthropod boring in a Permian calamitalean. Palaeontographica Abteilung B 302, 3–35. https://doi.org/10.1127/palb/2021/0073

Rothwell, G.W., Erwin, D.M., 1987. Origin of seed plants: an aneurophyte/seed-fern link elaborated. American Journal of Botany 74, 970–973. https://doi.org/10.1002/j.1537-2197.1987.tb08702.x

Rothwell, G.W., Karrfalt, E.E., 2008. Growth, development, and systematics of ferns: Does *Botrychium* s.*l.* (Ophioglossales) really produce secondary xylem?. American Journal of Botany 95, 414–423. https://doi.org/10.3732/ajb.95.4.414

Rothwell, G.W., Serbet, R., 1994. Lignophyte phylogeny and the evolution of spermatophytes: a numerical cladistic analysis. Systematic Botany 19, 443. https://doi.org/10.2307/2419767

Rothwell, G.W., Dunn, M.T., Scott, A.C., 2022. Reconstructing the *Tetrastichia bupatides* Gordon plant; a Devonian–Mississippian hydrasperman gymnosperm from Oxroad Bay, Scotland and Ballyheigue, Ireland. Review of Palaeobotany and Palynology 296, 104551. https://doi.org/10.1016/j.revpalbo.2021.104551

Rothwell, G.W., Scheckler, S.E., Gillespie, W.H., 1989. *Elkinsia* gen. nov., a Late Devonian gymnosperm with cupulate ovules. Botanical Gazette 150, 170–189. https://doi.org/10.1086/337763

Rowe, N.P., Galtier, J., 1989. A lower Carboniferous plant assemblage from La Serre (Montagne Noire, France). Part I. Review of Palaeobotany and Palynology 61, 239–271. https://doi.org/10.1016/0034-6667(89)90034-1

Rowe, N.P., Speck, T., 2003. Hydraulics and mechanics of plants: novelty, innovation and evolution, in: The Evolution of Plant Physiology. Elsevier Academic Press, Kew, UK, pp. 297–325.

Rowe, N.P., Speck, T., 1998. Biomechanics of plant growth forms: the trouble with fossil plants. Review of Palaeobotany and Palynology 102, 43–62. https://doi.org/10.1016/S0034-6667(98)00013-X

Sahoo, S.K., Gilleaudeau, G.J., Wilson, K., Hart, B., Barnes, B.D., Faison, T., Bowman, A.R., Larson, T.E., Kaufman, A.J., 2023. Basin-scale reconstruction of euxinia and Late Devonian mass extinctions. Nature 615, 640–645. https://doi.org/10.1038/s41586-023-05716-2

Salmaninezhad, F., Mostowfizadeh-Ghalamfarsa, R., Cacciola, S.O., 2024. *Pythium banihashemianum* sp. nov. and *Globisporangium izadpanahii* sp. nov.: Two new oomycete species from rice paddies in Iran. Journal of Fungi 10, 1–18. https://doi.org/10.3390/jof10060405

Sanders, H., Rothwell, G.W., Wyatt, S.E., 2009. Key morphological alterations in the evolution of leaves. International Journal of Plant Sciences 170, 860–868. https://doi.org/10.1086/600135

Schabilion, J.T., Baxter, R.W., 1971. A reconsideration of the Pennsylvanian arthrophyte *Sphenophyllum gilkineti* Leclercq. Botanical Gazette 132, 304–307. https://doi.org/10.1086/336594

Scheckler, S. E., 1978. Ontogeny of progymnosperms. 11. Shoots of Upper Devonian archaeopteridales. Canadian Journal of Botany 56, 3136–3170. https://doi.org/10.1139/b78-376

Scheckler, S.E., 1976. Ontogeny of progymnosperms. I. Shoots of Upper Devonian aneurophytales. Canadian Journal of Botany 54, 202–219. https://doi.org/10.1139/b76-020

Scheckler, S.E., 1975. *Rhymokalon*, a new plant with cladoxylalean anatomy from the Upper Devonian of New York State. Canadian Journal of Botany 53, 25–38. https://doi.org/10.1139/b75-004

Scheckler, S.E., Banks, H.P., 1971a. Anatomy and relationships of some Devonian progymnosperms from New York. American Journal of Botany 58, 737–751. https://doi.org/10.1002/j.1537-2197.1971.tb10028.x

Scheckler, S.E., Banks, H.P., 1971b. *Proteokalon* a new genus of progymnosperms from the Devonian of New York state and Its bearing on phylogenetic trends in the group. American Journal of Botany 58, 874–884. https://doi.org/10.1002/j.1537-2197.1971.tb10042.x

Schulze-Lefert, P., 2004. Knocking on the heaven's wall: pathogenesis of and resistance to biotrophic fungi at the cell wall. Current Opinion in Plant Biology 7, 377–383. https://doi.org/10.1016/j.pbi.2004.05.004

Schweitzer, H.-J., Giesen, P., 1980. Über *Taeniophyton inopinatum*, *Protolycopodites devonicus* und *Cladoxylon scoparium* aus dem Mitteldevon von Wuppertal. Palaeontographica Abteilung B 173, 1–25.

Scott, A.C., Galtier, J., Clayton, G., 1984. Distribution of anatomically-preserved floras in the lower Carboniferous in western Europe. Transactions of the Royal Society of Edinburgh 75, 311–340. https://doi.org/10.1017/S026359330001395X

Seago, J.L., 2020. Revisiting the occurrence and evidence of endodermis in angiosperm shoots. Flora 273, 151709. https://doi.org/10.1016/j.flora.2020.151709

Sepkoski, J.J., 1986. Phanerozoic overview of mass extinction, in: Raup, D.M., Jablonski, D. (Eds.), Patterns and Processes in the History of Life. Springer Berlin Heidelberg, Berlin, Heidelberg, pp. 277–295. https://doi.org/10.1007/978-3-642-70831-2_15

Serbet, R., Rothwell, G.W., 1992. Characterizing the most primitive seed ferns. I. A reconstruction of *Elkinsia polymorpha*. International Journal of Plant Sciences 153, 602–621. https://doi.org/10.1086/297083

Serlin, B.S., Banks, H.P., 1978. Morphology and anatomy of *Aneurophyton*, a progymnosperms from the Late Devonian of New York. Palaeontographica Americana 8, 343–359.

Shun-Liang, B., 2001. Ni-Ir anomaly, microtektites, and the biotic crisis across the Devonian–Carboniferous boundary, southern China. International Geology Review 43, 265–275. https://doi.org/10.1080/00206810109465013

Sigoillot, J.-C., Berrin, J.-G., Bey, M., Lesage-Meessen, L., Levasseur, A., Lomascolo, A., Record, E., Uzan-Boukhris, E., 2012. Fungal strategies for lignin degradation, in: Advances in Botanical Research. Elsevier, pp. 263–308. https://doi.org/10.1016/B978-0-12-416023-1.00008-2

Sleeman, A.G., Higgs, K., Sevastopulo, G.D., 1983. The stratigraphy of the Late Devonian—early Carboniferous rocks of South County Wexford. Bulletin Geological survey of Ireland 3, 141–158.

Smart, M.S., Filippelli, G., Gilhooly, W.P., Ozaki, K., Reinhard, C.T., Marshall, J.E.A., Whiteside, J.H., 2023. The expansion of land plants during the Late Devonian contributed to the marine mass extinction. Commun Earth Environ 4, 449. https://doi.org/10.1038/s43247-023-01087-8

Smoot, E.L., 1984. Phloem anatomy of the Carboniferous pteridosperm *Medullosa* and evolutionary trends in gymnosperm phloem. Botanical Gazette 145, 550–564. https://doi.org/10.1086/337490

Snigirevskaya, N.S., 1984. The root systems of archaeopterids in the Upper Devonian of Donets basin. Yezhegodnik Vsesoyuznogo Paleontologicheskogo Obschestva 27, 28–41.

Snigirevskaya, N.S., 1959. On the morphology and the anatomy of the genus *Sphenophyllum*. Paleontologicheskiy Zhurnal 2, 109–22.

Snigirevsky, S.M., 1992. New species of the genus *Cladoxylon* (Cladoxylaceae) from the Late Devonian of the Donetz Basin. Vopr Paleontol 10, 173–178.

Snigirevsky, S.M., Lyubarova, A.P., 2021. The N. S. Snigirevskaya's collections of fossil plants in Komarov Botanical Institute with an account of her life and work. Palaeobotany 12, 5–33. https://doi.org/10.31111/palaeobotany/2021.12.5

Solms-Laubach, H. de, 1896. Ueber die seinerzeit von Unger beschriebenen strukturbietenden Pflanzenreste des Unterculm von Saalfeld in Thüringen. Schropp.

Solms-Laubach, H. de, 1910. Ueber die in den Kalksteinen des Culm von Glätzisch-Falkenberg in Schlesien erhaltenen strukturbietenden Pflanzenreste. IV. Völkelia refracta, Steloxylon ludwigii. Zeitschrift für Botanik 2 529–54.

Soria, A., Meyer-Berthaud, B., 2005. Reconstructing the Late Devonian cladoxylopsid *Pietzschia schulleri* from new specimens from southeastern Morocco. International Journal of Plant Sciences 166, 857–874. https://doi.org/10.1086/431233

Soria, A., Meyer-Berthaud, B., 2004. Tree fern growth strategy in the Late Devonian cladoxylopsid species *Pietzschia levis* from the study of its stem and root system. American Journal of Botany 91, 10–23. https://doi.org/10.3732/ajb.91.1.10

Soria, A., Meyer-Berthaud, B., 2003. Occurrence of whorled organotaxis in the cladoxylopsid *Pietzschia polyupsilon* Read and Campbell (Lower Carboniferous, USA). Review of Palaeobotany and Palynology 124, 29–49. https://doi.org/10.1016/S0034-6667(02)00246-4

Soria, A., Rowe, N.P., Galtier, J., Speck, T., 2006. Having or lacking secondary growth: consequences on the mechanical architecture of Paleozoic cladoxylopsids (fern-like plants). Presented at the 5th Plant Biomechanics Conference, Stockholm.

Soria, A., Meyer-Berthaud, B., Scheckler, S.E., 2001. Reconstructing the architecture and growth habit of *Pietzschia levis* sp. nov. (Cladoxylopsida) from the Late Devonian of southeastern Morocco. International Journal of Plant Sciences 162, 911–926. https://doi.org/10.1086/320773

Speck, T., Rowe, N.P., 2003. Modelling primary and secondary growth processes in plants: a summary of the methodology and new data from an early lignophyte. Philosophical Transactions of the Royal Society of London. Series B: Biological Sciences 358, 1473–1485. https://doi.org/10.1098/rstb.2003.1347

Stalpers, J.A., 1978. Identification of wood-inhabiting Aphyllophorales in pure culture. Centraalbureau voor schimmelcultures Baarn 16.

Stein, W.E., 1993. Modeling the evolution of stelar architecture in vascular plants. International Journal of Plant Sciences 154, 229–263. https://doi.org/10.1086/297106

Stein, W.E., 1982a. *Iridopteris eriensis* from the Middle Devonian of North America, with systematics of apparently related taxa. Botanical Gazette 143, 401–416. https://doi.org/10.1086/337316

Stein, W.E., 1982b. The Devonian plant *Reimannia*, with a discussion of the class Progymnospermopsida. Palaeontology 25, 605–622.

Stein, W.E., Beck, C.B., 1992. New information on *Bostonia perplexa*—an unusual member of the Calamopityaceae from North America. Review of Palaeobotany and Palynology 72, 73–102. https://doi.org/10.1016/0034-6667(92)90177-I

Stein, W.E., Beck, C.B., 1983. *Triloboxylon arnoldii* from the Middle Devonian of western New York. Contributions from the Museum of Paleontology 26, 257–288.

Stein, W.E., Beck, C.B., 1978. *Bostonia perplexa* gen. et. sp. nov., A Calamopityan axis from the New Albany Shale of Kentucky. American Journal of Botany 4, 459–465. https://doi.org/10.1002/j.1537-2197.1978.tb06093.x

Stein, W.E., Hueber, F.M., 1989. The anatomy of Pseudosporochnus: *P. Hueberi* from the Devonian of New York. Review of Palaeobotany and Palynology 60, 311–359. https://doi.org/10.1016/0034-6667(89)90049-3

Stein, W.E., Berry, C.M., Morris, J.L., Hernick, L.V., Mannolini, F., Ver Straeten, C., Landing, E., Marshall, J.E.A., Wellman, C.H., Beerling, D.J., Leake, J.R., 2020. Mid-Devonian *Archaeopteris* roots signal revolutionary change in earliest fossil forests. Current Biology 30, 421-431.e2. https://doi.org/10.1016/j.cub.2019.11.067

Stein, W.E., Berry, C.M., Hernick, L.V., Mannolini, F., 2012. Surprisingly complex community discovered in the mid-Devonian fossil forest at Gilboa. Nature 483, 78–81. https://doi.org/10.1038/nature10819

Stein, W.E., Mannolini, F., Hernick, L.V., Landing, E., Berry, C.M., 2007. Giant cladoxylopsid trees resolve the enigma of the Earth's earliest forest stumps at Gilboa. Nature 446, 904–907. https://doi.org/10.1038/nature05705

Stein, W.E., Wight, D.C., Beck, C.B., 1984. Possible alternatives for the origin of Sphenopsida. Systematic Botany 9, 102–118. https://doi.org/10.2307/2418412

Stewart, W.N., Rothwell, G.W., 1993. The origin of the Sphenopsida, in: Paleobotany and the Evolution of Plants. New York, pp. 180–189.

Strullu-Derrien, C., Gèze, M., Spencer, A.R.T., De Franceschi, D., Kenrick, P., Selosse, M.-A., Knoll, A.H., 2021. An expanded diversity of oomycetes in Carboniferous forests: reinterpretation of *Oochytrium lepidodendri* (Renault 1894) from the Esnost chert, Massif Central, France. PLoS ONE 16, e0247849. https://doi.org/10.1371/journal.pone.0247849

Strullu-Derrien, C., Rioult, J., Strullu, D., 2009. Mycorrhizas in Upper Carboniferous *Radiculites* -type cordaitalean rootlets. New Phytolologist 182, 561–564. https://doi.org/10.1111/j.1469-8137.2009.02805.x

Stubblefield, S.P., Taylor, T.N., Beck, C.B., 1985. Studies of Paleozoic fungi. IV. Wood-decaying fungi in *Callixylon newberryi* from the Upper Devonian. American Journal of Botany 72, 1765–1774. https://doi.org/10.1002/j.1537-2197.1985.tb08449.x

Stubblefield, S.P., Taylor, T.N., Miller, C.E., Cole, G.T., 1984. Studies of Paleozoic fungi. III. Fungal parasitism in a Pennsylvanian gymnosperm. American Journal of Botany 71, 1275–1282. https://doi.org/10.1002/j.1537-2197.1984.tb11983.x

Sun, Q., Rost, T.L., Matthews, M.A., 2008. Wound-induced vascular occlusions in *Vitis vinifera* (Vitaceae): Tyloses in summer and gels in winter[1]. American Journal of Botany 95, 1498–1505. https://doi.org/10.3732/ajb.0800061

Suwannarach, N., Kumla, J., Bussaban, B., Hyde, K.D., Matsui, K., Lumyong, S., 2013. Molecular and morphological evidence support four new species in the genus *Muscodor* from northern Thailand. Annals of Microbiology 63, 1341–1351. https://doi.org/10.1007/s13213-012-0593-6

Swart, H.J., 1975. Callosities in fungi. Transactions of the British Mycological Society 64, 511–515. https://doi.org/10.1016/S0007-1536(75)80152-5

Szabo, L.J., Bushnell, W.R., 2001. Hidden robbers: The role of fungal haustoria in parasitism of plants. Proceedings of the National Academy of Sciences 98, 7654–7655. https://doi.org/10.1073/pnas.151262398

Tanrattana, M., Meyer-Berthaud, B., Decombeix, A.-L., 2018. *Callixylon wendtii* sp. nov., a new species of archaeopteridalean progymnosperm from the Late Devonian of Anti-Atlas, Morocco. Earth Environ. Earth and Environmental Science Transactions of the Royal Society of Edinburgh 108, 373–385. https://doi.org/10.1017/S1755691017000457

Taylor, T.N., Krings, M., 2010. Paleomycology: the rediscovery of the obvious. PALAIOS 25, 283–286. https://doi.org/10.2110/palo.2010.S03

Taylor, T.N., Krings, M., 2005. Fossil microorganisms and land plants: associations and interactions. Symbiosis 40, 119–135.

Taylor, T.N., Taylor, E.L., 1997. The distribution and interactions of some Paleozoic fungi. Review of Palaeobotany and Palynology 95, 83–94. https://doi.org/10.1016/S0034-6667(96)00029-2

Taylor, T.N., Krings, M., Taylor, E.L., 2015. Fossil fungi. Academic Press.

Taylor, T.N., Krings, M., Galtier, J., Dotzler, N., 2012. Fungal endophytes in *Astromyelon*-type (Sphenophyta, Equisetales, Calamitaceae) roots from the Upper Pennsylvanian of France. Review of Palaeobotany and Palynology 171, 9–18. https://doi.org/10.1016/j.revpalbo.2011.11.009

Taylor, T.N., Krings, M., Dotzler, N., Galtier, J., 2011. The advantage of thin section preparations over acetate peels in the study of late Paleozoic fungi and other microorganisms. PALAIOS 26, 239–244. https://doi.org/10.2110/palo.2010.p10-131r

Taylor, E.L., Taylor, T.N., Krings, M., 2009. Paleobotany: the biology and evolution of fossil plants. Academic Press.

Taylor, T.N., Klavins, S.D., Krings, M., Taylor, E.L., Kerp, H., Hass, H., 2004. Fungi from the Rhynie chert: a view from the dark side. Earth and Environmental Science Transactions of The Royal Society of Edinburgh 94, 457–473. https://doi.org/10.1017/S026359330000081X

Taylor, T.N., Remy, W., Hass, H., 1992. Fungi from the Lower Devonian Rhynie Chert: Chytridiomycetes. American Journal of Botany 79, 1233–1241. https://doi.org/10.1002/j.1537-2197.1992.tb13726.x

Terreaux De Felice, H.T., Decombeix, A.-L., Galtier, J., 2019. Anatomy, affinities, and evolutionary implications of new silicified stems of *Sphenophyllum* Brongniart, 1828 from the early Carboniferous (Mississippian) of France and Germany. Geodiversitas 41, 587–599. https://doi.org/10.5252/geodiversitas2019v41a14

Toledo, S., Bippus, A.C., Atkinson, B.A., Bronson, A.W., Tomescu, A.M.F., 2021. Taxon sampling and alternative hypotheses of relationships in the euphyllophyte plexus that gave rise to seed plants: insights from an Early Devonian radiatopsid. New Phytologist 232, 914–927. https://doi.org/10.1111/nph.17511

Toledo, S., Bippus, A.C., Tomescu, A.M.F., 2018. Buried deep beyond the veil of extinction: Euphyllophyte relationships at the base of the spermatophyte clade. American Journal of Botany 105, 1264–1285. https://doi.org/10.1002/ajb2.1102

Tomescu, A.M.F., 2021. The stele – A developmental perspective on the diversity and evolution of primary vascular architecture. Biological Reviews 96, 1263–1283. https://doi.org/10.1111/brv.12699

Tomescu, A.M.F., 2009. Megaphylls, microphylls and the evolution of leaf development. Trends in Plant Science 14, 5–12. https://doi.org/10.1016/j.tplants.2008.10.008

Tomescu, A.M.F., Groover, A.T., 2019. Mosaic modularity: an updated perspective and research agenda for the evolution of vascular cambial growth. New Phytologist 222, 1719–1735. https://doi.org/10.1111/nph.15640

Tomescu, A.M.F., McQueen, C.R., 2022. A protoxylem pathway to evolution of pith? An hypothesis based on the Early Devonian euphyllophyte *Leptocentroxyla*. Annals of Botany 130, 785–798. https://doi.org/10.1093/aob/mcac083

Trivett, M., 1993. An architectural analysis of *Archaeopteris*, a fossil tree with pseudomonopodial and opportunistic adventitious growth. Botanical Journal of the Linnean Society 111, 301–329. https://doi.org/10.1006/bojl.1993.1022

Unger, F., 1856. Schiefer und sandsteinflora, in: Beitrag Zur Paläontologie Des Thüringer Waldes. K.-k. Hof-u. Staatsdruckerei, pp. 139–186.

Van der Plaats-Niterink, A.J., 1981. Monograph of the genus *Pythium*. Studies in Mycology 21, 1–242.

Veenma, Y.P., Davies, N.S., Higgs, K.T., McMahon, W.J., 2023. Biogeomorphology of Ireland's oldest fossil forest: plant-sediment and plant-animal interactions recorded in the Late Devonian Harrylock Formation, Co. Wexford. Palaeogeography, Palaeoclimatology, Palaeoecology 621, 111579. https://doi.org/10.1016/j.palaeo.2023.111579

Wagner, C.A., Taylor, T.N., 1982. Fungal chlamydospores from the Pennsylvanian of North America. Review of Palaeobotany and Palynology 37, 317–328. https://doi.org/10.1016/0034-6667(82)90005-7

Walker, C., Harper, C.J., Brundrett, M.C., Krings, M., 2018. Looking for arbuscular mycorrhizal fungi in the fossil record, in: Transformative Paleobotany. Elsevier, pp. 481–517. https://doi.org/10.1016/B978-0-12-813012-4.00020-6

Walsh, P.T., 1968. The Old Red Sandstone west of Killarney, Co. Kerry, Ireland. Proceedings of the Royal Irish Academy. Section B: Biological, Geological, and Chemical Science 66, 9–26.

Wan, M., Yang, W., He, X., Liu, L., Wang, J., 2017. First record of fossil basidiomycete clamp connections in cordaitalean stems from the Asselian–Sakmarian (lower Permian) of Shanxi Province, North China. Palaeogeography, Palaeoclimatology, Palaeoecology 466, 353–360. https://doi.org/10.1016/j.palaeo.2016.11.050

Wang, Q., 2011. Correct author citation of the Late Devonian plant *Archaeopteris* (Progymnospermopsida). Paleontological Journal 45, 347–349. https://doi.org/10.1134/S0031030111030142

Wang, Z., Geng, B.-Y., 1997. A new Middle Devonian plant: *Metacladophyton tetraxylum* gen. et sp. nov. Palaeontographica Abteilung B 85–102.

Wang, D., Liu, L., 2015. A new Late Devonian genus with seed plant affinities. BMC Evolutionary Biology 15. https://doi.org/10.1186/s12862-015-0292-6

Wang, S., Sun, K., Cui, J., Ma, S., 2009. Fossil Flora of China. Volume 1: Fossil Plants from Coal Balls in China. Higher Education Press, Beijing.

Warmbrodt, R.D., Evert, R.F., 1979. Comparative leaf structure of several species of homosporous leptosporangiate ferns. American Journal of Botany 66, 412–440. https://doi.org/10.1002/j.1537-2197.1979.tb06242.x

Whiteside, J.H., Grice, K., 2016. Biomarker records associated with mass extinction events. Annual Review of Earth and Planetary Sciences 44, 581–612. https://doi.org/10.1146/annurev-earth-060115-012501

Williamson, W.C., 1892. The Genus *Sphenophyllum*. Nature 47, 11–13. https://doi.org/10.1038/047011c0

Williamson, W.C., 1874. III. On the organization of the fossil plants of the coal-measures.—Part V. Asterophyllites. Philosophical Transactions of the Royal Society of London 164, 41–81. https://doi.org/10.1098/rstl.1874.0003

Williamson, W.C., Scott, D.H., 1894. Further observations on the organization of the fossil plants of the coal- measures. —Part I. Calamites, *Calamostachys*, and *Sphenophyllum.* Philosophical Transactions of the Royal Society of London 185, 863–959. https://doi.org/10.1098/rstb.1894.0019

Wilson, J.P., Montañez, I.P., White, J.D., DiMichele, W.A., McElwain, J.C., Poulsen, C.J., Hren, M.T., 2017. Dynamic Carboniferous tropical forests: new views of plant function and potential for physiological forcing of climate. New Phytologist 215, 1333–1353. https://doi.org/10.1111/nph.14700

Wilson, M.L., Eggert, D.A., 1974. Root phloem of fossil tree-sized arthrophytes. Botanical Gazette 135, 319–328. https://doi.org/10.1086/336768

Xu, H.-H., Berry, C.M., Stein, W.E., Wang, Y., Tang, P., Fu, Q., 2017. Unique growth strategy in the Earth's first trees revealed in silicified fossil trunks from China. Proceedings of the National Academy of Sciences 114, 12009–12014. https://doi.org/10.1073/pnas.1708241114

Xu, H.-H., Berry, C.M., Wang, Y., Marshall, J.E.A., 2011. A New Species of *Leclercqia* Banks, Bonamo et Grierson (Lycopsida) from the Middle Devonian of North Xinjiang, China, with a Possible Climbing Habit. International Journal of Plant Sciences 172, 836–846. https://doi.org/10.1086/660195

Xu, Y.-M., Arnold, A.E., U′Ren, J.M., Xuan, L.-J., Wang, W.-Q., Gunatilaka, A.A.L., 2020. Teratopyrones A–C, Dimeric Naphtho-γ-Pyrones and Other Metabolites from *Teratosphaeria* sp. AK1128, a Fungal Endophyte of *Equisetum arvense*. Molecules 25, 5058. https://doi.org/10.3390/molecules25215058

Xue, J., Hao, S., Basinger, J.F., 2010. Anatomy of the Late Devonian *Denglongia hubeiensis*, with a discussion of the phylogeny of the Cladoxylopsida. International Journal of Plant Sciences 171, 107–120. https://doi.org/10.1086/647925

Zalessky, M., 1911. Etude sur l'anatomie du *Dadoxylon Tchihatcheffi* Goepp. sp. Mem. Comite Geol. de Russe, NS 68, 29.

Zeilinger, S., Gupta, V.K., Dahms, T.E.S., Silva, R.N., Singh, H.B., Upadhyay, R.S., Gomes, E.V., Tsui, C.K.-M., Nayak S, C., 2016. Friends or foes? Emerging insights from fungal interactions with plants. FEMS Microbiology Reviews 40, 182–207. https://doi.org/10.1093/femsre/fuv045

Zimmermann, W., 1930. Die Phylogenie der Pflanzen: ein Überblick über Tatsachen und Probleme. G. Fischer.

8. Appendices

Appendix A, supplementary data for chapter 1

Code map	Biozone	Stratigraphy	Name in literature	References
SBS	VI (?)	Carboniferous (Basal Mississipian)	76/2188 (?) or 76/2273(?)	Sleeman et al. (1983)
HBB	LE	Upper Devonian (uppermost Famennian)	Higgs locality H Locality 1	Sleeman et al. (1983) Matten (1995)
HH	LL		76/2271 Locality 7 Locality 4 Upper Sandeel Bay plant bed	Sleeman et al. (1983) Matten (1989) Matten (1995) Veenma et al. (2023)
SN	LL (?)		76/2192 (?)	Sleeman et al. (1983)
TC	LL (?)		Not reported	Not reported
TT	LL (?)		Locality 2 (?) Fossil log jam in the Harrylock Bay section	Matten (1995) Veenma et al. (2023)
GP	LL (?)		Not reported	Not reported

Appendix A.1. List of the localities with details of their ages, previous names found in the literature, and references. « ? » is used when the ages and the name and/or its previous name are inferred from maps of Sleeman et al. (1983) and/or Matten (1995).

TITLE-ABS-KEY (fossil AND plants) AND PUBYEAR < 2025 AND (LIMIT-TO (DOCTYPE,"ar")) AND (LIMIT-TO (EXACTSRCTITLE,"Review Of Palaeobotany And Palynology") OR LIMIT-TO (EXACTSRCTITLE,"Palaeogeography Palaeoclimatology Palaeoecology") OR LIMIT-TO (EXACTSRCTITLE,"International Journal Of Plant Sciences") OR LIMIT-TO (EXACTSRCTITLE,"American Journal Of Botany") OR LIMIT-TO (EXACTSRCTITLE,"Plos One") OR LIMIT-TO (EXACTSRCTITLE,"Quaternary Science Reviews") OR LIMIT-TO (EXACTSRCTITLE,"Quaternary International") OR LIMIT-TO (EXACTSRCTITLE,"Nature") OR LIMIT-TO (EXACTSRCTITLE,"Cretaceous Research") OR LIMIT-TO (EXACTSRCTITLE,"Science") OR LIMIT-TO (EXACTSRCTITLE,"Scientific Reports") OR LIMIT-TO (EXACTSRCTITLE,"Palaios") OR LIMIT-TO (EXACTSRCTITLE,"Acta Palaeobotanica") OR LIMIT-TO (EXACTSRCTITLE,"Historical Biology") OR LIMIT-TO (EXACTSRCTITLE,"New Phytologist") OR LIMIT-TO (EXACTSRCTITLE,"Quaternary Research") OR LIMIT-TO (EXACTSRCTITLE,"Botanical Journal Of The Linnean Society") OR LIMIT-TO (EXACTSRCTITLE,"Geology") OR LIMIT-TO (EXACTSRCTITLE,"Geobios") OR LIMIT-TO (EXACTSRCTITLE,"Paleontological Journal") OR LIMIT-TO (EXACTSRCTITLE,"Palaeoworld") OR LIMIT-TO (EXACTSRCTITLE,"Annals Of Botany") OR LIMIT-TO (EXACTSRCTITLE,"Nature Communications") OR LIMIT-TO (EXACTSRCTITLE,"Proceedings Of The Royal Society B Biological Sciences") OR LIMIT-TO (EXACTSRCTITLE,"Paleobiology") OR LIMIT-TO (EXACTSRCTITLE,"Palaeontology") OR LIMIT-TO (EXACTSRCTITLE,"Canadian Journal Of Earth Sciences") OR LIMIT-TO (EXACTSRCTITLE,"Journal Of Quaternary Science") OR LIMIT-TO (EXACTSRCTITLE,"Journal Of Paleontology") OR LIMIT-TO (EXACTSRCTITLE,"Palaeobiodiversity And Palaeoenvironments") OR LIMIT-TO (EXACTSRCTITLE,"Palynology") OR LIMIT-TO (EXACTSRCTITLE,"Palaeontologia Electronica") OR LIMIT-TO (EXACTSRCTITLE,"Lethaia") OR LIMIT-TO (EXACTSRCTITLE,"BMC Evolutionary Biology") OR LIMIT-TO (EXACTSRCTITLE,"Stratigraphy And Geological Correlation") OR LIMIT-TO (EXACTSRCTITLE,"Bulletin Of The Geological Society Of America") OR LIMIT-TO (EXACTSRCTITLE,"Sedimentary Geology") OR LIMIT-TO (EXACTSRCTITLE,"Acta Geologica Sinica English Edition") OR LIMIT-TO (EXACTSRCTITLE,"Geological Journal") OR LIMIT-TO (EXACTSRCTITLE,"Earth And Planetary Science Letters") OR LIMIT-TO (EXACTSRCTITLE,"Acta Botanica Sinica"))

Appendice A.2 Scopus advanced search request for research articles including « fossil» and «plants» in their titles, keywords, or abstracts from the first citation through 2025 (in selected journals).

Note that a subselection of the journal included in Scopus has been done to avoid the selection of journals including the words fossil and plant but where not paleontological papers.

TITLE-ABS-KEY (fossil AND fungi) AND PUBYEAR < 2025 AND (LIMIT-TO (DOCTYPE , "ar")) AND (LIMIT-TO (EXACTSRCTITLE , "Review Of Palaeobotany And Palynology") OR LIMIT-TO (EXACTSRCTITLE , "Palaeogeography Palaeoclimatology Palaeoecology") OR LIMIT-TO (EXACTSRCTITLE , "American Journal Of Botany") OR LIMIT-TO (EXACTSRCTITLE , "Plos One") OR LIMIT-TO (EXACTSRCTITLE , "Proceedings Of The National Academy Of Sciences Of The United States Of America") OR LIMIT-TO (EXACTSRCTITLE , "Quaternary Science Reviews") OR LIMIT-TO (EXACTSRCTITLE , "Quaternary International") OR LIMIT-TO (EXACTSRCTITLE , "Nature") OR LIMIT-TO (EXACTSRCTITLE , "Cretaceous Research") OR LIMIT-TO (EXACTSRCTITLE , "Science") OR LIMIT-TO (EXACTSRCTITLE , "Scientific Reports") OR LIMIT-TO (EXACTSRCTITLE , "Palaios") OR LIMIT-TO (EXACTSRCTITLE , "Acta Palaeobotanica") OR LIMIT-TO (EXACTSRCTITLE , "Historical Biology") OR LIMIT-TO (EXACTSRCTITLE , "New Phytologist") OR LIMIT-TO (EXACTSRCTITLE , "Quaternary Research") OR LIMIT-TO (EXACTSRCTITLE , "Botanical Journal Of The Linnean Society") OR LIMIT-TO (EXACTSRCTITLE , "Geology") OR LIMIT-TO (EXACTSRCTITLE , "Geobios") OR LIMIT-TO (EXACTSRCTITLE , "Paleontological Journal") OR LIMIT-TO (EXACTSRCTITLE , "Palaeoworld") OR LIMIT-TO (EXACTSRCTITLE , "Annals Of Botany") OR LIMIT-TO (EXACTSRCTITLE , "Paleobiology") OR LIMIT-TO (EXACTSRCTITLE , "Palaeontology") OR LIMIT-TO (EXACTSRCTITLE , "Canadian Journal Of Earth Sciences") OR LIMIT-TO (EXACTSRCTITLE , "Journal Of Quaternary Science") OR LIMIT-TO (EXACTSRCTITLE , "Journal Of Paleontology") OR LIMIT-TO (EXACTSRCTITLE , "Palaeobiodiversity And Palaeoenvironments") OR LIMIT-TO (EXACTSRCTITLE , "Palaeontologia Electronica") OR LIMIT-TO (EXACTSRCTITLE , "Lethaia") OR LIMIT-TO (EXACTSRCTITLE , "BMC Evolutionary Biology") OR LIMIT-TO (EXACTSRCTITLE , "Stratigraphy And Geological Correlation") OR LIMIT-TO (EXACTSRCTITLE , "Earth And Planetary Science Letters") OR LIMIT-TO (EXACTSRCTITLE , "Acta Botanica Sinica"))

Appendice A.3 Scopus advanced search request for research articles including « fossil » and «fungi» in their titles, keywords, or abstracts from the first citation through 2025 (in selected journals).

Note that a subselection of the journal included in Scopus has been done to avoid the selection of journals including the words fossil and fungi, but where not paleontological papers.

Appendix B, supplementary data for chapter 3

Specimen number	Included in stele morphotype	Included in emission pattern	Included in PCA
A 168	No	No	No
MN 204	Yes (morphotype 1)	No	Yes (cluster 2)
MN 205	No	No	No
MN 206	Yes (morphotype 1)	No	Yes (cluster 3)
MN 207	Yes (morphotype 1)	No	No
MN 208	Yes (morphotype 1)	No	No
MN 209	Yes (morphotype 1)	Yes (emission type 4)	No
Specimen number	Included in stele morphotype	Included in emission pattern	Included in PCA
MN 292	Yes (morphotype 1)	Yes (emission type 1)	Yes (cluster 3)
MN 400	Yes (morphotype 2)	Yes (emission type 5)	No
MN 719	Yes (morphotype 4)	No	No

MN 742	Yes (morphotype 1)	No	No
MN 751	No	No	No
MN 759	Yes (morphotype 1)	Yes (emission type 1)	No
MN 765	Yes (morphotype 1)	No	No
MN 766	Yes (morphotype 1)	No	No
MN 809	Yes (morphotype 1)	No	No
MN 821	No	No	No
MN 832	No	No	No
MN 837	No	No	No
MN 844	Yes (morphotype 1)	No	Yes (cluster 3)
MN 852	No	No	No
Specimen number	Included in stele morphotype	Included in emission pattern	Included in PCA
MN 879	No	No	No
MN 902	No	No	No
MN 904	Yes (morphotype 2)	No	No

MN 905	Yes (morphotype 1)	No	No
MN 906	No	No	No
MN 910	Yes (morphotype 1)	No	No
MN 918	Yes (morphotype 1)	No	Yes (cluster 2)
MN 920	Yes (morphotype 1)	Yes (emission type 2)	Yes (cluster 2)
MN 921	Yes (morphotype 3)	No	No
MN 922	No	No	No
MN 923	No	No	No
MN 924	No	No	No
MN 925	Yes (morphotype 1)	Yes (emission type 2)	Yes (cluster 3)
MN 926	Yes (morphotype 1)	No	Yes (cluster 2)
Specimen number	Included in stele morphotype	Included in emission pattern	Included in PCA
MN 947	Yes (morphotype 1)	Yes (emission type 2)	No
MN 950	No	No	No
MN 951	Yes (morphotype 1)	Yes (emission type 2)	No

MN 952	No	No	No
MN 952 bis	Yes (morphotype 1)	No	No
MN 953	Yes (morphotype 1)	No	No
MN 954	No	No	No
MN 958	Yes (morphotype 1)	Yes (emission type 2)	Yes (cluster 1)
MN 958 bis	Yes (morphotype 1)	No	Yes (cluster 1)
MN 966	No	No	No
MN 969	No	No	No
MN 969 bis	Yes (morphotype 1)	No	No
MN 982	No	No	No
Total sp : 53	Total sp : 32	Total sp : 12	Total sp : 13

Appendix B.1 List of all the *Cladoxylon* from the Montagne Noire with details of their different uses in the study.

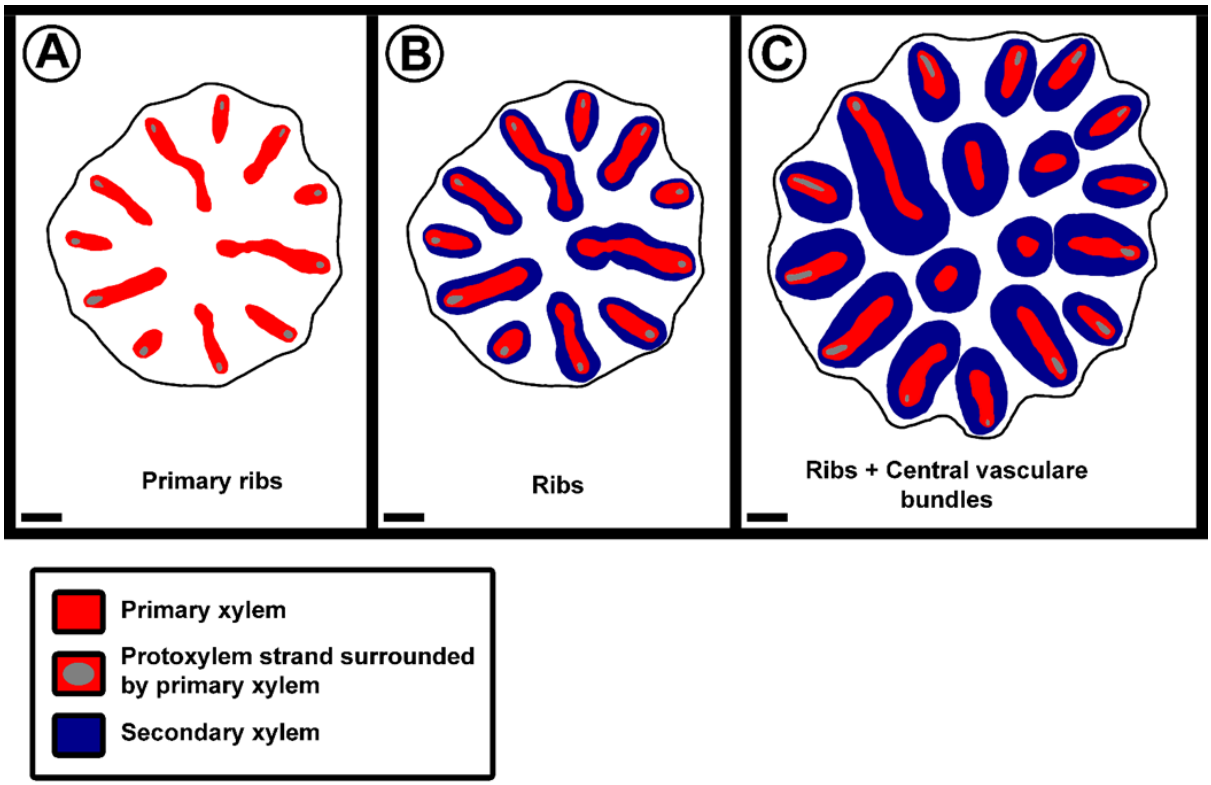

Appendix B.2 Illustration of the vocabulary used in describing steles. (A) Stele with only the primary ribs represented. (B) Stele with only ribs represented. (C) Complete stele with central vascular bundles represented.

Sp_number	Diameter	Total_ribs	X1_area	X2_area	Min_X1RibsL	Max_X1RibsL	Min_Ribs_ Lenght	Max_Ribs_ Lenght	Min_X1_ Roudness	Max_X1_ Roudness	Min_Ribs_ Roudness	Max_Ribs_Roud ness
MN 204	6.7	11	6.96	10.43	0.82	2.86	1.08	3.21	0.18	0.64	0.28	0.8
MN 206	6.4	9	4.14	19.242	0.62	2.14	1.31	3.27	0.17	0.85	0.62	0.91
MN 223	6.5	12	6.7	10.93	0.65	2.36	1.19	2.8	0.15	0.58	0.29	0.68
MN 268	10.6	14	11.236	38.17	1.19	3.65	1.74	4.55	0.12	0.4	0.44	0.75
MN 292	8	12	7.48	22.87	0.63	2.45	1.1	3.33	0.21	0.96	0.5	0.89
MN 844	8.4	10	7.47	24	0.87	2.51	1.45	3.4	0.24	0.67	0.54	0.89
MN 876	7.3	10	6.34	12.28	0.94	2.52	1.13	3.16	0.2	0.55	0.43	0.8

Sp_number	Diameter	Total_ribs	X1_area	X2_area	Min_X1RibsL	Max_X1RibsL	Min_Ribs_Lenght	Max_Ribs_Lenght	Min_X1_Roudness	Max_X1_Roudness	Min_Ribs_Roudness	Max_Ribs_Roudness
MN 920	4.9	10	3.34	5.457	0.6	1.84	0.99	2.02	0.15	0.55	0.31	0.82
MN 920 (D)	4.6	10	3.92	3.83	0.74	2.07	0.97	2.15	0.16	0.44	0.29	0.68
MN 925	7.8	13	7.94	19.71	0.81	2.94	1.21	3.47	0.12	0.65	0.34	0.93
MN 926	5.9	13	9.47	2.41	0.95	2.67	0.95	2.82	0.18	0.6	0.25	0.61
MN 958	5.2	10	2.936	11.324	0.55	1.5	0.81	2.23	0.24	0.72	0.59	0.94
MN 958 (D)	5.7	10	2.88	11.48	0.48	1.42	0.85	2.33	0.22	0.73	0.48	0.96
MN 958 bis	3.3	8	1.872	2.308	0.42	1.12	0.56	1.32	0.3	0.83	0.43	0.94

Appendix B.3 Stele morphotype 1 PCA characters.

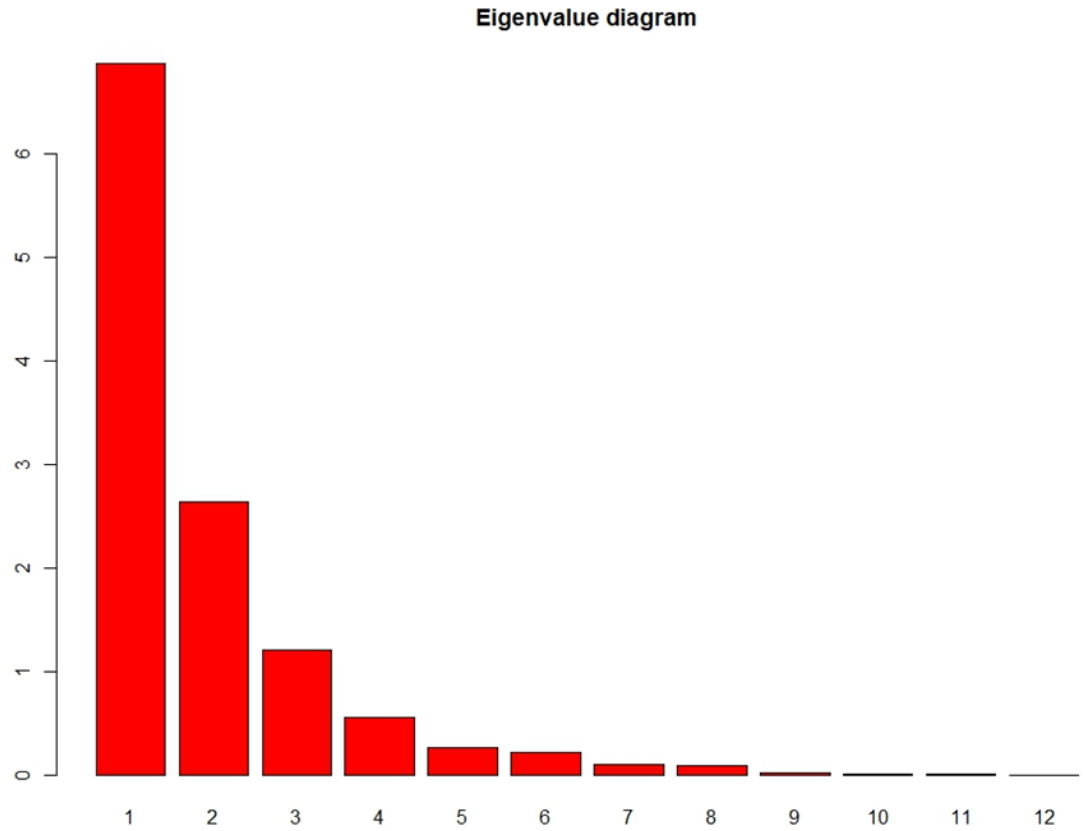

Appendix B.4 Eigenvalue diagram of the stele morphotype 1 PCA.

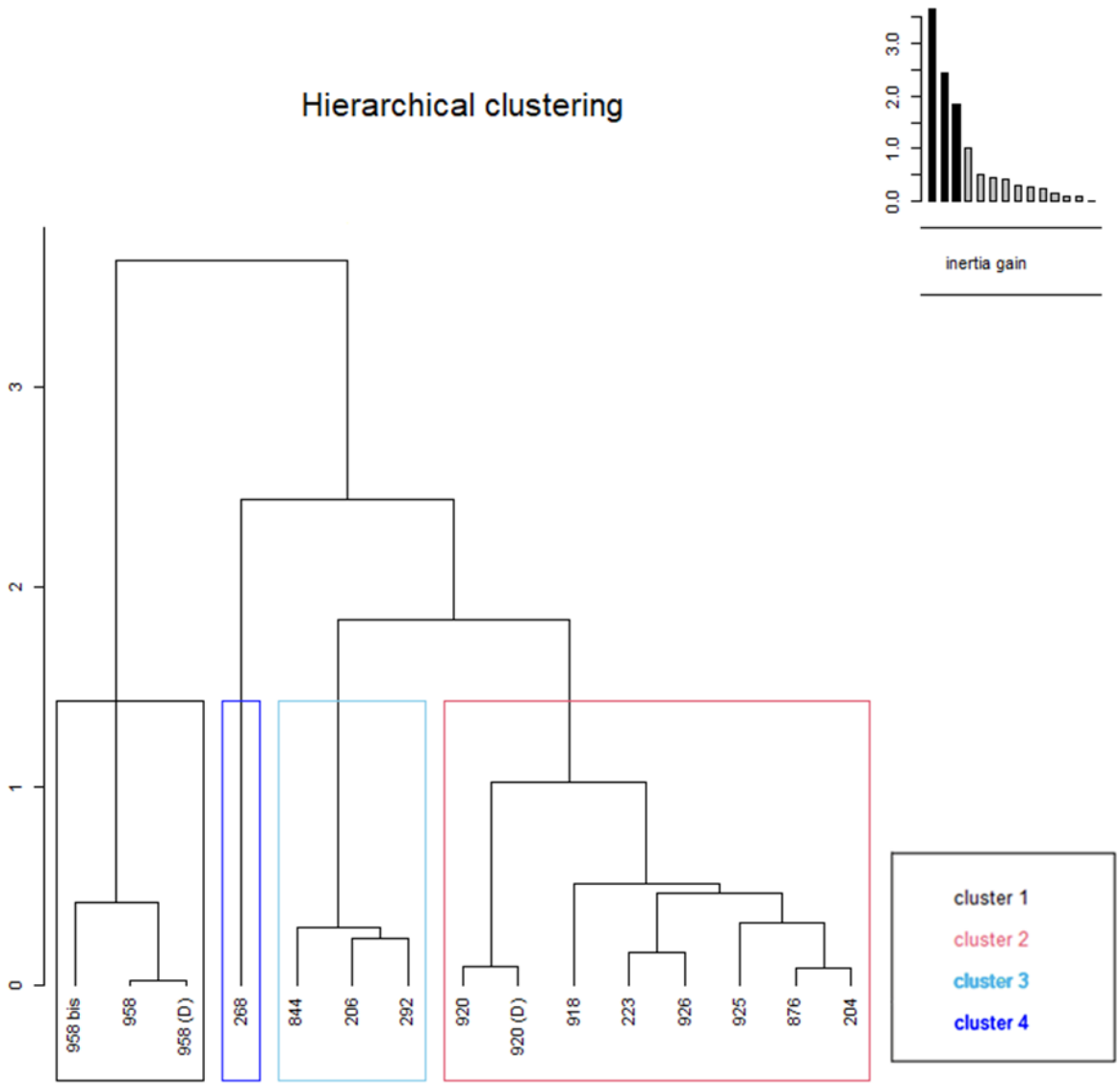

Appendix B.5 Hierarchical clustering tree.

Appendix C, supplementary data for chapter 4

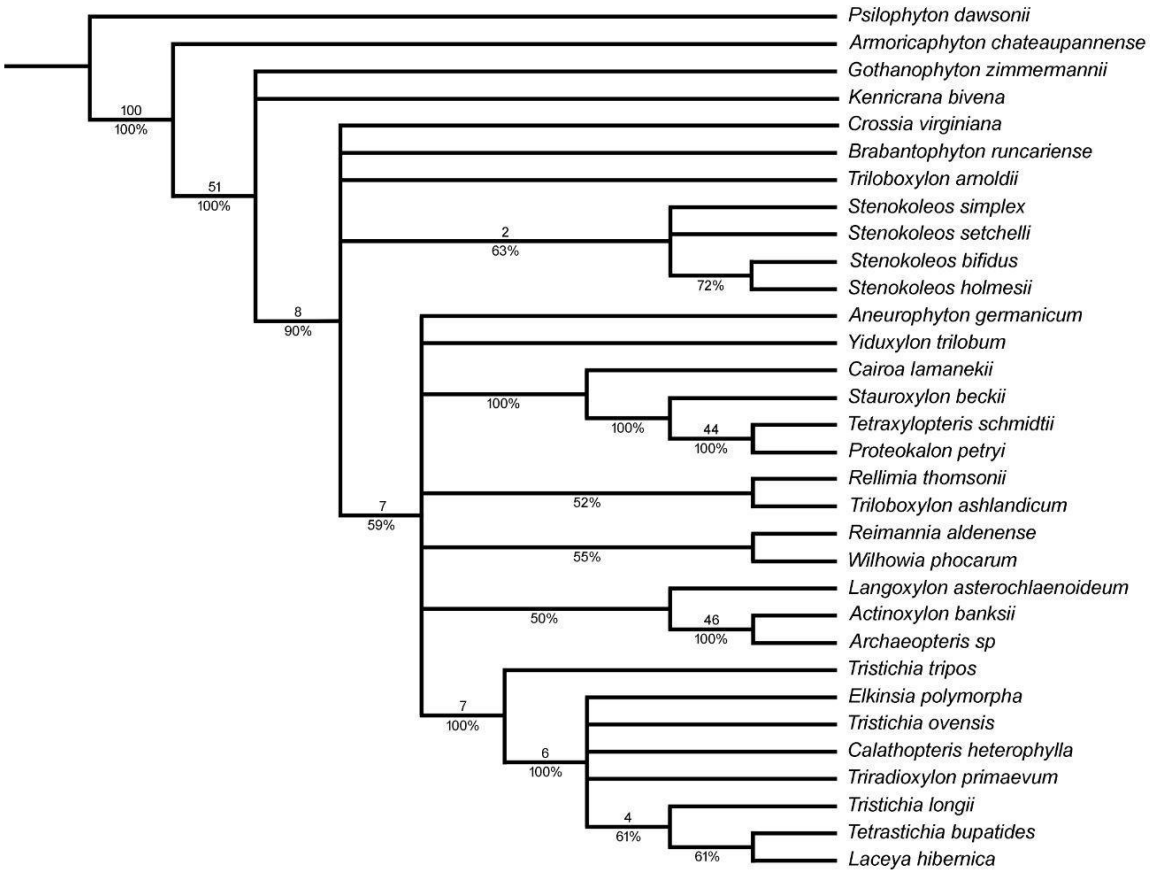

Appendix C.1 Analysis with discrete characters only, 50% majority rule tree; numbers at node are bootstrap value ≥2 above and frequency of tree with this node ≥50% below (32 taxa, 41 characters, 208 most parsimonious trees, length 110, RI=0.587, CI=0.436).

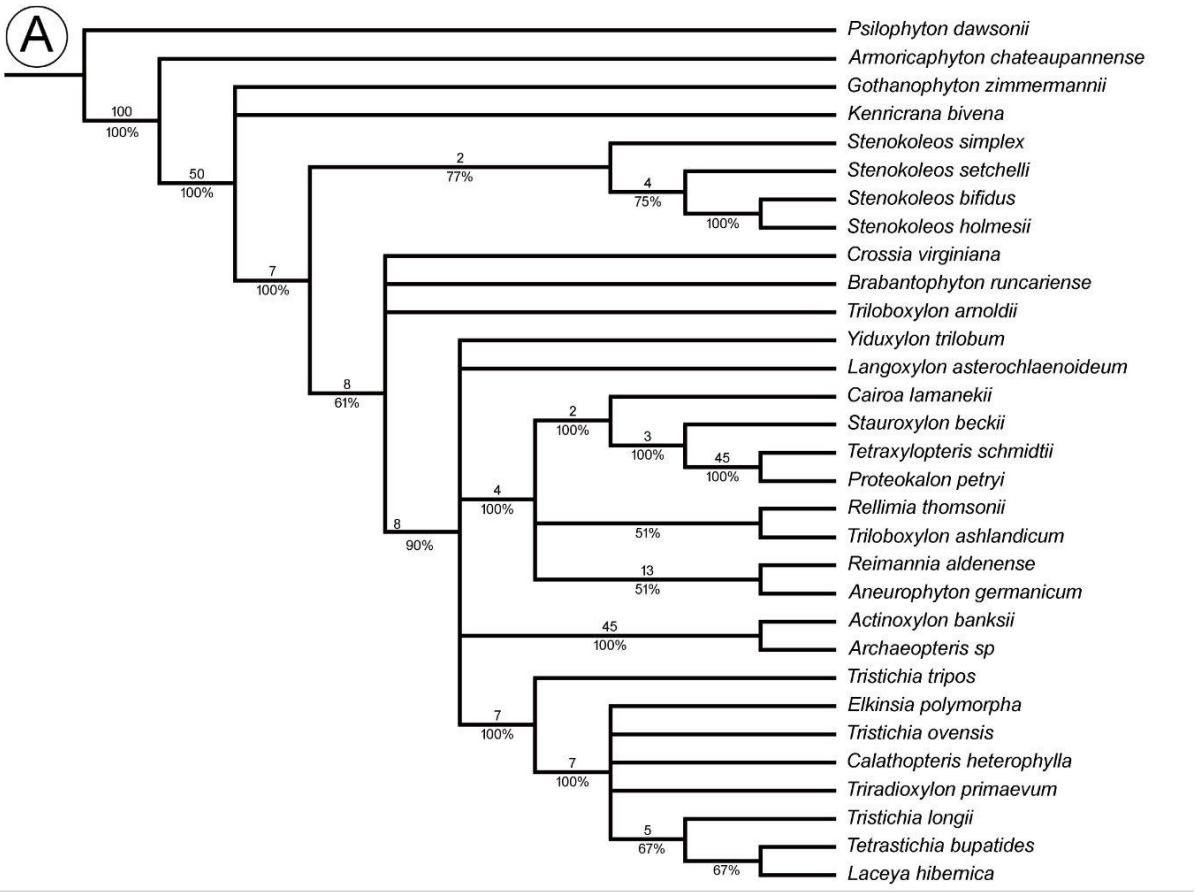
A
Psilophyton dawsonii
Armoricaphyton chateaupannense
Gothanophyton zimmermannii
Kenricrana bivena
Stenokoleos simplex
Stenokoleos setchelli
Stenokoleos bifidus
Stenokoleos holmesii
Crossia virginiana
Brabantophyton runcariense
Triloboxylon arnoldii
Yiduxylon trilobum
Langoxylon asterochlaenoideum
Cairoa lamanekii
Stauroxylon beckii
Tetraxylopteris schmidtii
Proteokalon petryi
Rellimia thomsonii
Triloboxylon ashlandicum
Reimannia aldenense
Aneurophyton germanicum
Actinoxylon banksii
Archaeopteris sp
Tristichia tripos
Elkinsia polymorpha
Tristichia ovensis
Calathopteris heterophylla
Triradioxylon primaevum
Tristichia longii
Tetrastichia bupatides
Laceya hibernica
B
Psilophyton dawsonii
Armoricaphyton chateaupannense
Gothanophyton zimmermannii
Kenricrana bivena
Triloboxylon arnoldii
Brabantophyton runcariense
Crossia virginiana
Stenokoleos simplex
Stenokoleos setchelli
Stenokoleos bifidus
Stenokoleos holmesii
Yiduxylon trilobum
Cairoa lamanekii
Stauroxylon beckii
Tetraxylopteris schmidtii
Proteokalon petryi
Rellimia thomsonii
Aneurophyton germanicum
Reimannia aldenense
Triloboxylon ashlandicum
Langoxylon asterochlaenoideum
Actinoxylon banksii
Archaeopteris sp
Tristichia tripos
Elkinsia polymorpha
Calathopteris heterophylla
Tristichia longii
Tetrastichia bupatides
Laceya hibernica
Tristichia ovensis
Triradioxylon primaevum

Appendix C.2 50% majority rule trees of analysis conducted without *Wilhowia phocarum*; numbers at node are: for A bootstrap value ≥2 above and frequency of tree with this node ≥50% below and for B bootstrap value ≥2 above and Bremer support ≥0.2 below.

(A) Analysis with discrete characters only (31 taxa, 41 characters, 88 most parsimonious tree, length 107, RI = 0.607, CI = 0.449). (B) Analysis with discrete and continuous characters (31 taxa, 50 characters, 3 most parsimonious tree, length 125.519, RI=0.576, CI=0.435).

nstates cont;

xread

50 32

&[cont]

Psilophyton_dawsonii 0.350-0.435 0.189-0.241 ? ?
0.248-0.394 ? ? ? ?

Stenokoleos_simplex 0.399-0.495 0.179-0.229 0.207-0.351 0.307-0.398
0.066-0.172 ? ? 0.808-1.000 ?

Stenokoleos_bifidus 0.525-0.649 0.609-0.754 0.392-0.577 0.799-1.000
0.223-0.364 ? ? 0.075-0.103 ?

Stenokoleos_holmesii 0.804-0.990 0.319-0.400 0.580-0.807 0.377-0.484
0.041-0.142 ? 0.004-0.009 0.482-0.602 ?

Stenokoleos_setchelli 0.598-0.739 0.379-0.474 0.142-0.272 0.637-0.801
0.413-0.596 ? 0.012-0.018 ? ?

Crossia_virginiana 0.683-0.842 0.631-0.782 0.496-0.705 0.731-0.916
0.363-0.536 ? ? 0.062-0.088 ?

Brabantophyton_runcariense 0.711-0.876 0.810-1.000 0.565-0.789 0.267-0.349
0.504-0.707 0.774-1.000 0.815-1.000 0.000-0.012 ?

Cairoa_lamanekii	0.165-0.209	0.197-0.251	0.549-0.769	0.227-0.301	0.000-0.092	0.149-0.235	?
?	?						
Rellimia_thomsonii	0.812-1.000	0.177-0.226	0.615-0.850	0.097-0.142	0.148-0.273	0.484-0.645	?
?	?						
Reimannia_aldenense	0.283-0.353	0.069-0.095	0.467-0.669	0.097-0.142	0.372-0.546	?	?
?	?						
Tetraxylopteris_schmidtii	0.000-0.007	0.254-0.320	0.637-0.877	0.105-0.151	0.083-0.193	0.539-0.713	?
?	0.000-0.093						
Aneurophyton_germanicum	0.318-0.396	0.296-0.372	0.539-0.757	0.307-0.398	0.050-0.152	0.118-0.197	?
?	0.139-0.263						
Proteokalon_petryi	0.525-0.649	0.124-0.162	0.434-0.628	0.090-0.133	0.050-0.152	0.138-0.223	?
?	0.510-0.716						
Triloboxylon_ashlandicum	0.414-0.513	0.221-0.281	0.545-0.765	0.051-0.085	0.330-0.495	0.173-0.265	?
?	0.046-0.149						
Triloboxylon_arnoldii	0.401-0.497	0.000-0.010	0.450-0.648	0.182-0.246	0.124-0.243	0.297-0.417	0.017-0.024
0.030-0.049	?						
Actinoxylon_banksii	0.432-0.535	?	0.352-0.528	0.399-0.510	0.192-0.327	0.219-0.322	?
?	0.742-1.000						
Wilhowia_phocarum	0.618-0.762	0.637-0.789	0.621-0.858	0.135-0.188	?	?	
?	0.002-0.014	?					
Gothanophyton_zimmermannii	0.780-0.961	0.647-0.802	0.454-0.652	0.000-0.023	0.330-0.495	?	0.011-0.017
?	?						
Elkinsia_polymorpha	0.473-0.585	0.406-0.506	0.571-0.796	0.273-0.356	0.628-0.859	0.366-0.502	0.001-0.005
0.101-0.135	?						
Tetrastichia_bupatides	0.292-0.364	0.043-0.062	0.417-0.607	0.168-0.228	0.165-0.294	0.000-0.054	?
0.034-0.054	?						

Tristichia_tripos 0.362-0.450 0.164-0.211 0.738-1.000 0.635-0.799 0.429-0.617 0.429-0.578 ? 0.023-0.040 ?

Tristichia_ovensi 0.083-0.109 0.093-0.124 0.609-0.843 0.155-0.213 0.000-0.092 0.207-0.307 0.000-0.004 0.065-0.092 ?

Tristichia_longii 0.325-0.404 0.142-0.184 0.387-0.572 0.386-0.495 0.330-0.495 0.346-0.476 0.007-0.012 0.097-0.131 ?

Laceya_hibernica 0.246-0.308 0.225-0.286 0.539-0.757 0.529-0.669 0.380-0.556 0.124-0.206 ? ? ?

Yiduxylon_trilobum 0.233-0.292 0.006-0.018 0.588-0.817 0.245-0.323 0.289-0.445 0.276-0.392 ? 0.081-0.112 ?

Calathopteris_heterophylla 0.664-0.819 0.215-0.273 ? ? 0.165-0.294 0.173-0.265 0.077-0.098 0.101-0.135 ?

Langoxylon_asterochlaenoideum 0.398-0.494 0.353-0.442 0.450-0.648 0.439-0.559 0.413-0.596 ? ? 0.049-0.072 ?

Triradioxylon_primaevum 0.083-0.109 0.041-0.060 ? ? 0.000-0.092 0.069-0.138 0.003-0.007 0.101-0.135 ?

Kenricrana_bivena 0.292-0.364 0.170-0.219 0.648-0.891 0.043-0.076 0.380-0.556 0.380-0.518 0.028-0.038 0.039-0.059 ?

Archaeopteris_sp 0.502-0.621 0.402-0.501 0.000-0.098 0.731-0.916 0.103-0.218 0.120-0.200 ? ? ?

Armoricaphyton_chateaupannense 0.432-0.535 0.643-0.797 ? ? 0.212-0.351 0.397-0.539 ? ? ?

Stauroxylon_beckii 0.523-0.646 0.170-0.219 0.474-0.678 0.289-0.376 0.743-1.000 0.104-0.180 ? 0.188-0.242 ?

&[num]

Psilophyton_dawsonii 0010-0--1--00-00-0--000100000----------0
223

Stenokoleos_simplex ?11141401110100l?0--000110?10---11013-110

Stenokoleos_bifidus ?111?1?0101010l?0--000??0?10---11013-??0

Stenokoleos_holmesii ?11131301011000l?0----1000?10---110?3-0-0

Stenokoleos_setchelli ??1?41401110100??0--000000?10---?????-??0

Crossia_virginiana ?1???13?11101001?1?1010110?10---??-1?-??0

Brabantophyton_runcariense ?11131311110100l?111000110?00---11013-??0

Cairoa_lamanekii ?03131[3 4]011100001?1?-00011000120?-0------0

Rellimia_thomsonii 00113130111001010111000000001100-0------0

Reimannia_aldenense ?01[1 2]3130101100l?0--00011010?----0------0

Tetraxylopteris_schmidtii 00224140111000l1?111010120001200-0------0

Aneurophyton_germanicum 0011?13010100001011100001000l100-0------0

Proteokalon_petryi ?02241[3 4]011110011?111000110011101-0------0

Triloboxylon_ashlandicum ?011313011100101?111000110101101-0------0

Triloboxylon_arnoldii ?11131301110000l?11110011O?00---1101????0

Actinoxylon_banksii ?111616001?00001?11-000110000---001-----1

Wilhowia_phocarum ?111?13011110201?0--00011000??[0 1]0-0--?-??0

Gothanophyton_zimmermannii ?111?1[4 5 6]011100000?0--??0?10?00---11003-??0

Elkinsia_polymorpha 111131301110100??111101110?00---0[0 1][0 1]112110

Tetrastichia_bupatides ?111[3 5]1[3 4 5 6]001001001[0 1]1?1101[1 2][1 2]0?10---0001[1 2 3]2110

Tristichia_tripos ?11131301110000l?1?1100110?10---000112?-0

Tristichia_ovensi ?111313010100001011110111O?10---000112110

Tristichia_longii ?11131301000000l?11110l110?10---110112??0

Laceya_hibernica ?111313000000000??11110l110?10---000112110

Yiduxylon_trilobum ?1113130?0?0000??11100011O?00---011112??0

Calathopteris_heterophylla ?11151501?101011?11110l110?10---000112110

Langoxylon_asterochlaenoideum ?111?1900100101100--000110?00---000?12??0

Triradioxylon_primaevum ?11131301010000l?11110l110?00---000112110

Kenricrana_bivena ?112414011110100-100010111?00---110012110

Archaeopteris_sp 1111[2 3 4 5]1[4 5 6 7 8 9]000000[1 2]0101110111?0000---0010[4 5][2 3]0-1

Armoricaphyton_chateaupannense ?010-0--1--10-00-101000100000----------0

Stauroxylon_beckii ?132414010001001[0 1]11100000?00????00012???0

;

Appendix C.3 Morphological matrix modified from Toledo et al. 2021 TEA ++ version including 50 characters (9 continuous, 41 discrete) and 32 taxa.